UNIVERSITY OF CALGARY

Precipitation, Aggregation, and Settling of Asphaltenes from *n*-Alkane Diluted Bitumens

by

Jairo Alberto Duran

A THESIS

SUBMITTED TO THE FACULTY OF GRADUATE STUDIES

IN PARTIAL FULFILMENT OF THE REQUIREMENTS FOR THE

DEGREE OF DOCTOR OF PHILOSOPHY

GRADUATE PROGRAM IN CHEMICAL AND PETROLEUM ENGINEERING

CALGARY, ALBERTA

SEPTEMBER, 2019

Abstract

Several industrial processes involve the precipitation, aggregation, and settling of asphaltenes from solvent diluted bitumen. Models and data that include the effect of solvent type, concentration, shear, and contact time on asphaltene precipitation and settling are required to design and optimize these processes but are lacking or are specific for conventional oils. In this thesis, the kinetics of asphaltene precipitation, aggregation and settling were investigated for *n*-heptane and *n*-pentane diluted bitumens at ambient conditions. The onset and amount of precipitation were measured in air and nitrogen. The size distribution, fractal dimension, and settling rates of the aggregates were also measured.

Asphaltene aggregates were found to be fused fractal structures that are insensitive to shear once formed. A semi-empirical correlation for their fractal dimension was proposed. Asphaltene precipitation in a nitrogen atmosphere was found to be time-dependent but reached an apparent equilibrium after tens of hours. A previously developed population balance model was adapted to include both nucleation and flocculation mechanisms and was tuned to match both precipitation amounts and aggregate sizes. Asphaltene precipitation in air did not reach an equilibrium likely because oxygen altered the asphaltenes. An oxidation rate term was introduced into the population balance model to match the precipitation data in air. The proposed model matched both yields and aggregate sizes over time for several bitumens and conventional oils to within 15% in nitrogen and 20% in air.

Asphaltene aggregates were found to have an approximately log normal size distribution but settled as a zone; that is, all aggregates settled at the same rate. The average aggregate size and fractal dimension reached a maximum at an *n*-alkane content of approximately 75 wt%. Settling rates are a function of the aggregate size and fractal dimension and reached a maximum at approximately the same *n*-alkane content. The settling rates were modeled with Stokes' law modified to include the fractal dimension of the aggregates and using the Sauter mean diameter for all aggregates. The model matched settling rates to within 20% of the maximum settling rate.

Keywords: asphaltene precipitation, bitumen, aggregation, size distribution, fractal dimension, kinetics, population balance, nucleation, settling rate, aeriation, oxidation.

Acknowledgements

This thesis has been the product of a few years of hard work and resilience. All this work would have been impossible without the constant support and advice of many persons along the way. First, to my supervisor, Dr. Harvey Yarranton, who gave me the opportunity to be part of his group and spent innumerable hours giving me guidance and advice to form a good PhD and an enthusiastic professional. Thanks to him for the long hours spent in academic discussions and editing papers. Also, thanks for showing me that is possible to be an excellent professor and a great family man. It was a pleasure being part of this research group and taking me to an unforgettable experience.

Also, I want to thank Mr. Florian Schoeggl for this constant support in the lab and the amazing conversations we often had. He showed me that to learn to fly is not that different than to learn to make research. Many thanks to Ms. Elaine Baydak, a constant support and whose different conversation topics made more bearable the many hours in the lab. I want to extend my gratitude to former and current members of the HOPP/AER research group. All of you were a constant source of trouble and laughs but also a huge source of personal and professional experiences from which to learn. Thanks for the great time and the many pleasant conversations over lunch.

To Karen, my friend and love. Thanks for being there all the way and being patient with my bad temper and my many absences during these years. Hope to make up for those in the many upcoming years. Thanks for your support and understanding.

To my family, particularly to my mom, Maria Patricia. You planted the seed on me to be curious and pursue my dreams. All the words I might write to thank all you have done for me would fall short.

To friends and colleagues, who provided many words of advice and cheer in the moments I needed them most. To many others that the memory fails to remember. People who directly or indirectly were a key part on the completion of my PhD.

And of course, to god: *"Ad maiorem Dei gloriam"*.

To my Mother and my lovely Karen,

Resilient women to whom I owe so much;

From whom I have received much love and advice.

"Begin. To begin is half the work, let half still remain; again begin this, and thou wilt have finished"

Marcus Aurelius

Table of Contents

List of Tables

List of Figures

List of Symbols

Symbol	*Definition*
A	Hamaker constant (J)
A_i	parameter for viscosity model
b	fitting parameter of equilibrium yield equation
B, C	fitting parameters for the correlation of immediate precipitation fraction
C_0	asphaltene supersaturation concentration (mol/m^3)
C_1	concentration of primary particles (mol/m^3)
C_i	concentration of aggregate of size i (mol/m^3)
C_s	asphaltene concentration at the particle surface (mol/m^3)
d_1	number mean diameter (m)
d_2	area mean diameter (m)
d_3	volume mean diameter (m)
d_{32}	Sauter mean diameter (m)
d_{43}	volume moment mean diameter (m)
d_i	aggregate diameter (m)
d_p	primary particle diameter (m)
D	diffusion coefficient of asphaltene nanoaggregates (m^2/s)
D_c	diameter of graduated cylinder (m)
D_B	diffusion coefficient of bitumen in the medium (m^2/s)
D_f	asphaltene fractal dimension
D_i	aggregate diffusion coefficient in the medium (m^2/s)
f	immediate precipitate fraction
f_i	number frequency of size distributions
F_{ad}	adhesion force (N)
F_i	volume frequency of size distributions
$F_{i,j}$	aggregation rate between aggregates of size i and j (mol/m^3·s)
g	acceleration of gravity (m/s^2)
h	radius of spherical boundary for asphaltene mass transfer (m)
k	exponent for the diffusivity model

k_A	conversion factor used in the nucleation model (mol/m^3)
k_B	Boltzmann constant (kg·m^2/s^2·K)
k_N	nucleation rate constant (1/s)
k_s	adhesion force decay rate (1/s)
$K_{i,j}$	collision kernel for aggregation (m^3/mol·s)
L	length of centrifuge tube (m)
m	exponent for FBRM calibration
$m_{agg,i}$	mass of one aggregate in the *i*-th bin (kg)
$M_{A,i}$	mass of asphaltenes in the *i*-th bin (kg)
$M_{W,A}$	molecular weight of an average asphaltene molecule (kg/mol)
n	number concentration (# particles/m^3); Richardson-Zaki exponent in Chapter 6.
$n_{agg,i}$	number of aggregates per bin per unit mass of oil (# aggregates/kg)
n_p	number of primary particles per aggregate
N	total number of bins
N_f	total number of aggregates
N_n	number of asphaltene molecules per nanoaggregate
r	asphaltene nuclei radius (m)
r_0	initial radius of asphaltene nanoaggregates (m)
r_c	centrifuge radius (m)
r_N	nucleation rate (mol/m^3·s)
r_{ox}	oxidation rate (mol/m^3·s)
R	universal gas constant (J/mol·K)
R_s	geometric scaling factor
Re	Reynolds number
s_i	separation efficiency of aggregates in the *i*-th bin
SG	specific gravity
T	system temperature (K)
TI	toluene insolubles
t_c	centrifugation time (s)
u_s	settling rate (m/s)
V_{agg}	volume of aggregates in suspension (m^3)

V_{sed}	volume of sediment (m^3)
V_{susp}	volume of aggregate suspension (m^3)
v_i	volume of settling layers (m^3)
w	precipitant content (wt%)
w_0	mass of oil per unit volume of mixture (kg/m^3)
$w_{A,C7}$	*n*-heptane asphaltene content of the oil (wt%)
w_i	weighting factor for FBRM calibration
w_o	equilibrium onset content (wt%)
w_u	asphaltene precipitate concentration (wt%)
W_A	*n*-pentane asphaltene content of the oil (wt%)
W_{ad}	Adhesion energy, (mJ/m^2)
W_{ij}	enhancement factor of the collision frequency
x	dimensionless interparticle distance; weighting factor in Eq. 6.11
$Y_{A,eq}$	asphaltene equilibrium yield (wt%)
$Y_{A,slow}$	yield of asphaltenes showing slow precipitation (wt%)

Greek Symbols

α	collision frequency ($m^3/mol \cdot s$)
α_{agg}	aggregate volume fraction
α_i	interaction parameter of viscosity model
α_m	volume fraction of fluid
β	collision efficiency
β_i	interaction parameter for density model
δ	Hildebrand solubility parameter ($MPa^{0.5}$)
Δx_i	distance travelled by aggregates during centrifugation (m)
μ	fluid viscosity (Pa·s)
ρ_A	asphaltene density (kg/m^3)
ρ_A	asphaltene aggregate density (kg/m^3)
ρ_m	medium density (kg/m^3)
ρ_o	crude oil density (kg/m^3)
ρ_s	particle density (kg/m^3)

φ_0	volume fraction of precipitant in the mixture
ϕ_i	aggregate porosity
Φ	van der Waals potential energy (J)
ω	angular velocity (rad/s)
χ	interaction parameter

Subscripts

asph	asphaltenes
A	asphaltenes
c	compacted
eff	effective
E	early
i	aggregate in the *i*-th bin
m	fluid medium
max	maximum diameter in the domain
med	medium
o	crude oil
onset	onset of precipitation at a fixed contact time
p	particle
res	residual
sed	sediment
susp	suspension
total	total
uc	uncompacted

Acronyms

AAD	Absolute average deviation
AARD	Absolute average relative deviation
AER	Alberta Energy Regulator
API	American Petroleum Institute
ASTM	American Society for Testing and Materials

EOS	equation of state
FBRM	Focused beam reflectace measurement
FTIR	Fourier transform infrared spectroscopy
ID	internal diameter
IR	infrared
JKR	Johnson-Kendall-Roberts model
MBI	multiple beam interferometry
MMBPD	millions of barrels per day
NBP	normal boiling point
ODE	ordinary differential equation
OF	objective function
PFT	paraffinic froth treatment
PSD	particle size distribution
RCF	relative centrifugal force
SAGD	steam-assisted gravity drainage
SANS	small-angle neutron scattering
SARA	saturates, aromatics, resins, and asphaltenes
SAXS	small-angle x-ray scattering
SFA	surface force apparatus
USAXS	ultra-small angel x-ray scattering
UV	ultraviolet
VDW	van der Waals

Chapter 1: Introduction

1.1 Background and Motivation

Crude oil is still the world's main energy source. The demand for oil was approximately 100 MMBPD in 2018 and is projected to increase by more than 16% over the next 20 years (OPEC, 2018). At the same time, the supply of conventional oil has declined over the past decade (NRC, 2018) and the industry is turning its attention to unconventional resources such as shale oil, tight gas, and oilsands as alternatives to conventional oil. Exploitation of these resources is expected to fill the gap in energy demand until renewable resources reach a mature state both technologically and economically (Ellaban *et al*., 2014; Till, 2017).

In Western Canada alone, there are approximately 165 billion barrels of recoverable oil sands bitumen, which can contribute a large portion of the forecasted demand and offer a potential opportunity for development (AER, 2019). Surface mining and *in-situ* recovery are the most common methods used to extract bitumen from oil sands. Traditional water-based extraction of bitumen from mined oil sand ore accounts for about half the production of bitumen in Alberta (AER, 2019). Thermal methods such as cyclic steam stimulation and steam-assisted gravity drainage (SAGD) account for most of the remaining production.

Bitumen is highly viscous (typically 10,000 to over 500,000 mPa·s at ambient conditions) and its viscosity must be reduced prior to pipeline transportation (Gray, 2015; Masliyah *et al.*, 2011; Zhang, 2012; Read and Whiteoak, 2003). One option to reduce its viscosity is to remove asphaltenes from the bitumen. Asphaltenes are the heaviest fraction of the bitumen and contribute most to its viscosity (Speight, 2006; Wiehe, 2008). Asphaltene precipitation can be initiated by changes in the composition, pressure, or temperature of the oil (Hirschberg *et al*., 1984; Andersen *et al*, 1998; Hammami *et al*., 2000). In deasphalting processes, asphaltenes are removed by adding a poor solvent (precipitant).

Both mining and *in situ* processes may use asphaltene rejection to facilitate the transport of oil and to provide added value to the product before reaching refineries. For example, in the paraffinic froth treatment process (PFT), a paraffinic solvent is added to the froth from the oil sands extraction process to precipitate asphaltenes (Long *et al*., 2004). The precipitated asphaltenes aggregate with the water and solids in the froth to promote settling and obtain a clean bitumen product. Recently, non-aqueous extraction of bitumen has been investigated as an alternative to aqueous extraction. In this type of process, a paraffinic solvent is added to the oil sand ore in multiple stages to precipitate asphaltenes, aggregate asphaltenes, water, and solids, and recover a partially upgraded bitumen (Hooshiar *et al*., 2012; Nikakhtari *et al*., 2013). This kind of process can produce a high-quality bitumen product that meets pipeline specifications; however, the cost associated with the recovery of large volumes of solvent compromises its transition to commercial scale (Gray, 2015; Nikakhtari *et al*., 2013).

Partial deasphalting is also an option to decrease the viscosity of bitumen from *in situ* processes prior to pipeline transport. In deasphalting processes, a paraffinic solvent is added to the bitumen to intentionally trigger asphaltene precipitation. The precipitated asphaltenes aggregate and are separated from the diluted oil by gravity settling (Gray, 2015; Northup and Sloan, 1996). The partially deasphalted bitumen product has a lower viscosity and less sulfur and metal content than the original bitumen, thus it has a higher value in the market (Gray, 2015).

All of these processes require the use of settlers to separate asphaltene aggregates. To design these operations and to size settling vessels, settling rates of asphaltene aggregates are a required input. To date, most of the data available in literature focuses on settling rates of aggregates from bitumen froth and are intended for PFT operations (Long *et al*., 2002, 2004; Zawala *et al*., 2012; Kosior *et al.*, 2018). Little information is available for settling rates of asphaltenes aggregates containing small quantities of solids and water (Rahmani *et al*., 2005a). Collecting these data and understanding the effect of different operational variables (such as solvent type and concentration, shear rate, and contact time) in the settling rates are vital to design and optimize the proposed strategies for bitumen extraction.

Settling rates depend on the size and density of the suspended aggregates and the density and viscosity of the fluid (the continuous media) (Long *et al*., 2004; Valinasab, 2006). The fluid properties can be determined experimentally or with correlations of mixtures from diluted crude oils. In contrast, the definition of size and density of the aggregates is not straightforward and different studies have used different definitions (Long *et al*., 2002, 2004; Rahmani *et al*., 2005a; Zawala *et al*., 2012; Kosior *et al.*, 2018). Asphaltene aggregates are usually viewed as irregular collections of smaller (primary) particles that are the result of a flocculation process (Rahmani *et al.*, 2005b*).* These primary particles originate from a phase transition or colloidal destabilization that occurs upon addition of solvent (Agrawal *et al*., 2012; Mullins, 2007). The kinetics of precipitation and the subsequent flocculation processes have been investigated separately for diluted bitumen mixtures but have not necessarily been considered together (Ferworn *et al*., 1993; Rastegari *et al*., 2004; Maqbool *et al*., 2009, 2011).

Settling models that account for the precipitation and flocculation kinetics are required to accurately model a settling process. In particular, it is necessary to predict the mass of precipitate, the diameter of the aggregated particles, and the aggregate porosity at the process residence time. The porosity can be used to determine the density of the aggregates if enough information about the composition of the solid matrix is known (Long *et al.*, 2004; Kosior *et al*., 2018). To date, there are no models that can simultaneously predict the mass of precipitate and the size of the asphaltene aggregates. Instead, independent models have been developed to determine the precipitation amounts or the aggregate size distributions from diluted crude oils as a function of time, type of solvent, composition, and shear rate. (Rastegari *et al*., 2004; Rahmani *et al*., 2003; Maqbool *et al*., 2011; Haji-Akbari *et al*., 2013). The main issue with these modeling approaches is that one or often more fitting parameters are required to adjust experimental data (that are laborious to obtain in the lab) and in most cases, the results cannot be translated to systems containing different crude oils, precipitants, temperatures, *etc*. Settling models based on Stokes' law have shown good results in predicting settling rates for aggregates in similar hydrocarbon systems (Long *et al*., 2004; Rahmani *et al*., 2005a); however, these models require some experimental data to set or tune their inputs.

This thesis investigates the kinetics of asphaltene precipitation and aggregation, and the settling rates of the asphaltene aggregates. Other necessary inputs for a settling model are also investigated including fluid properties and the aggregate size and density. The effect of the solvent type, solvent content, mixing rate, and contact time on the kinetics are evaluated. A mathematical model is proposed to describe the kinetics of asphaltene precipitation/aggregation from the nanometer to the micrometer scale. The results of this model are used as inputs for another model developed to predict settling rates of asphaltene aggregates.

The thesis is organized in a manuscript-based format. In each results chapter, a literature review is provided for the material relevant to that chapter. A brief overview of the literature is provided below to provide general background material and to establish an overall context for the research issues.

1.2 Literature Review

Crude oil is a complex mixture of hydrocarbons with a wide variety of chemical composition and properties. Crude oils are classified by the oil's API gravity and viscosity as conventional oils, heavy oils, and bitumens, Table 1.1 (Speight, 2006; Meyers, 2004; Gray, 1994). Crude oils must be characterized into a set of pseudo-components for phase behavior modeling and process simulation and the characterization approach depends on the type of oil. Conventional oils are typically characterized using distillation-based methods such as ASTM D86, D2892, and IP 123 (Riazi, 2005). Heavy oils and bitumens contain less volatiles than conventional oils, (as little as 25 wt% of a bitumen is distillable, Castellanos-Diaz *et al*., 2014); therefore, distillation only provides a limited characterization. Bitumens are more commonly characterized using SARA (saturates, aromatics, resins, and asphaltenes) fractionation (Fan and Buckley, 2002). This thesis focuses on the asphaltenes.

Table 1.1. UNITAR Classification of conventional crude oils, heavy oils and bitumens (Gray, 1994; Khayan, 1982).

Classification	Viscosity mPa·s	Density kg/m^3	API Gravity
Conventional oil	$<10^2$	<900	>20
Heavy oil	10^2-10^5	900-1000	10-20
Bitumen	$>10^5$	>1000	<10

Asphaltenes are a solubility class defined as the crude oil components that are insoluble in an *n*-alkane but completely soluble in aromatic solvents like benzene or toluene (Speight, 2006; Gray, 2015). They consist of thousands or perhaps millions of different molecular species (McKenna *et al.*, 2013). They are the densest, highest molecular weight, most polar oil fraction and have the largest content of heteroatoms (nitrogen, oxygen, and sulfur) and metals (such as vanadium, nickel, and chromium) in the oil (Speight, 2006; Rodgers and McKenna, 2011). Asphaltenes are known to contribute significantly to the viscosity of the oil and to its susceptibility to fouling and coke formation.

The molecular structures of asphaltenes and their state in the oil are still debated (Moir, 2018; Mullins *et al*., 2008; Arnaud, 2009). Asphaltene molecules are thought to consist of island (sometimes called continental) and/or archipelago type of structures, Figure 1.1. The island model consists of a polycyclic aromatic core with alkyl side chains located at the periphery. The archipelago model consists of several smaller polynuclear aromatic cores linked by alkyl groups and with alkyl side chains at the periphery. The continental structure is the traditional view but is inconsistent with the distribution of reaction products obtained from asphaltenes (Gray *et al*., 2011; Strausz and Lown, 2003). There is now strong evidence from high resolution mass spectrometry that both structures are present in crude oils (McKenna *et al*., 2019; Chacon- Patiño *et al*. 2017).

The aggregation tendency of asphaltenes is considered to be a consequence of the type of molecules comprising the asphaltene fraction (Mullins *et al*., 2012; McKenna *et al*., 2013). The traditional view (Dickie and Yen, 1967) considers that asphaltene aggregation results from π-π stacking between aromatic cores. This view considers that asphaltene molecules consist mainly of

island type molecules. In contrast, archipelago structures can interact through a variety of mechanisms including π-π stacking, acid-base interactions, and hydrogen bonding (Gray *et al.*, 2011). Chacon-Patiño *et al*. (2017, 2018) recently showed that stronger aggregation/adsorption forces and interfacial activity are found in asphaltene samples that contained almost exclusively archipelago structures.

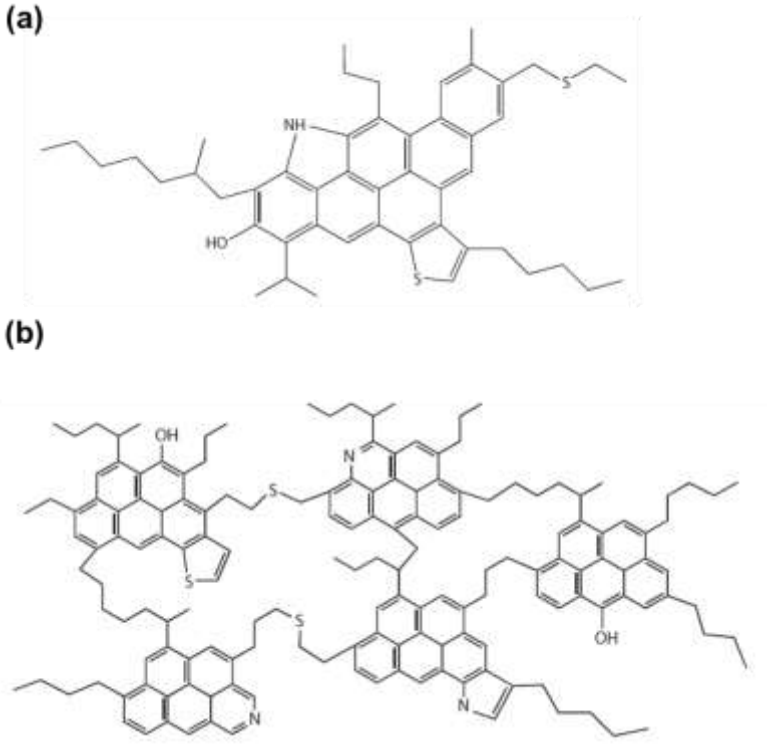

Figure 1.1. Example of proposed asphaltene molecular structures: a) island (continental) model; b) archipelago model. Image retrieved from Kelland (2014).

Whatever the mechanism, it has been established that asphaltenes self-associate and form molecular nanoaggregates in the oil that are approximately 1 to 5 nm in diameter (Hoepfner *et al*., 2013; Betancourt *et al*., 2009). It has not been resolved if asphaltene nanoaggregates are colloidal particles suspended in the oil or macromolecular assemblies in solution with the oil (Mullins, *et al* 2012; Yarranton *et al.*, 2007). This issue is important for understanding the mechanism of asphaltene precipitation. The colloidal approach suggests that asphaltene nanoaggregates are stabilized by resins, thus, active sites for asphaltene-asphaltene interaction are inaccessible

(Janardhan and Mansoori, 1993; Hoepfner and Fogler, 2013). Addition of poor solvent depletes the concentration of resins around the asphaltene assemblies and asphaltenes start to aggregate. The macromolecular approach posits that the asphaltenes are in solution with all of the other oil components and they undergo a conventional phase transition when the precipitant is added.

Asphaltene Precipitation

This thesis focuses on asphaltene precipitation caused by the addition of a poor solvent (precipitant). At ambient conditions, the asphaltenes precipitate as particles that are first detected as approximately 0.5 μm in diameter and grow over time (Agrawal *et al.*, 2012; Angle *et al*., 2006). At higher temperatures (>100ºC), asphaltenes come out of solution as liquid droplets that coalesce into a second phase (Mancilla-Polanco *et al*., 2019). Asphaltene precipitation has been shown to be reversible when the precipitant content is reduced (Beck *et al*., 2005), temperature is increased (Chaisoontornyotin *et al*., 2017), or pressure is increased (Hammami *et al*., 2000). In some cases, there is a hysteresis; for example, Beck *et al*. (2005) measured yields in a cycle of precipitant addition (asphaltene precipitation) and removal (asphaltene dissolution). They observed higher amounts of precipitate in the precipitation cycle than the dissolution cycle but found that all of the precipitate could be redissolved when more precipitant was removed. Liquid phase formation and reversibility are more consistent with the macromolecular approach.

Regardless of the mechanism, most studies on asphaltene precipitation have focused on the determination of conditions (pressure, temperature, precipitant content, and contact time) at which precipitation occurs (onset of precipitation) and the amount (yield) of asphaltenes precipitated above the onset (Mousavi-Dehghani *et al.*, 2004; Hammami *et al*., 2000; Alboudwarej *et al*., 2003; Wattana *et al*., 2003; Angle *et al*., 2006). The amount of asphaltene precipitation has been shown to increase (lower solubility) when pressure decreases (and fluid density decreases) (Hammami *et al*., 2000; Panuganti *et al*., 2012) and the precipitant content increases (Akbarzadeh *et al*., 2004; Andersen and Birdi, 1990). Asphaltene solubility increases with temperature up to about 100ºC (Andersen *et al*., 1998; Akbarzadeh *et al*., 2005). Above this temperature, asphaltene solubility decreases (Johnston *et al*., 2017). The precipitant type also has a significant effect on asphaltene solubility (Wiehe *et al*., 2005; Hu and Guo, 2005; Wiehe, 2008). For example, asphaltene yields

increase and the onset of precipitation shift to lower precipitant contents when the carbon number of the precipitant decreases from 7 to 3 and slightly decreases at higher carbon numbers. More recently, asphaltene solubility has been found to be affected by the contact time with the precipitant (Beck *et al*., 2005; Maqbool *et al.,* 2009). Asphaltene yields tend to increase with longer contact times and onsets of precipitation shifted to lower values in experiments that were conducted for several months (Maqbool *et al*., 2009; Vilas-Bôas Fávero *et al*., 2017). At high precipitant contents (>75 wt% *n*-heptane), the time dependence was brief (a few seconds to minutes) while at lower *n*-alkane contents this behavior was observed for several hundred hours.

Asphaltene precipitation is usually modeled with thermodynamic equilibrium approaches based on regular solution theory or equations of state (Akbarzadeh *et al*, 2005; Arya *et al*., 2017; Punnapala and Vargas, 2013). The models are tuned to match the available precipitation data which are usually collected after several hours of contact and assumed to be at equilibrium. However, asphaltenes yield has been found to increase over several hours to even months. Neglecting the kinetic effects may give misleading results because the data used to tune the model is not at equilibrium or because the process to be modeled has a short residence time and is not well represented with an equilibrium model. Most industrial operations have residence times that vary from seconds to few hours far less than the time required to reach equilibrium (Beck *et al*., 2005; Maqbool *et al*., 2009; Shafiee, 2014). Contact of oxygen from air has also been found to alter the kinetics of precipitation (Beck *et al*., 2005). Higher asphaltene yields have been observed in air than in nitrogen (anaerobic environment) at the same solvent content and time. Most data are collected in air and therefore may not represent an equilibrium condition.

Asphaltene Aggregates

This thesis focuses on asphaltene aggregation at ambient conditions where the asphaltenes precipitate as particles which form aggregates. At these conditions, observable asphaltene precipitation is related to asphaltene aggregation because only particles/aggregates that exceed approximately 1 μm are detected by optical methods. Even larger aggregates are required to physically separate the precipitated asphaltenes. Hence, asphaltene yields may depend on the size distribution of the aggregates.

Asphaltene aggregation have been studied for mixtures of *n*-alkanes with a variety of model oils and bitumens as a function of precipitant content, shear, and temperature (Ferworn *et al*., 1993; Rastegari *et al*., 2004; Calles *et al*. 2008; Seifried *et al*., 2013; Rahmani *et al*., 2003). The aggregates are usually examined with an optical microscope and the observed sizes range from 1 to approximately 400 μm in diameter (Ferworn *et al*., 1993; Angle *et al*., 2006). Asphaltene aggregates sizes have been observed to increase with precipitant content (Ferworn *et al*., 1993; Rastegari *et al*., 2004) and temperature (Daneshvar, 2005; Long *et al*., 2004). Aggregate sizes have been found to be 3 to 5 times larger in *n*-pentane than in *n*-heptane (Seifried *et al*., 2013; Kosior *et al*., 2018), and to increase with increased temperature between 30 to 70ºC (Daneshvar, 2005; Torkaman *et al.*, 2017). At higher temperatures (up to 100ºC) aggregate sizes decreased slightly. The effect of mixing on the aggregate sizes is less clear. While in some studies the aggregate size decreased significantly at higher shear rates (Rahmani *et al*., 2003; Shafiee, 2014; Rastegari *et al*., 2004), other authors have reported that aggregates sizes in fact increased at higher shear rates because flocculation is favored over breakage, particularly after short mixing times (Soleimani-Khormakala *et al*., 2018; Zawala *et al*., 2012). In all cases, steady sizes were reached within 1 or more hours under mixing.

The asphaltene aggregates are believed to form by a flocculation process in which primary particles interact and stick to each other to form larger structures. The primary particles are assumed to be either nano-aggregates (Torkaman *et al*., 2017; Nassar *et al*., 2015) or nucleated asphaltene phase particles with a diameter of approximately 1 μm (Rahmani *et al*., 2003; Rastegari *et al*., 2004). The aggregates are believed to be fractal structures; that is, their diameter is related to the number of primary particles in the aggregate through the fractal dimension. Most irregular shapes found in nature have been found to follow a fractal relation, including asphaltenes aggregates (Janardhan and Mansoori, 1993; Hewett, 1994; Hoepfner *et al*., 2013). Asphaltene aggregates have been identified to follow a fractal relationship at both the sub-micron and at the micrometer scale. At the nanometer scale, studies using small angle x-ray and neutron scattering (SAXS and SANS) have shown that asphaltene nanoaggregates in model oils produce emission data that is characteristic of fractal structures (Hoepfner *et al.*, 2013; Eyssautier *et al.*, 2012; Long *et al.*, 2013).

At the micrometer scale, the fractal dimension of asphaltene aggregates can be obtained using optical microscopy or from flocculation models (Rastegari *et al*., 2004; Daneshvar, 2005; Rahmani *et al*., 2005b). Flocculation models will be discussed later and give fractal dimensions of micrometer scale asphaltene aggregates in the order of 1.6 to 3 (Rastegari *et al*., Rahmani *et al.*, 2003; Shafiee, 2014). The micrographic method involves taking images of individual flocs and correlating the area (or an arbitrary length) with the perimeter of the floc (Daneshvar, 2005; Rahmani *et al*., 2005b). The method requires the collection of multiple images of different non-overlapping flocs and therefore has only been used for model oils where the concentration of aggregates is relatively low. Fractal dimensions from the micrographic method are typically lower than the obtained with flocculation models. For example, Rahmani *et al.* (2005b) obtained fractal dimensions in the rage of 1.1 to 1.5 and Daneshvar (2005) obtained a value of 1.6 using a similar micrographic method. These values correspond to branched two-dimensional structures that do not appear to correspond to the three-dimensional structures observed in the micrographs reported in the same studies.

Fractal dimensions have not been directly reported as a function of the temperature but the aggregate density (proportional to the fractal dimensions as will be discussed later) was reported to increase with temperature (up to 60ºC) for aggregates from diluted bitumen froth. To date, there are no available data for fractal dimensions or aggregate density as a function of temperature for aggregates consisting of asphaltenes alone. Shafiee (2014) reported lower fractal dimensions with increased precipitant content, however that study was made at a relatively narrow range of *n*-heptane contents (88 to 95 wt% *n*-heptane in Athabasca bitumen).

Asphaltene Aggregation Models

In classical flocculation for a well-mixed system, a dynamic equilibrium between flocculation (aggregation) and disintegration is established over time (Rahmani *et al*., 2003). A dynamic equilibrium implies that a sudden increment in shear rate would break the flocs but the flocs would be restored if the original shear conditions were reestablished. At steady state conditions, a constant average aggregate size would be observed. This type of flocculation is typically modeled

with population balance model based on Smoluchowski's early work on coagulation (Smoluchowski, 1917) and several researchers have applied this approach to asphaltene aggregation (Rahmani *et al*., 2003; Rastegari *et al*., 2004; Daneshvar, 2005; Shafiee, 2014; Nassar *et al*., 2015; Torkaman *et al*., 2017). The aggregation/disintegration rate terms are functions of the shear regime and temperature. The output of the model is the floc size distribution as a function of time. One issue with most approaches found in literature is that they require several assumptions which introduce several adjustable parameters. Hence, the models are not predictive or even easily tunable for a different system.

A population balance model predicts a distribution of aggregates in terms of the number of primary particles in the aggregate. It is necessary to translate the number of particles per aggregate into a diameter and porosity to compare with measured size distributions and for use in settling calculations. The fractal dimension of the flocs provides a mathematical relationship between the aggregate size and the number of primary particles in the aggregate. Similarly, the fractal dimension can be used to determine the porosity of the aggregate if the densities of the primary particle and fluid medium are known (Long *et al*., 2004; Kosior *et al*., 2018). The fractal dimension is commonly used as an adjustable parameter to fit the flocculation model to measured aggregate sizes (Rahmani *et al*., 2005b; Rastegari *et al*., 2004).

Asphaltene Aggregation/Precipitation Models

Most of the asphaltene flocculation models consider the time-evolution of aggregate size distributions and do not consider the relationship between aggregate size and the detected amount of asphaltene precipitation. The amount of precipitated asphaltenes is simply taken as an input based on a yield measurement at a fixed contact time or calculated from a thermodynamic equilibrium model (Rastegari *et al*., 2004; Shafiee, 2014). Maqbool *et al*. (2011) proposed a precipitation model that used a population balance to determine the aggregate size distribution over time and a Stokes' law settling equation to determine the detectable yield over time. In this case, the total concentration of "unstable" asphaltenes was an adjustable input parameter for the model rather than providing a fixed asphaltene yield measured at a given time. This approach fitted yield data over time using a single fitting parameter and predicted successfully the time of

appearance of ~0.5 μm particles (the onset detection time as it was defined). Although the proposed model is based in Smoluchowski's approach and can provide both yields and aggregate sizes over time, the model has not been shown to match both aggregate size and yields. And yet, both variables are key inputs to model settling rates.

Settling of Asphaltene Aggregates

Settling rates of asphaltene aggregates have been investigated for *n*-alkane diluted froth and model oils (Long *et al*., 2002, 2004; Long and Dabros, 2005; Zawala *et al*., 2012; Kosior *et al*., 2018; Rahmani *et al*., 2005a). Settling rates for these systems have been measured using visual methods, ultrasound, or light scattering (UV or IR) as a function of the mixture composition, temperature, solids and water content, and shear rate. Larger aggregates are obtained at higher precipitant contents and temperatures. Denser aggregates are formed with increased shear and higher solids and water contents (Long *et al*., 2004; Kosior *et al*., 2018). Since denser and larger aggregates settle faster, higher settling rates are observed at higher precipitant contents and at higher water and solids contents. These tendencies are expected to apply to asphaltene aggregates from diluted bitumen.

The settling rates of aggregates of asphaltenes, water, and solids have been fitted with models based on Stokes' law (Long *et al*., 2002; Rahmani *et al*., 2005a; Zahabi *et al*., 2010). One challenge has been the identification of the type of settling occurring at different conditions. For example, hindered settling was observed in suspensions with a high concentration of aggregates (Long *et al*., 2004). In this type of settling, rates are usually lower than predicted by Stokes' law. In contrast, highly porous aggregates had higher settling rates than expected; therefore, an aggregate permeability was introduced in the modeling approach (Rahmani *et al*., 2005a). Some studies have measured settling rates for individual aggregates rather than for the bulk suspension (Rahmani *et al*., 2005a; Zawala *et al*., 2012; Kosior *et al*., 2018). With this methodology, the size and density of aggregates can be investigated in isolation; however, it is difficult to obtain a representative set of aggregates.

Another challenge is that the density of the aggregates cannot be easily estimated because the solid matrix is not made of asphaltenes alone. The asphaltenes attach to the surfaces of mineral solids and water droplets which are then trapped within the structures of asphaltene aggregates as they form (Long *et al*., 2004; Zahabi *et al*., 2010). The average density of the aggregates can be determined from settling experiments from a settling model (Long *et al*., 2004; Rahmani *et al*., 2005a). Aggregate densities (or porosities) can also be determined from independent measurements of the volume of settled aggregates; however, once settled, the aggregates size and morphology may change (Kosior *et al*., 2018, Daneshvar, 2005).

Although the input parameters for a settling model are established, it has been difficult to independently verify the input values and the model assumptions. In addition, the settling rates of asphaltenes from diluted bitumen with little solids and water droplets has not been investigated. However, these are the conditions expected for the partial deasphalting processes and bitumen polishing stages in proposed non-aqueous extraction processes. A study on asphaltene aggregate settling also has the advantage that the aggregates consist only of asphaltenes, reducing the uncertainty of the settling model inputs and allowing a more rigorous test of any proposed settling model.

1.3 Research Objectives

The main objective of this thesis was to develop a model to predict settling rates of asphaltene aggregates from *n*-alkane diluted bitumen mixtures. Since the main unknown inputs for the settling calculation were the size and porosity (fractal dimension) of the asphaltene aggregates, a model was also developed to determine aggregate size distributions and fractal dimensions as a function of precipitant type, precipitant content, shear rate and contact time. A population balance approach was proposed that accounted for both yields and aggregate sizes over time. Hence, it is a combined model for asphaltene precipitation and aggregation. Since oxygen from air alters asphaltene precipitation, the model was adapted to include an oxidation rate term. In this way, the model can be applied to data collected in the laboratory (in air) and predict conditions in the field (anaerobic). The data required to develop the models were measured in *n*-alkane diluted bitumens at ambient conditions and include: density and viscosity, asphaltene precipitation onsets and yields in air and

in nitrogen, size distributions and fractal dimensions of asphaltene aggregates, and settling rates of asphaltene aggregates.

The specific objectives of this thesis were to:

1. measure the density and viscosity of the *n*-heptane and *n*-pentane diluted bitumens used in this study (required model inputs).
2. fit the density and viscosity data using existing mixing rules.
3. measure the effect of oxygen from air on asphaltene precipitation (yields and onsets) at ambient temperature.
4. measure the effect of precipitant content (*n*-pentane and *n*-heptane) on asphaltene aggregate sizes and fractal dimensions.
5. measure the effect of shear on the aggregate size and fractal dimension during their formation and over time.
6. evaluate the capability of the Smoluchowski population balance approach to match both yields and aggregate size distributions of precipitated asphaltenes over time, and adapt the model as required to match yield and aggregate size data.
7. adapt the population balance model developed for anaerobic conditions and use it to account for the incremental yield observed in air (from Objective 3).
8. measure the settling rates of asphaltene aggregates precipitated from *n*-pentane and *n*-heptane diluted bitumen at ambient conditions. This includes settling rate data collected in a separate study from the same research group (Casas, 2018).
9. develop and test a Stokes' Law based model to predict settling rates of asphaltene aggregates from diluted bitumens.

1.4 Brief Overview of Chapters

This thesis is divided into seven chapters that have been written to be read independently with relevant background and literature review included in each chapter. Each of the results chapters is based on a research article prepared for publication. References to the published articles are provided in a footnote in the first page of each chapter. Since this is a manuscript-based thesis, some redundancy may be found in the literature review in each chapter. To minimize repetition,

the experimental methods have been included in a separate chapter (*Chapter 2*). An overview of the following chapters is provided below.

Chapter 2 describes the materials and chemicals used to prepare diluted crude oil and bitumen samples. A description of the methodologies and apparatuses used to measure the density and viscosity of diluted crude oil and bitumen mixtures is presented. The procedures to measure yields and onsets of precipitation in air and nitrogen atmospheres are described in detail. The methodology followed to prepare asphaltene aggregates and measure aggregate size distributions and settling rates is also discussed. A new method to measure fractal dimensions of asphaltene aggregates is described.

Chapter 3 presents a study on the nature of asphaltene aggregates. The size and structure of aggregates is evaluated as a function of shear and time. The concept that asphaltenes aggregates are reversible flocs is tested and it is shown that asphaltene aggregates are instead fused structures that are insensitive to shear after they formed. Adhesion force data is analyzed and supports the hypothesis that asphaltenes lose their stickiness over time and will not further flocculate or re-flocculate after being shattered. The change in the aggregate structure at different dilutions is also investigated and the assumption that asphaltenes are fractal structures is validated. A semi-empirical correlation for the fractal dimension as a function of the concentration of destabilized asphaltenes is proposed.

Chapter 4 presents the yield and onset data collected for different crude oils diluted with *n*-heptane at 21ºC in anaerobic conditions. The data shows that both onsets and yields are time-dependent but reach constant values after tens of hours. A population balance model from literature is tested but failed in describing both yields and aggregate sizes over time. The concept of precipitation viewed as a continuous aggregation process from the nanoscale is reevaluated and replaced instead by the concept that asphaltene precipitation is a simultaneous nucleation/growth/aggregation process based on the observations presented in *Chapter 3*. The population balance model is reformulated to include the physics of these three mechanisms. Asphaltene yields and aggregate sizes are fitted with the proposed model.

Chapter 5 discusses the effect of oxygen of air in asphaltene precipitation. Kinetic data collected in air is compared to the anaerobic data of *Chapter 4*. Yields in air increased for as long as the experiments were conducted, and onsets decreased continually over time, so no apparent equilibrium conditions were reached. The potential mechanisms by which oxygen affects the asphaltene solubility or alters chemically different components of the oil are discussed. Bitumen aeration results are presented and support the idea that asphaltenes are altered by oxygen from the air. The population balance model formulated in *Chapter 4* is modified to account for the "oxidation" effect on asphaltene yields. The model is tested against data from literature.

In *Chapter 6* the data collected in previous chapters are used as inputs to test a settling model based on Stokes' law. Settling rates are presented for different diluted bitumen mixtures (from a separate investigation and from this study). The trapping of solids and water droplets into the asphaltene aggregate structures is confirmed by examining the concentration profiles during settling and zone settling is identified as the predominant settling mechanism. The magnitude of the hindered effect is assessed and is shown that is negligible for the systems considered in this study. A straightforward methodology is proposed to apply the settling model using the Sauter mean diameter as the representative size of the aggregates. The robustness of the model is tested, and it is shown that predicted settling rates have low deviations given the uncertainties on the input parameters.

Chapter 7 provides a summary of the major findings of this thesis and presents a list of suggestions for future work in this area.

1.5 Statement of Contribution

This thesis is the product of a total of four research articles. A bibliographic citation of each paper (if available at the date of preparation of this document) is provided in the first page of each chapter. Multiple authors have contributed in the preparation of the articles; however, Duran was the main author or was a major contributor for these papers. Duran's contributions include: developing the micrographic method; developing a method to calibrate the FBRM measurements;

modeling and analyzing the results for all of the chapters; measuring the majority of the data presented in the thesis (density and viscosity, aggregate sizes, fractal dimensions, and settling rates).

Some data were collected by a colleague (Casas) and some were obtained from the literature. In particular, the density and viscosity of the *n*-pentane/WC-B-A3 mixture were measured by Casas (2017). Both Casas (2017) and the author measured the aggregate size distributions of the *n*-heptane/WC-B-A3 system and the fractal dimensions from the *n*-pentane/WC-B-B2 system. Aggregate sizes and settling rates for the *n*-pentane/WC-B-A3 mixture were all measured and originally reported by Casas (2017). The aeration experiments of Section 2.9 were part of an unpublished work from the same research group and were performed by James Beck. The surface force apparatus measurements of Section 2.11 were performed at the University of Alberta in Dr. Hongbo Zeng's lab with samples provided by the author. Literature references are provided for data taken from other sources such as the density and viscosity of crude oils and solvents.

1.6 Chapter References

Akbarzadeh, K.; Alboudwarej, H.; Svrcek, W.Y.; Yarranton, H.W. (2005). A Generalized Regular Solution Model for the Prediction of Asphaltene Precipitation from *n*-Alkane Diluted Heavy Oils and Bitumens. *Fluid Phase Equilib*., 232, 159-170.

Akbarzadeh, K.; Dhillon, A.; Svreck, W.Y.; Yarranton, H.W. (2004). Methodology for the Characterization and Modeling of Asphaltene Precipitation from Heavy Oils Diluted *n*-Alkanes. *Energy Fuels,* 18, 1434-1441.

Agrawal, P.; Schoeggl, F.F.; Satyro, M.A.; Taylor, S.D.; Yarranton, H.W. (2012). Measurement and Modeling of the Phase Behavior of Solvent Diluted Bitumens. *Fluid Phase Equilib*., 334, 51–64.

Alberta Energy Regulator (AER). (2019). ST98: Alberta Energy Outlook. Alberta Energy Regulator, Calgary, AB.

Alboudwarej, H.; Akbarzadeh, K.; Beck, J.; Svrcek, W.Y.; Yarranton, H.W. (2003). Regular Solution Model for Asphaltene Precipitation from Bitumens and Solvents. *Energy Fuels,* 49 (11), 2948-2956.

Andersen, S.I.; Birdi, K.S. (1990). Influence of Temperature and Solvent on the Precipitation of Asphaltenes. *Fuel Sci. Techn. Int.,* 8, 51-74.

Andersen, S.I.; Lindeloff, N.; Stenby, E.H. (1998). Investigation of Asphaltene Precipitation at Elevated Temperature, *Petr. Sci. Technol*., 16 (3-4), 323-334.

Angle, C.W.; Long, Y.; Hamza, H.; Lue, L. (2006). Precipitation of Asphaltenes from Solvent-diluted Heavy Oil and Thermodynamic Properties of Solvent-diluted Heavy Oil Solutions. *Fuel*, 85, 492-506.

Arnaud, C.H. (2009). Digging into Asphaltenes. *Chem Eng. News,* 87 (38), 12-17. Gray, M.R.; Tykwinski, R.R.; Stryker, J.M.; Tan, X. (2011). Supramolecular Assembly Model for Aggregation of Petroleum Asphaltenes. *Energy Fuels,* 25 (7), 3125-3134.

Arya, A.; Liang, X.; Von Solms, N.; Kontogeorgis, G.M. (2017). Modeling of Asphaltene Precipitation from Crude Oil with the Cubic Plus Association Equation of State. *Energy Fuels,* 31 (2), 2063-2075.

Beck, J.; Svrcek, W.Y.; Yarranton, H.W. (2005). Hysteresis in Asphaltene Precipitation and Re-dissolution. *Energy Fuels,* 19 (3), 944-947.

Betancourt, S.S.; Ventura, G.T.; Pomerantz, A.E.; Viloria, O.; Dubost, F.X.; Zuo, J.; Monson, G.; Bustamante, D.; Purcell, J.M.; Nelson, R.K.; Rodgers, R.P.; Reddy, C.M.; Marshall, A.G.; Mullins, O.C. (2009). Nanoaggregates of Asphaltenes in a Reservoir Crude Oil and Reservoir Connectivity. *Energy Fuels*, 23 (3), 1178-1188.

Calles, J. A.; Dufour, J.; Marugán, J.; Peña, J. L.; Giménez-Aguirre, R.; Merino-García, D. (2008). Properties of Asphaltenes Precipitated with Different *n*-Alkanes. A Study to Assess the Most Representative Species for Modeling. *Energy Fuels*, 2 (22), 763-769.

Casas, Y. (2017). Settling Rate of Asphaltenes and Solids from Diluted Bitumen. MSc. Thesis. University of Calgary.

Castellanos-Diaz, O.; Sanchez-Lemus, M.C.; Schoeggl, F.F.; Satyro, M.A.; Taylor, S.D.; Yarranton, H.W. (2014). Deep-Vacuum Fractionation of Heavy Oil and Bitumen, Part I: Apparatus and Standardized Procedure. *Energy Fuels,* 28 (5), 2857-2865.

Chacon-Patiño, M.L.; Rowland, S.M.; Rodgers, R.P. (2017). Advances in Asphaltene Petroleomics. Part 1: Asphaltenes are Composed of Abundant Island and Archipelago Strctural Motifs. *Energy Fuels,* 31 (12), 13509-13518.

Chacon-Patiño, M.L; Rowland, S.M.; Rodgers, R.P. (2018). Advances in Asphaltene Petroleomics. Part 3. Dominance of Island or Archipelago Structural Motif is Sample Dependent. *Energy Fuels*, 32 (9), 9106-9120.

Chaisoontornyotin, W.; Bingham, A.W.; Hoepfner, M.P. (2017). Reversibility of Asphaltene Precipitation Using Temperature-Induced Aggregation. *Energy Fuels*, 31, 3392-3398.

Daneshvar, S. (2005). Asphaltene Flocculation in Diluted Bitumen Systems. MSc. Thesis. University of Calgary.

Dickie, J.P.; Yen, T.F. (1967). Macrostructures of Asphaltic Fractions by Various Instrumental Methods. *Anal. Chem.*, 39, 1847-1852.

Ellaban, O.; Abu-Rub, H.; Blaabjerg, F. (2014). Renewable Energy Resources: Current Status, Future Prospects and their Enabling Technology. *Renew. Sust. Energ. Rev.*, 39, 748-764.

Eyssautier, J.; Frot, D.; Barré, L. (2012). Structure and Dynamics Properties of Colloidal Asphaltene Aggregates. *Langmuir*, 28 (33), 11997-12004.

Fan, T.; Buckley, J.S. (2002). Rapid and Accurate SARA Analysis of Medium Gravity Crude Oils. *Energy Fuels*, 16, 1571-1575.

Ferworn, K.A.; Svrcek, W.Y.; Mehrotra, A.K. (1993). Measurement of Asphaltene Particle Size Distributions in Crude Oils Diluted with *n*-Heptane. *Ind. Eng. Chem. Res*., 32, 955-959.

Gray, M.R. (1994). *Upgrading Petroleum Residues and Heavy Oils*. Marcel Dekker, Inc., New York, NY.

Gray, M.R. (2015). *Upgrading Oilsands Bitumen and Heavy Oil*. First Edition. The University of Alberta Press, Edmonton, AB.

Gray, M.R.; Tykwinski, R.R.; Stryker, J.M.; Tan, X. (2011). Supramolecular Assembly Model for Aggregation of Petroleum Asphaltenes. *Energy Fuels*, 25 (7), 3125-3134.

Haji-Akbari, N.; Masirisuk, P.; Hoepfner, M.P.; Fogler, H.S. (2013). A Unified Model for Aggregation of Asphaltenes. *Energy Fuels*, 27 (5), 2497-2505.

Hammami, A.; Phelps, C.H.; Monger-McClure, T.; Little, T.M. (2000). Asphaltene Precipitation from Live Oils: An Experimental Investigation of Onset Conditions and Reversibility. *Energy Fuels*, 14(1), 14-18.

Hewett, T.A. (1994). Fractal Methods for Fracture Characterization. In *Stochastic Modeling and Geostatistics.* Yarus, J.M. and Chambers R.L. (Eds.), AAPG Publications, Tulsa, OK.

Hirschberg, A.; deJong, N.J.; Schipper, B.A.; Meijer, J.G. (1984). Influence of Temperature and Pressure on Asphaltene Flocculation. *SPE J*. (24), 283-291.

Hoepfner, M.P.; Fogler, H.S. (2013). Multiscale Scattering Investigations of Asphaltene Cluster Breakup, Nanoaggregate Dissociation, and Molecular Ordering. *Langmuir*, 29 (49), 15423-15432.

Hoepfner, M.P.; Vilas-Bôas Fávero C.; Haji-Akbari, N.; Fogler, H.S. (2013) The Fractal Aggregation of Asphaltenes. *Langmuir*, 29, 8799-8808.

Hooshiar, A.; Uhlik, P.; Ivey, D.G.; Liu, Q.; Etsell, T.H. (2012). Clay Minerals in Nonaqueous Extraction of Bitumen from Alberta Oil Sands: Part 1. Nonaqueous Extraction Procedure. *Fuel Process. Technol*., 94 (1), 80-85.

Hu, Y.-F.; Guo, T.-M. (2005). Effect of Temperature and Molecular Weight of n-Alkane Precipitants on Asphaltene Precipitation. *Fluid Phase Equilib.,* 192, 13-25.

Janardhan, A.S.; Mansoori, G.A. (1993). Fractal Nature of Asphaltene Aggregation. *J. Pet. Sci. Eng.*, 9 (1), 17-27.

Johnston, K.A.; Schoeggl, F.F.; Satyro, M.A.; Taylor, S.D.; Yarranton, H.W. (2017). Phase Behavior of Bitumen and *n*-pentane. *Fluid Phase Equil*. 442, 1-19.

Kelland, M.A. (2014). *Production Chemicals for the Oils and Gas Industry*. Second Edition. CRC Press, Boca Raton, FL.

Khayan, M. (1982). Proposed Classification and Definitions of Heavy Crude Oils and Tar Sands. In *The Future of Heavy Crude and Tar Sands*. R.F. Meyer, J.C. Wynn, and J.C. Olson (Eds.) UNITAR, New York, NY.

Kosior, D.; Ngo, E.; Xu, Y. (2018). Aggregates in Paraffinic Froth Treatment: Settling Properties and Structure. *Energy Fuels*, 32, 8268-8276.

Long, B.; Chodakowski, M.; Shaw, J.M. (2013). Impact of Liquid-Vapor to Liquid-Liquid-Vapor Phase Transitions on Asphaltene-Rich Nanoaggregate Behavior in Athabasca Vacuum Residue + Pentane Mixtures. *Energy Fuels*, 27, 1779-1790.

Long, Y.; Dabros T. (2005). Monitoring the Settling of Water-Solids-Asphaltenes Aggregates Using In-line Probe Coupled with a Near-Infrared Spectrophotometer. *Energy Fuels*. 19 (4), 1542-1547.

Long, Y.; Dabros, T.; Hamza, H. (2002). Stability and Settling Characteristics of Solvent-diluted Bitumen Emulsions. *Fuel*, 81 (15), 1945-1952.

Long, Y.; Dabros, T.; Hamza, H. (2004). Structure of Water/Solids/Asphaltenes Aggregates and Effect of Mixing Temperature on Settling Rate in Solvent-Diluted Bitumen. *Fuel*, 83 (7-8), 823-832.

Mancilla-Polanco, A.; Johnston, K.; Richardson, W.D.L.; Schoeggl, F.F.; Zhang, Y.; Yarranton, H.W.; Taylor, S.D. (2019). Phase Behavior of Heavy-Oil/Propane Mixtures. *SPE J*., 24 (2), 596-617.

Maqbool, T.; Balgoa, A.T.; Fogler, H.S. (2009). Revisiting Asphaltene Precipitation from Crude oils: A Case of Neglected Kinetic Effects. *Energy Fuels*, 23, 3681-3686.

Maqbool, T.; Raha, S.; Hoepfner, M.P.; Fogler, H.S. (2011). Modeling the Aggregation of Asphaltene Nanoaggregates in Crude Oil-precipitant Systems. *Energy Fuels*. 25(4), 1585-1596.

Masliyah, J.H.; Czarnecki, J.; Xu, Z. (2011). *Handbook of Theory and Practice of Bitumen Recovery from Athabasca Oil Sands. Volume 1: Theoretical Basis.* First Edition. Kingsley Publishing Services, Edmonton, AB.

McKenna, A.M.; Chacon-Patiño, M.L.; Weisbrod, C.R.; Blakney, G.T.; Rodgers, R.P. (2019). Molecular-Level Characterization of Asphaltenes Isolated from Distillation Cuts. *Energy Fuels,* 33 (3), 2018-2029.

McKenna, A.M.; Donald, L.J.; Fitzsimmons, J.E.; Juyal, P.; Spicer, V.; Standing, K.G.; Marshall, A.G.; Rodgers, R.P. (2013). Heavy Petroleum Composition. 3. Asphaltene Aggregation. *Energy Fuels*, 27 (3), 1246-1256.

McKenna, A.M.; Marshall, A.G.; Rodgers, R.P. (2013). Heavy Petroleum Composition. 4. Asphaltene Compositional Space. *Energy Fuels,* 27 (3), 1257-1267.

Meyers, R.A. (2004). *Handbook of Petroleum Refining Processes.* Third Edition. McGraw Hill, New York, NY.

Moir, M.E. (2018). Asphaltenes, What Art Thou?: Asphaltenes and the Boduszynski Continuum. *ACS Symp. Ser. Am. Chem. Soc.,* 1282, 3-24.

Mousavi-Dehghani, S.; Riazi, M.; Vafaie-Sefti, M.; Mansoori, G. (2004). An Analysis of Methods for Determination of Onsets of Asphaltene Phase Separations. *J. Pet. Sci. Eng*., 42, 145-156.

Mullins, O.C.; Martinez-Haya, B.; Marshall, A.G. (2008). Contrasting Perspective on Asphaltene Molecular Weight. This Comment vs the Overview of A.A. Herod, K.D. Bartle, and R. Kandiyoti. *Energy Fuels*, 22 (3), 1765-1773.

Mullins, O.C.; Sabbah, H.; Eyssautier, J.; Pomerantz, A.E.; Barre, L.; Andrews, A.B.; Ruiz-Morales, Y.; Mostowfi, F.; McFarlane, R.; Goual, L.; Lepkowicz, R.; Cooper, T.; Orbulescu, J.; Leblanc, R.M.; Edwards, J.; Zare, R.N. (2012). Advances in Asphaltene Science and the Yen-Mullins Model. *Energy Fuels*, 26 (7), 3986-4003.

Mullins, O.C.; Sheu, E.Y.; Hammami, A., Marshall, A. (Eds.). (2007). *Asphaltenes, Heavy Oils, and Petroleomics*. Springer, New York, NY.

Nassar, N.N.; Betancur, S.; Acevedo, S.; Franco, C.A.; Cortes, F.B. (2015). Development of a Population Balance Model to Describe the Influence of Shear and Nanoparticles on the Aggregation and Fragmentation of Asphaltene Aggregates. *Ind. Eng. Chem. Res.*, 54, 8201-8211.

Natural Resources Canada (NRC). (July 2018). Energy Fact Book 2018-2019. Available from: https://www.nrcan.gc.ca/energy-facts/20061.

Nikakhtari, H.; Vagi, L.; Choi, P.; Liu, Q.; Gray, M. R. (2013). Solvent Screening for Non-Aqueous Extraction of Alberta Oil Sands. *Can. J. Chem. Eng*., 91 (6), 1153–1160.

Northup, A.H.; Sloan, H.D. (1996). Advances in Solvent Deasphalting Technology. AM-96-55. NPRA Annual Meeting, San Antonio, TX.

Organization of the Petroleum Exporting Countries (OPEC). (September 2018). 2018 World Oil Outlook 2040. Available from: http://woo.opec.org.

Panuganti, S.R.; Vargas, F.M.; Gonzalez, D.L.; Kurup, A.S.; Chapman, W.G. (2012). PC-SAFT Characterization of Crude Oils and Modeling of Asphaltene Phase Behavior. *Fuel*, 93, 658-669.

Punnapala, S.; Vargas, F.M. (2013). Revisiting the PC-SAFT Characterization Procedure for an Improved Asphaltene Precipitation Prediction. *Fuel*, 108, 417-429.

Rahmani, N.; Dabros, T.; Masliyah, J.H. (2005a). Settling Properties of Asphaltene Aggregates. *Energy Fuels*, 19 (3), 1099-1108.

Rahmani, N.; Dabros, T.; Masliyah, J.H. (2005b). Fractal Structure of Asphaltene Aggregates. *J. Colloid Interface Sci*., 285 (2), 599-608.

Rahmani, H.; Masliyah, J.H.; Dabros, T. (2003). Characterization of Asphaltene Aggregation and Fragmentation in a Shear Field. *AIChE J.*, 49 (7), 1645-1655.

Rastegari, K.; Svrcek, W.Y.; Yarranton, H.W. (2004). Kinetics of Asphaltene Flocculation. *Ind. Eng. Chem. Res*., 43, 6861-6870.

Read, J.; Whiteoak, D. (2003). Shell Bitumen Handbook. 5th edition. In *4.5. Bitumen Quality*. ICE Publishing, London, UK.

Riazi, M.R. (2005). *Characterization and Properties of Petroleum Fractions*. First Edition. ASTM International, Baltimore, MD.

Rodgers, R.P.; McKenna, A.M. (2011). Petroleum Analysis. *Anal. Chem*., 83, 4665-4687.

Seifried, C. M.; Crawshaw, J.; Boek, E.S. (2013). Kinetics of Asphaltene Aggregation in Crude Oil Studied by Confocal Laser-Scanning Microscopy. *Energy Fuels*, 27 (4), 1865-1872.

Shafiee, M. Kinetics of Asphaltene Precipitation and Flocculation from Diluted Bitumen. (2014). MSc. Thesis. University of Calgary.

Smoluchowski, M. (1917). Versuch Einer Mathematischen Theorie der Koagulations Kinetis Kolloider Losungen. *Z. Physik. Chem*., 92, 129-168.

Soleimani-Khormakala, H.; Torkaman, M.; Bahrami, M. (2018). The Effect of Shear Rate on Aggregation and Fragmentation of Asphaltene Aggregates. *J. Dispension Sci. Technol.*, 40 (6), 836-845.

Speight, J.G. (2006). *The Chemistry and Technology of Petroleum*. Fourth Edition. CRC Press, Boca Raton, FL.

Strausz, O.P.; Lown, E,.M. (2003). *The Chemistry of Alberta Oil Sands, Bitumens, and Heavy Oils.* Alberta Energy Research Institute (AERI), Calgary, AB.

Till, A. (2017). Measuring Technology Maturity: Theoretical Aspects. In *Measuring Technology Maturity: Operationalizing information from Patents, Scientific Publications, and the Web* (pp. 35-85). Berlin, Springer Gabler.

Torkaman, M.; Bahrami, M.; Dehghani, M. (2017). Influence of Temperature and Stability of Asphaltenes. I. Perikinetic Aggregation. *Energy Fuels*, 31, 11169-11180.

Valinasab, M. (2006). The Effect of Bitumen Extraction Conditions on Froth Treatment Effectiveness. MSc. Thesis, University of Calgary.

Vilas-Bôas Fávero, C.; Maqbool, T.; Hoepfner, M.; Haji-Akbari, N.; Fogler, H.S. (2017). Revisiting the Flocculation Kinetics of Destabilized Asphaltenes. *Adv. Colloid Interface Sci.*, 244, 267-280.

Wattana, P.; Wojciechowski, D.J.; Bolanos, G.; Fogler, H.S. (2003). Study of Asphaltene Precipitation Using Refractive Index Measurement. *Petr. Sci. Technol*., 21 (3-4), 591-613.

Wiehe, I.A. (2008). *Process Chemistry of Petroleum Macromolecules*, CRC Press, Boca Raton, FL.

Wiehe, I.A.; Yarranton, H.W.; Akbarzadeh, K.; Rahimi, P.M.; Teclemariam, A. (2005). The Paradox of Asphaltene Precipitation with Normal Paraffins. *Energy Fuels*, 19, 1261-1267.

Yarranton, H.W.; Fox, W.A.; Svrcek, W.Y. (2007). Effect of Resins on Asphaltene Self-association and Solubility. *Can. J. Chem. Eng.*, 85 (5), 635-642.

Zahabi, A.; Gray, M.R.; Czarnecki, J.; Dabros, T. (2010). Flocculation of Silica Particles from a Model Oil Solution: Effect of Adsorbed Asphaltenes. *Energy Fuels*, 24 (6), 3616-3623.

Zawala, J.; Dabros, T.; Hamza, H.A. (2012). Settling Properties of Aggregates in Paraffinic Froth Treatment. *Energy Fuels*, 26, 5775-5781.

Zhang, M. (2012). Role of Bitumen Viscosity in Bitumen Recovery from Athabasca Oil Sands. MSc. Thesis. University of Alberta.

Chapter 2: Experimental Methods

This chapter presents a description of the experimental methods used in this thesis. A list of chemicals and crude oil and bitumen samples is provided and their properties are reported. The apparatus and methodology used to measure density and viscosity of the samples and of the diluted mixtures are explained. The preparation of suspensions of asphaltene aggregates and the methods used to measure the aggregate size distributions are discussed. The development of a method to measure fractal dimensions of aggregates based on the sediment volumes is described. The procedure used to measure yields and onsets of precipitation in air and nitrogen atmospheres is explained. The method used to aerate bitumen samples at different temperatures is presented. The methods used to measure settling rates are described in detail. Finally, adhesion tests of asphaltene samples studied here were performed elsewhere but the method is summarized here.

2.1 Crude Oils Samples and Chemicals

The oils used in this thesis are listed in Table 2.1. The samples are labeled as follows: "WC" indicates Western Canada, "B" indicates bitumen, "A3" and "B2" denote the source reservoirs, and the number in brackets is the sample number. The four Western Canadian bitumen samples (WC-B-B2, WC-B-A3, WC-B-A0, and WC-B-B2(1)) each came from a steam-assisted gravity drainage (SAGD) process. These samples were supplied by Shell Canada Ltd. (WC-B-B2 and WC-B-B2(1)), Japan Canada Oil Sands (WC-B-A3), and Syncrude Canada Ltd. (WC-B-A0). Samples WC-B-B2 and WC-B-B2(1) have the same origin but WC-B-B2 was from the top of the sample pail and had a relatively low water and solids content. WC-B-B2(1) was from the bottom 20% of the same sample pail and had a higher water and solids content than the other samples, probably because some settling occurred during storage. Three additional oils, one bitumen (MX-B-A1), one heavy oil (EU-HO-A1), and one light oil (MSB), were provided by Schlumberger Ltd. Technical grade toluene (99.5% purity), *n*-pentane (>98%) and *n*-heptane (>99%) were obtained from VWR International LLC. Nitrogen and air were 99.99% pure and were purchased from Praxair Canada Inc.

The oil samples received from Schlumberger and Syncrude had been processed prior to receipt to remove water and solids. The WC-B-B2 and WC-B-A3 bitumens initially contained a significant amount of water. For these samples, the free water was decanted and the remaining bitumen/water was distilled at 110ºC. After distillation, the samples were passed through a 5 µm Sterlitech silver membrane filter and then through a 2.5 µm filter to remove mineral solids. Details of this procedure are reported elsewhere (Ramos-Pallares, 2017). Karl Fischer titration was used to measure the residual water content for all samples and it was less than 0.8 wt% in all cases, Table 2.1.

Samples WC-B-B2 and WC-B-A3 were used for most experiments of this thesis (aggregation and precipitation kinetics), while sample WC-B-B2(1) was used only in the settling experiments. The WC-B-A0 bitumen was used only in the aeration experiments in Chapter 5. The MX-B-A1, EU-HO-A1, and MSB oils were used in the determination of the kinetics of asphaltene precipitation/aggregation (Chapters 4 and 5).

Table 2.1. Properties of the crude oils and bitumens used in this work (at 20ºC).

Sample	Density kg/m^3	Viscosity[a] mPa·s	Water wt %	TI[d] wt%	C7-Asph. wt%	C5-Asph. wt%
WC-B-B2	1153.5	437,000	0.71	0.69	17.3	19.4
WC-B-A3	1008.8 [b]	153,000 [b]	0.79	0.16	12.0	14.5
MX-B-A1	1006.5	831,600	0.64	0.18	22.0	24.2
EU-HO-A1	962.1	5,036	0.15	0.09	2.7	6.5
MSB	872.3	18.1	0.08	0.02	0.7	3.6
WC-B-B2(1)	1013.9	89,200	4.90	0.16	17.3	19.4
WC-B-A0[c]	1014.0	33,737	0.10	0.80	12.7	14.6

a) Ramos-Pallares *et al.* (2016); b) Marquez (2019); c) Peramanu *et al.* (2001); d) TI = toluene insoluble.

The asphaltene content of the samples (both *n*-pentane insoluble C5-asphaltenes and *n*-heptane insoluble C7-asphaltenes) was determined gravimetrically following the method described by Alboudwarej *et al.* (2002) and are provided in Table 2.1. The densities and viscosities of the oils in Table 2.1 were measured previously and reported elsewhere (Ramos-Pallares *et al.*, 2016;

Marquez, 2019; Peramanu *et al*., 2001). Asphaltene and solids composition of the WC-B-A0 sample were originally reported by Alboudwarej *et al.* (2003).

2.2 Density and Viscosity of Mixtures

Densities of the WC-B-A3 and WC-B-B2 bitumens were measured elsewhere (Marquez, 2019; Ramos-Pallares *et al*., 2016). Densities of the WC-B-B2(1) bitumen and for mixtures of each crude oil from Table 2.1 with *n*-heptane and *n*-pentane were measured in this study at 21°C and atmospheric pressure using an Anton Paar DMA 4500M density meter. The procedure for the density measurements is reported elsewhere (Ramos-Pallares *et al*., 2016) and summarized below. The instrument precision was ±0.01 kg/m^3 and the repeatability of the measurements was ±0.05 kg/m^3.

To measure the density of the mixtures, samples of *n*-heptane or *n*-pentane diluted oil were prepared in the range of 20 to 90 wt% *n*-alkane. Below the onset the density of the whole mixture was measured. Above the onset, the density of the precipitate-free fluid was measured. A known mass of bitumen or crude oil was placed in a 30 mL glass tube and *n*-alkane was added dropwise until the desired concentration was achieved. For bitumen samples, the mixture was stirred first manually with a spatula and later, when the viscosity was sufficiently low, with a magnetic bar. For lighter oils, only magnetic agitation was used. Once the *n*-alkane addition was completed, the tube was sealed and sonicated for 1 h. The samples were left to settle for 24 h after the addition of *n*-alkane. Then, a sample of the supernatant was taken with a syringe and transferred to the density meter to make the measurement. At *n*-alkane contents above approximately 45 wt% with *n*-pentane and 50 wt% with *n*-heptane, some asphaltenes had precipitated and were not included in the sample.

Ramos-Pallares *et al*. (2016) collected data for diluted bitumen viscosities with different solvents below the onset of precipitation. The viscosities were measured using an Anton Paar Model MCR-52 cone-and-plate rheometer equipped with a temperature controller. Details of the procedure are provided elsewhere (Ramos-Pallares *et al*., 2016). The repeatability on the viscosities was ± 5%.

2.3 Preparation of Asphaltene Aggregates

To prepare suspensions of asphaltene aggregates in mixtures of bitumen and *n*-heptane or *n*-pentane, the bitumen and the precipitant were mixed in two stages, pre-dilution and precipitation. The pre-dilution step consisted on adding enough precipitant to lower the viscosity of the bitumen and obtain a homogeneous mixture without triggering asphaltene precipitation. To avoid asphaltene precipitation in the pre-dilution stage, the target precipitant content was kept below the onset of precipitation (about 45 wt% *n*-heptane or *n*-pentane). At this point the viscosity of the mixture was sufficiently low to allow for rapid and homogeneous mixing in the precipitation stage. In the precipitation stage, enough *n*-heptane or *n*-pentane was added to initiate asphaltene precipitation and permit the formation of aggregates at the targeted mixture composition.

The suspensions were prepared in a 500 mL glass beaker equipped with a four-angle blade impeller with 50 mm diameter. A known mass of bitumen was placed in the beaker and precipitant was added at approximately 1 mL/minute while stirring manually with a spatula. At 45 wt% precipitant, the mixture was sonicated for 50 minutes. To compensate for precipitant evaporation, more *n*-heptane or *n*-pentane was added to maintain a constant mass (about 1 mL per hour). At this point, a few droplets were taken from the beaker and observed in the microscope to confirm that no asphaltene precipitation had occurred. Next, the mixer was turned on at the specified mixing rate, the mass of precipitant to precipitate asphaltenes was added to reach the final content, and the measurement of aggregate size distribution was started.

After the pre-dilution stage, the FBRM probe (of Section 2.4) and the impeller were placed in the beaker containing the pre-diluted bitumen. The mixer was turned on at the specified rotational speed (195, 275 or 330 rpm) and the remaining mass of *n*-alkane was added to achieve the final poor solvent content. The total volume of mixture in the beaker was set at 200 mL in all cases. The second stage of *n*-heptane or *n*-pentane was added in less than 10 seconds using a separatory funnel. Then, the FBRM apparatus was turned on and the size distribution measurements taken. To measure aggregate size distributions of asphaltene aggregates from the MX-B-A1 bitumen, EU-HO-A1, and MSB oil, suspensions were prepared with the same procedure but the FBRM probe was not immersed in the fluid, because these samples were investigated with the

micrographic method described in Section 2.4.1. For these samples, the impeller speed was set always at 195 rpm.

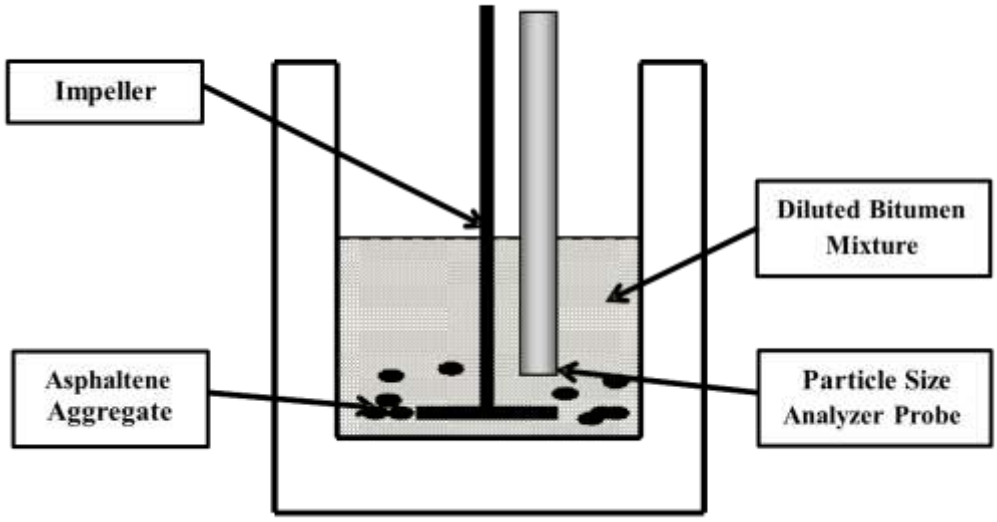

Figure 2.1. Schematic of the setup used to measure aggregate size distributions using the FBRM method.

2.4 Aggregate Size Measurements

Two methods were used to measure the size distributions of suspended asphaltene aggregates: the micrographic method (optical microscopy) and the Focused Beam Reflectance Measurement (FBRM) method. Both methods were required to examine the full range of precipitant contents above the onset of precipitation.

The FBRM method is a rapid, non-intrusive technique that measures the aggregate sizes *in-situ*. However, the FBRM measures chord length distributions that must be calibrated to an independent measurement to obtain particle size distributions (Allen, 2003). The FBRM also cannot distinguish between particles and aggregates, and can count overlapping particles as a single larger particle. The micrographic method can be accurate when a large number of aggregates are measured; however, it is an intrusive measurement and the sample could be altered during the analysis. It can also be challenging to obtain a representative sample and the image processing is laborious. The

FBRM method was suitable for relatively high dilutions (> 60 wt% *n*-heptane or *n*-pentane). The microscopic method was used to calibrate the FBRM and to measure the aggregate size distributions at conditions near the onset of precipitation where the concentration of asphaltenes aggregates was too low for an accurate FBRM measurement.

Micrographic Method

A Carl Zeiss Axiovert S100 optical microscope equipped with an Axiocam video camera was used to capture asphaltene aggregate images. For each image, a sample was collected using a pipette from the beaker containing the asphaltene suspension (see Section 2.3). Two droplets of the sample were placed on a microscope glass slide with coverslip and several images were taken. Preliminary tests with multiple samples indicated that at least sixteen images per sample with each image having no less than 15 particle measurements were enough to obtain a repeatable distribution (a total of 240 particles). Each image was processed using ImageJ software and its distribution was calculated from the maximum diameters of 250 to 3000 aggregates. Note, the *maximum diameters* of the aggregates were measured because it is a consistent measurement and corresponds to the porosity and density methodology presented in Section 3.1.2.

The aggregates were counted at two magnifications: aggregates smaller than 40 μm were measured using 16 images at 40x magnification and aggregates larger than 40 μm were measured using one image at 10x magnification. Since the areas of each magnification were matched, the distributions at 10x and 40x magnifications were simply added together to obtain an average distribution. The repeatability of the volume moment mean diameter with this method was ± 9.5 μm for *n*-heptane diluted systems and ± 12.9 μm for the *n*-pentane dilute bitumen based on six repeats and a 90% confidence interval.

Focused Beam Reflectance Method

A Lasentec Model D600 Particle Size Analyzer was used to measure asphaltene aggregate distributions with the FBRM technique. The apparatus is equipped with stainless steel probe that encases a laser beam (wavelength 780 nm) that rotates in a circular path at 4500 rpm (2 m/s). The probe is immersed in a beaker equipped with a four-angle blade impeller that contains the liquid

suspension. Chord lengths are measured when the beam intersects a particle from edge to edge and scattered light is reflected back to a photodetector. The photodetector in the probe generates a pulse that represents the two points at the edge of the particle. Since the laser velocity and the pulse time are known, a chord length is calculated for each particle/aggregate detected (Clain *et al*., 2015; Xu, 2000).

The primary chord length distribution is constructed from the chord length measurements of hundreds of particles. The size range is divided into Cartesian or logarithmic intervals (bins) and the number count for each bin is reported. The number count is the number of particles intersected by the laser in its circular path over 1 second. This value does not represent the real concentration of particles in the mixture, but can be used as a qualitative indicator (Greaves *et al.*, 2008). Number or volume weighted frequency distributions are calculated from the bin counts. The experiments were carried out with measuring time intervals of 30 seconds to obtain sufficient counts per interval and avoid noise in the distribution. The coarse electronics setting was used in this study since it provides higher resolution for aggregated particles and aggregates (Lasentec, 2002).

The experimental chord length volume frequency distributions were calibrated to match volume moment frequencies from the microscopic method using a weighting factor given by:

$$w_i = \frac{d_i^m}{\sum_{i=1}^{N} d_i^m} N \tag{2.1}$$

where w_i is the weighting factor of particle size i, N is the number of discrete bin sizes in the distribution, and m is an exponent tuned for the calibration. The calibrated frequencies are then given by:

$$F_i = w_i \frac{n_i}{n_T} \tag{2.2}$$

where F_i is the volume moment frequency and n_T is the total particle counts per measurement (summation over all the bin sizes). A calibration exponent of zero (no calibration) was found to best match the microscopic method distributions. In other words, the chord length distributions from the FBRM measurements were equivalent to number frequency distributions from the micrographic method. A complete description of the calibration procedure and results is provided in Appendix A.

For convenience, most of the results of this thesis are presented in terms of an average diameter rather than a distribution. The volume moment mean diameter (henceforth termed the volume mean diameter) was used in the aggregation studies (Chapters 3 and 4) since it is proportional to the average mass of the aggregates. The volume mean diameter was calculated from each volumetric distribution (F_i) as follows:

$$d_{4,3} = \sum_i F_i d_i = \frac{\sum f_i d_i^4}{\sum f_i d_i^3} \tag{2.3}$$

where $d_{4,3}$ is the volume mean diameter. This average diameter can also be calculated from the number frequencies (f_i). The volume mean diameters were repeatable to ± 6.4% based on a 90% confidence interval. For the MSB oil, the repeatability of the volume mean diameter from the micrographic method was ± 3.2 µm. The volume mean diameters from the FBRM method were repeatable to ± 6.4 µm for *n*-heptane diluted systems and ± 12.9 µm for the *n*-pentane diluted WC-B-A3 bitumen, based on a 90% confidence interval in both cases. Other definitions of the average diameter of a particle size distribution can be defined for different applications and are discussed in the following section.

Representation of Average Size

All of the measured volume frequency distributions obtained from the FBRM and micrographic methods were approximately log-normal. Hence, the changes in the distribution can be tracked using a mean diameter. To simplify the presentation of the results, only the mean diameter of the aggregates is reported. The volume moment mean diameter was selected for the studies of asphaltene aggregation because it provides an estimate of the center of mass of the particle distribution. However other definitions of average diameter can be used and are particularly important in the settling study of Chapter 6. The different definitions of mean diameter that are used in Chapter 6 are provided in Table 2.2. The use of the mean diameters in the settling calculation will be discussed later.

Table 2.2. Different definitions of "average" particle size of the asphaltene aggregate distribution used in this work.

Name	Mathematical Form	Notes
Number Mean Diameter	$d_1 = \sum_{i=1}^{N} f_i d_i$	Simple arithmetic mean.
Area Mean Diameter	$d_2 = \left[\sum_{i=1}^{N} f_i d_i^2\right]^{1/2}$	Approximates diameter with mean surface area.
Volume Mean Diameter	$d_3 = \left[\sum_{i=1}^{N} f_i d_i^3\right]^{1/3}$	Approximates diameter with mean particle volume.
Volume/Area Mean Diameter (Sauter Diameter)	$d_{32} = \frac{\sum_{i=1}^{N} f_i d_i^3}{\sum_{i=1}^{N} f_i d_i^2}$	Ratio *V/A* of the particle population.
Volume Moment Mean Diameter	$d_{43} = \frac{\sum_{i=1}^{N} f_i d_i^4}{\sum_{i=1}^{N} f_i d_i^3}$	Mean density (mass) of distribution of particles.

2.5 Fractal Dimension from Sediment Volumes

The sediment volume method was proposed to determine the fractal dimension of asphaltene aggregates (D_f) based on the volume occupied by their settled sediment, as illustrated in Figure 2.2. The method is derived from the total volume occupied by non-overlapping spherical aggregates with a polydisperse size distribution, given by,

$$V_{total} = N_f \frac{\pi}{6} \sum_{i=1}^{N} f_i d_i^3 \tag{2.4}$$

where N_f is the total number of aggregates, f_i the number frequency of the *i-th* bin size, and d_i is the bin diameter. The total number of aggregates is determined from the mass of precipitate as follows,

$$N_f = \frac{m_A}{\sum_{i=1}^{N} f_i m_i} \tag{2.5}$$

where m_A is the mass of precipitate and m_i is the mass of the i^{th} aggregate. The mass of the i^{th} aggregate is given by,

$$m_i = \frac{\pi}{6} n_p d_p^3 \rho_A \tag{2.6}$$

where d_p is the diameter of the primary unit and ρ_A is the asphaltene density of 1200 kg/m^3 (Yarranton and Masliyah, 1996). Initially, the primary units were defined as the asphaltene nano-aggregates with an assumed diameter of 2.5 nm (Mostowfi *et al.*, 2009; Maqbool *et al*., 2011). In Chapter 4, the primary particle diameter is calculated from a growth model and is different for each system. Calculated primary particles were in the order of 200 to 1500 nm (see Section 4.3.4). The number of primary particles in the aggregate is related to the aggregate diameter through the fractal dimension as follows (Rahmani *et al.*, 2005),

$$n_p = \left(\frac{d_{agg}}{d_p}\right)^{D_f} \tag{2.7}$$

Equation 2.7 is substituted into Eq. 2.6 to obtain the following expression,

$$m_i = \frac{\pi}{6} \rho_A d_p^3 \left(\frac{d_i}{d_p}\right)^{D_f} \tag{2.8}$$

Finally, Equations 2.4, 2.5, and 2.8 are combined to obtain the volume of sediment, V_{sed}, given by,

$$V_{sed} = \frac{m_A \sum_{i=1}^{N} f_i \left(\frac{d_i}{d_p}\right)^3}{\rho_A \sum_{i=1}^{N} f_i \left(\frac{d_i}{d_p}\right)^{D_f}} \tag{2.9}$$

The sediment volume, mass of precipitate, and the aggregate size distribution are directly measured. The only unknown is the fractal dimension and it is calculated iteratively to match the measured sediment volume.

To measure the sediment volume, the diluted bitumen mixture prepared for the aggregation experiments was poured into a 250 mL graduated cylinder with an inside diameter of 3.5 cm. The asphaltene aggregates started to settle immediately and the interface position was visually tracked over time when possible. A flashlight with an incandescent bulb was focused on the interface with a magnifying glass to improve the visibility of the settling material. Settling curves were prepared by plotting the position of the interface versus time. The initial "uncompacted" sediment volume was defined as the point where there was a substantial change on the settling curve; that is, the end of the free settling stage. The final "compacted" volume was measured at 24 hours in all cases. The repeatability of the uncompacted and compacted sediment volumes were ± 4 and ± 1 mL, respectively, based on 4 repeats and 90% confidence interval.

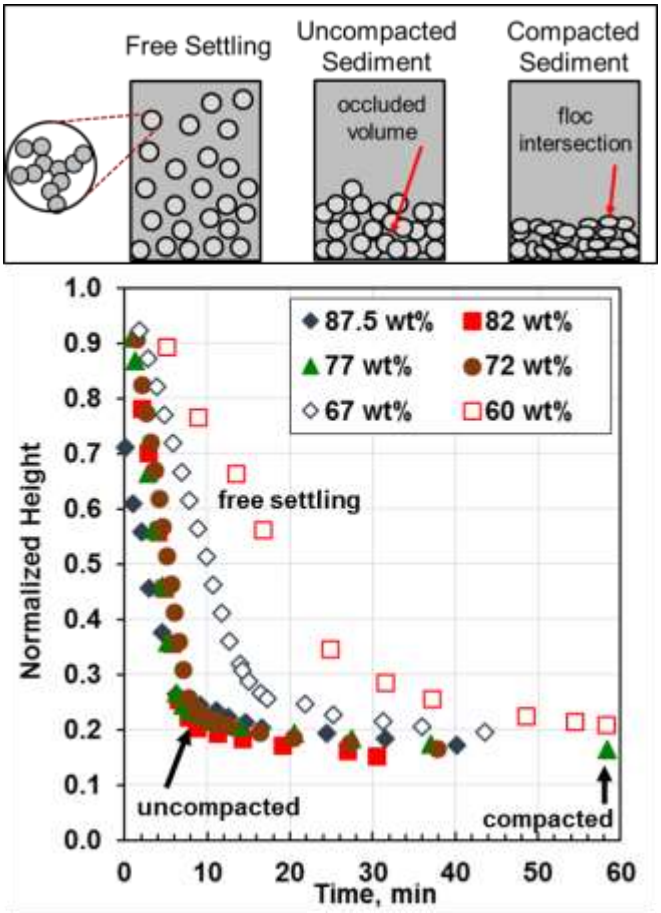

Figure 2.2. Settling of asphaltene aggregates in *n*-heptane diluted WC-B-B2 bitumen at 21ºC and identification of the three stages of the process: free settling, formation of the final sediment layer, and sediment compaction. Normalized height is the measured height of interface divided by the initial liquid height.

To apply Equation 2.9, the mass of precipitate was measured gravimetrically after each experiment and the aggregate size distribution taken as the last FBRM measurement before the start of the settling experiment. It was assumed that aggregates size distributions did not change significantly when the suspension was poured in a graduated cylinder. This assumption is expected to be valid because, as will be shown in Chapter 3, the aggregates appear to be fused structures that are unaffected by the low shear rates encountered when pouring.

The fractal dimension was calculated from both the uncompacted and the final compacted sediment volumes. At the uncompacted condition, the aggregates are less likely to have deformed during the settling process but there may be a significant volume of occluded fluid trapped between them. Therefore, the volume may be too large, and the calculated fractal dimension would be too small (smaller fractal dimensions correspond to more porous structures with larger volumes). At the compacted conditions, the sediment has less occluded volume but the aggregates may have collapsed under the weight of the sediment and deformed compared to the original shape and size. Therefore, the volume may be too small and the calculated fractal dimension would be too large. Hence this method cannot establish an exact fractal dimension but provides a range for the fractal dimension. The repeatability of the compacted and uncompacted fractal dimensions is ±0.08 in both cases.

2.6 Determination of the Onset of Precipitation

The aggregation and settling experiments must be performed at precipitant contents above the onset of precipitation. In Chapter 1, the onset of precipitation was defined as the lowest precipitant content at which asphaltene precipitation is first observed after a fixed contact time. For aggregation experiments this time was 24 hours. In contrast, the onset of precipitation for settling experiments was defined to 1.5 hours, because this is the average time to complete one of these experiments. A gravimetric method and a micrographic method were used to determine the onsets. Both methods are outlined below.

Gravimetric Method

The onset was determined from a series of asphaltene yield measurements in *n*-heptane or *n*-pentane diluted crude oil after a given contact time with the precipitant. The measurement of asphaltene yields is described in Section 2.8.

Yields were measured for a series of samples prepared with *n*-heptane or *n*-pentane contents ranging from 20 wt% to 95 wt% and left to equilibrate by the same contact time. The onset at each contact time for each crude oil or bitumen was determined by extrapolating the yield data to zero

yield as shown in Figure 2.3. Based on the scatter in the yield data, the precision of the extrapolated yields was ± 1 wt% solvent.

Micrographic Method

The onset of asphaltene precipitation was also determined from micrographs taken for a series of diluted crude oil or bitumen samples with different precipitant contents each at a specified contact time. The samples were prepared with the same procedure as used for the gravimetric measurements. For the crude oils containing a small amount (< 0.02 wt%) of inorganic solids (MSB and EU-HO-A1), a few drops of each mixture were placed on glass slides covered with a coverslip and a micrograph was prepared. A Carl Zeiss Axiovert S100 optical microscope equipped with and Axiocam video camera was used to capture images and Axiovision and ImageJ were used for image analysis. The onset of asphaltene precipitation at each contact time was determined as the lowest mass percent of *n*-heptane or *n*-pentane at which precipitated asphaltene particles were observed. The resolution limit of the microscope is approximately 0.5 µm.

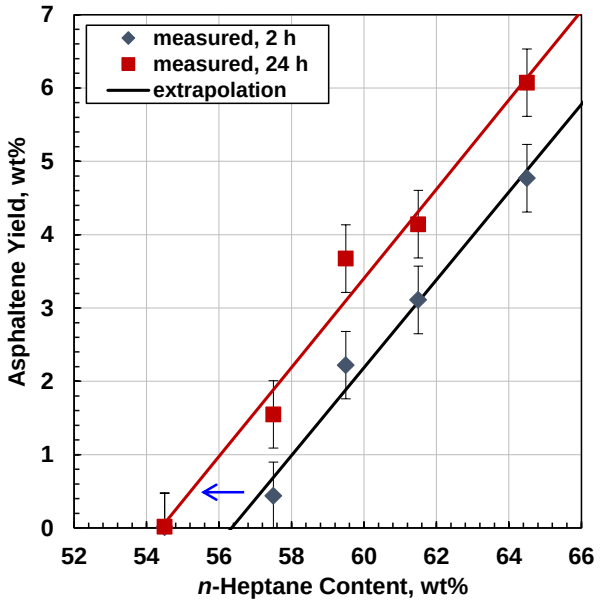

Figure 2.3. Gravimetric determination of the onset of asphaltene precipitation from *n*-heptane diluted WC-B-A3 bitumen at 2 and 24 h contact time by extrapolation of data to zero yield. The onsets at 2 and 24 h were 56.3 ± 1 and 54.4 ± 1 wt% *n*-heptane, respectively. Yields are reported on a TI-free basis.

For the crude oils containing inorganic solids (MX-B-A1 and 'WC' bitumens), the solids can obscure the detection of precipitation near the onset. Therefore, these bitumen samples were filtered beforehand using Sterlitech silver membranes to remove fine solids and water. The samples were first passed through a 5 µm filter and then through a 2.5 µm filter. Then, the filtered samples were diluted with the desired mass ratio of *n*-heptane or *n*-pentane as described above, and then observed in the microscope.

Micrographs were prepared near the expected onset at each contact time (between 1 minute and 250 hours) at intervals of 0.5 wt% *n*-heptane or *n*-pentane. The precipitant content ranged from 5 wt% below to 5 wt% above the gravimetric onset concentration determined beforehand. The lower boundary of the reported onset is the precipitant content of the micrograph with the highest precipitant content and no observable precipitate particles (0.5 µm particles). The upper boundary is the precipitant content of the micrograph with the lowest precipitant content and observable precipitate. The onset of precipitation at that contact time is taken as the midpoint precipitant content (*n*-heptane or *n*-pentane) with a precision of half the interval between the precipitant contents of the two micrographs (± 0.3 wt%).

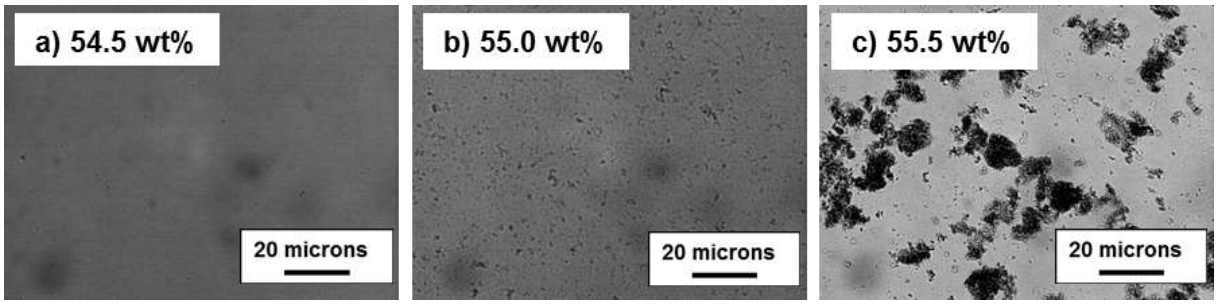

Figure 2.4. Micrographs showing the onset of asphaltene precipitation from *n*-heptane diluted WC-B-A3 bitumen at a) 54.5 wt%, b) 55.0 wt%, and c) 55.5 wt% *n*-heptane at 21ºC and 24 hours contact time.

Results from both methods were consistent within the experimental error of each method. To illustrate this point, Figure 2.4 shows a series of images for the *n*-heptane diluted WC-B-A3 bitumen at 24 hours of contact. No particles were detected below 54.5 wt% *n*-heptane, a small number of particles appear at 55.0 wt% *n*-heptane, and a large number of particles are observed at 55.5 wt% *n*-heptane. Hence, the onset is 55.0 ±0.5 wt%. The micrographic onsets of precipitation at 24 hours contact are compared with the gravimetric onsets in Table 2.3. The onsets from both methods agree within the experimental error.

Table 2.3. Comparison of onsets of precipitation obtained from the two methods used in this thesis. Validation was made for *n*-heptane diluted WC-B-A3 and WC-B-B2 bitumens at 24 hours of contact time.

Sample	Gravimetric Method wt% *n*-Heptane	Micrographic Method wt% *n*-Heptane
WC-B-A3	54.4 ±1	55.0 ±0.5
WC-B-B2	48.5 ±1	48.0 ±0.5

2.7 Sample Pretreatment for Yield Measurements

Asphaltene precipitation yields tend to increase in the presence of oxygen in the samples (Beck *et al*., 2005) and therefore oxygen-free oil samples and precipitants were used in the measurement of yields unless otherwise indicated. For the MX-B-A1, MSB, and EU-HO-A1 crude oils, approximately 300 g of sample were placed in a 500 mL Buchner flask and immersed in water bath at 21 or 50ºC. Then, the flask was connected to a nitrogen supply inlet with the outlet open to the atmosphere. Nitrogen was bubbled through each oil for 24 hours. After removal from the water bath, the crude oil samples were used immediately. Since the crude oils may contain volatile components that were lost during the bubbling, the mass of the oils was measured before and after treatment to determine losses. The MX-B-A1 and EU-HO-A1 were treated at 50°C and the losses were less than 1.6 wt%. The MSB oil was treated at 21ºC and the loss was less than 0.8 wt%. The bubbling time was modified slightly for each run as required to ensure that the mass of volatile losses per mass of oil were the same for each sample; in other words, to ensure that all the final samples were the same. The compositions reported in Table 2.1 were obtained after treating the samples with nitrogen, but the viscosity and density were obtained using untreated samples.

Bitumen samples were treated in a slightly different way because the high viscosity of the sample prevented effective degassing. A sample of 500 g of bitumen was placed in flask and kept in a Thermo Scientific Labline vacuum oven at 70ºC for three days. Then, the flask was placed in a water bath at 50ºC, and nitrogen was bubbled for 5 days. A vacuum line was connected at the outlet to enhance flow. After the removal from the water bath, the bitumen was continuously purged with nitrogen for another two days. Note, any potential evaporation of light components from the bitumen during purging was not monitored because these dead bitumen samples had previously been shown to only release volatiles at temperatures above 120ºC (Castellanos *et al*., 2014); therefore, volatile losses were considered negligible. Finally, the precipitant (*n*-heptane for the kinetic experiments of Chapter 4) was purged with nitrogen in the same way as the MSB oil for three hours (instead of 24 h) before it was added to the crude oil or bitumen.

2.8 Measurement of Asphaltene Yields

Measurements in Nitrogen

The yield measurements in anaerobic environment were carried out at ambient conditions inside an inflatable glove box filled with 99.99% nitrogen using the pretreated oil samples and precipitants. The glove box was first vacuumed and then filled with nitrogen. This cycle was repeated for four times to ensure an oxygen-free environment and then the glove box was sealed. Diluted crude oil or bitumen samples were prepared by adding a known mass of pretreated crude oil to a clean 30 mL centrifuge tube. A specified mass of degassed *n*-heptane was then added to achieve the desired weight percent of precipitant. The *n*-heptane was added at a rate of approximately 1 mL/minute while the mixture was carefully mixed manually with a spatula. When the viscosity of the mixture was sufficiently low, a magnetic bar was used to stir the mixture while *n*-heptane addition continued dropwise. The mixtures were then sonicated for 60 minutes and left to settle for the desired equilibration time. Time zero was defined as the time at which the last drop of *n*-heptane was added to the crude oil.

After a specified contact time, the samples were centrifuged using a Hettrich Model EBA 12 centrifuge for five minutes at 4000 rpm (centrifuge radius = 0.2 m; centrifuge tube length = 8.5 cm), equivalent to a relative centrifugal force (RCF) of 1735 G. The supernatant was carefully removed with a pipette and the remainder of the fluid was poured into a VWR grade 696 glass microfiber filter. The remaining sediment (precipitated asphaltenes and entrained continuous phase) were washed with 20 mL of *n*-heptane and the mixture was sonicated for 30 minutes and centrifuged for five minutes at 4000 rpm. The washing step was repeated twice or until a colorless supernatant was obtained. The precipitated material was left to dry in a Thermo Scientific Labline vacuum oven at 60ºC and 20 kPa for one week.

Note, this sediment still contains mineral solids and organic compounds that co-precipitate with the asphaltenes (*e.g*., carbenes, carboids, *etc*.) but are insoluble in toluene. To obtain the toluene insoluble (TI) content, the precipitate was dissolved in 25 mL of toluene, sonicated for one hour and centrifuged at 4000 rpm for 10 minutes. The supernatant was decanted and additional toluene was added. This procedure was repeated until the toluene solution was colorless. The remaining TIs were dried and weighed as described previously for the asphaltene precipitate. Asphaltene precipitation yields were calculated as the mass of precipitate less the mass of TI all divided by the initial mass of crude oil; that is, the asphaltene yields were all determined on a TI-free basis. The repeatabilities of the yields measured inside the glove box were ± 0.6 wt% for the WC-B-B2 and WC-B-A3, ± 0.6 wt% for MX-B-A1, ± 0.02 wt% for the MSB, and ± 0.03 wt% for EU-HO-A1 sample.

Measurements in Air

Asphaltene yields were determined in air using the same procedure as for the nitrogen atmosphere experiments except it was performed in open air instead of in a glove box. In air, asphaltene yields were also collected using *n*-pentane as precipitant. The determination of asphaltene and toluene insoluble contents was made following the same gravimetric procedure. The repeatabilities of the yields in air were ± 0.4 wt% for the WC-B-B2 and WC-B-A3, ± 0.5 for MX-B-A1, ± 0.02 for the EU-HO-A1, and ± 0.02 for the MSB oil. These repeatabilities are lower than the values reported

in nitrogen because it was simpler to control the addition of precipitant and the measurement of weights outside the glove box.

2.9 Bitumen Aeration

The effect of aeriation of bitumen on asphaltene precipitation yields was investigated using the WC-B-A0 sample. The sample was deoxygenated prior to these tests following the procedure described in Section 2.7. To aerate the bitumen at 40 and 70°C, approximately 100 g of bitumen was placed in a glass tube (ID=4 cm; L= 35 cm) containing approximately 3 cm^3 of grit. Air was introduced into the test tube through an outlet underneath the grit. The aeration rate was maintained at 10 cm^3/s (20°C and 0.1 MPa), corresponding to 360 to 900 cm^3 air / g bitumen / hour. At this flow rate, the air stream broke up within the grit into small bubbles about 1 mm in diameter. The total aeration time was 5 days. The test tube was heated with an electrical heating band and a thermocouple was placed in the center of the bitumen bed. The temperature was kept to ± 2ºC from the target temperature. For the aeration at 21ºC, approximately 40 g of bitumen was loaded instead of 100 g to avoid high pressure drops caused by the high viscosity of bitumen at this temperature. Otherwise, the procedure was the same. Experiments with the aerated samples were started immediately after the aeration procedure. Asphaltene yields were measured at 21ºC and 24 h contact time with aerated samples following the method provided in Section 2.8.

2.10 Settling Rates

The settling rates of asphaltene aggregates were measured with two methods: the visual method and the sampling method. The visual method was performed when the asphaltene aggregate concentration was high (> 60 wt% *n*-pentane or 70 wt% *n*-heptane) and the solution was transparent enough to track the interface over time. The sampling method was used for lower asphaltene aggregate concentrations and opaque solutions where the interface was not clearly visible. Details on the sampling method are discussed elsewhere (Casas, 2017).

Visual Method

The suspension of asphaltene aggregates was prepared following the method described in Section 2.3. After 1 h mixing, the suspension was poured into a 250 mL graduated cylinder with an internal diameter of 3.5 cm. Aggregates started to settle immediately and the interface position was visually tracked over time. A flashlight with an incandescent light bulb was focused on the interface with a magnifying glass to improve the visibility of the settling asphaltenes. The height of the interface was plotted as a function of time to obtain a "settling curve". The settling rate was determined in the free-settling region as the slope of the first data points in the settling curve. The repeatability of the settling rate was ±0.02 cm/min (about 5.5%) based on 3 repeats with a 90% confidence interval.

Sampling Method

The asphaltene suspension was poured into a graduated cylinder with the same specification as in the visual method. The mixture was left to settle for a specified time between 10 minutes and 2 hours. Then, a 50 mL glass syringe with a stainless-steel needle (length = 30 cm, diameter = 1 mm) was used to remove layers of fluid in sequence from top to bottom. Ten layers of approximately 20 mL each were collected. This method could only be applied if the settling time was greater than 10 minutes because at least 4 minutes were required to recover all the samples. The data are all reported at the midpoint time, hence the error in the reported times with this method is ± 2 minutes (Casas, 2017).

Each layer was transferred into a 30 mL glass vial to measure its volume and mass. The samples were washed and centrifuged with a similar procedure used in the determination of yields. In this case, samples were centrifuged for 5 minutes at 4000 rpm (equivalent to a relative centrifugal force of 1735 G) to separate asphaltene aggregates from the supernatant. The supernatant was decanted from the vial using a 10 mL pipette. The precipitate was washed using 20 mL of precipitant (fresh *n*-heptane or *n*-pentane, the same precipitant used to prepare the suspension), followed by 60 minutes sonication. After this time, the sample was centrifuged again, and the supernatant was removed. This washing procedure was performed twice or until the supernatant was colorless. The precipitate was dried for 1 day in a fume hood and then dried in a Thermo Scientific Labline

vacuum oven at 60°C and 20 kPa for 4 days. Finally, the mass of precipitated asphaltenes + inorganic solids was measured.

To determine the mass of toluene insolubles, 20 mL of toluene were added to the tube with the dry sediment and sonicated for 30 minutes. The sample was then centrifuged, and the supernatant was removed with a pipette. The washing steps with toluene were repeated for at least three times. The sample was dried for 4 days, and the mass of toluene insolubles was measured. The mass of precipitated asphaltenes was obtained as the mass of solids obtained in the previous step minus the mass of toluene insolubles. Since the volume of the layer and the mass and density of precipitate are known the solid volume fraction of the layer was calculated as follows,

$$\phi_i = \frac{m_{A,i}}{\rho_A V_i} \tag{2.10}$$

where ϕ_i is the asphaltene volume fraction of layer i, $m_{A,i}$ is the mass of asphaltenes in the layer, and V_i, is the volume of the layer. The same approach was used to calculate the TI volume fraction, but the asphaltene mass is replaced by the mass of TI. The asphaltene density was taken as 1200 kg/m^3 (Yarranton and Masliyah, 1996), and 2500 kg/m^3 was used for the toluene insolubles, which is the average density for minerals typically found in oil sands (Bowman, 1967; Van and Bang, 2013). The volume of the layer was determined from the height of fluid and diameter of the tube to where the layer samples were transferred. The repeatability for the solid volume fractions was ±0.002.

The asphaltene volume fraction data was used to create a concentration profile over the height of the fluid column at each settling time. Above the interface, the solid content was nearly constant and significantly lower than immediately below the interface (See Section 6.3.5). The interface was selected as the midpoint between the uppermost layer of constant low solids content and the lowest layer where the solids content suddenly increases. Since the layer thickness is 2.0 cm, the uncertainty for the position of the interface is ±1 cm.

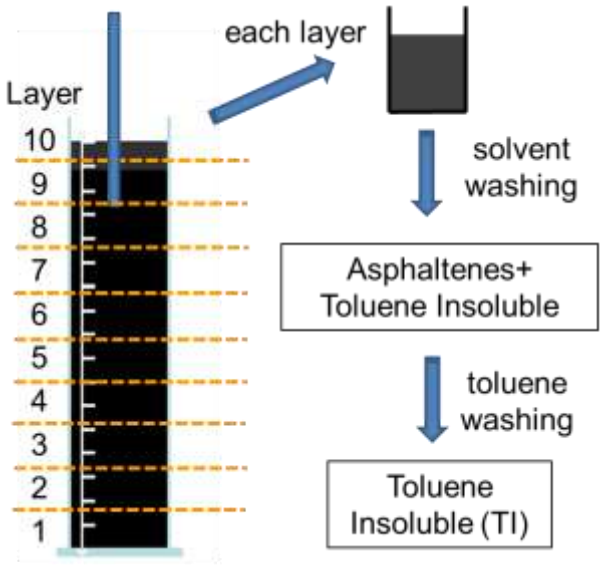

Figure 2.5: Methodology followed to measure settling rates of asphaltene aggregates using the sampling method. The sampling time per layer was 25 s. 10 samples of 20 mL each were collected over 4 minutes. Image retrieved from Casas (2017).

Consistency between Methods

To compare the methods used to measure settling rates, asphaltenes aggregates were prepared from a mixture of a diluted WC-B-B2(1) bitumen at 62.5 wt% *n*-heptane and 21°C. At this concentration, both the visual and sampling method could be applied with confidence. Figure 2.6 shows that the location of the interface is systematically lower for the sampling method. However, the slope is identical within the error of the measurements: 0.36 ± 0.10 cm/min for the sampling method and 0.37 ± 0.02 cm/min for the visual method. Only the slope is required to determine the settling rate. Therefore, both methods provide the same quality of settling rate data and together they provide data over a broad range of conditions. The range of applicability of each method for the different mixtures investigated is provided in Table 2.4.

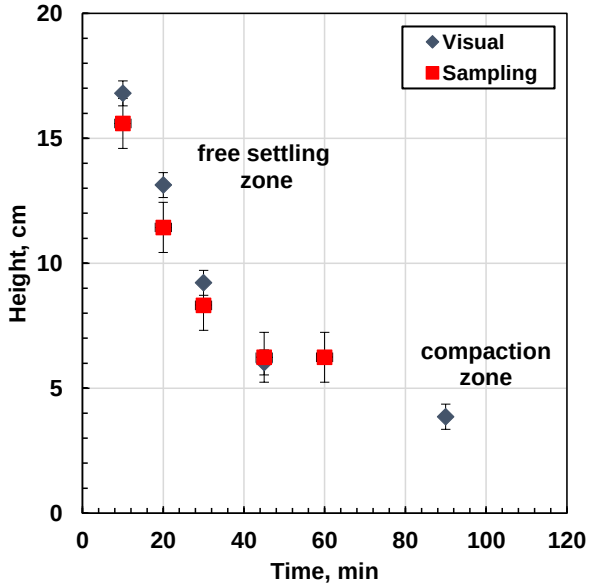

Figure 2.6. Comparison of settling curves from visual and sampling methods for a mixture of *n*-heptane and WC-B-B2(1) bitumen at 62.5 wt% precipitant content at 21°C and 1 atm.

Table 2.4. Range of applicability of the visual and sampling methods to measure the settling rate of asphaltene aggregates in diluted bitumen mixtures.

Mixture	Method	Precipitant Content, wt%
n-pentane/WC-B-A3	visual[†]	60.0 - 95.0
n-heptane/WC-B-A3	sampling	60.0 - 72.0
n-heptane/WC-B-A3	visual	72.0 - 95.0
n-heptane/WC-B-B2*	sampling	55.0 - 62.5
n-heptane/WC-B-B2*	visual	62.5 - 90.5

[†] tracking the lower interface only (See Section 6.3.5). * Refers to both WC-B-B2 and WC-B-B2(1) samples.

2.11 Adhesion Measurements

A surface forces apparatus (SFA) was employed to measure the interaction forces of asphaltenes in mixtures of 50 vol% toluene and 50 vol% *n*-heptane (heptol). These experiments were conducted by Dr. Hongbo Zeng at the University of Alberta. Asphaltenes were extracted with *n*-heptane from the WC-B-B2 and WC-B-A3 samples following the procedure described by Alboudwarej *et al.* (2002) and sent to Dr. Zeng's lab. Details of the SFA method are provided

elsewhere (Zhang *et al.*,2016; Wang *et al.*, 2012; Hwang *et al.*, 2012; Israelachvili *et al.*, 2010). Briefly, two cylindrical silica disks with a 2 cm radius were prepared by gluing thin (1−5 μm) back-silvered mica sheets to their surface. The disks were mounted in the SFA chamber in a cross-cylinder geometry, which is locally equivalent to a sphere of radius *R* against a flat surface at a separation distance of $D \ll R$. A volume of 200 μL of a 500 ppm asphaltene/heptol solution was injected between the mica surfaces. The absolute separation distance between the two mica surfaces was determined with multiple beam interferometry (MBI) employing the fringes of equal chromatic order. The interaction force (*F)* between two mica surfaces in the asphaltene solution was measured as a function of the separation distance (*D)*. The reference distance ($D = 0$) was determined from an independent measurement of the point at which two bare mica surfaces come into contact in air. The adhesion energy per unit area (W_{ad}) was determined from the measured adhesion force (F_{ad}) based on the Johnson−Kendall−Roberts (JKR) model where $W_{ad}=F_{ad}/1.5\pi R$ (Huang *et al.*, 2017; Israelachvili 2011).

2.12 Chapter References

Alboudwarej, H.; Akbarzadeh, K.; Beck, J.; Svrcek, W.Y.; Yarranton, H.W. (2003). Regular Solution Model for Asphaltene Precipitation from Bitumens and Solvents. *Energy Fuels*, 49 (11), 2948-2956.

Alboudwarej, H.; Beck, J.; Svrcek, W.Y.; Yarranton, H.W. (2002). Sensitivity of Asphaltene Properties to Separation Techniques. *Energy Fuels*, 16(2), 462-469.

Allen, T. (2003). *Powder Sampling and Particle Size Determination*, Elsevier, Amsterdam, The Netherlands.

Beck, J., Svrcek, W.Y., Yarranton, H.W. (2005). Hysteresis in Asphaltene Precipitation and Re-dissolution, *Energy Fuels*, 19 (3), 944-947.

Bowman, C.W. (1963). *Molecular and Interfacial Properties of Athabasca Tar Sands*. No. 13 in Proceedings of the 7th World Petroleum Congress, Vol. 3, Elsevier Publishing Co., 583-603.

Casas, Y. (2017). Settling Rate of Asphaltenes and Solids from Diluted Bitumen. MSc. Thesis. University of Calgary.

Castellanos-Diaz, O.; Sánchez, M.C.; Schoeggl, F.F.; Satyro, M.A.; Taylor, S.D.; Yarranton, H.W. (2014). Deep Vacuum Fractionation of Heavy Oil and Bitumen: Part 1. Apparatus and Standardized Procedure. *Energy Fuels*, 28 (5), 2857-2865.

Clain, P.; Ndoye, F.T.; Delahaye, A.; Fournaison, L.; Lin, W.; Dalmazzone, D. (2015). Particle Size Distribution of TBPB Hydrates by Focused Beam Reflectance Measurement (FBRM) for Secondary Refrigeration Application. *Int. J. Refrig*., 50, 19-31.

Greaves, D.; Boxall, J.; Mulligan, J.; Montesi, A.; Creek, J.; Sloan, D.E.; Koh, C.A. (2008). Measuring the Particle Size of a Known Distribution Using the Focused Beam Reflectance Measurement Technique. *Chem. Eng. Sci*., 63(22), 5410-5419.

Huang, J.; Liu, X.; Qiu, X.; Xie, L.; Yan, B.; Wang, X.; Huang, Q.; Zeng, H. (2017). Octadecyltrichlorosilane Deposition on Mica Surfaces: Insights into the Interface Interaction Mechanism. *J. Phys. Chem. B*, 121 (14), 3151-3161.

Hwang, D.S.; Harrington, M.J.; Lu, Q.; Masic, A.; Zeng, H.; Waite, J.H. (2012). Mussel Foot Protein-1 (mcfp-1) Interaction with Titania Surfaces. *J. Materials Chem*., 22 (31), 15530-15533.

Israelachvili, J. N. (2011). *Intermolecular and Surface Forces*. Academic Press, Amsterdam, The Netherlands.

Israelachvili, J.; Min, Y.; Akbulut, M.; Alig, A.; Carver, G.; Greene, W.; Kristaiansen, K.; Meyer, E.; Pesika, N.; Rosenberg, K.; Zeng, H. (2010). Recent Advances in the Surface Forces Apparatus (SFA) Technique. *Rep. Prog. Phys*., 73 (3), 036601.

Lasentec. (2002). *FBRM Control Interface Version 6.0 User Manual*. Lasentec Inc.

Maqbool, T.; Raha, S.; Hoepfner, M.P.; Fogler, H.S. (2011). Modeling the Aggregation of Asphaltene Nanoaggregates in Crude Oil-Precipitant Systems. *Energy Fuels*, 25 (4), 1585-1596.

Marquez, A.A. (2019). Viscosity of Characterized Visbroken Heavy Oils. MSc. Thesis. University of Calgary.

Mostowfi, F.; Indo, K.; Mullins, O.C.; McFarlane, R. (2009). Asphaltene Nanoaggregates Studied by Centrifugation. *Energy Fuels*, 23(3), 1194-1200.

Peramanu, S.; Singh, C.; Agrawala, M.; Yarranton, H.W. (2001). Investigation of the Reversibility of Asphaltene Precipitation. *Energy Fuels*, 15 (4), 910-917.

Rahmani, N.; Dabros, T.; Masliyah, J.H. (2005). Fractal Structure of Asphaltene Aggregates. *J. Colloid Interface Sci*., 285 (2), 599-608.

Ramos-Pallares, F. (2017). The Viscosity and Thermal Conductivity of Heavy Oils and Solvents. PhD. Dissertation. University of Calgary.

Ramos-Pallares, F.; Lin, H.; Yarranton, H.W.; Taylor, S.D. (2017). Prediction of the Liquid Viscosity of Characterized Crude Oils by Use of the Generalized Walther Model. *SPE J*., 22 (5), 1487-1505.

Ramos-Pallares, F.; Schoeggl, F.F.; Taylor, S.D.; Satyro, M.A. Yarranton, H. W. (2016). Predicting the Viscosity of Hydrocarbon Mixtures and Diluted Heavy Oils Using the Expanded Fluid Model. Energy Fuels, 30(5), 3575-3595.

Van, A.L.; Bang, D.P.V. (2013). Hindered Settling of Sand/mud Flocs Mixtures: From Model Formulation to Numerical Validation. *Adv. Water Resour*., 53, 1-11.

Wang, J.; Lu, Q.; Harbottle, D.; Sjöblom, J.; Xu, Z.; Zeng, H. (2012). Molecular Interactions of a Polyaromatic Surfactant C5Pe in Aqueous Solutions Studied by a Surface Forces Apparatus. *J. Phys. Chem. B*, 116 (36), 11187-11196.

Xu, R. (2000). *Particle Characterization: Light Scattering Methods*. Kluwer Academic Publishers, New York, NY.

Yarranton, H.W.; Masliyah, J.H. (1996). Molar Mass Distribution and Solubility Modeling of Asphaltenes. *AIChE J*. 42(12), 3533-3543.

Yarranton, H.W.; van Dorp, J.J.; Verlaan, M.L.; Lastovka, V. (2013). Wanted Dead or Live: Crude-Cocktail Viscosity – A Pseudocomponent Method to Predict the Viscosity of Dead Oils, Live Oils, and Mixtures. *J. Can. Pet. Technol*., 52 (3), 176-191.

Zhang, L.; Shi, C.; Lu, Q.; Liu, Q.; Zeng, H. (2016). Probing Molecular Interactions of Asphaltenes in Heptol Using a Surface Forces Apparatus: Implications on Stability of Water-in-Oil Emulsions. *Langmuir*, 32 (19), 4886-4895.

Chapter 3: Nature of Asphaltene Aggregates

In this contribution[1], the size and fractal dimension of asphaltene aggregates were investigated for two Western Canadian bitumens (WC-B-B2 and WC-B-A3) diluted with *n*-heptane at concentrations above the onset of precipitation. The asphaltenes formed approximately log-normal size distributions with volume mean diameters of tens to hundreds of micrometers, depending mainly on the *n*-heptane content. The distributions were established in less time than the first measurement could be obtained (about 30 seconds) and changed relatively little afterwards. The average aggregate size increased with increasing *n*-heptane content but reached a plateau value at 70 to 80 wt% *n*-heptane.

The fractal dimension reached a maximum at a similar *n*-heptane content. Micrographic images and fractal dimensions indicated that, near the onset of precipitation, compact linear and planar aggregate structures dominated. At higher *n*-heptane contents up to approximately 75 wt% *n*-heptane the aggregates remained compact but became more three-dimensional. At higher *n*-heptane contents, larger, looser structures were formed that could be broken under sufficient shear but did not re-aggregate. The results were consistent with a simultaneous nucleation, growth, and flocculation processes where the precipitating material was initially sticky but lost its stickiness over time. The loss in stickiness was confirmed with surface force adhesion measurements.

3.1 Introduction

It is well known that asphaltenes can precipitate from crude oils upon changes in pressure and temperature or when a paraffinic solvent is added to the oil (Wiehe, 2008). In fact, asphaltenes are defined as the fraction of the oil that is insoluble in normal alkanes (*i.e.*, *n*-pentane or *n*-heptane) but soluble in toluene. Asphaltene precipitation is often considered to be an undesirable flow assurance issue but solvent induced precipitation is also a necessary step in some commercial

[1] This chapter is based on the following published work: Duran, J.A.; Casas, Y.A.; Xiang, L.; Zhang, L.; Zeng, H.; Yarranton, H.W. (2019). Nature of Asphaltene Aggregates. *Energy Fuels,* 33 (5), 3694-3710.

heavy oil processes, such as partial deasphalting and oil sands froth treatment, and for potential new processes such as non-aqueous oil sand extraction. In partial deasphalting, the asphaltenes are precipitated and settled to improve the quality of the product oil (Gray, 2015). In oil sands froth treatment, the asphaltenes are precipitated to flocculate with and settle suspended water droplets and solids (Romanova *et al*., 2006). In non-aqueous extraction, asphaltene precipitation is one option to aggregate and remove fine solids from the bitumen product (Wu and Dabros, 2012, Pal *et al.*, 2015). The effectiveness of these gravity settling processes depends significantly on the size and density distribution of the precipitated asphaltene particles and/or aggregates. In this chapter, the size and structure of these aggregates is examined as a first step in developing a method to predict settling rates at different process conditions. Two terms are defined here to aid in the following discussion. Aggregation is defined as the formation of a larger particle from smaller particles and/or precipitating molecules regardless of the mechanism. Flocculation is defined as the formation of aggregates from primary particles as a result of electrostatic or dispersion forces.

Before examining the literature on aggregate sizes and properties, two limitations are set on the conditions considered in this chapter. The first limitation is on the morphology of the precipitated asphaltenes. In crude oils diluted with *n*-pentane or higher carbon number *n*-alkanes at temperatures below approximately 90°C, asphaltenes appear to precipitate as approximately 1 μm in diameter glassy particles (Agrawal *et al.*, 2012) that aggregate into structures up to several hundred microns in diameter (Ferworn *et al.*, 1993; Rastegari *et al.*, 2004; Rahmani *et al.*, 2005a). At temperatures above approximately 90°C, the asphaltene-rich phase is in a glass/liquid transition and, above 130°C, is fully liquid (Agrawal *et al.*, 2012; Johnston *et al.*, 2017). The settling processes considered in this study are at lower temperatures and therefore only the glassy particles and aggregates are considered.

The second limitation relates to the definition of the onset of precipitation; that is, the solvent (precipitant) content at which asphaltenes are presumed to have precipitated. Asphaltenes in the oil are thought to exist as nanoaggregates that either act as a colloidal dispersion stabilized by resin molecules (Mullins *et al.*, 2012; Eyssautier *et al.*, 2012; Park and Mansoori, 1988) or as macromolecules in solution with the oil (Agrawala and Yarranton, 2001). The colloidal description

of asphaltene precipitation assumes that dilution with a precipitant depletes the resins surrounding the nanoaggregates allowing them to flocculate into micrometer-scale structures. Precipitation is only observed when the particles reach a detectable size and the time to reach a detectable size may depend on the precipitant content (Maqbool *et al.*, 2009). Hence, the precipitant content (onset condition) at which the particles are detected is time dependent. The macromolecular explanation assumes that dilution with a precipitant induces a phase transition and that a glassy asphaltene-rich phase nucleates, grows, and possibly flocculates as well. A phase transition has an equilibrium onset condition, but it still may take some time to reach equilibrium. In this study, only conditions at which micrometer-scale particles are observed are examined. In this chapter, the onset of precipitation is defined as the precipitant content at which the particles are first detected at 24 hours after contact. The time dependence of the onset is not considered here but will be accounted for in Chapters 4 and 5.

The choice of the colloidal or the macromolecular approach does have one implication for this study. In the colloidal approach, the aggregates are assumed to be collections of smaller primary particles held together by electrostatic and van der Waals forces and therefore their size distribution is expected to be shear sensitive. In the macromolecular approach, it is not known if the particle growth and flocculation processes are simultaneous or sequential. Hence, the precipitated material could form fused solids and flocs. If the structures are fused solids, they could be shattered under shear but would not necessarily be able to re-flocculate.

3.1.1 Size of Asphaltene Aggregates

Caution is advised when examining aggregate size data from different sources. First, aggregate sizes are reported on a different basis depending on the technique employed; for example, number mean diameters are typically reported for microscopy or time of transition methods, while volume or Sauter mean diameters are reported for FBRM techniques (Kempkes *et al*, 2008; Allen, 2003). Second, it is challenging to measure broad particle size distributions and different methods have different errors. For example, the time of transition and FBRM techniques measure chord length distributions and many authors simply report the chord length distribution as the diameter

distribution. With microscopic methods, it is challenging to obtain a representative sample. Therefore, this review focuses on the trends in the data rather than direct numerical comparisons.

Size distributions of asphaltenes aggregates have been measured with laser time of transition methods (Ferworn *et al*., 1993; Rastegari *et al*., 2004), focused beam reflectance method (FBRM) (Calles *et al*., 2008; Daneshvar, 2005; Shafiee, 2014), and confocal laser-scanning microscopy (Seifried *et al., 2013*). In addition, Angle *et al*. (2006) observed asphaltenes precipitated from model oils with a microscope. A consistent observation from the model oils and diluted bitumens used in these studies is that the precipitated asphaltenes are first observed as 0.5 to 5 μm diameter particles. In all cases, these "primary" particles begin growing/aggregating immediately after the addition of precipitant, reaching diameters of tens to hundreds of micrometers over minutes to hours (Rassamdana and Sahimi, 1996; Rastegari *et al.*, 2004; Ferworn *et al*., 1993; Calles *et al*., 2008; Seifried *et al.*, 2013). The aggregate structures appear to be collections of the primary particles and therefore have been interpreted to be the result of a secondary flocculation process after the primary precipitation process. It is also possible that only flocculation occurs (or simultaneous precipitation and flocculation) and that the primary particles and flocs are really the same basic structures grown to different sizes. In other words, the particles/flocs were continuously growing from the nano-aggregate scale and simply reached a detectable size at a diameter of approximately 1 μm.

In general, unimodal size distributions were observed and the average steady-state aggregate size was found to increase as the asphaltene content increased and the precipitant content increased. Inconsistent trends have been reported at high precipitant contents. Rastegari *et al.*, (2004) found that the average aggregate sizes decreased at *n*-heptane contents above 85 wt% in a model oil consisting of asphaltenes in *n*-heptane and toluene. In contrast, Ferworn *et al*. (1993) observed that the average aggregate sizes reached a plateau at high dilutions in mixtures of *n*-heptane and heavy oil. Calles *et al*. (2008) reported that asphaltene aggregate sizes from an *n*-alkane diluted crude oil residue increased at higher *n*-alkane contents.

A consistent observation was that the average aggregate sizes were larger in a stronger precipitant (Daneshvar, 2005; Calles *et al*. 2008). For example, aggregates in *n*-pentane diluted bitumen were up to five times larger than the aggregates in *n*-heptane diluted bitumen at the same dilution, shear and temperature (Daneshvar, 2005). Seifried *et al.* (2013) confirmed this effect for a crude oil diluted with *n*-hexane or *n*-heptane and related the average aggregate size to the solubility parameter of the precipitant.

3.1.2 Structure of Asphaltene Aggregates

Microscopic, SAXS or SANS observations suggest that asphaltene aggregates are fractal-like structures made up of smaller particles (Rahmani *et al.*, 2005b; Hoepfner *et al*, 2013). Rahmani *et al.* (2005b) assumed that asphaltene aggregates are made up of small spheres as shown in Figure 3.1 and that the number of primary particles scales to the aggregate diameter according to Eq. 2.4. The diameter of the aggregate was defined as its maximum diameter and, in this case, the porosity of the aggregate is given by,

$$\phi = 1 - n_p \left(\frac{d_p}{d_{agg}}\right)^3 \tag{3.1}$$

where ϕ is the porosity of the aggregate. Equation 2.7 is substituted into Equation 3.1 to obtain the following expression,

$$\phi = 1 - \left(\frac{d_p}{d_{agg}}\right)^{3-D_f} \tag{3.2}$$

The density of a fractal aggregate defined by its maximum diameter is then given by,

$$\rho_{agg} = \rho_m + \left(\rho_p - \rho_m\right)\left(\frac{d_p}{d_{agg}}\right)^{3-D_f} \tag{3.3}$$

where ρ_m and ρ_p are the densities of the surrounding fluid and of the asphaltenes, respectively. Eqs. 3.2 and 3.3 demonstrate that, for fractal structures, the porosity and density are not constant but rather scale with the size of the aggregate.

Although the fractal nature of asphaltene aggregates has been recognized, measurements of the fractal dimensions are relatively scarce. Several studies have reported fractal dimensions for asphaltene nano-aggregates (below the onset of precipitation) using small angle *x*-ray (SAXS) and neutron scattering (SANS) techniques (Hoepfner *et al.*, 2013; Eyssautier *et al.*, 2011; Long *et al.*,

2013). Scattering data are commonly adjusted to mathematical functions that describe the emission data and the fractal dimension is a fitted parameter. Eyssautier *et al*. (2011) reported the fractal dimension of soluble asphaltenes (nanoaggregates) to be 2.1 after fitting SANS and SAXS data of an asphaltene-toluene mixture (5 g/L). Similarly, Long *et al.* (2013) studied the morphology of asphaltene nanoaggregates from *n*-pentane diluted vacuum residue between 50-170ºC using SAXS. They reported fractal dimensions from 1.8 to 2.6 in the solvent-rich phase and observed that the nanoaggregates became more compact (higher fractal dimensions) as the *n*-pentane content increased. Hoepfner *et al.* (2013) used time-resolved SANS to investigate the size and fractal dimension of asphaltene nanoaggregates in model oils and crude oils diluted with *n*-heptane and reported fractal dimensions between 1.3 and 2.0 below the onset of precipitation.

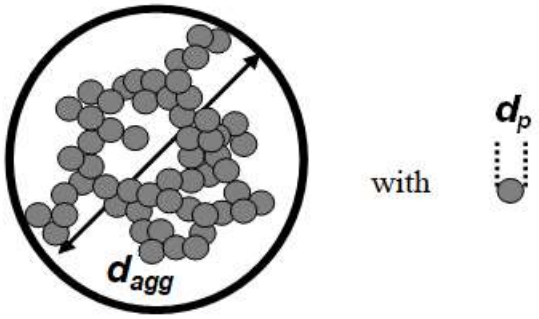

Figure 3.1. Schematic of an asphaltene aggregate with the characteristic length defined as the maximum diameter of the aggregate.

All of these results apply to colloidal or macromolecular structures at the nanometer scale and is unclear if the same fractal dimension applies to precipitated/aggregated asphaltenes at the micrometer scale. At larger scales, Rastegari *et al.* (2004) investigated the fractal dimension of suspended asphaltene aggregates in model oils at precipitant contents well above the onset of precipitation. Based on the mass of precipitate and the particle size distribution of the aggregates, the fractal dimension was estimated to be at least 1.6. Similarly, Rahmani *et al.* (2005b) calculated the fractal dimension of asphaltene aggregates formed in toluene-heptane mixtures and established a range of 1.1 to 1.5 from the slope of a *log-log* plot of the aggregate settling rate against the longest dimension of the aggregates. In a follow up study, Rahmani *et al.* (2005c) used the

projected area diameter instead of the largest distance and obtained fractal dimensions in the range of 1.3 to 2.0.

Higher values for the fractal dimension have been reported for asphaltenes from diluted bitumen systems. Daneshvar (2005) estimated the fractal dimension in the range of 2 to 3, while Shafiee (2014) narrowed the range to 2.1 to 2.4 for aggregates formed from *n*-heptane diluted Athabasca bitumen. In both studies, large volumes of precipitant were used (> 87 wt% *n*-heptane) and the estimation of D_f required the measurement of sediment volumes of the aggregates and their mass. The effect of the precipitant content in the fractal dimension was not investigated and it was assumed to be independent of the *n*-heptane content. Long *et al.* (2013) examined the asphaltene-rich phase from *n*-pentane diluted vacuum residue between 50-170ºC with SAXS and observed structures with fractal dimensions above 3, which they interpreted as structures with a solid core and rough fractal surface.

3.1.3 Objectives

There is still considerable uncertainty in the size distribution and fractal dimension of asphaltene aggregates at conditions relevant for commercial gravity settling processes; that is, in paraffinic solvent diluted crude oil above the onset of asphaltene precipitation. The objective of this chapter is to assess the effect of the precipitant content on asphaltene aggregates sizes and fractal dimensions. The aggregate size distributions were measured as a function of time after *n*-heptane was added to two different bitumen samples. The asphaltene fractal dimensions were estimated from the method discussed in Section 2.5. Micrographs of asphaltene aggregates obtained at different precipitant contents were taken and the morphological characteristics of the aggregates were examined at different conditions. To assist in interpreting some of the results, the adhesion forces between asphaltene films were also measured over time. The data are intended for use in settling calculations but also provide insight on the precipitation/aggregation mechanism. The interpretation of the data involves combining the results from several different measurements. Therefore, the results are first presented individually and then discussed together.

3.2 Results and Discussion

3.2.1 Asphaltene Yields and Precipitate Concentration

The asphaltene yields and the concentration of the precipitated asphaltenes are required for determining the fractal dimension and interpreting the aggregation data. Figure 3.2a shows the yield of precipitated asphaltenes as a function of the *n*-heptane content for each diluted bitumen and Figure 3.2b shows mass fraction of precipitated asphaltenes calculated from the yield data. The yields and precipitate concentrations were higher in WC-B-B2 bitumen than WC-B-A3 bitumen because it had a higher asphaltene content (Table 2.1). For both bitumens, the yields initially increased steeply but the slope decreased significantly at approximately 70 wt% *n*-heptane content. The concentration of precipitated asphaltenes increased with increasing *n*-heptane content until the same point and then decreased at higher *n*-heptane contents because the yield was nearly constant and the increase in *n*-heptane content simply diluted the mixture.

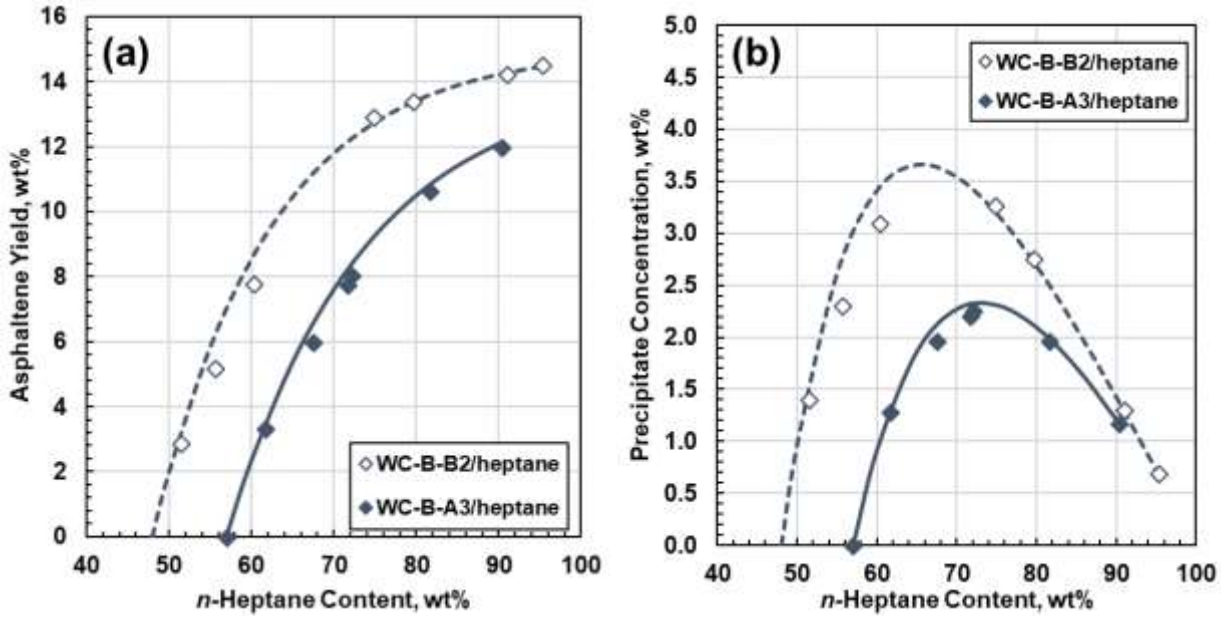

Figure 3.2. Yield (a) and asphaltene precipitate concentration (b) as a function of *n*-heptane content at 21ºC after 24 hours contact time. The symbols are data; the lines are empirical equations fitted to the yield data and provided as visual aids.

3.2.2 Size of Asphaltene Aggregates

General Observations

Figure 3.3a shows a volume frequency distribution measured with the FBRM for a typical aggregation experiment with *n*-heptane diluted bitumen. This distribution and all the others measured in this study were approximately log-normal. Since there was little variation in the shape of the distributions, the results will be discussed in terms of volume mean diameters for the sake of simplicity. Note, mean diameters were chosen over median values because the former gives a better indication of the center of mass on the distribution. Figure 3.3b confirms that the FBRM distribution matches the microscopic method distribution.

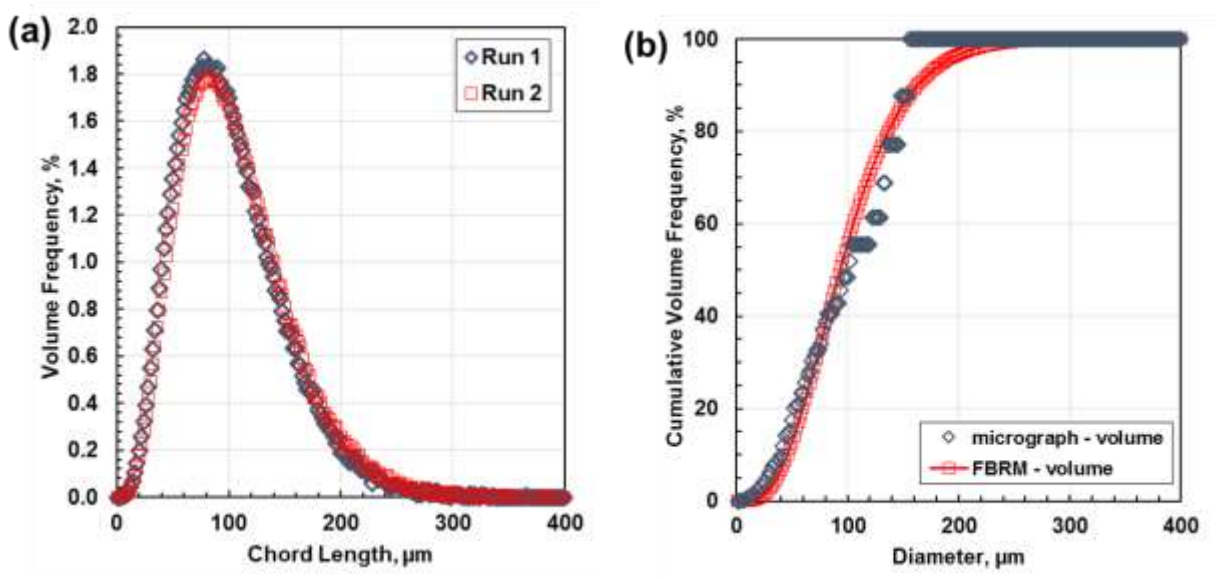

Figure 3.3. Volume distribution of asphaltene aggregates in a mixture of 5 wt% WC-B-A3 bitumen and 95 wt% *n*-heptane at 195 rpm, 21ºC, and after 60 minutes mixing: a) volume frequency distribution from FBRM method; b) comparison of cumulative frequency distributions from FBRM and micrographic methods.

Figures 3.4 and 3.5 show the evolution of the aggregate mean diameters and number counts, respectively, over the course of 3 hours for several WC-B-B2/*n*-heptane mixtures at a mixing speed of 195 rpm. There are two points of interest: 1) the initial mean diameters; 2) the change of mean diameters over time. The initial volume mean diameters, measured at 30 seconds of contact time,

were already over a hundred micrometers. Visual observations based on micrographs (not shown here) indicate that precipitation occurs almost instantaneously above the onset condition. Hence, the initial aggregation is rapid compared, for example, to a process residence time of approximately 15 minutes for oil sands froth treatment (Tipman and Long, 1999).

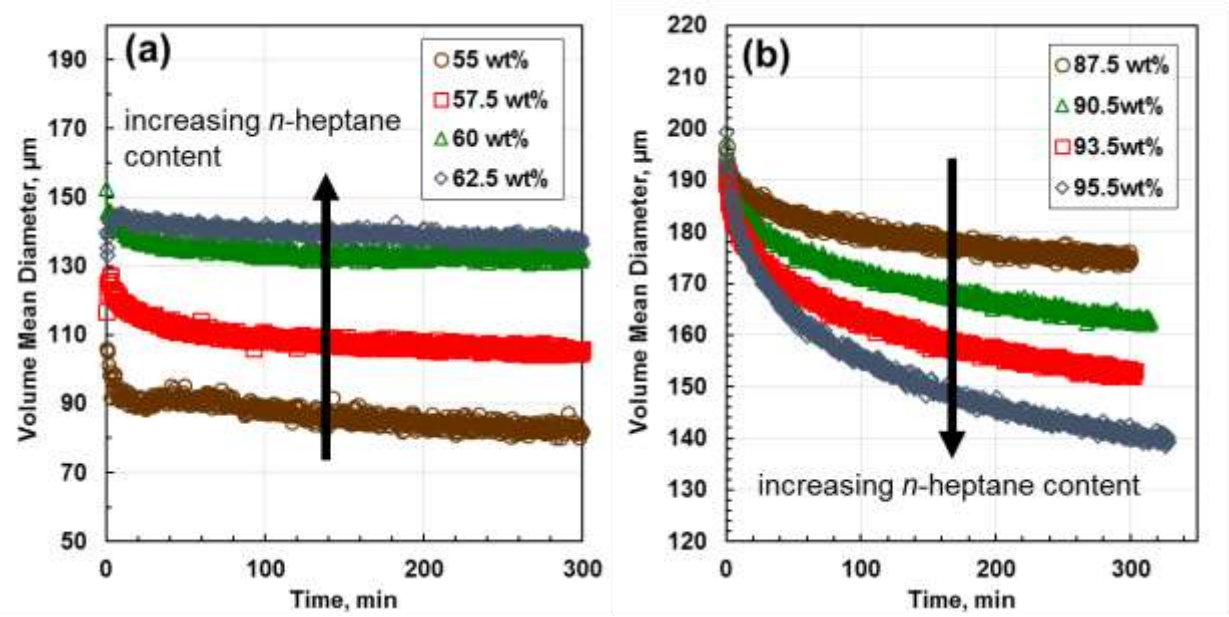

Figure 3.4. FBRM volume mean diameter of asphaltene aggregates in *n*-heptane diluted WC-B-B2 bitumen at 195 rpm: a) near onset; b) at high dilution. Note, the vertical scale is different in each plot.

The initial volume mean diameters and number counts both increased with increasing *n*-heptane content until reaching a plateau above approximately 80 wt% *n*-heptane. The volume mean diameters evolved differently over time at different *n*-heptane contents. At *n*-heptane contents below 65 wt%, the mean diameter and number count did not change significantly over time indicating a stable population. In contrast, at *n*-heptane contents above 85 wt%, the mean diameter decreased over time while the number count increased, consistent with shattering. Similar trends were observed for the WC-B-A3 bitumen.

Initial Asphaltene Aggregate Size

The initial volume mean diameter for *n*-heptane diluted WC-B-B2 bitumen (Figure 3.6a) and WC-B-A3 bitumen (Figure 3.6b) both increased with increasing *n*-heptane content up to approximately 80 wt% *n*-heptane. Above 80 wt% *n*-heptane the volume mean diameters reached plateaus of approximately 200 μm for the WC-B-B2 bitumen and 85 μm for the WC-B-A3 bitumen.

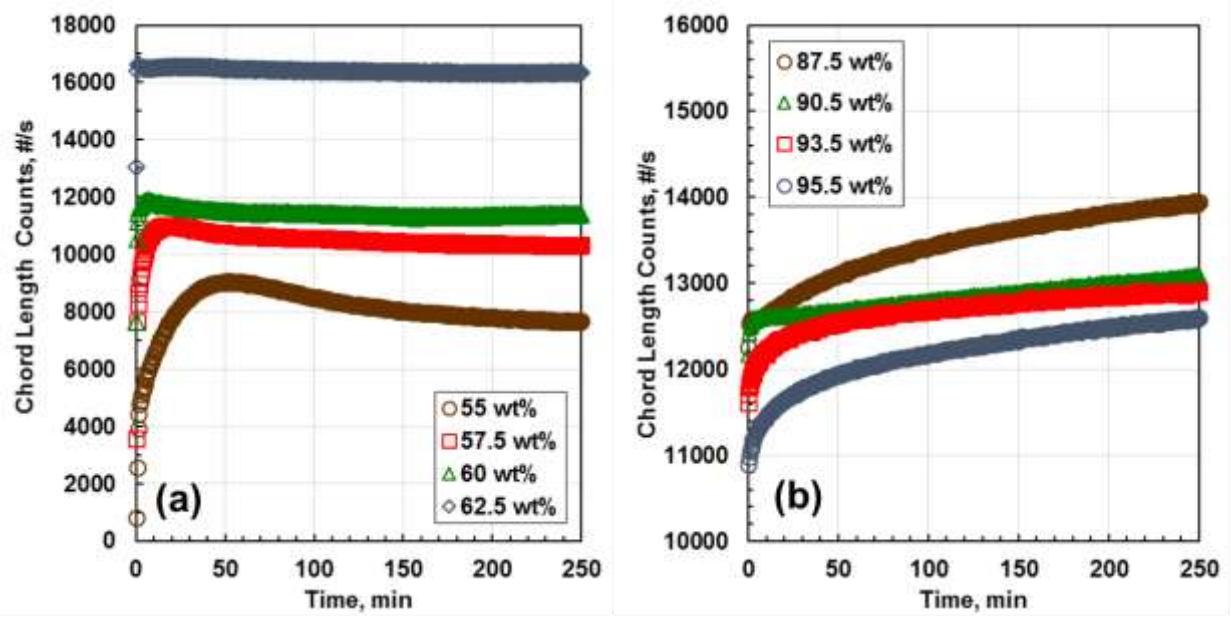

Figure 3.5. FBRM number count of asphaltene aggregates in *n*-heptane diluted WC-B-B2 bitumen at 195 rpm: a) near onset; b) at high dilution. Note, the vertical scale is different in each plot.

Figure 3.7 shows the effect of shear on the initial mean diameter of asphaltenes aggregates measured at three types of shear condition: 1) zero shear (micrographs taken with no agitation applied after the second addition of precipitant); 2) impeller mixer at speeds of 195, 275 and 330 rpm (FBRM method); 3) sonication (micrographic method). Sonication provides a large mixing energy relative to the mixer. For the WC-B-B2 bitumen, shear had little effect on the initial diameter between 195 to 330 rpm at all *n*-heptane contents (Figure 3.7a). For the WC-B-A3 bitumen, the initial diameters under "zero shear" and at 195 rpm were almost identical within the experimental error (Figure 3.7b). Hence, measurement up to 195 rpm are representative of the

initial zero-shear size of the aggregates. Further increases in shear decreased the initial aggregate sizes.

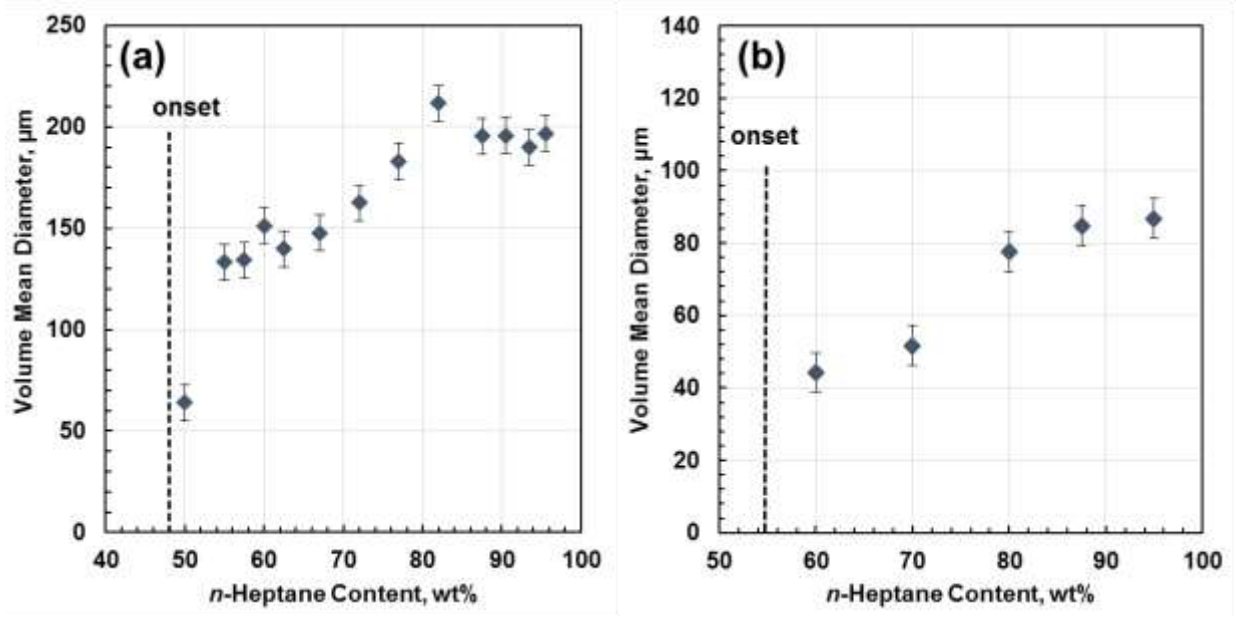

Figure 3.6. Initial aggregate mean diameter (measured at 30 seconds) for *n*-heptane diluted bitumen at 195 rpm and 21ºC: a) WC-B-B2; b) WC-B-A3. Note vertical axes have different scales.

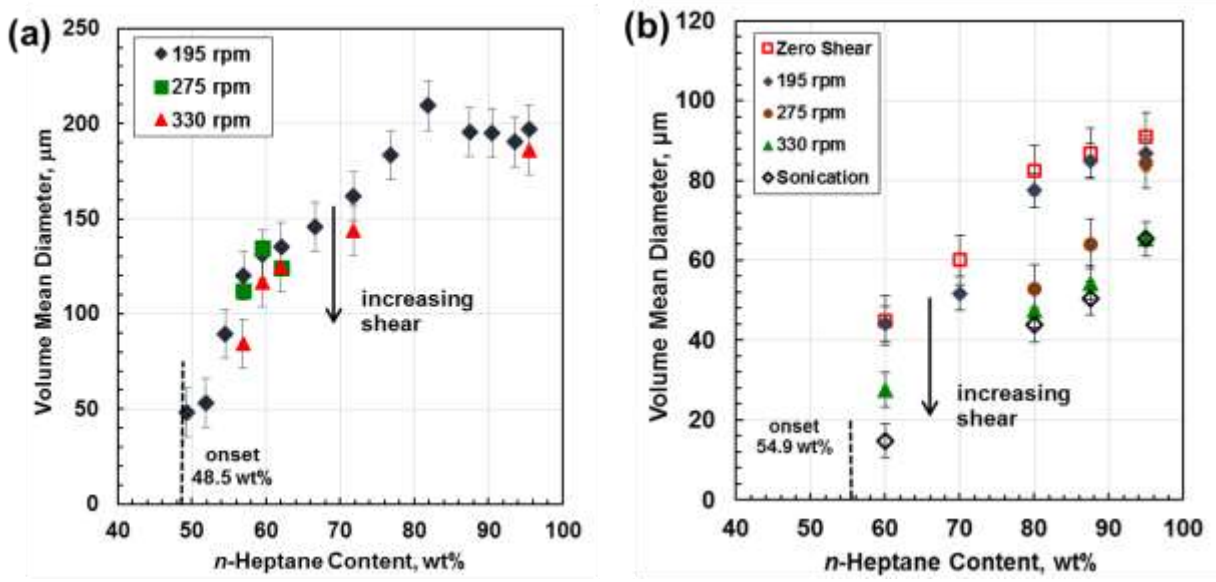

Figure 3.7. Effect of shear on the initial diameter of asphaltene aggregates from *n*-heptane diluted bitumen at 21ºC: a) WC-B-B2; b) WC-B-A3. Note vertical axes have different scales.

Aggregate Size Over Time

Figures 3.8a and 3.8b present the initial and final aggregate mean diameters for mixtures of *n*-heptane with WC-B-B2 and WC-B-A3 bitumen, respectively. Below approximately 80 wt% *n*-heptane, there is little or no change in the aggregate size over time (3 hours) at any of the mixing speeds considered in this study. In other words, the aggregates formed at the lower *n*-heptane contents are shear insensitive over time. Above 80 wt% *n*-heptane, the mean diameter of the aggregates after 3 hours under shear is always lower than the initial size, consistent with shattering. To summarize, asphaltene aggregates appear to be somewhat sensitive to shear during their formation but after a short time, the structures formed at low *n*-heptane contents become shear independent. At higher dilutions, asphaltene aggregates are still affected by shear after their formation.

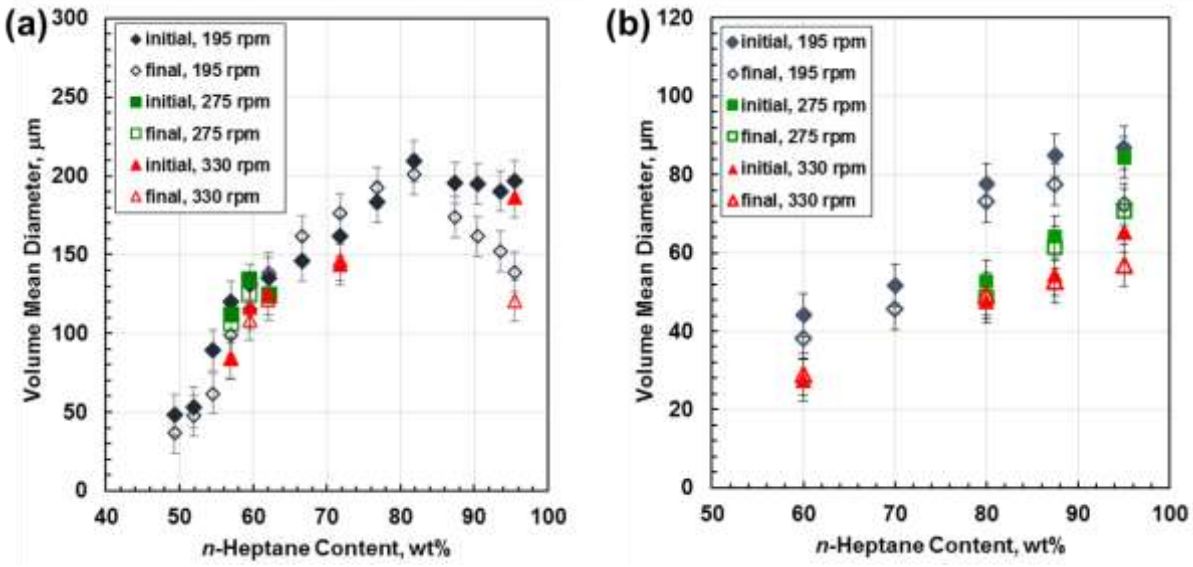

Figure 3.8. Effect of shear rate on the aggregate mean diameter from *n*-heptane diluted bitumen after 3 hours at 21ºC. (a) WC-B-B2 bitumen; (b) WC-B-A3 bitumen. Closed and open symbols are the initial and final (3 hours) volume mean diameters, respectively.

3.2.3 Structure and Fractal Dimension of Asphaltene Aggregates

Micrographic Observations

Figures 3.9 and 3.10 show micrographs of the asphaltene aggregates from WC-B-B2 and WC-B-A3 bitumen, respectively, at *n*-heptane contents from the onset to 95 wt%. Near the onset, the aggregates from the WC-B-B2 bitumen appear to be more planar structures while the aggregates from the WC-B-A3 bitumen are more linear. The aggregates from the WC-B-A3 bitumen are smaller than those formed from the WC-B-B2 bitumen. In both cases, the aggregates tended to have looser, more porous structures at higher *n*-heptane contents.

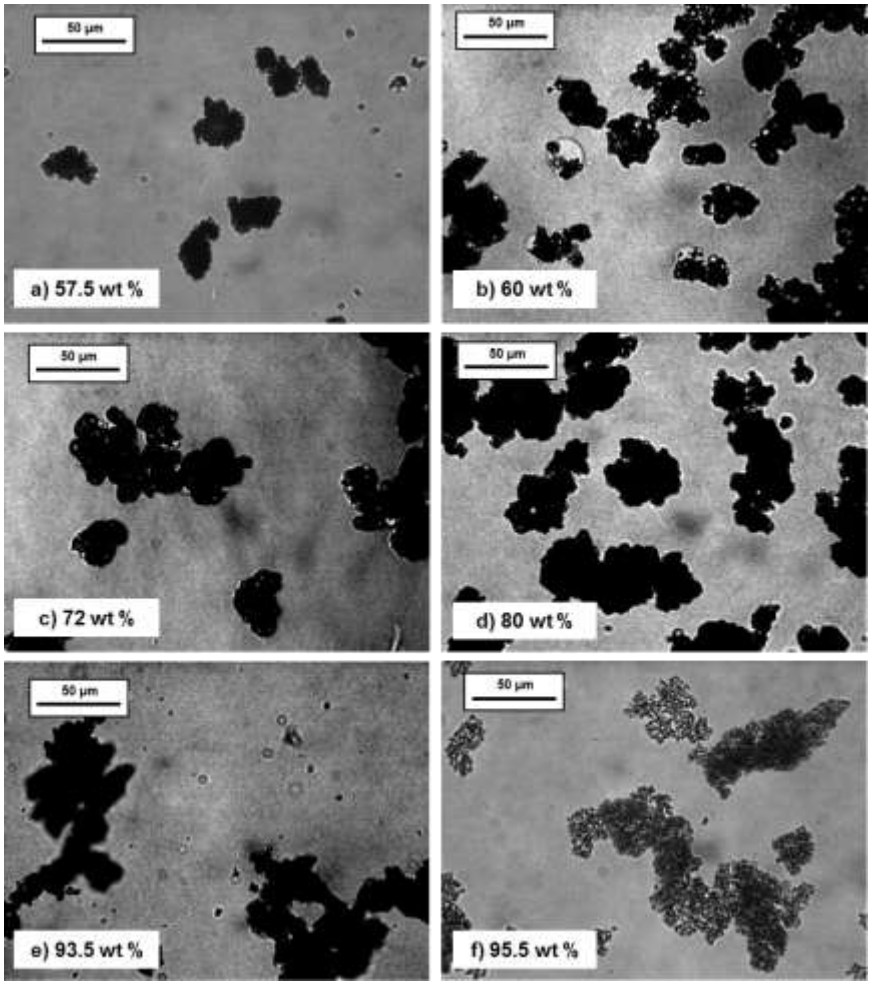

Figure 3.9. Micrographs of asphaltene aggregates from *n*-heptane diluted WC-B-B2 bitumen after 1 hour mixing at 195 rpm.

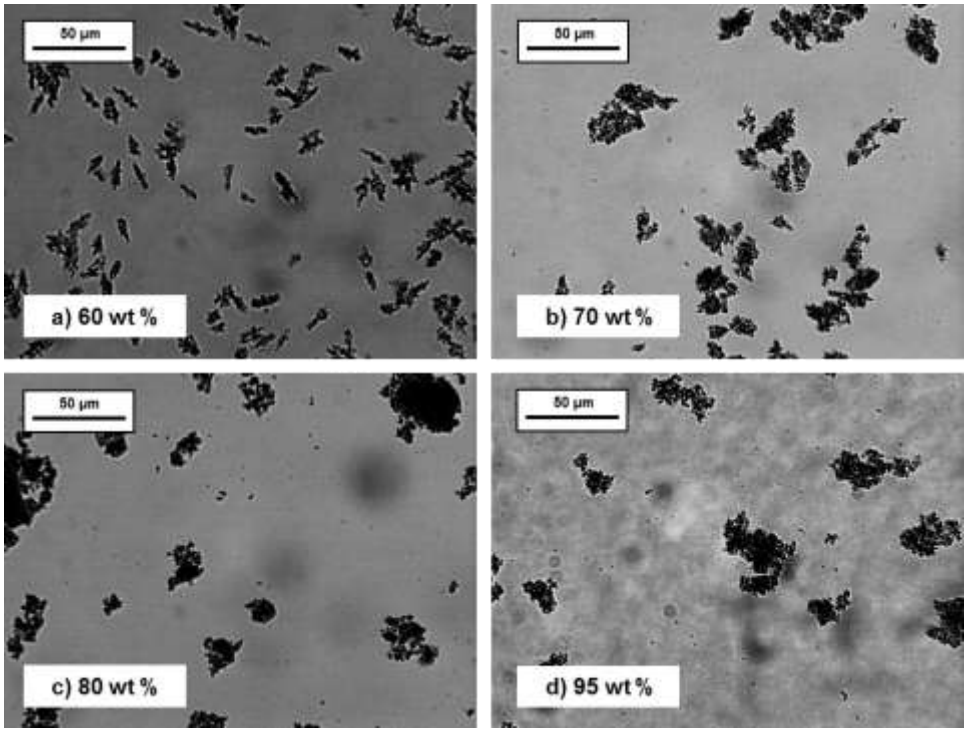

Figure 3.10. Images of asphaltene aggregates from *n*-heptane diluted WC-B-A3 bitumen after 1 hour mixing at 195 rpm.

Fractal Dimension

Figure 3.11 shows the fractal dimensions determined for *n*-heptane diluted WC-B-B2 bitumen (Figure 3.11a) and WC-B-A3 bitumen (Figure 3.11b) at 195 rpm. All of the calculated fractal dimensions ranged from 1 to 3 as expected for three-dimensional fractal structures (Mandelbrot, 1982). The fractal dimensions from the uncompacted volumes were smaller than the compacted volumes because the same mass of aggregates were occupying a larger space. The fractal dimensions increased with increasing precipitant content to a maximum and then decreased at high dilutions. The maximum fractal dimension for both bitumens occurred at a similar *n*-heptane content (70 to 80 wt%) where the largest diameters and highest asphaltene concentrations were observed.

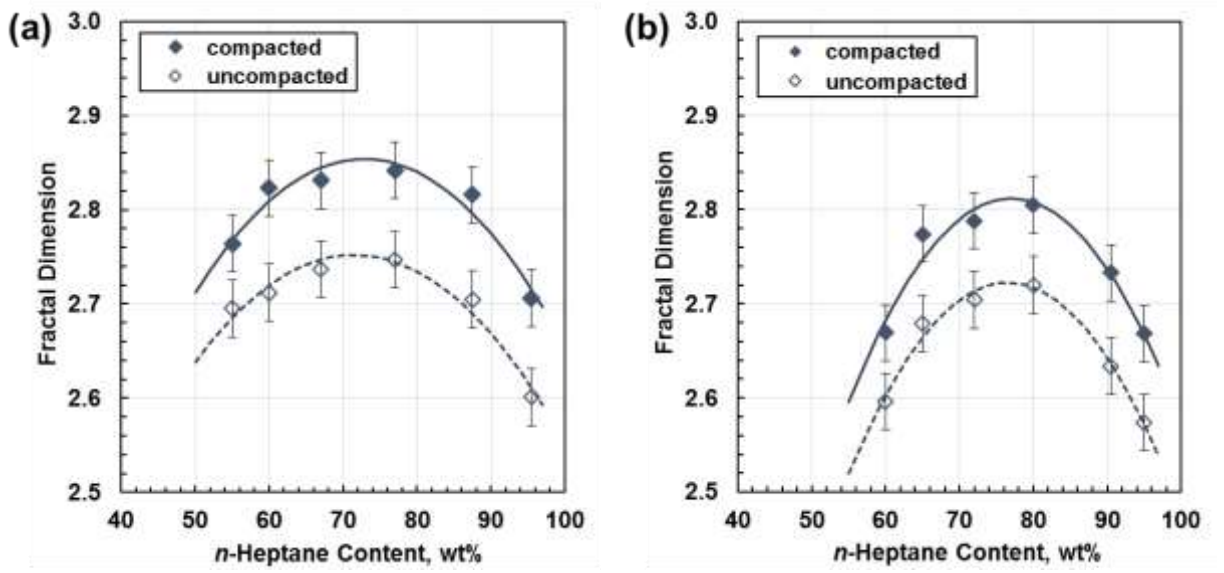

Figure 3.11. Fractal dimensions from sediment volumes at 195 rpm and 21ºC. Compacted and uncompacted curves give the estimated range for D_f. (a) *n*-heptane diluted WC-B-B2; (b) *n*-heptane diluted WC-B-A3. Lines are provided as visual aids.

The fractal dimensions in Figure 3.11 are consistent with the floc structures shown in Figures 3.9 and 3.10. As shown in Figure 3.12, fractal dimensions close to 2 indicate the presence of either planar structures or highly porous material. As fractal dimension increases, structures become more three-dimensional and less porous. The aggregates formed from WC-B-B2 bitumen just above the onset are rounded structures with a fractal dimension of approximately 2.7 and are likely planar structures. At intermediate *n*-heptane contents, the aggregates are more compact with a fractal dimension of approximately 2.8. At higher *n*-heptane contents, the aggregates appear to be three-dimensional rather than planar but have looser, branched structures and the fractal dimension is lower. The trends for the aggregates from the WC-B-A3 bitumen are similar except that the aggregates formed near the onset are more linear in structure and the aggregates formed at higher dilution are slightly looser.

One potential issue affecting the accuracy of the results is the diameter of the primary units used to calculate the fractal dimension (See Eq. 2.9). In this study, the diameter of the primary units was set at 2.5 nm, the value reported by Mostowfi *et al*. (2009) and used elsewhere (Maqbool *et*

al., 2011; Tavakkoli *et al.*, 2016). However, the size of the asphaltene nanoaggregates may be as large as 50 nm and may increase with increasing *n*-alkane content (Hurtado *et al.*, 2011). Given this uncertainty in the diameter of the primary units, a sensitivity analysis was performed. Increasing the diameter of the primary unit to 10 and 100 nm decreased the fractal dimensions by 0.01 and 0.09, respectively, a deviation of less than 4%. Calculations starting with detectable particle sizes (approximately 1 μm) as primary units (Daneshvar, 2005; Shafiee, 2014) will predict even lower fractal dimensions. In Chapter 6, the definition of the diameter of the primary particles is reevaluated and the values for the fractal dimensions are updated to be used in the precipitation/aggregation and settling models. The fractal dimensions decreased by about 0.15 units compared to the values shown in Figure 3.11, but the tendencies discussed here are maintained. A detailed discussion on the primary particle diameters is presented in Section 4.3.4.

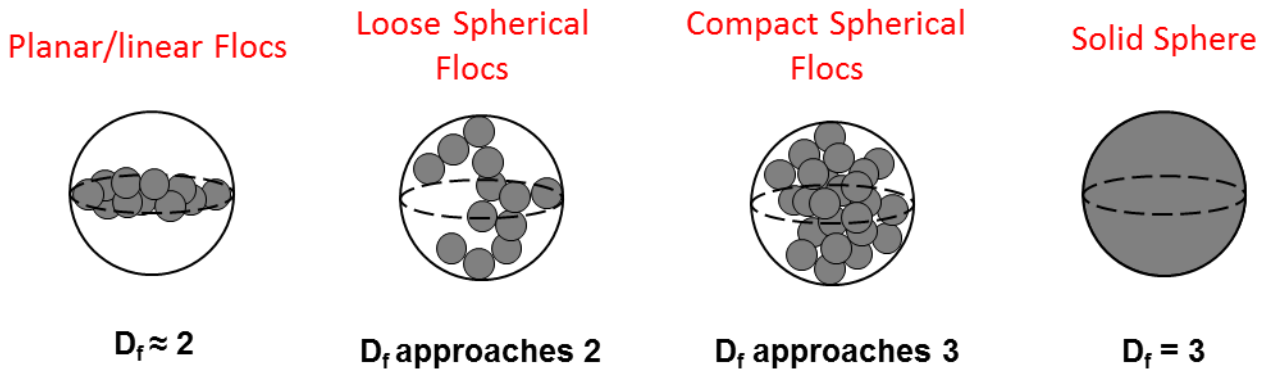

Figure 3.12. Representations of aggregate structures as a function of their fractal dimension.

Effect of Shear Rate and Time on Fractal Dimension

Figures 3.13a shows the effect of shear on the fractal dimension of aggregates in mixtures of *n*-heptane and WC-B-B2 bitumen. At any given *n*-heptane content, the fractal dimensions at 275 rpm and 330 rpm were nearly identical to the fractal dimension at 195 rpm. In other words, the fractal dimension of the asphaltene aggregates is shear insensitive. Data at different mixing conditions were not collected for the WC-B-A3 bitumen due to time constraints.

Figure 3.13b shows the evolution of fractal dimensions over time for aggregates in mixtures of *n*-heptane and WC-B-B2 bitumen near the onset (60 wt% *n*-heptane) and at high dilution (95 wt% *n*-heptane). The samples were prepared as discussed in Section 2.3, stirred at 195 rpm for the specified time, and then poured in a graduated cylinder and the sediment volumes measured. The first data point corresponds to a mixing time of 15 minutes and therefore no information is available on the behavior of the fractal dimension in the first minutes after the aggregates are formed. As expected for shear insensitive aggregates, no changes in the fractal dimension were observed for the duration of the experiment.

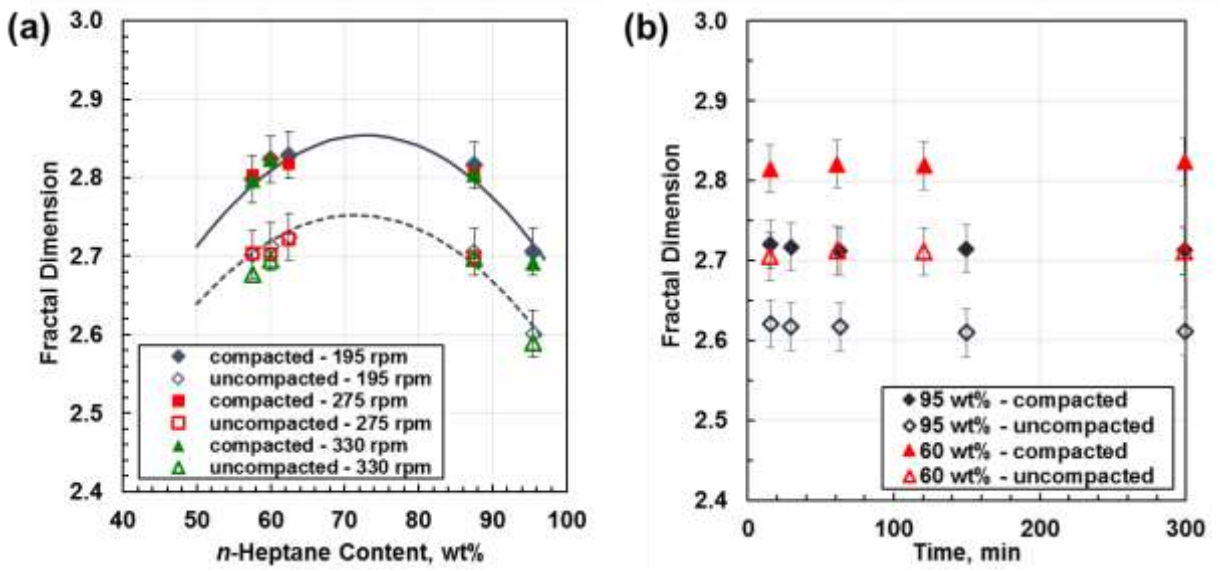

Figure 3.13. The effects of shear rate (a) and time (b) on the fractal dimension of asphaltene aggregates (*n*-heptane diluted WC-B-B2 bitumen) at 21ºC. The lines are visual aids.

3.2.4 Nature of Asphaltene Aggregates

Two key observations from the data reported in Sections 3.2.1 and 3.2.2 are that:

1. the asphaltene aggregates have compact structures near the onset of precipitation but looser structures at high dilution.
2. the compact aggregates are shear insensitive while the looser structures are somewhat shear sensitive.

A hypothesis is that asphaltenes aggregates are not flocs but are fused structures that in some cases can be shattered under sufficient shear. To test this hypothesis, the size of the aggregates in mixtures of WC-B-B2 and *n*-heptane were measured over a sequence of high and low shear rates. If the aggregates are capable of flocculating, then a switch from high shear to low shear would result in larger aggregates and a switch from low shear to high shear would result in smaller aggregates.

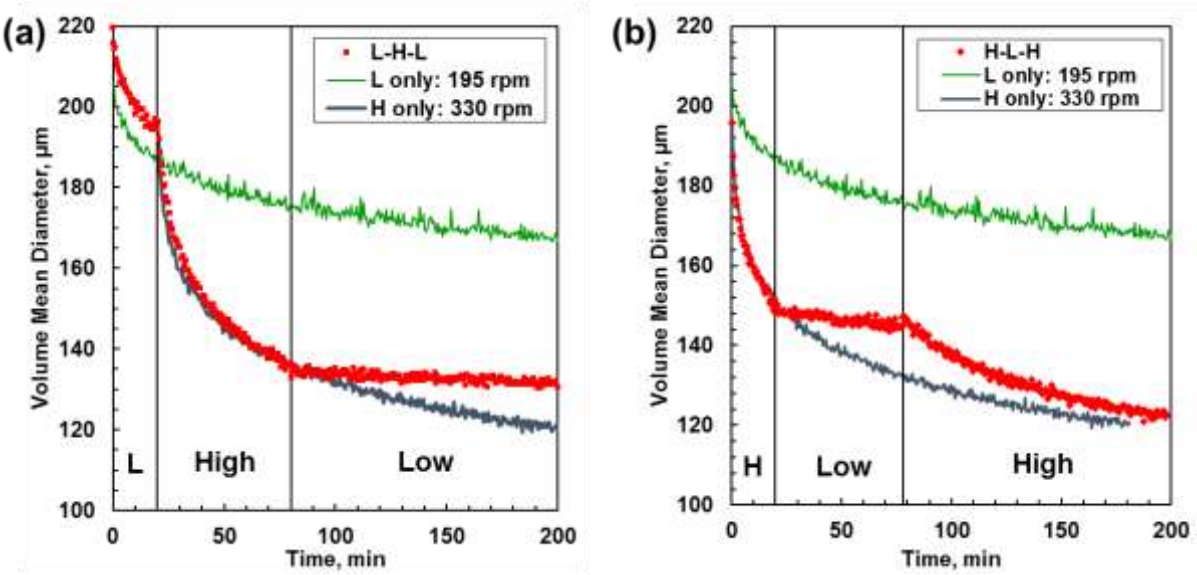

Figure 3.14. Effect of changing shear rate on volume mean diameter of asphaltene aggregated in a mixture of WC-B-B2 and *n*-heptane (95.5 wt%): a) low-high-low shear sequence; b) high-low-high shear sequence. Low shear = 195 rpm mixer speed; high shear = 330 rpm.

First consider the effect of changing shear rate on aggregates in WC-B-B2 bitumen at a high *n*-heptane content of 95.5 wt%. Recall that the aggregates at this condition shattered under sufficient shear. Figure 3.14a shows that as the shear rate increased (from a mixer speed of 195 to 330 rpm), the volume mean diameter decreased (and while not shown here, the number count increased); that is the aggregates were shattering. In fact, the change in volume mean diameter at the higher shear rate closely match the change in diameter over time observed when mixing at only 330 rpm. When the shear rate was reset back to the original mixing speed, the aggregate size became constant. Figure 3.14b confirms that reducing the shear rate resulted in a constant aggregate size. When the

shear rate increased, the volume mean diameter decreased again indicating that shattering has recommenced. Not once did the aggregate size increase with a reduction in shear; hence, there is no evidence for flocculation.

Figure 3.15 shows the same sequence of shear rates for WC-B-B2 bitumen at a relatively low *n*-heptane content of 57.5 wt%. Recall that at *n*-heptane contents below 65 wt% the aggregates sizes were almost the same at all shear conditions. Figure 3.15 demonstrates that the volume mean diameter (and the number count) did not change when the shear rate changed either to higher or lower shear rates. One apparent exception was the small increase in the measured volume mean diameter in Figure 3.15a when the shear rate was increased. However, this increase is attributed to a measurement artifact for the following reasons: 1) increased shear rate is expected to decrease the aggregate size; 2) there was no step change in the number count (Figure 3.15b) as would be expected if flocculation was occurring; 3) the volume mean diameter instantly returned to the original value when the shear rate was reduced again. It is more likely that the increased impeller speed redistributed the aggregates so that more of larger aggregates passed in front of the laser probe.

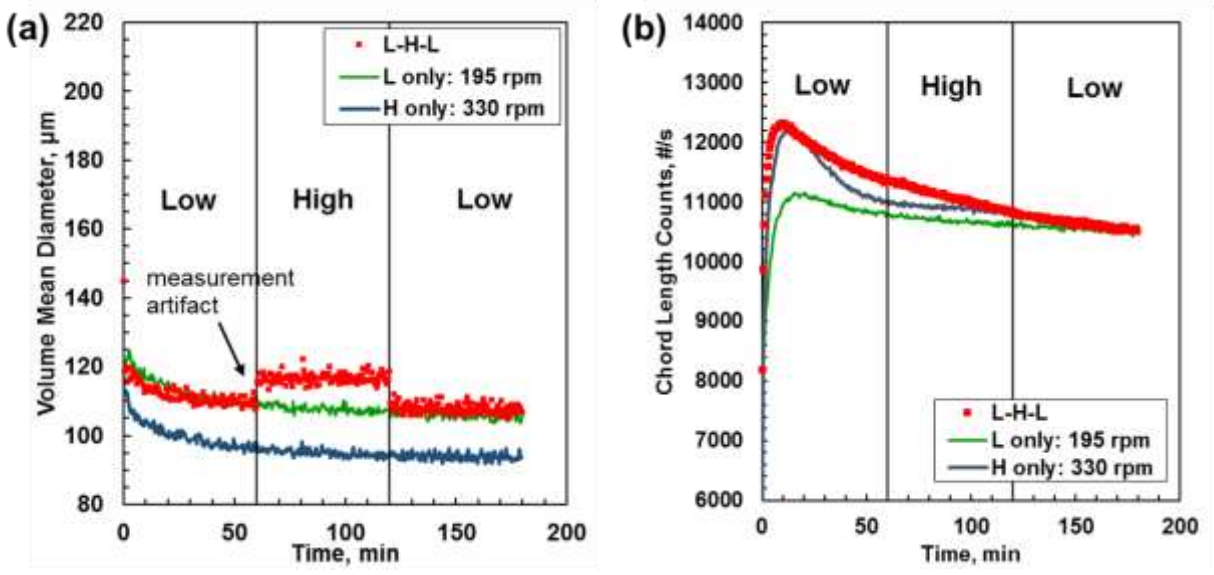

Figure 3.15. Effect of low-high-low shear sequence on volume mean diameter (a) and number count (b) of asphaltene aggregates in a mixture of WC-B-B2 and *n*-heptane (57.5 wt%). Low shear = 195 rpm mixer speed; high shear = 330 rpm.

Figure 3.15a also shows that the volume mean diameter of the aggregates decreases slightly over time. At first glance, this decrease could be taken as evidence of shattering. However, Figure 3.15b shows that the number count also decreased continuously over time. Shattering would increase the number count. It is more likely that some settling occurred over time decreasing the number of large aggregates detected. Therefore, it was concluded that neither flocculation nor shattering was observed at *n*-heptane contents below 65 wt%.

3.2.5 Nucleation/Growth, Flocculation, and Stickiness

The formation of fused particles is consistent with a nucleation and growth mechanism. However, the structure of the aggregates formed at high dilution appear to be collections of smaller particles, more consistent with flocculation. In addition, the initial aggregate size decreases with increased shear as expected with flocculation and shattering. One hypothesis is that growth and flocculation occur simultaneously. As particles nucleate and grow, they can collide with other particles, flocculate, and continue to grow as an aggregate. The aggregates formed near the onset are dominated by the growth mechanism or flocculate early in the growth process and form more compact strongly fused structures that are resistant to shear. The aggregates formed at high dilution flocculate late in the growth process and form looser more fragile structures that can be partially shattered with sufficient shear.

One question that arises is: if the growing particles can flocculate while forming why does the flocculation stop later on? It is possible that the molecules within and particularly on the surface of the aggregates rearrange over time such that active functional groups (with high cohesion forces) become embedded and therefore unavailable for further interaction with other aggregates (Wang *et al.,* 2012; Natarajan *et al.,* 2014). Surface force data suggested that asphaltene layers progressively dwindle over time (30 minutes) in the presence of a poor environment (pure *n*-heptane) and atomic force microscopy showed that morphological changes occur over this time, most likely polar branches reorienting and pointing away from the bulk fluid (Natarajan *et al.,* 2014).

To test this hypothesis, SFA was applied to investigate the adhesion of WC-B-B2 and WC-B-A3 asphaltenes adsorbed on surfaces *in situ* and in real time. The surfaces were mica conditioned in 500 ppm asphaltene solutions of 50 vol% toluene and 50 vol% heptane (heptol). Figures 3.16(a,b) and 3.17(a,b) show the force-distance curves for the two respective asphaltenes. The adsorbed asphaltene layer forms in less than 2 min. This layer consists of surface active asphaltene molecules that adsorb onto the mica as monomers or nanoaggregates to form a compact film (Zhang *et al.*,2016; Wang *et al.*, 2010; Natarajan *et al*., 2014). Subsequently, with the increase of aging time from 10 to 90 min, the asphaltene layer thickness increases continuously reaching thickness of 11.5 nm (WC-B-B2) and 10.0 nm (WC-B-A3). However, the growth rate slows down, indicating that less asphaltenes from the bulk solution could adsorb onto the growing asphaltene layer over time.

The adhesion force was determined from the measured force curves between the asphaltene layers during separation (Figures 3.16b and 3.17b). Figures 3.16c and 3.17c show that, over the course of 30 minutes, the normalized adhesion force (F_{ad}/R) decreased from 9.3 mN/m (W_{ad} = 2.0 mJ/m^2) to 1.3 mN/m (W_{ad} = 0.26 mJ/m^2) for WC-B-B2 and from 9.5 mN/m (W_{ad} = 2.0 mJ/m^2) to 2.6 mN/m (W_{ad} = 0.55 mJ/m^2) for WC-B-A3. The adhesion for both cases decreased to less than 1 mN/m after 90 min. The gradually weakening of the adhesion between the adsorbed asphaltene layers is consistent with a conformational change of asphaltene molecules on the surface of the aggregate layer. Functional groups and segments in asphaltene molecules with relatively higher adhesion would tend to embed into the asphaltene layer while other chains or groups which have more affinity to the bulk solvent environment would extend into the solvent. The extended groups likely provide steric hindrance between the approaching asphaltene films reducing their adhesion. The generated steric hindrance could also impede further adsorption of asphaltene molecules onto the "rearranged" asphaltene layer, consistent with the layer thickness becoming stable over time. The SFA results confirm the hypothesis that the precipitated WC-B-B2 and WC-B-A3 asphaltenes lose their stickiness over time. A loss of stickiness could explain why asphaltene aggregates stop flocculating after aging.

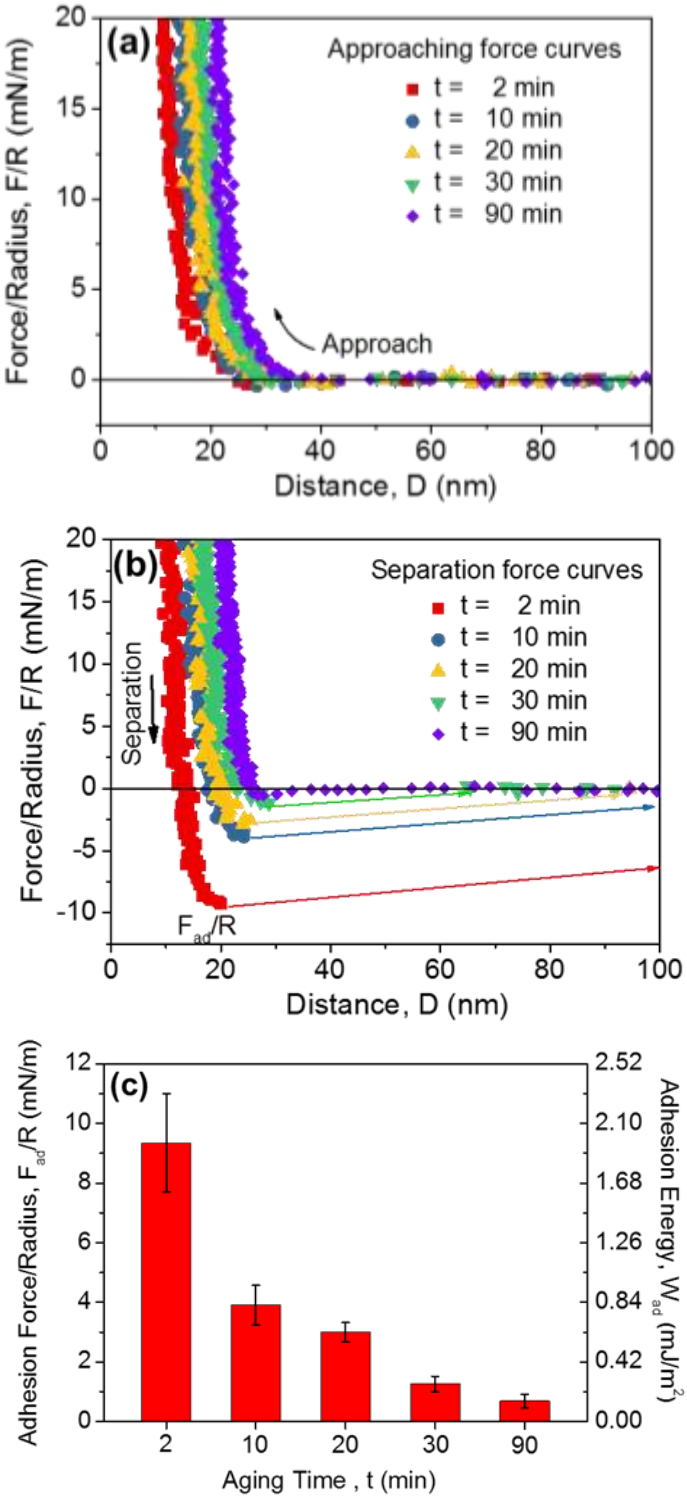

Figure 3.16. Forces of WC-B-B2 asphaltene layers interacting in heptol: a) force-distance profile for approach; b) force-distance profile for separation after approach; c) normalized adhesion force (F_{ad}/R) and adhesion energy (W_{ad}) as a function of the adsorption time (t).

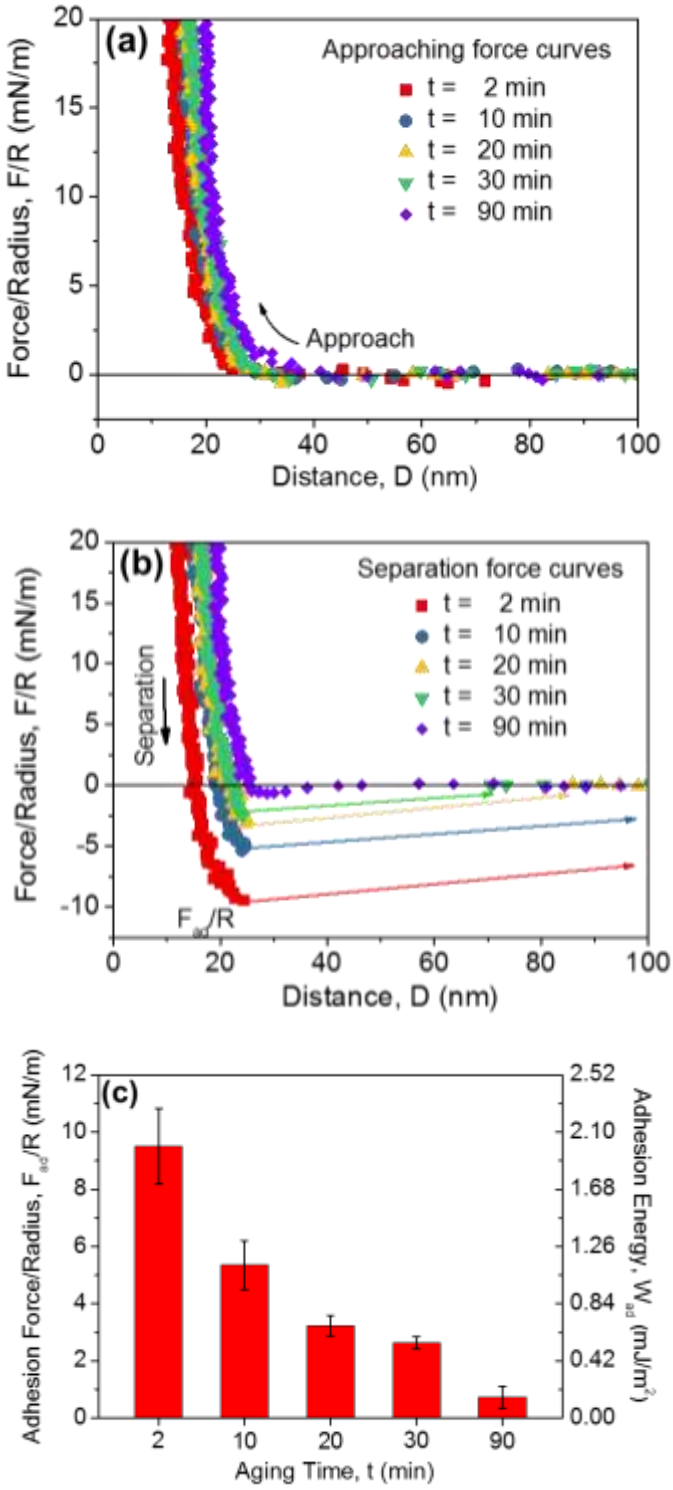

Figure 3.17. Forces of WC-B-A3 asphaltene layers interacting in heptol: a) force-distance profile for approach; b) force-distance profile for separation after approach; c) normalized adhesion force (F_{ad}/R) and adhesion energy (W_{ad}) as a function of the adsorption time (t).

3.2.6 Effects of *n*-Heptane Content and Shear on Asphaltene Aggregates

Effect of n-Heptane Content on Initial Aggregate Size

The results in Section 3.2.1 demonstrate that the aggregate size reaches a plateau value at an *n*-heptane content of approximately 80 wt% (Figure 3.6). If the initial particle size is dictated by traditional flocculation (that is, a balance between flocculation and shattering), then the volume mean diameter is expected to scale to the number of primary particles and therefore to the concentration of precipitated asphaltenes. The expected trend is less obvious with a nucleation and growth mechanism because both nucleation and growth rates are expected to increase with increasing particle concentration. The particle size will depend on the relative magnitude of each rate: slow nucleation and fast growth will give large particles and *vice versa*. Nonetheless, low concentrations are expected to give small particles.

Figure 3.18a shows the initial volume mean diameter versus particle concentration for each *n*-heptane diluted bitumen. The initial volume mean diameters can only partly be explained in terms of the precipitate concentrations. The larger volume mean diameters in the WC-B-B2 bitumen compared with the WC-B-A3 bitumen are consistent with the higher precipitate concentration but do not correlate only to the precipitate concentration. The increase in aggregate size with increasing *n*-heptane content is also consistent with the increasing precipitate concentration but only up to about 70 wt% *n*-heptane. Above 70 wt% *n*-heptane, the aggregate size continued to increase even though the precipitate concentration decreased (inflection points on Figure 3.18a).

It appears that a second factor affects asphaltene aggregation, such as the compatibility of the precipitated asphaltenes with the surrounding fluid. A mixture with a large proportion of precipitant will have a low solubility parameter compared with the asphaltenes (Akbarzadeh *et al.*, 2005). The large difference in solubility parameter between the asphaltenes and the surrounding medium is likely to increase the relative attraction between asphaltenes and hence to create larger aggregates. In other words, interaction forces between asphaltene-asphaltene molecules (or nanoaggregates) are expected to be larger in a poor solvent environment.

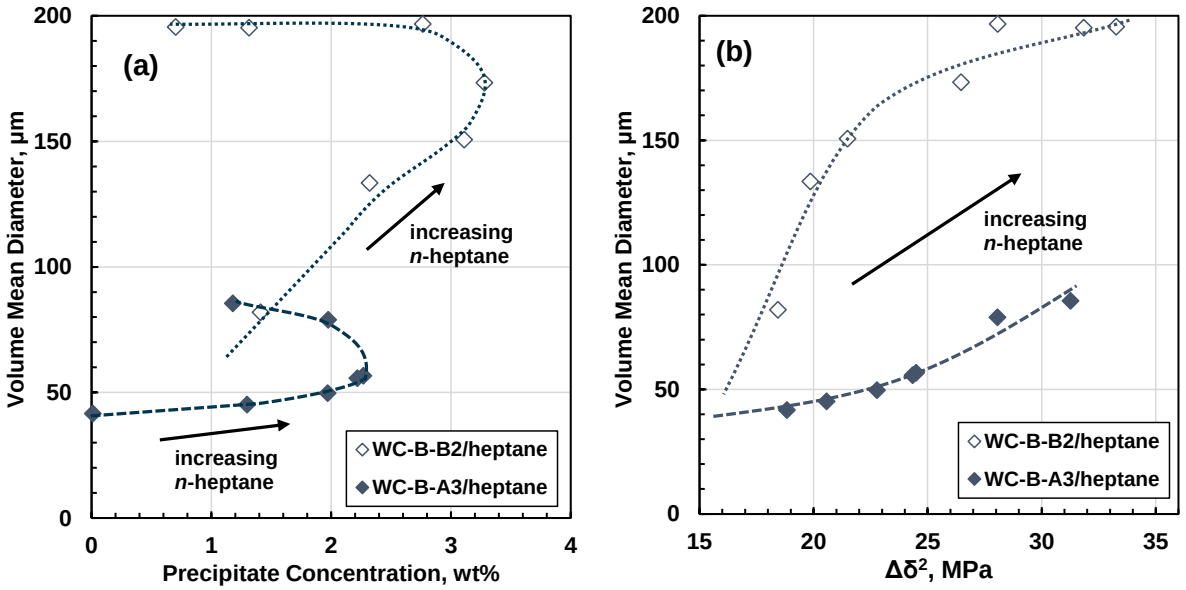

Figure 3.18. Variation of the initial volume mean diameter of the asphaltene aggregates with: a) the concentration of precipitated asphaltenes; b) asphaltene yield (amount of precipitate). Symbols are data for *n*-heptane diluted bitumen at 195 rpm and 21ºC; lines are provided as a visual aid.

Zhang *et al*. (2016) showed that interactions between asphaltenes change from pure repulsion in a good solvent (toluene) to weak adhesion in a poor medium (heptol) and that the adhesion force increased with increasing *n*-heptane content. Wang *et al.* (2010) correlated the adhesion force with the interaction parameter ($\chi \sim \Delta\delta^2$ where $\Delta\delta$ is the difference between the solubility parameter of the asphaltenes and the medium), as an indicator of the quality of the fluid medium. At low χ values (good solvent), adhesion forces between asphaltenes were almost null and rapidly increased with increasing *n*-heptane content. At intermediate *n*-heptane contents (between volume fraction of toluene from 0.2 to 0.7, corresponding to χ = 0.3 to 1) nearly constant adhesion was found and increased by three times at χ >1. These results suggest that at high *n*-heptane contents (more than 65 wt% *n*-heptane for WC-B-B2 bitumen and 70 wt% *n*-heptane for the WC-B-A3) the asphaltene-asphaltene attraction forces increase significantly and therefore the aggregate size could continue to increase even though the precipitate concentration decreases. Figure 3.18b shows that the initial volume mean diameter did indeed increase monotonically with $\Delta\delta^2$ for each *n*-heptane diluted bitumen. However, the larger aggregate sizes in the WC-B-B2 bitumen versus the WC-B-A3 bitumen cannot be explained by the solubility parameters alone. The reason for the difference is

not known at this time but could indicate a difference between the asphaltenes from each oil; for example, the WC-B-B2 asphaltene nanoaggregates may stick to each other more readily when they collide above the onset of precipitation. The SFA measurements (Figures 3.16a and 3.17a) show a relatively thicker confined asphaltene layer (~ 11.5 nm) of WC-B-B2 asphaltenes adsorbed on the surface compared to that of the WC-B-A3 asphaltene (~ 10 nm). The thicker layer is consistent with greater initial adsorption and likely initial adhesion.

Effect of n-Heptane Content on Fractal Dimension

The results reported in Section 3.2.2 show that the fractal dimension reaches a maximum at an *n*-heptane content of approximately 75 wt% (Figure 3.11) near where the concentration of precipitated asphaltenes reaches a maximum (Figure 3.2b). Figure 3.19 confirms that the fractal dimension correlates to the precipitate concentration for both bitumens. Near the onset, the precipitate concentration is low and little or early flocculation favours the formation of small linear or planar aggregates with low fractal dimensions. At *n*-heptane contents of approximately 75 wt%, the precipitate concentration reaches a maximum and more primary units will be available in the system. A simultaneous nucleation/growth and flocculation process favours the formation of spherical and more compact (higher fractal dimension) aggregates. At higher dilutions, flocculation late in the growth process favours the formation of fewer but larger, loose aggregate structures. Hence, the correlation may be fortuitous in that the reasons for the change in fractal dimension are different at low versus high concentration. Nonetheless, the correlation may be consistent for different bitumens. As will be discussed in Chapter 6, this correlation can be improved by considering the diffusion of asphaltene nanoaggregates/particles through the fluid media.

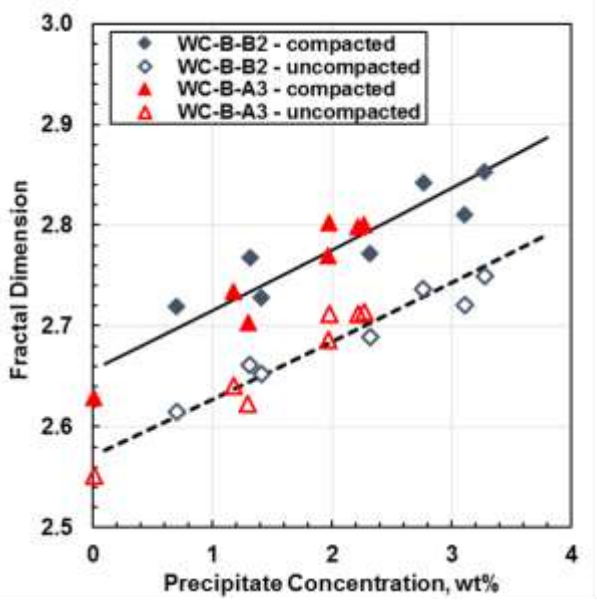

Figure 3.19. Effect of the asphaltene concentration on the fractal dimension of aggregates. Symbols are data for *n*-heptane diluted bitumen at 195 rpm and 21ºC; lines are provided as a visual aid.

3.2.7 Effect of Shear on Aggregate Size

Figure 3.20 shows that shear starts to have an impact on the initial size of the aggregates above the transition between laminar and turbulent flow; that is, above a Reynold's number of approximately 2000 (Norwood and Metzner, 1960). The Reynold's number for this system is defined as $Re = D_{im} \cdot \rho_m \cdot v/\mu_m$, where D_{im} is the impeller diameter (50 mm) and v is the impeller speed. The Reynold's number at which the transition occurs increases with increasing *n*-heptane content, consistent with stronger adhesion forces at higher *n*-heptane contents. Hence, at initial conditions, the effect of shear appears to depend mainly on the stickiness of the aggregates. This effect is addressed in detail later (Section 4.3.4).

Once the aggregates have formed, they lose their stickiness and the effect of shear depends on their structure. Near the onset of precipitation, the aggregates are compact fused structures. Shear has little effect on their size. At higher dilutions, the looser aggregate structures are more easily shattered and therefore their size is shear sensitive. Interestingly, the fractal dimension is not shear sensitive at any conditions even when the structures are broken into fragments. In other words, the

fragments have the same fractal dimension as the original structure, consistent with the fractal assumption.

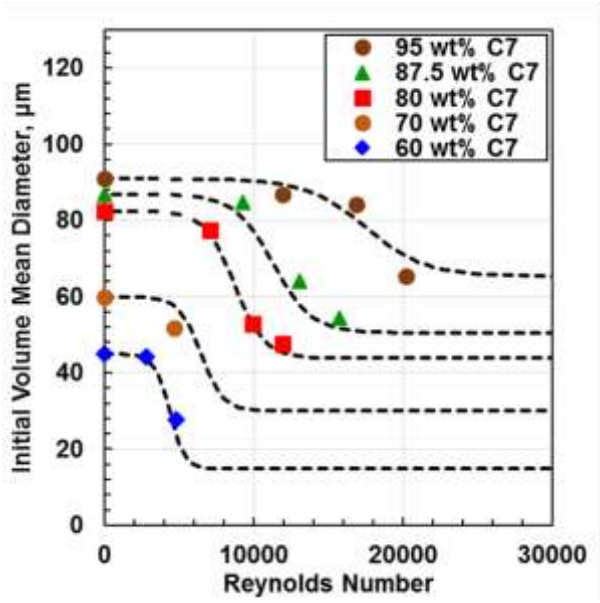

Figure 3.20. Effect of shear on the initial diameter of asphaltene aggregates from *n*-heptane diluted WC-B-A3 bitumen at 21ºC. Dashed lines are provided as visual aid but are close to a sigmoid function.

3.3 Conclusions

Asphaltene aggregate sizes and structures were investigated for two Western Canadian bitumen samples diluted with *n*-heptane. Above the onset of precipitation, the initial aggregate size increases with increasing *n*-heptane content reaching a plateau value at approximately 80 wt% *n*-heptane. The initial aggregates size is smaller at higher shear rates. The fractal dimension of the aggregates reaches a maximum value at approximately 75 wt% *n*-heptane. Near the onset of precipitation, the aggregates have compact structures. At high dilution, their structures are looser. Once formed, the aggregates near the onset are insensitive to shear while the aggregates formed at high dilution can be shattered into smaller sizes at sufficient shear. The results are consistent with a combined mechanism of nucleation/growth and flocculation for aggregate formation. The aggregates are initially sticky allowing for flocculation. They lose their stickiness over time so that they no longer flocculate and can only be shattered (if loosely structured).

The results have several implications for settling processes involving precipitated asphaltenes. Settling rates will be highest for large compact aggregates; that is, at large volume mean diameters and high fractal dimensions. Therefore, the settling rate is expected to reach a maximum at 70 to 80 wt% *n*-heptane. The expected maximum in the settling rate approximately coincides with the maximum in the precipitated asphaltene concentration. Since the aggregate size and fractal dimension are relatively shear insensitive, the settling rate will not be significantly altered by upstream shear conditions. However, some reduction in aggregate size and settling rates will occur if the mixture is sheared at *n*-heptane contents above the maximum settling rate condition.

3.4 Chapter References

Agrawal, P.; Schoeggl, F.F.; Satyro, M.A.; Taylor, S.D.; Yarranton, H.W. (2012). Measurement and Modeling of the Phase Behavior of Solvent Diluted Bitumens. *Fluid Phase Equil*., 334, 51-64.

Agrawala, M.; Yarranton, H.W. (2001). An Asphaltene Association Model Analogous to Linear Polymerization. *Ind. Eng. Chem. Res*., 40 (21), 4664-4672.

Akbarzadeh, K.; Alboudwarej, H.; Svrcek, W.Y.; Yarranton, H.W. (2005). A Generalized Regular Solution Model for Asphaltene Precipitation from *n*-Alkane Diluted Heavy Oils and Bitumens. *Fluid Phase Equil*., 232, 159-170.

Allen, T. (2003). *Powder Sampling and Particle Size Determination*, Elsevier, Amsterdam, The Netherlands.

Angle, C.W.; Long, Y.; Hamza, H.; Lue, L. (2006). Precipitation of Asphaltenes from Solvent-diluted Heavy Oil and Thermodynamic Properties of Solvent-diluted Heavy Oil Solutions. *Fuel*, 85, 492-506.

Calles, J. A.; Dufour, J.; Marugán, J.; Peña, J. L.; Giménez-Aguirre, R.; Merino-García, D. Properties of Asphaltenes Precipitated with Different *n*-Alkanes. (2008). A Study to Assess the Most Representative Species for Modeling. *Energy Fuels*, 2 (22), 763-769.

Daneshvar, S. (2005). Asphaltene Flocculation in Diluted Bitumen Systems. MSc. Thesis. University of Calgary.

Eyssautier, J.; Frot, D.; Barré, L. (2012). Structure and Dynamics Properties of Colloidal Asphaltene Aggregates. *Langmuir*, 28 (33), 11997-12004.

Eyssautier, J.; Levitz, P.; Espinat, D.; Jestin, J.; Gummbel, J.; Grillo, I.; Barré, L. (2011). Insight into Asphaltene Nanoaggregate Structure Inferred by Small Angle Neutron and X-ray Scattering. *J. Phys. Chem. B.*, 115 (21), 6827-6837.

Ferworn, K.A.; Svrcek, W.Y.; Mehrotra, A.K. (1993). Measurement of Asphaltene Particle Size Distributions in Crude Oils Diluted with *n*-Heptane. *Ind. Eng. Chem. Res*., 32, 955-959.

Gray, M.R. (2015). *Upgrading Oilsands Bitumen and Heavy Oil*, University of Alberta Press, Edmonton, AB.

Hoepfner, M.P.; Vilas Boas Favero, C.; Haji-Akbari, N.; Fogler, H.S. (2013). The Fractal Aggregation of Asphaltenes. *Langmuir*, 29 (28), 8799-8808.

Hurtado, J.L.A.; Chodakowski, M.; Long, B.; Shaw, J.M. (2011). Characterization of Physically and Chemically Separated Athabasca Asphaltenes Using Small-Angle X-ray Scattering. *Energy Fuels*, 25 (11), 5100-5112.

Johnston, K.A.; Schoeggl, F.F.; Satyro, M.A.; Taylor, S.D.; Yarranton, H.W. (2017). Phase Behavior of Bitumen and *n*-pentane. *Fluid Phase Equil*. 442, 1-19.

Kempkes, M.; Eggers, J.; Mazzotti, M. (2008). Measurement of Particle Size and Shape by FBRM and in situ Microscopy. *Chem. Eng. Sci*., 63 (19), 4656-4675.

Long, B.; Chodakowski, M.; Shaw, J.M. (2013). Impact of Liquid-Vapor to Liquid-Liquid-Vapor Phase Transitions on Asphaltene-Rich Nanoaggregate Behavior in Athabasca Vacuum Residue + Pentane Mixtures. *Energy Fuels*, 27, 1779-1790.

Mandelbrot, B. (1982). *The Fractal Geometry of Nature*. W.H. Freeman and Co., New York, NY.

Maqbool, T.; Balgoa, A.T.; Fogler, H.S. (2009). Revisiting Asphaltene Precipitation from Crude Oils: A Case of Neglected Kinetic Effects. *Energy Fuels*, 23 (7), 3681-3686.

Maqbool, T.; Raha, S.; Hoepfner, M.P.; Fogler, H.S. (2011). Modeling the Aggregation of Asphaltene Nanoaggregates in Crude Oil-Precipitant Systems. *Energy Fuels*, 25, 1585-1596.

Mostowfi, F.; Indo, K.; Mullins, O.C.; McFarlane, R. (2009). Asphaltene Nanoaggregates Studied by Centrifugation. *Energy Fuels*, 23 (3), 1194-1200.

Mullins, O.C.; Sabbah, H.; Eyssautier, J.; Pomerantz, A.E.; Barre, L.; Andrews, A.B.; Ruiz-Morales, Y.; Mostowfi, F.; McFarlane, R.; Goual, L.; Lepkowicz, R.; Cooper, T.;

Orbulescu, J.; Leblanc, R.M.; Edwards, J.; Zare, R.N. (2012). Advances in Asphaltene Science and the Yen-Mullins Model. *Energy Fuels*, 26 (7), 3986-4003.

Natarajan, A.; Kuznicki, N.; Harbottle, D.; Masliyah, J.; Zeng, H.; Xu, Z. (2014). Understanding Mechanisms of Asphaltene Adsorption from Organic Solvent on Mica. *Langmuir*, 30 (31), 9370-9377.

Norwood, K.W.; Metzner, A.B. (1960). Flow Patterns and Mixing Rates in Agitated Vessels. *AIChE J.*, 6 (3), 432-437.

Pal, K.; Branco, L.P.N.; Heintz, A.; Choi, P.; Liu, P.; Seidl, P.R.; Gray, M.R. (2015). Performance of Solvent Mixtures for Non-aqueous Extraction of Alberta Oil Sands. *Energy Fuels*, 29 (4), 2261-2267.

Park, S.J.; Mansoori, G.A. (1988). Aggregation and Deposition of Heavy Organics in Petroleum Crudes, *Energy Sources*, 10 (2), 109-125.

Rahmani, N.; Dabros, T.; Masliyah, J.H. (2005a). Online Optical Monitoring of Asphaltene Aggregation. *Ind. Eng. Chem. Res*., 44(1), 2005, 75-84.

Rahmani, N.; Dabros, T.; Masliyah, J.H. (2005b). Fractal Structure of Asphaltene Aggregates. *J. Colloid Interface Sci*., 285 (2), 599-608.

Rahmani, N.; Dabros, T.; Masliyah, J.H. (2005c). Settling Properties of Asphaltene Aggregates. *Energy Fuels*, 19 (3), 1099-1108.

Rassandama, H.; Sahimi, M. (1996). Asphalt Flocculation and Deposition: II. Formation and Growth of Fractal Aggregates, *AIChE J*., 42 (12), 3319-3332.

Rastegari, K.; Svrcek, W.Y.; Yarranton, H.W. (2004). Kinetics of Asphaltene Flocculation. *Ind. Eng. Chem. Res*., 43, 6861-6870.

Romanova, U.G.; Valinasab, M.; Stasiuk, E.N.; Yarranton, H.W. (2006). The Effect of Oil Sands Bitumen Extraction Conditions on Froth Treatment Performance. *J. Can. Pet. Technol*., 45 (9), 36-45.

Seifried, C. M.; Crawshaw, J.; Boek, E.S. (2013). Kinetics of Asphaltene Aggregation in Crude Oil Studied by Confocal Laser-Scanning Microscopy. *Energy Fuels*, 27 (4), 1865-1872.

Shafiee, M. (2014). Kinetics of Asphaltene Precipitation and Flocculation from Diluted Bitumen. MSc. Thesis, University of Calgary.

Tavakkoli, M.; Chen., A.; Sung, C.; Kidder, K.M.; Lee., J.J.; Alhassan, S.M.; Vargas, F.M. (2016). Effect of Emulsified Water on Asphaltene Instability in Crude Oils. *Energy Fuels*, 30 (5), 3676-3686.

Tipman, R.N.; Long, Y. (1999). Solvent Process for Bitumen Separation from Oil Sands Froth. US Patent 5,876,592.

Wang, J.; Opedal, N.; Lu, Q.; Xu, Z.; Zeng, H.; Sjoblom, J. (2012). Probing Molecular Interactions of an Asphaltene Model Compound in Organic Solvents Using a Surface Forces Apparatus (SFA). *Energy Fuels*, 26 (5), 2591-2599.

Wang, S.; Liu, J.; Zhang, L.; Masliyah, J.; Xu, Z (2010). Interaction Forces between Asphaltene Surfaces in Organic Solvents. *Langmuir*, 26 (1), 183-190.

Wiehe, I.A. (2008). *Process Chemistry of Petroleum Macromolecules*, CRC Press, Boca Raton, FL.

Wu, J.; Dabros, T. (2012). Process for Solvent Extraction from Oil Sand. *Energy Fuels*, 26 (2), 1002-1008.

Zhang, L.; Shi, C.; Lu, Q.; Liu, Q.; Zeng, H. (2016). Probing Molecular Interactions of Asphaltenes in Heptol Using a Surface Forces Apparatus: Implications on Stability of Water-in-Oil Emulsions. *Langmuir*, 32 (19), 4886-4895.

Chapter 4: Kinetics of Asphaltene Precipitation/Aggregation from Diluted Crude Oil

In this contribution[2], asphaltene precipitation kinetics were investigated for four crude oils with different asphaltene contents, each diluted with *n*-heptane at room conditions. The yields of precipitated asphaltenes (mass of precipitated asphaltenes divided by mass of bitumen in feed) were measured gravimetrically and the diameters of the aggregated asphaltene particles were measured using both microscopy and the focused beam reflectance method. The measurements were performed at anaerobic conditions. The data were first modeled with the geometric population balance proposed by Maqbool *et al.* (2011a). This approach matched the yield data but not the aggregate diameters, nor did it account for the rapid (almost instantaneous) precipitation and aggregation observed in heavy oils. The model was adapted to include a simultaneous nucleation/growth/aggregation mechanism as follows: 1) the primary particles size was increased to the micrometer scale; 2) the fraction of "instantaneously" unstable asphaltenes was explicitly accounted for; 3) a nucleation term was introduced for more slowly precipitating material; 4) the collision frequency was modified to include interparticle attraction, and; 5) the experimentally observed loss of interparticle adhesion over time was explicitly accounted for in the collision efficiency. Correlations were proposed for most of the model parameters. The minimum required inputs for the model are the temperature, precipitant content, and the equilibrium asphaltene yield. The proposed model matched both yield and aggregate size kinetic data from this study and the literature.

4.1 Introduction

Asphaltenes are defined as the crude oil components that are insoluble in *n*-alkanes such as *n*-pentane or *n*-heptane but are soluble in aromatic solvents such as toluene or benzene (Speight, 2006). It is well established that asphaltenes can precipitate upon a change in the composition, pressure, or temperature of the oil (Hirschberg *et al*., 1984; Hammami *et al*., 2000; Andersen and

[2] This chapter is based on the following published work: Duran, J.A.; Schoeggl, F.F.; Yarranton, H.W. (2019). Kinetics of Asphaltene Precipitation/Aggregation from Diluted Crude Oil. *Fuel,* 255, 115859.

Birdi, 1990; Andersen *et al*., 1998). At ambient conditions, asphaltenes can precipitate and grow to particle sizes of 1 μm or larger in diameter (Ferworn *et al*., 1993; Rastegari *et al*., 2004). At higher temperatures, they come out of solution as liquid droplets which tend to coalesce into a continuous liquid phase (Agrawal *et al*., 2012; Johnston *et al*., 2017). This study focuses on the precipitation of particles from precipitant (poor solvent) diluted crude oils at room temperature and pressure.

Asphaltene precipitation is generally viewed as a flow assurance issue in the oil industry but it is also a key step in several processes including solvent deasphalting in refineries and paraffinic froth treatment in mined oil sand processing (Long *et al*., 2004; Gray, 2015). Most previous work in this area has focused on the onset conditions (temperature, pressure, or composition) at which asphaltene precipitation is first detected and the yield (amount) of precipitation (Carnahan, 2000; Mousavi-Dehghani *et al.*, 2004; Mullins *et al*., 2007; Wiehe, 2008). These data were assumed to be collected at equilibrium conditions and have been used in various equilibrium models including regular solution theory (Alboudwarej *et al*., 2003; Akbarzadeh *et al*., 2005) and equations of state (Agrawal *et al*., 2012; Arya *et al*., 2017; Punnapala and Vargas, 2013). However, the amount of asphaltene precipitation in fact depends on the contact time between the oil and precipitant (Maqbool *et al*., 2009; Vilas-Bôas *et al*., 2017). Therefore, it is not clear if the reported data represent equilibrium values. Nor have precipitation kinetics been accounted for in precipitation models.

The residence time in process situations involving asphaltene precipitation is generally on a time scale of minutes to few hours and may not be enough to reach equilibrium. Hence, the kinetics of precipitation can have a direct impact on industrial operations. For example, if precipitation continues after a separation step is completed then there is potential for fouling in downstream process units. In addition, precipitation kinetics can potentially be used to advantage; for example, by flocculating and removing water and solids near the onset of precipitation before there is time for significant asphaltene precipitation to occur. Therefore, data and models of asphaltene precipitation kinetics at process conditions are required for the design and operation of processes involving asphaltene precipitation.

4.1.1 Kinetic Data for Asphaltene Precipitation

Most studies on asphaltene precipitation have measured either the yield or onset of precipitation from crude or model oils diluted with a precipitant (often called solvent or diluent) such as *n*-heptane. The onset of precipitation is defined as the precipitant content at which precipitation is first detected and has been determined by refractive index measurements, spectrophotometry, or optical microscopy (Buckley *et al*., 1999; Wattana *et al*., 2003; Angle *et al*., 2006). The contact time between the precipitant and the oil for the onset measurements ranged from few seconds to 24 hours. The yield is defined as the mass of precipitated asphaltenes divided by the mass of oil in the feed. The yield of precipitated asphaltenes is typically measured gravimetrically usually after approximately 24 hours of contact time with the precipitant (Hirschberg *et al*., 1984; Alboudwarej *et al*., 2002; Buenrostro-Gonzalez *et al*., 2004). In general, kinetic effects are neglected and data for asphaltene onsets and yields over time are relatively scarce.

More recently, the kinetics of asphaltene precipitation has been investigated for *n*-alkane diluted crude and model oils (Maqbool *et al*., 2009, 2011a; Beck *et al*., 2005; Haji-Akbari *et al*., 2015; Khoshandam and Alamdari, 2010; Yang *et al*., 2018; Chaisoontornyotin *et al*., 2017). Khoshandam and Alamdari (2010) investigated the kinetics of precipitation in a model oil (0.15 g asphaltenes/kg toluene) using *n*-heptane as precipitant and found that the concentration of soluble asphaltenes decreased continuously over 2 h and then reached a plateau. Similar results were reported by Yang *et al.* (2018) and Chaisoontornyotin *et al.* (2017) for an *n*-heptane diluted model oil (4.3 wt% Athabasca asphaltenes in toluene). They reported that equilibrium conditions were reached within 3 h in all cases at various precipitant contents and temperatures between -10 and 40ºC. The time to reach equilibrium in model oils was found to decrease with increased asphaltene content in the model oil and with increasing *n*-heptane concentration (Haji-Akbari *et al.,* 2014, 2015).

Asphaltene yields from diluted oils were found to increase over several days after the addition of precipitant (Maqbool *et al*., 2009; Beck *et al*., 2005; Chaisoontornyotin *et al*., 2018). Chaisoontornyotin *et al.* (2018) studied the kinetics of asphaltene precipitation from a solids-free Athabasca bitumen and reported significant yields after short contact times (< 30 min) particularly

at high precipitant contents (heptane/toluene mixtures in their case). They identified rapid precipitation rates at high precipitant contents; however, approximately 50 h were required to attain equilibrium yields at precipitant contents near the onset. In the same study, it was observed that equilibrium yields were attained much faster in oils containing inorganic solids. Beck *et al*. (2005) also found that equilibrium yields from *n*-heptane diluted Athabasca bitumen were attained after approximately 50 h in a nitrogen atmosphere. They observed that the amount of precipitate was already significant at early times (less than 20 min) and increased slowly over the next several hours.

Maqbool *et al.* (2009) identified the detection time at which asphaltene particles appeared at a given *n*-heptane content from several crude oils, where detection time was defined as the contact time at which 0.5 μm particles appeared. The detection time increased as the *n*-heptane content decreased and ranged from less than a second to several months. When the onset was rapid, the yields approached plateau values within a few hours. At lower *n*-heptane contents, the yields exhibited slow kinetics.

Maqbool *et al.* (2009) and Hoepfner *et al.* (2013) hypothesized a flocculation process that starts with destabilized primary nanoaggregates (asphaltene nanoparticles or molecular nanoaggregates) that aggregate over time into larger flocs; that is, the size distribution of the precipitated asphaltenes changes with time. They set the maximum possible yield as the amount of "destabilized" asphaltenes which must be determined independently from a measurement or an equilibrium calculation. They noted that the actual yield will depend on the separation method employed to obtain the mass of precipitated asphaltenes. In other words, more effective separation methods will report higher yields because these methods separate smaller aggregates from the suspension. Hence, precipitation and aggregation are connected both through the separation method and via the amount of destabilized asphaltenes.

4.1.2 Modeling the Kinetics of Asphaltene Precipitation/Aggregation

Models of aggregation kinetics are commonly based the population balance approach applied by Smoluchowski (1917) to Brownian coagulation (Zahnow *et al*, 2011; Thomas *et al*., 1999; Family *et al*., 1989; Elimelech *et al*., 1995; Friedlander, 2000; Jeldres *et al*, 2018). In this approach, aggregation occurs by the transport, collision, and adhesion of particles to form larger structures. The rate of aggregation between two particles of size *i* and *j* is given by (Thomas *et al*., 1999),

$$\mathrm{F}_{i,j} = \alpha_{i,j}\beta_{i,j}n_i n_j = K_{i,j}n_i n_j \tag{4.1}$$

where F_{ij} is the rate of aggregation between particles of size *i* and *j*, α is the collision frequency, β is the collision efficiency, $K_{i,j}$ is the collision kernel, and *n* is the particle number concentration. The collision *frequency* accounts for the probability of collisions between particles and depends on the transport mechanism of the particles/aggregates in the medium (Balakin *et al*., 2010; Kusters *et al*., 1997; Feke and Schowalter, 1983). The collision *efficiency* depends on the type and magnitude of the interaction forces that drive the aggregation process, such as electrostatic or van der Waals forces (Bäbler, 2008; Balakin *et al*., 2012). For simplicity, these two terms are sometimes combined into the collision kernel.

The Smoluchowski model counts all possible binary collisions that form aggregates of size *k*. The discretized model is given by (Friedlander, 2000),

$$\frac{dC_k}{dt} = \frac{1}{2}\sum_{i+j=k} K_{i,j}C_i C_j - \sum_{i=1}^{N} K_{i,k}C_i C_k \tag{4.2}$$

where the number concentration from Eq. 4.1 has been substituted by the molar concentrations, *C*. This population balance only considers particle aggregation. In some studies, the consumption of aggregates by shattering/breakage mechanisms has also been considered (Rastegari *et al*., 2004; Zahnow *et al*., 2011; Rahmani *et al*., 2003; Nassar *et al*., 2015). Since the experimental observations reported in Chapter 3 suggest that asphaltene aggregates are mostly fused structures that are insensitive to shear particularly near onset conditions (See Section 3.5), breakage mechanisms are not considered in this study. In other words, particles can aggregate but not disaggregate.

There are four main considerations when applying the population balance: 1) the size of the primary (non-aggregated) particles; 2) the relationship between the number of particles in the

aggregate (the output of the population balance) and the size and density of the aggregate (the factors that control settling); 3) the functional form of the reaction kernel; 4) the reduction of the number of equations to a tractable solution. Each consideration is discussed below.

Primary Particle Size

Asphaltenes molecules have molecular weights in the order of 1000 g/mol (Rodgers and McKenna, 2011; Betancourt *et al.*, 2009) and are believed to self-associate in crude oils into nano-aggregates with diameters in the order of 2.5 nm (Hoepfner *et al*., 2013). Some asphaltene aggregation models take the nano-aggregates as the primary particles (Maqbool *et al*., 2011a; Torkaman *et al.*, 2017). Precipitation is then considered to be an aggregation driven process. Other models assume that asphaltenes first precipitate in a phase transition and then aggregate. These models take the precipitated particle as the primary unit with a diameter in the order of 1 µm (Rastegari *et al*., 2004; Rahimi and Nazar, 2010) or even 30 µm (Rahmani *et al*, 2005).

Aggregate Dimensions

Asphaltene aggregates have been shown to have fractal-like structures where the following scaling relationship can be applied (Rahmani *et al*., 2005),

$$d_i \propto n_{p,i}^{1/D_f} \tag{4.3}$$

where the diameter of the aggregates in the different bins, d_i, is based on the number of primary units per aggregate, $n_{p,i}$, and D_f is the fractal dimension. The diameter of an irregular fractal aggregate must be defined and the most straightforward approach is to set it equal to the longest dimension of the aggregate (Rastegari *et al*., 2004; Nassar *et al*., 2015; Solemaini-Khormakala *et al*., 2018). This definition means that the aggregate includes all of the material enclosed within a sphere equal to the maximum diameter as shown in Figure 3.1. An alternative is to use the area equivalent diameter of the aggregates based on their projected area from micrographic images (Rahmani *et al*., 2005; Zawala *et al*., 2012). As will be discussed later in Section 4.2.1, the porosity and density of the aggregate can be calculated from the number of primary particles within the aggregate and the diameter of the aggregate obtained from Eq. 4.3.

Collision Kernel

The collision kernel is the product of the collision frequency and the collision efficiency, and the two terms can be determined independently or in combination. First consider the collision frequency. If Brownian motion is the transport mechanism responsible for the collisions of suspended particles/aggregates, the collision frequency can be defined as follows (Maqbool *et al*., 2011a; Nassar *et al*., 2015),

$$\alpha_{i,j} = 2\pi\left(D_i + D_j\right)\left(d_i + d_j\right) \tag{4.4}$$

where D is the diffusivity of an aggregate. The Stokes-Einstein equation is substituted for the diffusivity to obtain the following expression (Maqbool *et al*., 2011a; Torkaman *et al*., 2017; Islam, 2004),

$$\alpha_{i,j} = \frac{2}{3}\frac{k_B T}{\mu_m}\frac{\left(d_i + d_j\right)^2}{d_i d_j} \tag{4.5}$$

where k_B is Boltzmann constant, μ_m, the viscosity of the medium, and T, the temperature of the system. Other functional forms for the collision frequency have been proposed for aggregation in shear flow (Rahmani *et al*., 2003; Rahimi and Nazar, 2010), during settling with Brownian motion (Safaie and Nazar, 2013), and simultaneous Brownian and shear-induced aggregation (Nassar *et al.*, 2015; Soleimani-Khormakala *et al.*, 2018; Torkaman *et al*., 2018).

The collision efficiency is usually set to unity (Rahmani *et al*., 2003; Nassar *et al*., 2015; Rahimi and Nazar, 2010) or treated as a fitting parameter (Maqbool *et al*., 2011a; Torkaman *et al*., 2018). The fitted collision efficiencies were found to increase with increasing *n*-heptane content (Maqbool *et al.*, 2011a), decreasing temperature (Torkaman *et al*., 2018), and decreasing shear rate (Soleimani-Khormakala *et al*., 2018). Other approaches ignore the flow regime and assume semi-empirical collision kernels (Rastegari *et al*., 2004; Khoshandam and Alamdari, 2010; Rahmani *et al*., 2003; Nassar *et al*., 2015; Rahimi and Nazar, 2010). In this case, the collision efficiency is implicitly set to a constant value and it is assumed that the collision frequencies are proportional to the collision volume or area of the aggregates raised to the power of an exponent. The exponent is used as a fitting parameter. These approaches included a shattering kernel to account for the simultaneous breakage of the aggregates and this kernel required another fitting parameter. In some cases, additional fitting parameters were introduced to the kernels.

Number of Equations

The population balance is a system of ordinary differential equations (ODEs) that must be solved simultaneously after establishing a size domain (upper and lower limit of *n*) and a set of initial conditions. The challenge is that tracking millions of individual primary particles produces thousands or more coupled ODEs that require long computational times to solve (Friedlander, 2000; Spicer and Pratsinis, 1996). The following approaches have been used to minimize the number of equations: restricting the aggregate size to a narrow range (Yudin *et al.*, 1998); grouping several primary particles into clusters that can play the role of primary units for the calculation (Rastegari *et al*., 2004; Rahmani *et al.*, 2003); defining aggregate sizes as a geometric progression of the particle volume (Nassar *et al*., 2015; Torkaman *et al*., 2017; Rahimi and Nazar, 2010; Spicer and Pratsinis, 1996), or; defining aggregate sizes as a geometric progression of the number of primary particles (Maqbool *et al*., 2011a).

Current State-of-the-Art

Most of the above studies either focused on the aggregate size distributions over time but did not considered asphaltene yield (Rastegari *et al*., 2004; Khoshandam and Alamdari, 2010; Rahmani *et al*., 2003; Nassar *et al*., 2015; Torkaman *et al*., 2017; Rahimi and Nazar, 2010). Maqbool *et al*. (2011a) focused on the yield over time with the aggregate size distribution as a key part of the model. They modeled the precipitation kinetics of *n*-heptane diluted Alaskan crude oil (10.9 wt% C7-asphaltenes). The yield was calculated from the calculated aggregate size distribution using a settling model based on Stokes' law. They defined the primary particles as asphaltene nano-aggregates and used a geometric scaling factor to reduce the number of ODEs from about 1 million to less than 40 for aggregates between 1 nm to 500 nm. The collision frequency was obtained from Eq. 4.5. The collision efficiency was assumed to be independent of the aggregate size and was tuned to match measured yields over time. The collision efficiency increased with the *n*-heptane content and the increase was attributed to the larger driving force for aggregation in a poorer solvent medium. The model predicted the time to detect ~0.5 μm particles at different temperatures within experimental error. The model was later extended to different light crude oils and model oils (Haji-Akbari *et al*., 2013, 2015). However, the predicted aggregate size distributions were only used to confirm onset times but were not rigorously confirmed with measurements beyond this

point. Although the Smoluchowski model can provide both yields and aggregate sizes over time, none of the studies to date have demonstrated directly that the model matches both aggregate size distributions and yields. And yet both size and yield are required to model settling and deposition.

4.1.3 Objectives

In this chapter, the capability of the Smoluchowski population balance approach to match both yields and aggregate size distributions of precipitated asphaltenes over time is evaluated. Onset, yields, and aggregate size distributions were measured at 21ºC as a function of time after *n*-heptane addition for a Western Canadian bitumen (WC-B-B2), a Mexican bitumen (MX-B-A1), an Alberta Mixed Sweet Blend (MSB), and a European heavy oil (EU-HO-A1). A more limited set of data were collected for a Western Canadian Bitumen (WC-B-A3) mixed with *n*-heptane and *n*-pentane at 21°C. Properties for these oils are reported in Table 2.1. The data were collected in a nitrogen atmosphere to simulate the anaerobic conditions found in the field. The population balance approach was adapted to match experimental data and correlations for the collision efficiency, primary particle diameter, and fraction of immediate precipitate were proposed to apply the model to different crude oils and precipitants. The predictive capabilities of the model were tested on precipitation data from one Alaskan oil and one Gulf of Mexico oil each diluted with *n*-heptane and originally reported by Maqbool *et al*. (2009, 2011b).

4.2 Preliminary Population Balance Model

4.2.1 Model Description

The geometric population balance proposed by Maqbool *et al*. (2011a) was selected as the initial approach because it is relatively simple to implement and is tuned to yield data using only one fitting parameter. The size of the aggregates in the domain are defined in terms of the geometric scaling factor, R_s. For $R_s = 2$ (used throughout this study), the aggregates in each bin contain double the number of primary units per aggregate than the immediate smaller bin (*i.e*., 1, 2, 4, 8,…, *N*); hence the i^{th} bin contains 2^{i-1} primary units. The number of aggregates in each bin is calculated over a series of time steps and the population balance at each time step is given by,

$$\frac{dC_k}{dt} = \frac{1}{2} K_{k-1,k-1} C_{k-1}^2 + C_{k-1} \sum_{j=1}^{k-2} K_{k-1,j} 2^{j-k+1} C_j$$

$$-C_k \sum_{j=1}^{k-1} K_{k,j} 2^{j-k} C_j - C_k \sum_{j=k}^{N-1} K_{k,j} C_j \quad (4.6)$$

The collision kernel assumes Brownian transport and that the collision efficiency is independent of the aggregate size; it is given by,

$$K_{i,j} = \frac{2}{3} \frac{RT}{\mu_m} \frac{(d_i + d_j)^2}{d_i d_j} \beta \quad (4.7)$$

The output of the population balance is a distribution of aggregates defined by the number of primary particles in the aggregate.

The following steps are required to determine the aggregate size distribution and yield from the population balance: 1) set the primary particle diameter and initial concentration; 2) solve the population balance equations to obtain the concentration and number frequency of aggregates in each bin size; 3) calculate the diameters and porosities of the aggregates in each bin size; 4) perform a settling calculation to determine the fraction of aggregates that are separated at the experiment conditions (yield); 5) iterate by adjusting the collision efficiency to match measured yields. Each step is discussed below.

Primary Particle Size and Concentration

An initial population of monodisperse primary particles with 2.5 nm diameters is assumed. The initial concentration of primary units (C_1 in kmol/m³) is given by,

$$C_1(t = 0) = \frac{Y_{A,eq} \varphi_0 \rho_0}{M_{w,A} N_n} \quad (4.8)$$

where $Y_{A,eq}$ is the equilibrium yield of asphaltenes, φ_0 is the volume fraction of precipitant in the mixture, and ρ_o is the crude oil density. The denominator represents the molecular weight of the primary unit where $M_{w.A}$ is the molecular weight of an average asphaltene molecule and N_n is the number of asphaltene molecules per nanoaggregate.

Number Frequency Distribution of Aggregates

The frequency of aggregates in each bin at each time step is determined as follows,

$$f_i = 100 \frac{n_{agg,i}}{\sum_{i=1}^{N} n_{agg,i}} \quad (4.9)$$

where f_i is the number frequency and $n_{agg,i}$ is the number of aggregates in the i^{th} bin (per kg oil) given by,

$$n_{agg,i} = \frac{M_{A,i}}{m_{agg,i}} \tag{4.10}$$

where $M_{A,i}$ is the total mass of asphaltenes and $m_{agg,i}$ is the mass of one asphaltene aggregate in the i^{th} bin. $M_{A,i}$ and $m_{agg,i}$ are given by,

$$M_{A,i} = \frac{2^{i-1} M_{w,A} N_n C_i}{w_0} \tag{4.11}$$

$$m_{agg,i} = \frac{\pi}{6} 2^{i-1} \rho_A d_p^3 \tag{4.12}$$

where w_0 is the mass of oil per unit volume of mixture and C_i is the molar concentration of asphaltenes in the i^{th} bin. The concentration of aggregates in each bin is determined from the population balance equations.

Aggregate Diameter and Density

The original approach assumed a constant porosity value for all aggregates. However, the porosity of asphaltene aggregate has been found to scale with the number of primary particles according to eq. 3.2. Therefore, the porosity of aggregates in the i^{th} bin is defined as follows,

$$\phi_i = 1 - \left(\frac{d_p}{d_i}\right)^{3-D_f} \tag{4.13}$$

where D_f is the fractal dimension and d_p is the diameter of the primary particles. Therefore, the model was modified to use the fractal dimension instead of porosity. For $R_s=2$, the diameter of the aggregates in each bin size is given by,

$$d_i = d_p 2^{\frac{i-1}{D_f}} \tag{4.14}$$

and their density is given by,

$$\rho_i = \rho_m + (\rho_A - \rho_m)\left(\frac{d_p}{d_i}\right)^{3-D_f} \tag{4.15}$$

where ρ_i is the density of the aggregates in the i^{th} bin and ρ_m and ρ_A are the densities of the fluid and the asphaltenes, respectively. Eq. 4.15 is similar to eq. 3.3 but different aggregate densities are defined for each bin.

Settling and Yield

The mass of precipitate per kg of oil in each bin size is given by,

$$Y_{A,i}(\mathrm{t}) = M_{A,i}(t)s_i = \frac{2^{i-1}M_{w,A}N_n s_i C_i(t)}{w_0} \tag{4.16}$$

where $Y_{A,i}$ is the yield of asphaltenes from the i^{th} bin and s_i is the fraction of asphaltenes in the i^{th} bin that are separated by centrifugation. The fraction of asphaltenes separated by centrifugation is determined from the following settling calculation based on Stokes' law (Maqbool *et al*., 2011a),

$$s_i = \frac{\Delta x_i}{L} = \frac{r_c}{L}\left\{1 - \exp\left[-\frac{(\rho_A - \rho_m)d_i^{D_f-1}\omega^2 t_c}{18\mu_m}\right]\right\} \tag{4.17}$$

where Δx_i is the distance the aggregates in the i^{th} bin move during the centrifugation time t_c, L is the length of the centrifuge tube, r_c is the radius of the centrifuge, and ω is the angular velocity. Eq. 4.17 is valid only for $\Delta x_i \leq L$. If $\Delta x_i > L$, s_i is set to unity. Finally, the total mass of precipitate per unit mass of oil is given by,

$$Y_A(\mathrm{t}) = \sum_{i=1}^{N} Y_{A,i}(t) \tag{4.18}$$

where Y_A is the asphaltene yield.

4.2.2 Model Implementation

Model Inputs

The number of required input parameters were reduced by setting several of the model inputs to fixed internal values. The primary particle molecular weight and aggregation number were set to their previously recommended values of 750 g/mol and 8, respectively (Maqbool *et al*., 2011a; Betancourt *et al*., 2009). The asphaltene density was set to 1200 kg/m³ (Yarranton and Masliyah, 1996). The following correlation, based on the "compacted" fractal dimension data reported in Figure 3.19, was used to determine the fractal dimension of the asphaltene aggregates in this chapter,

$$\log(D_f) = 0.009508w_u + 0.04243 \tag{4.19}$$

where w_u is the precipitate concentration in wt%; that is, the concentration of unstable asphaltenes, given by,

$$w_u = \frac{Y_{A,eq}}{100}(100 - w) \tag{4.20}$$

The calculated fractal dimensions were approximately 2.65 for the low asphaltene content oils (MSB and EU-HO-A1) and ranged from 2.5 to 2.8 for the WC-B-B2, and MX-B-A1 bitumens, depending on the *n*-heptane concentration. The correlation of Eq. 4.19 fitted the compacted fractal dimension to within 10%. Since the settling model of Chapter 6 is very sensitive to the input fractal dimensions, the correlation of Eq. 4.19 was modified to provide errors below 3% (See Section 6.3.4). Nevertheless, the correlation provided here still provides small deviations for the fractal dimension.

Table 4.1. Values of centrifugation parameters used in this study.

Parameter	Value
Centrifuge radius, m	0.2
Centrifuge tube length, m	0.085
Centrifugation time, s	300
Angular velocity, rad/s	418.9

The remaining inputs for the aggregation model are the centrifuge parameters, the component and mixture density and viscosity, the temperature, the mass concentration of *n*-heptane in the mixture, the concentration of destabilized asphaltenes at equilibrium, and the collision efficiency. The centrifugation parameters used in this study are provided in Table 4.1. The density and viscosities for the oils in this study were taken from Table 2.1. Densities for the oil/precipitant mixtures were measured at 21ºC and were correlated with the excess volume mixing rule (Saryazdi *et al*., 2013). The viscosity of the diluted crude oil mixtures was calculated with the modified Walther model (Ramos-Pallares *et al*., 2017). The fitted density and viscosity models are presented in Appendix B and summarized in Section 6.3.2. The temperature and *n*-heptane concentration were specified for each case. The concentration of destabilized asphaltenes at equilibrium was determined from the yield measurements for each case. The collision efficiency is a fitting parameter.

Model Algorithm

The algorithm employed to solve the population balance model is shown in Figure 4.1 and was implemented in Matlab™. The input parameters are the *n*-heptane content, the amount of destabilized asphaltenes, the collision efficiency at the given mixture composition, and the

centrifugation parameters. In addition, the largest aggregate diameter considered in the size domain was defined as d_{max} = 500 μm to limit the matrix size and because most observed aggregates were smaller than 500 μm.

In the next step, the initial conditions for the model are set. The concentration of the monodisperse population of primary units is calculated from Eq. 4.8. The density and viscosity of the mixture are calculated as a function of the solvent content. The fractal dimension of the aggregates is calculated from Eq. 4.19. The number of bins are defined to include diameters from 2.5 nm to 500 μm. Since the fractal dimension is a function of the *n*-heptane content, the number of bins also varies with composition. The total number of bins, *N*, is given by,

$$N = 1 + \frac{D_f \ln\left(\frac{d_{max}}{d_p}\right)}{\ln(2)} \tag{4.21}$$

The number of particles per aggregate is assigned to each bin (2^{i-1} for the i^{th} bin). For fractal dimensions in the range of 2 to 3, the number of bins (thus the number of ODEs) ranged from 37 to 54. Then, the aggregate diameters for each bin size are calculated from Eq. 4.14, the aggregate porosity from Eq. 4.13, and the separation efficiency from Eq. 4.17.

In the innermost loop, the collision kernel values are calculated and the population balance equations (a system of discretized ODE) is solved using the *ode45* function (based on the Runge-Kutta formulas for 4th and 5th orders). The solution is the aggregate concentration for each bin. Then, the diameter distribution and mean diameter are calculated from Eqs. 4.9-4.12. At this point the following check on the number of primary particles was performed,

$$C_1(t=0) - \sum_{i=1}^{N} 2^{i-1} C_i(t) = 0 \tag{4.22}$$

This check was converted to an asphaltene mass balance by multiplying Eq. 4.22 by the molecular weight of the aggregates, $M_{w,A} N_n$. If the error in the mass balance is larger than a threshold value (1×10^{-8} kg), the time step is decreased to 10% of its current value.

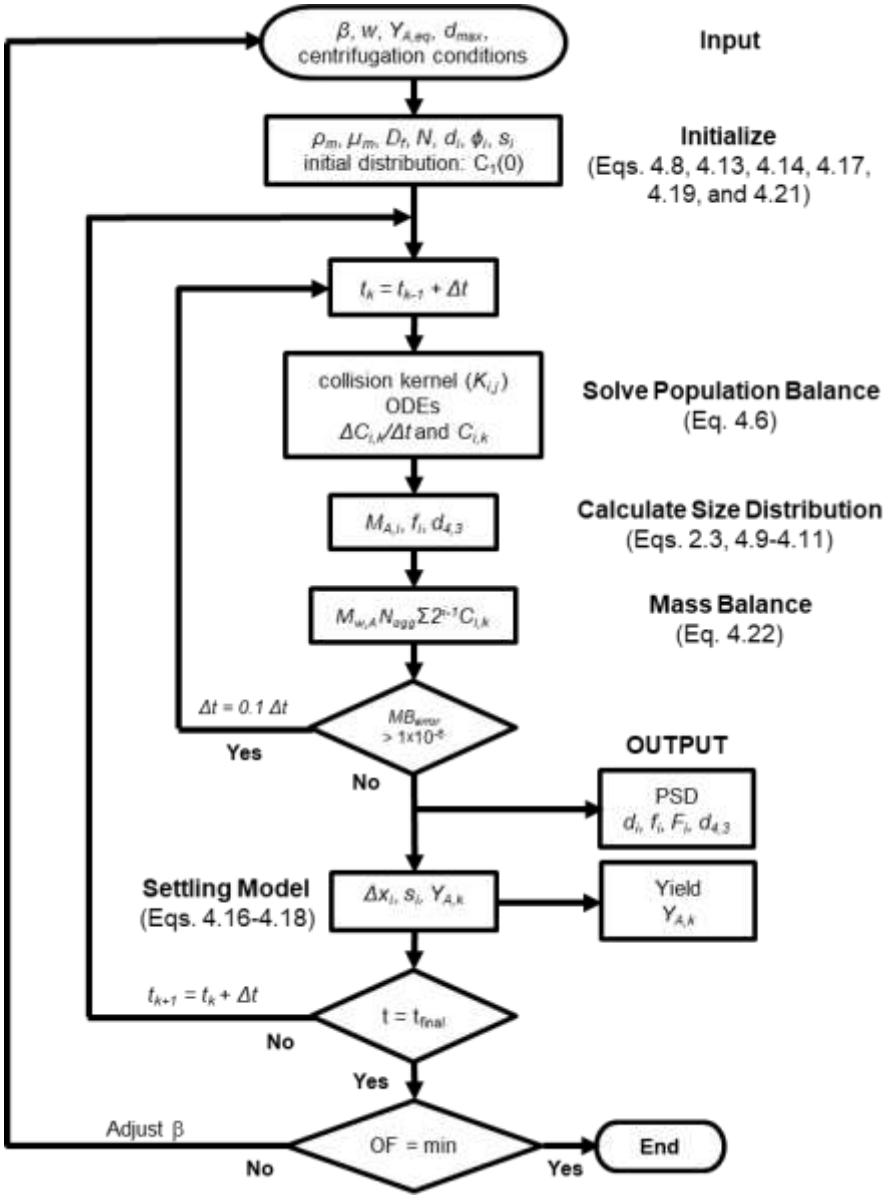

Figure 4.1. Calculation algorithm used to solve the discretized population balance. The subscript *k* is the time-step index.

In the middle loop, the mass detected as precipitate is determined from the settling model (Eqs. 4.16-4.18). Then, the time increment is applied to start the next iteration. This iterative process is repeated until the time reaches a defined maximum simulation time (500 h in this study). The outputs of the routine are the yield and volume mean diameter as a function of time.

In the outermost loop, the input collision efficiency is adjusted to best fit the yield data. For each crude oil system and at each precipitant content, the collision efficiency, β, is iterated to minimize the following objective function (OF),

$$OF = \min_{0 \le \beta \le 1} \frac{1}{n} \sum_{j=1}^{n} \left(Y_{j,\text{experimental at t}} - Y_{j,\text{ model at t}} \right)^2 \quad (4.23)$$

where n is the number of experimental yield points. The function *fminsearch* in Matlab™ was used as minimization tool.

4.3 Results and Discussion

First, the measured onsets, yields, and size distributions for the first five crude oils from Table 2.1 mixed with *n*-heptane are presented. The onset data are required for some model parameter correlations presented later. The yields and size distributions are used to assess and modify the proposed population balance model. The ability of the preliminary population balance model to match the data is discussed. A revised population balance model is developed and applied to the measured data. Finally, the revised model is tested against data from the literature.

The WC-B-B2, MX-HO-A1, MSB, and EU-HO-A1 oils constitute the Development Dataset. The data for the WC-B-B2 bitumen and *n*-heptane mixtures are discussed in detail and the results for the other three oils are summarized because similar behavior was observed for these oils. The WC-B-A3 bitumen provides a limited Supplemental Dataset including yield and aggregate size data with *n*-heptane and *n*-pentane. The size distributions are used for model development and the yields are used to test the model.

4.3.1 Development Dataset

Onsets of Asphaltene Precipitation

Figure 4.2a to 4.2c shows the micrographs for the diluted WC-B-B2 samples at 56.5, 57.0, and 57.5 wt% *n*-heptane, respectively, at three different contact times. The first appearance of particles was a haze that is challenging to see in the printed micrograph because the particle diameters are smaller than 0.5 µm. At 56.5, 57.0, and 57.5 wt% *n*-heptane, this haze appeared after 70, 40, and less than 1 minute, respectively. Subsequently, clearly defined particles and aggregates appeared gradually over tens of minutes. Therefore, the appearance of the haze is interpreted as the onset of

precipitation. Figure 4.2c shows that for this system, the instantaneous onset of precipitation (where particles appear immediately after mixing the precipitant with the oil) was 57.3 ± 0.3 wt% *n*-heptane. Table 4.2 shows that the onsets shift to lower *n*-heptane contents with increasing contact time, consistent with a time dependent process. The gradual increment in the number of particles over time observed in the micrographs also confirms that asphaltene precipitation is a time dependent process.

The onset of precipitation was also determined from extrapolated asphaltene yields as was shown in Figure 2.3. The yields were measured in a nitrogen atmosphere except at contact times less than one hour. The short contact time data were collected in air. The yields in air and nitrogen have been shown to be the same for contact times less than 48 h (Beck *et al*., 2005). The yield data are provided in Appendix C. Figure 4.3 shows that the onsets over time initially decreased but reached a plateau value after approximately 150 hours of contact time. A limiting value is contrary to the findings of Maqbool *et al.* (2009) who observed that the onsets in an air atmosphere continued to decrease even after several months of contact. However, the presence of air may alter the observed asphaltene precipitation kinetic behavior by promoting oxidation reactions (or oxygen catalyzed reactions) that increase the amount of unstable (insoluble) asphaltenes, causing the onsets to shift over time as will be discussed in Chapter 5.

Table 4.2. Onset of asphaltene precipitation in *n*-heptane diluted WC-B-B2 bitumen at 21ºC and 1 atm at various contact times.

Contact Time (h)	Microscopic Onset (wt% *n*-heptane)	Gravimetric Onset (wt% *n*-heptane)
< 0.02	57.3 ±0.3	-
0.7	56.8 ±0.3	-
1.2	56.3 ±0.3	-
2.0	-	56.5 ± 1

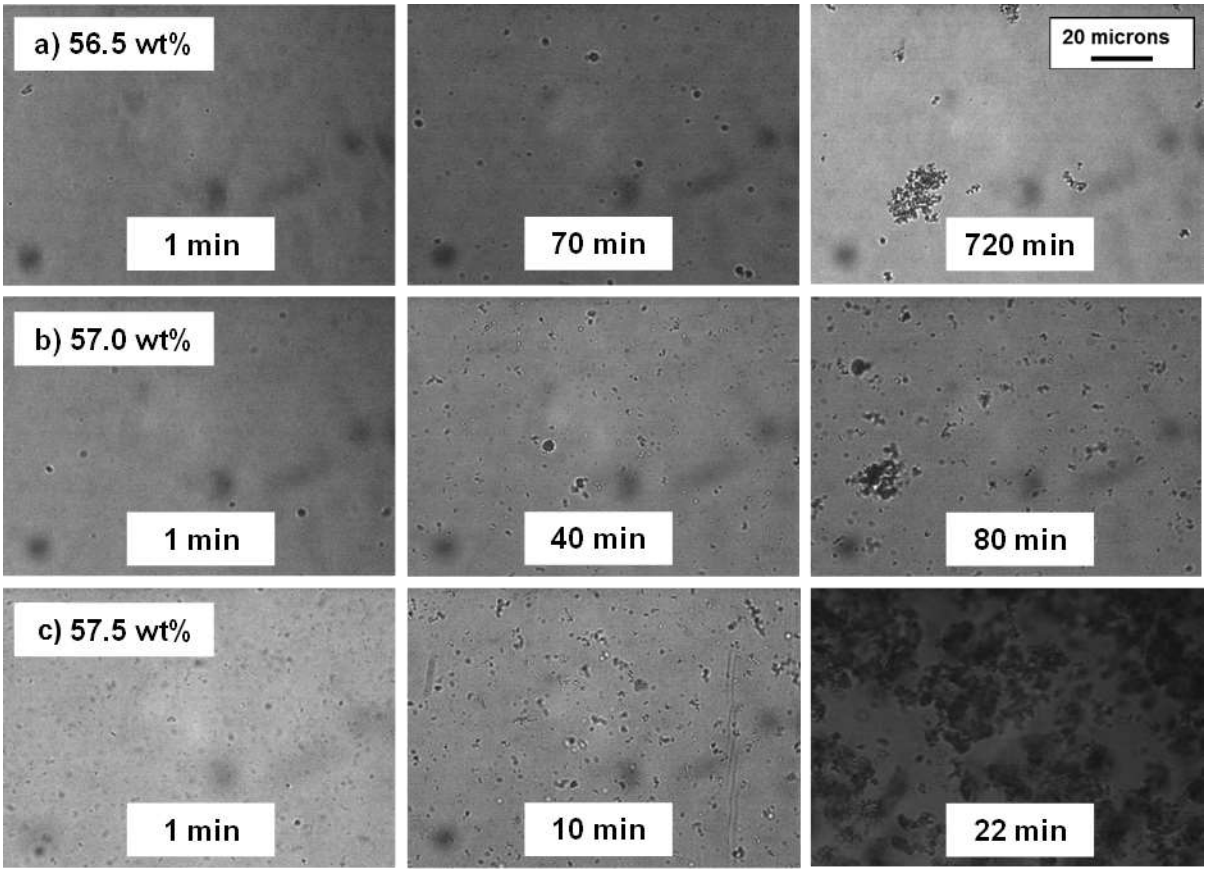

Figure 4.2. Micrographs showing the onset of asphaltene precipitation from *n*-heptane diluted WC-B-B2 bitumen at a) 56.5 wt%, b) 57.0 wt%, and c) 57.5 wt% *n*-heptane at 21ºC.

The data collected in this study suggest that a thermodynamic equilibrium is eventually reached in anaerobic conditions. The equilibrium onset for the WC-B-B2 bitumen was 53.7 ±0.5 wt% *n*-heptane. Equilibrium requires reversibility. While reversibility was not tested in this study, asphaltene precipitation has been found to be reversible when the precipitate content is reduced (Beck *et al*., 2005), temperature is increased (Beck *et al*., 2005; Chaisoontornyotin *et al*., 2017), and pressure is increased (Hammami *et al*., 2000). Beck *et al.* (2005) observed a hysteresis between the precipitation and redissolution of the asphaltenes that could be overcome by heating. The hysteresis is consistent with a kinetic factor in precipitation and dissolution.

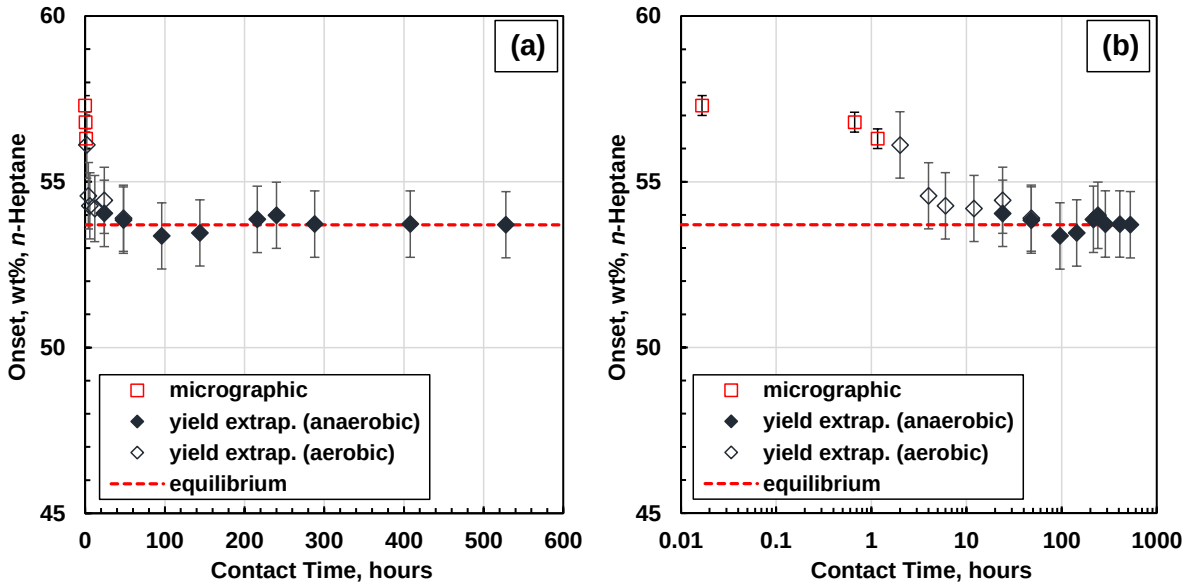

Figure 4.3. Comparison of micrographic and gravimetric onset of precipitation for the *n*-heptane diluted WC-B-B2 bitumen at 21ºC and 1 atm: a) Cartesian coordinates; b) semi-log coordinates.

The onset of precipitation was also measured for the other oils in *n*-heptane following the same procedures. Yield data and micrographs are also provided in Appendix C. The onsets determined by the micrographic method were within ±0.7 wt% *n*-heptane of the onsets obtained by the extrapolated yield method, almost within the measurement error (±0.5 wt% for each method). For the MSB and EU-HO-A1 oils (one light and one heavy oil), the particles when first detected were smaller than observed for the other oils (less than 0.5 µm in comparison to 1 to 5 µm) but eventually grew to larger sizes, suggesting that the particles of these oils grow relatively more slowly.

Figure 4.4 shows the onsets over time for the MX-B-A1, MSB, and EU-HO-A1 oils. In all cases, the onsets decreased in the first 50 to 150 hours but eventually reached a plateau. Equilibrium (or ultimate) onsets for all four oils are presented in Table 4.3. All the yield data for the following kinetic analysis were collected at *n*-heptane concentrations above the equilibrium onsets estimated for each system.

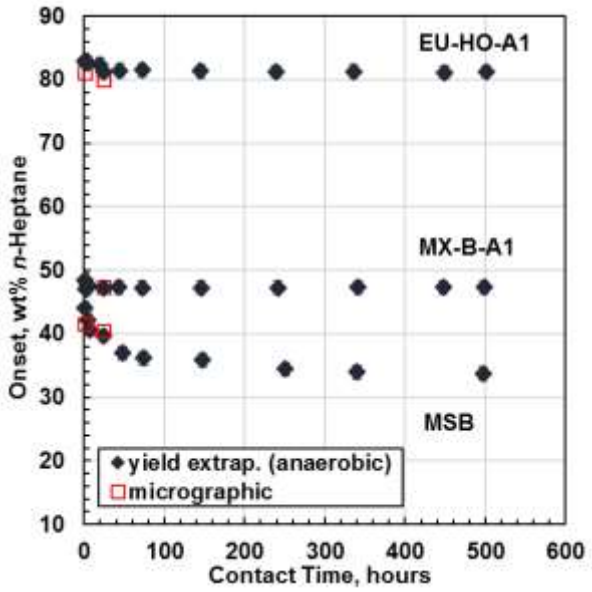

Figure 4.4. Comparison of the onsets of asphaltene precipitation in *n*-heptane diluted MX-B-A1, MSB, and EU-HO-A1 oils at 21ºC and 1 atm. Error bars are ±1 wt% for extrapolated onsets, and ±0.3 wt% for micrographic onsets.

Table 4.3. Equilibrium onsets of asphaltene precipitation in *n*-heptane diluted crude oil at 21ºC and 1 atm. Data collected in anaerobic conditions. The errors for the onsets are ±0.5 wt%.

Sample	Equilibrium Onset wt% *n*-heptane
WC-B-B2	53.7
MX-HO-A1	47.3
MSB	34.5
EU-HO-A1	79.9

Asphaltene Precipitation Yields

Figure 4.5a shows the yields from the WC-B-B2 bitumen over time at *n*-heptane contents from 54.5 to 64.5 wt%. The yields increased monotonically over time and reached a plateau in less than 150 h. The rate of precipitation is similar to data reported for other bitumens (Beck *et al.*, 2005; Chaisoontornyotin *et al*., 2017). The plateau value is interpreted as the equilibrium yield. The plateau value was reached more rapidly as the *n*-heptane content increased.

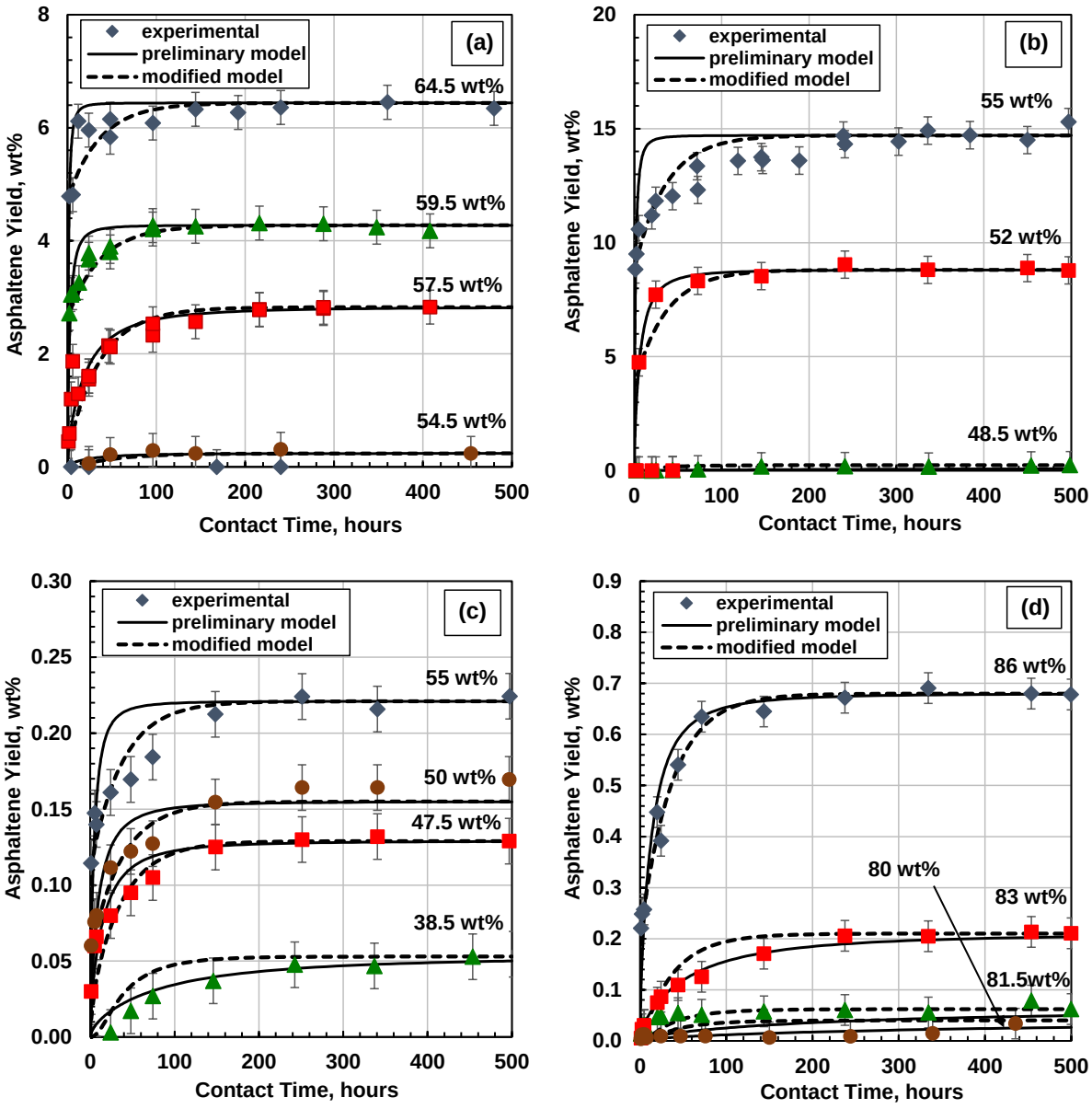

Figure 4.5. Measured and modeled asphaltene yields from *n*-heptane diluted crude oils over time in a nitrogen atmosphere at 21ºC and 1 atm: a) WC-B-B2; b) MX-B-A1; c) MSB; d) EU-HO-A1. Error bars in yields are ±0.6 wt% (WC-B-B2), ± 0.6 wt% (MX-B-A1), ±0.02 wt% (MSB), and ±0.03 wt% (EU-HO-A1). Symbols are data; solid lines correspond to the preliminary model, and dashed lines to the modified model.

At *n*-heptane contents near the onset of precipitation, the yields increased slowly over time. At higher precipitant contents, a significant amount of asphaltenes precipitated almost

instantaneously and then the yields increased slowly over time. Near the equilibrium onset (53.7 wt% *n*-heptane), no precipitate was observed initially but particles appeared after some time. Similar trends were observed for the other oils as shown in Figure 4.5. The rate of precipitation observed in the MSB, and EU-HO-A1 oils is consistent with rates observed for other light or medium oils reported elsewhere (Maqbool *et al.*, 2009; Torkaman *et al.*, 2017; Rahimi and Nazar, 2010). The equilibrium yields are a required input for the population balance model and are shown in Figure 4.6. For convenience, they were correlated as an empirical function of the *n*-heptane content as follows,

$$Y_{A,eq} = w_{A,C7}\{1 - exp[-b(w - w_o)]\} \tag{4.24}$$

where $Y_{A,eq}$ is the equilibrium yield, $w_{A,C7}$ is the C7-asphaltene content of the oil in wt% from Table 2.1, w is the mass percent of *n*-heptane in the mixture, and w_o is the equilibrium onset (wt% *n*-heptane) from Table 4.3. The fitted values of parameter b were 0.04, 0.12, 0.0175, and 0.028 for the WC-B-B2, MX-B-A1, MSB, and EU-HO-A1 oils, respectively. The correlation fit the data with an AAD of 0.26 wt% (WC-B-B2), 0.66 wt% (MX-B-A1), 0.01 wt% (MSB), and 0.19 wt% (EU-HO-A1).

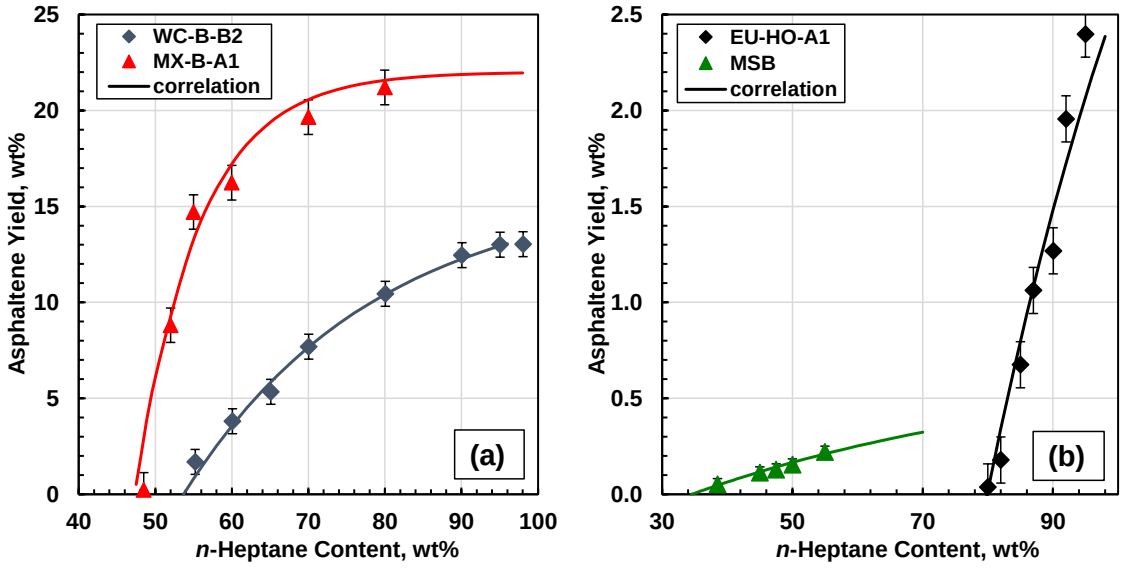

Figure 4.6. Equilibrium yields from *n*-heptane diluted crude oils at 21°C in a nitrogen atmosphere: a) high asphaltene content oils; b) low asphaltene content oils.

Aggregate Size Distributions

Figure 4.7 shows the initial volume mean diameters for the mixtures of *n*-heptane and WC-B-B2 bitumen. The mean diameters increased significantly immediately above the onset and approached a plateau value at approximately 80 wt% *n*-heptane. The mean diameters for the other oils also increased above the onset but diameters far above the onset were not investigated.

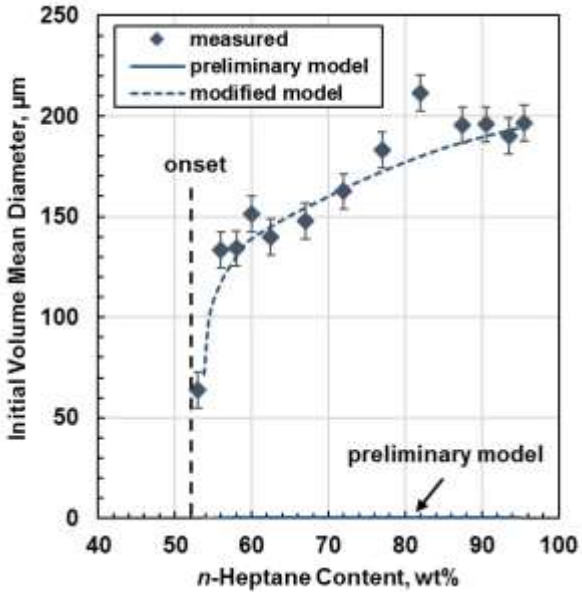

Figure 4.7. Measured and modeled initial volume mean diameter of asphaltene aggregates in *n*-heptane diluted WC-B-B2 bitumen at 21ºC. Symbols are data; solid line correspond to the preliminary model, and dashed line to the modified model.

Figure 4.8 shows the growth (increase in volume mean diameter) of the aggregates from the four oils over time. The trends are different for the high asphaltene content oils versus the low asphaltene content oils. The aggregates from the WC-B-B2 and MX-B-A1 bitumens (Figure 4.8a and 4.8b, respectively) reached tens of micrometers within a few seconds and remain almost unchanged over time except at high dilution (> 85 wt% *n*-heptane). Above this concentration, the aggregates from the WC-B-B2 bitumen appear to partially shatter under shear; however, the final diameter is only 5 to 10 µm lower than the initial diameter. In contrast, the aggregates from the MSB and EU-HO-A1 oils (Figure 4.8c and 4.8d, respectively) were much smaller and grew at a slower rate for a longer time. This slow aggregation rate is consistent with the rates observed for

other crude and model oils (Maqbool *et al*., 2009; Khoshandam and Alamdari, 2010). All the oils in those studies had asphaltene contents below 3 wt%. The difference in growth rates in low and high asphaltene content oils will be discussed later.

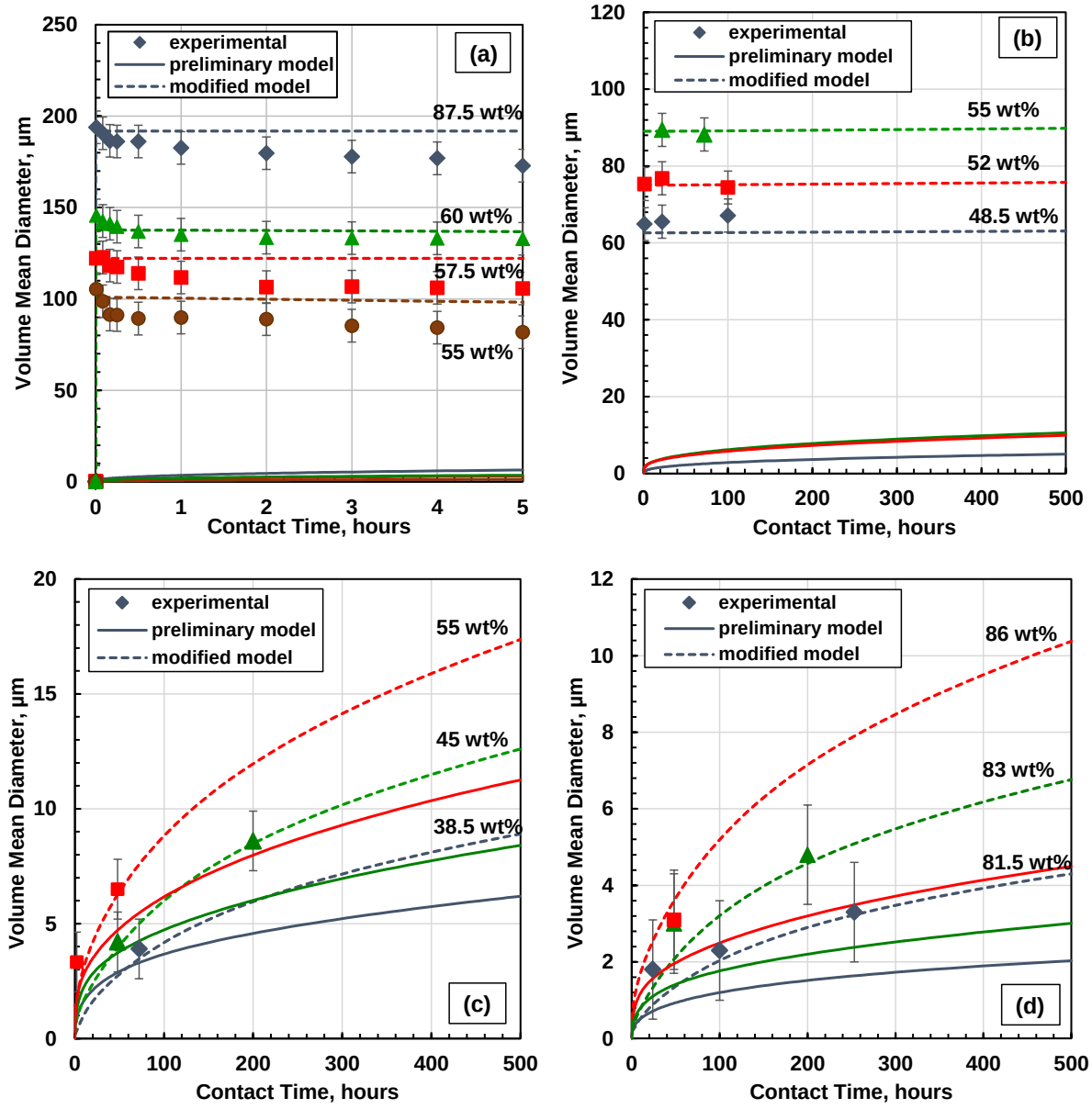

Figure 4.8. Comparison between the measured and predicted volume mean diameters of asphaltene aggregates for *n*-heptane diluted crude oils at 21ºC. a) WC-B-B2; b) MX-B-A1; c) MSB; d) EU-HO-A1. Reported diameters for the WC-B-B2 bitumen were measured with the FBRM method (See Section 2.4). Symbols are data; solid lines correspond to the preliminary model, and dashed lines to the modified model.

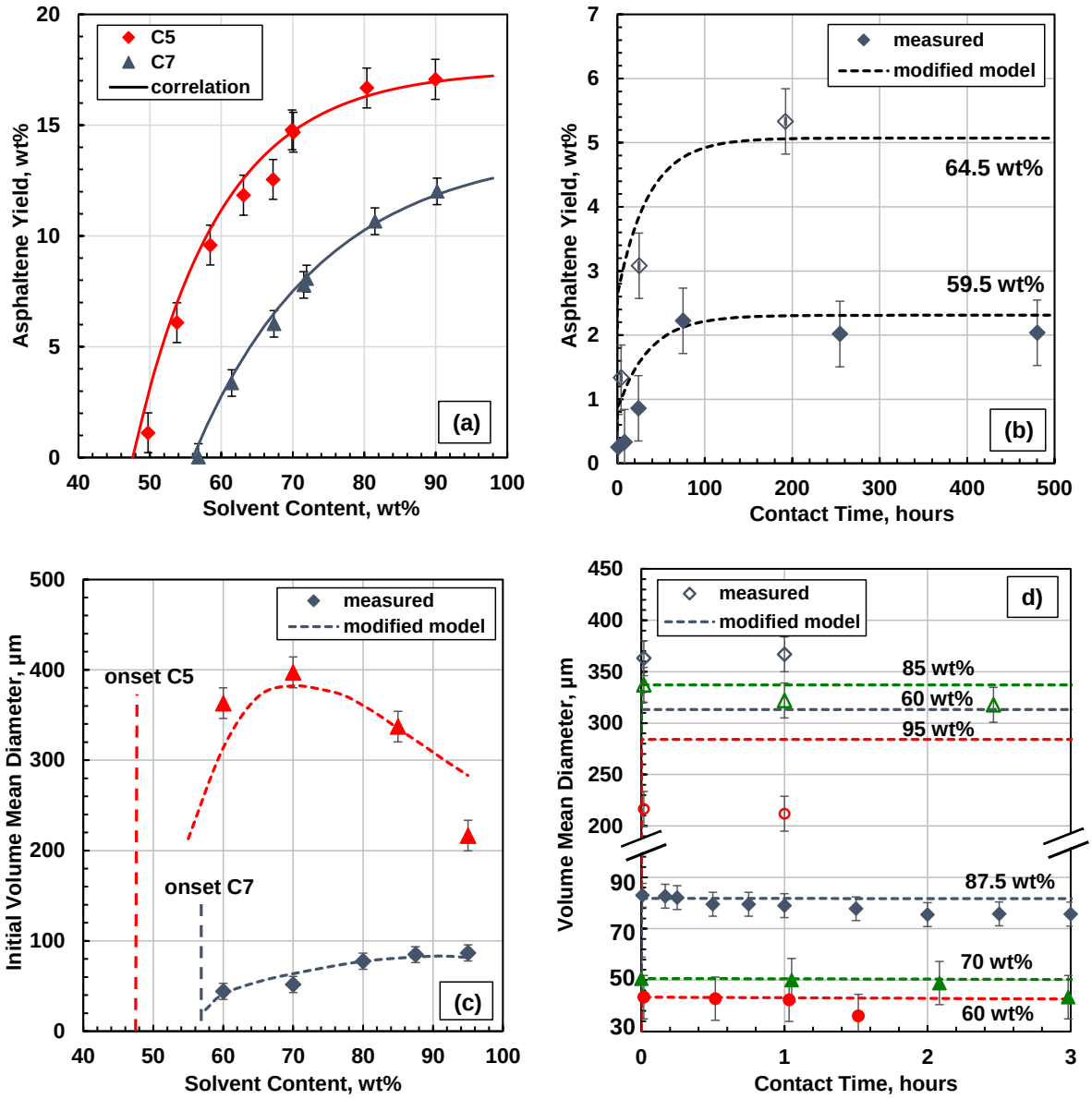

Figure 4.9. Measured and modeled (modified model) asphaltene yields and aggregate mean diameters for the diluted WC-B-A3 bitumen in *n*-heptane and *n*-pentane at 21ºC: a) asphaltene yields at 24 h contact time in nitrogen atmosphere; b) asphaltene yield over time in *n*-heptane; c) volume mean diameters at 30 s; d) volume mean diameter over time in *n*-pentane and *n*-heptane.

4.3.2 Supplemental Dataset

The supplemental dataset includes onsets, yields, and aggregate sizes for WC-B-A3 bitumen with *n*-heptane and *n*-pentane at 21°C. The aggregate diameters in *n*-heptane for this sample were

reported in Section 3.3. The results for this bitumen in *n*-heptane were similar to the results for the WC-B-B2 bitumen. The asphaltenes were significantly less soluble (higher yields) in *n*-pentane than in *n*-heptane, as shown in Figure 4.9a. The equilibrium onsets were 47.6 ± 0.3 wt% *n*-pentane and 56.0 ± 0.3 wt% *n*-heptane.

The equilibrium yields for these systems were taken as the yields at 24 hours and are expected to be within 7% of the equilibrium value based on the data from the WC-B-B2 bitumen. The equilibrium yields were correlated with Eq. 4.24 with *b* equal to 0.055 for the *n*-heptane diluted system (AAD = 0.27 wt%), and 0.082 for *n*-pentane (AAD = 0.68 wt%). The increment in yield over time in *n*-heptane is shown in Figure 4.9b; the yields were not measured over time in *n*-pentane.

Figure 4.9c shows that the asphaltene aggregate diameters in *n*-pentane are approximately 4 times larger than the diameters in *n*-heptane. Figure 4.9d shows the time dependent behavior of aggregate diameter in the two solvents. In both cases, aggregate diameters exhibit a steep increase over the first minutes and remain almost unchanged over time. For the *n*-heptane diluted WC-B-A3, no reliable data was obtained with the FBRM method below 75 wt%, therefore only diameters obtained with micrographs are reported in this region. For the *n*-pentane diluted mixture, only the micrographic method was employed.

4.3.3 Performance of the Preliminary Population Balance Model

The geometric population balance described in Section 4.2 was tested on the yield and particle size data for the crude oils of the development dataset. The remaining unspecified input parameter was the amount of unstable asphaltenes for the calculation of the concentration of primary particles (Eq. 4.8). This amount was taken as the fitted equilibrium yield from Eq. 4.24. The collision efficiencies were tuned to match the yield curves for each oil as shown in Figure 4.5 (solid lines). The fitted efficiencies and average absolute deviations (AAD) for the yields are provided in Table 4.4. The model fitted the measured yields to within 0.5 wt%. The collision efficiencies were almost insensitive to the *n*-heptane content and therefore a single collision efficiency was fitted for each oil. In contrast, Maqbool *et al*. (2011a) found that collision efficiencies increased with precipitant

content. The difference could be caused by the presence of air in the Maqbool *et al*. study. The collision efficiencies for three of the four oils are in the same order of magnitude while that of the EU-HO-A1 oil is an order of magnitude lower. The collision efficiencies did not correlate with the asphaltene content or other properties of the oils.

Table 4.4. Collision efficiencies obtained for the preliminary population balance model.

Crude Oil	β	AAD Yields (wt%)	AARD Diameters (%)
WC-B-B2	0.0051	0.25	99
MX-HO-A1	0.0070	0.51	96
MSB	0.0050	0.02	28
EU-HO-A1	0.00023	0.03	54

Asphaltene aggregate size distributions were obtained from the population balance model using the collision efficiencies reported in Table 4.4. Since the collision efficiencies were obtained from minimization of yield data only, the diameters obtained from the population balance model are predictions. Figure 4.8 (solid lines) shows that in all cases the model captures the trend in particle growth rate over time but under-predicts the volume mean aggregate diameters from start to finish. In other words, the model fails to account for the early rapid aggregation process, particularly for the oils with high asphaltene content. The predicted diameters are approximately 50% too low for the two oils with low asphaltene content (MSB and EU-HO-A1) and 1-2 orders of magnitude too low for the heavy oils (WC-B-B2 and MX-HO-A1).

The model could be retuned to match the measured diameters but the required collision efficiencies would exceed 100% (by several orders of magnitude when attempting to match the WC-B-B2 data). In addition, a large β value causes large aggregates to form very rapidly giving a high separation efficiency and high yields almost immediately. In other words, the model can be adjusted to predict yields or diameters but not both at the same time. It appears that the preliminary model is not capturing all of the physics of the precipitation/flocculation process.

4.3.4 Modified Population Balance Model

The two main challenges in modeling the data are: 1) at *n*-heptane contents near the onset, to predict a small number of large aggregates at early times (low yield but large diameter) followed by a slow increase in yield and size; 2) at higher dilutions, to predict the almost instantaneous high initial yields followed by a slow increase in yield and size. Both challenges can be addressed if asphaltene precipitation is treated as a simultaneous nucleation/growth and aggregation process. Therefore, the population balance model was modified to include particle nucleation and growth as outlined below.

Particle Growth and Primary Particles

There is evidence in the literature that asphaltene precipitation is a phase transition; for example, asphaltene-rich phases are liquids at temperatures above 100°C rather than colloidal dispersions (Johnston *et al*., 2017). It then follows that the asphaltene particles at lower temperatures nucleate and grow in a process analogous to crystal growth. To assess the feasibility of this hypothesis, the growth of an asphaltene particle was modeled based on the mass of asphaltenes transported from the medium to the surface of the particle through a spherical boundary with radius *h.* The flux of material through the spherical volume is obtained from Fick's first law as follows,

$$J(t) = -4\pi r^2 D \frac{dC}{dr} \tag{4.25}$$

where *J(t)* is the flux at time *t*, *r* is the particle radius, and *D* and *C* are the diffusivity and concentration of the unstable asphaltenes, respectively. At constant flux, Eq. 4.25 is integrated to obtain the following expression for the particle growth rate,

$$\frac{dr}{dt} = \frac{D}{\rho}\left(\frac{C_0 - C_s}{r} - \frac{\rho r^2}{h^3}\right) \tag{4.26}$$

where C_0 is the asphaltene supersaturation concentration in the mixture, C_s, the concentration near the surface of the particle, and ρ, the density of the asphaltene particle. Assuming that $C_s \rightarrow 0$ and that $h >> r$, Eq. 4.26 can be simplified to obtain the following expression,

$$\frac{dr}{dt} = \frac{1}{r}\frac{DC_0}{\rho} \tag{4.27}$$

Eq. 4.27 is integrated to obtain the following analytical solution,

$$r(t) = \left(\frac{2DC_0}{\rho}t + r_0^2\right)^{1/2} \tag{4.28}$$

where r_0 is the initial radius of the asphaltene nucleus. Eq. 4.28 only applies for constant flux; that is, negligible depletion of unstable asphaltenes beyond the boundary *h*. It also assumes that *h* is fixed and therefore is only an approximation of the actual diffusion process.

Eq. 4.28 was applied to the oils in this study to calculate the diameter that the nuclei could reach within an arbitrary time limit of 0.1 seconds. A time of 0.1 s is a typical time frame for mineral crystals to form stable particles (Nguyen *et al.*, 2014; Markov, 2003) and is consistent with the near instantaneous formation of aggregates observed experimentally. The initial diameter of the unstable asphaltene nanoaggregates was set to 2.5 nm (Mostowfi *et al.*, 2009) and the asphaltene density was set to 1200 kg/m³ (Yarranton and Masliyah, 1996). The supersaturation concentration, C_0 (kg/m^3) was determined from the experimental equilibrium yields. The diffusion coefficients were approximated with the following correlation for *n*-heptane diluted bitumen (Grimaldos, 2018),

$$D_B = \frac{2.35 \cdot 10^{-12} T}{\mu_m^{0.35}} \tag{4.29}$$

where D_B is the bitumen diffusivity in the mixture (m²/s) here taken as the asphaltene diffusivity, and μ_m is the viscosity of the mixture in mPa·s.

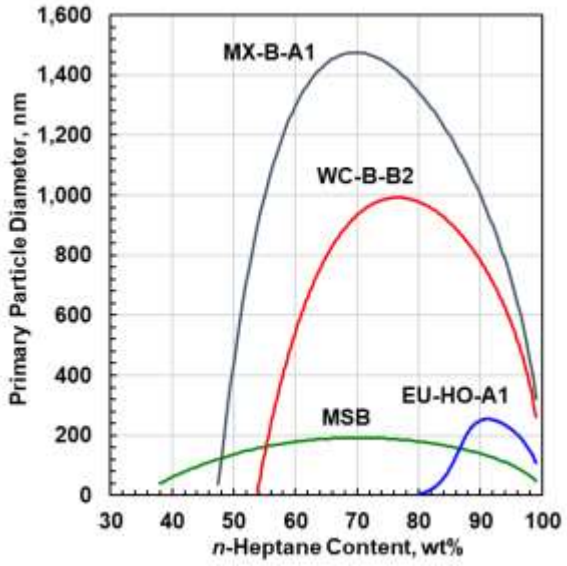

Figure 4.10. Diameter of asphaltene primary particles calculated with constant flux diffusion model after a growth time of 0.1 s.

Figure 4.10 shows the calculated diameter of the particles for each oil after 0.1 s of growth. The diameter of the particles depends on the concentration of unstable asphaltenes which initially increases above the onset of precipitation as more asphaltenes precipitate but then decreases at higher *n*-heptane contents as precipitation levels off but the mixture becomes more dilute. Hence, there is a maximum diameter for each oil. It is striking that the calculated particle diameters are significant (> 100 nm) at most precipitant contents above the onset. In other words, it is likely that the primary particle diameters are much larger than 2.5 nm. The maximum diameters range from 200 nm to 1.5 µm. These values are consistent with apparent primary particle sizes reported in the literature which range from 200 nm to 2 µm (Rastegari *et al*., 2004; Yang *et al*., 2018; Headen *et al*., 2009; Alhammadi *et al*., 2017).

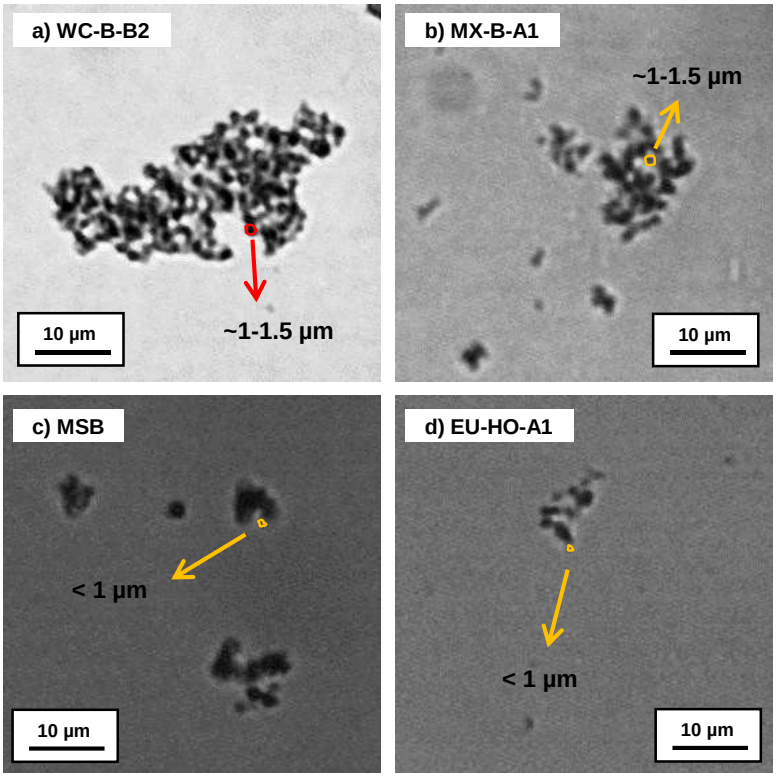

Figure 4.11. Primary particles of asphaltene aggregates in *n*-heptane diluted crude oils after 5 min of contact time: a) WC-B-B2 at 90.5 wt% *n*-heptane; b) MX-B-A1 at 87.5 wt% *n*-heptane; c) MSB at 45 wt% *n*-heptane; d) EU-HO-A1 at 86 wt% *n*-heptane.

Therefore, the primary particle diameter from the preliminary population balance model was modified from 2.5 nm to diameters at the 100+ nm scale. As noted above, the diffusion model is only an approximation and the actual primary particles sizes are unknown. In this study, the primary particle sizes were set to a fixed value equal to the maximum calculated value for each oil; that is, 1000 nm for WC-B-B2, 1500 nm for MX-B-A1, 200 nm for MSB, and 250 nm for the EU-HO-A1 oil. These diameters are similar to the qualitative estimates of the primary particle diameters from the micrographs shown in Figure 4.11.

Particle Nucleation

Asphaltenes come out of solution when the difference of solubility parameters between the asphaltene macromolecular assemblies (nanoaggregates) and the medium reaches certain threshold (Akbarzadeh *et al.*, 2005). However, the formation of new phase requires the appearance of small particles or nuclei that overcome an energy barrier and some degree of supersaturation is necessary for nucleation and precipitation to begin (Leite and Ribeiro, 2012). Nucleation is expected to occur simultaneously for a partially soluble homogeneous material but not necessarily for a polydisperse material like asphaltenes. Asphaltenes are thought to exist in the oil as a polydisperse distribution of solubilities, molecular weights, and other properties (Yarranton and Masliyah, 1996; Barrera *et al*., 2013). Hence, it follows that molecular aggregates having different properties could have different stability thresholds with different degrees of supersaturation at a given condition and; therefore, come out of solution at different times. The most insoluble asphaltenes (molecules or nano-aggregates) might nucleate first followed by the less insoluble material. It is also possible that initially soluble nano-aggregates undergo a molecular rearrangement to form a mixture of soluble and insoluble nano-aggregates and molecules. Hence, nucleation may continue over time.

Time dependent nucleation means that only some of the ultimately unstable asphaltenes will be available at first and the remainder will appear over time. This hypothesis is consistent with the observation of instantaneous high initial yields followed by a slowly increasing yields, as shown in Figure 4.12. At precipitant contents well above the equilibrium onset of precipitation (86 wt% *n*-heptane in Figure 4.12), a large fraction of asphaltenes are initially unstable and nucleate rapidly

forming large aggregates that can be separated as a precipitate. Over time, the rest of asphaltenes start to nucleate, grow, and aggregate to form large aggregates, which are eventually added to the detected precipitate. In contrast, near onset conditions (83 wt% *n*-heptane in this example), only a small fraction of asphaltenes, if any, are initially unstable and only over time do more nucleate, grow, and aggregate into detectable precipitate.

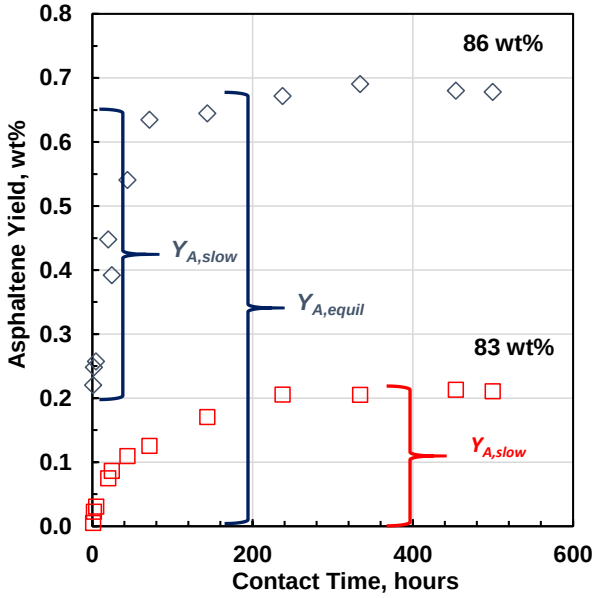

Figure 4.12. Change in yield over time observed near and well above the equilibrium onset of precipitation. The data (symbols) is from the *n*-heptane diluted EU-HO-A1 oil at 21ºC.

Therefore, the preliminary population balance was modified to include a nucleation rate as a generation term in the balance of for the primary units only, as follows,

$$\frac{dC_1}{dt} = -C_1 \sum_{j=i}^{N-1} K_{1,j} C_j + \dot{r}_N \tag{4.30}$$

Assuming that the rate of nuclei generation is proportional to the rate of yield increase observed in the yield curve (Figure 4.12), the nucleation rate is given by,

$$\dot{r}_N = \frac{dc_{1,gen}}{dt} = k_A k_N Y_{A,slow} \exp(-k_N t) \tag{4.31}$$

where k_N is the nucleation rate constant, k_A is a factor to convert from mass to molar concentration, and $Y_{A,slow}$ is the equilibrium yield of the asphaltenes that precipitate slowly over time. The conversion factor is given by,

$$k_A = \frac{(1-w)\rho_m}{M_w N_n} \tag{4.32}$$

where w is the mass fraction of *n*-heptane and ρ_m is the medium density. The slow equilibrium yield term is given by,

$$Y_{A,slow} = (1-f)Y_{A,eq} \tag{4.33}$$

where f is the fraction of immediate precipitation and is obtained experimentally. The fraction of asphaltenes that come out of solution immediately upon precipitant addition was taken as the first data point in the yield measurements. For example in Figure 4.12, approximately 30% of the asphaltenes destabilized at 86 wt% *n*-heptane are collected as precipitate after a few minutes of contact time.

Collision Frequency

In the preliminary population balance model, the collision frequency factor, $\alpha_{i,j}$, is based on Brownian collisions between non-interacting aggregates. As discussed before, if the Brownian collision frequency is used, the collision efficiencies required to fit the data were unrealistically high, at least 3 orders of magnitude greater than unity. Brownian collisions do not account for the attraction between particles but asphaltene aggregates are attracted to each other via van de Waals interaction forces. Several authors have related the collision efficiency to the Hamaker constant, a measure of the van der Waals forces (Bäbler, 2008; Balakin *et al*., 2012; Vanni and Baldi, 2002; Alam, 1987). Hamaker (1937) and Chu *et al*. (1967) introduced an explicit correction factor for the collision frequency of interacting particles by modeling the adhesion originated from van der Waals forces of two colliding spherical particles. They showed that for two particles of diameters d_i, and d_j, the van de Waals potential is given by,

$$\phi(x) = -\frac{A_{eff}}{6}\left[\frac{2d_i d_j}{f_1} + \frac{2d_i d_j}{f_2} + \ln\left(\frac{f_1}{f_2}\right)\right] \tag{4.34}$$

where x is the dimensionless separation distance between the particles ($x = d_j/r$ for $d_j > d_i$) and A_{eff} is the Hamaker constant. The parameters f_1 and f_2 are given by,

$$f_1 = 4\left(\frac{d_j}{x}\right)^2 - \left(d_i + d_j\right)^2 \tag{4.35}$$

$$f_2 = 4\left(\frac{d_j}{x}\right)^2 - \left(d_i - d_j\right)^2 \tag{4.36}$$

The additional attraction from the van der Waals forces experienced by the particles is as follows,

$$W_{i,j} = \frac{1}{4}\left(d_i + d_j\right)\int_0^{x_L} \exp\left[\frac{\phi(x)}{k_B T}\right] dx \tag{4.37}$$

where $W_{i,j}$ is the enhancement factor of the collision frequency and the upper limit of the integral is given by,

$$x_L = \frac{2}{\frac{d_i}{d_j}+1} \tag{4.38}$$

In the model, the integral in Eq. 4.37 was solved numerically using the Gauss-Kronrod quadrature algorithm (Shampine, 2008).

The revised collision frequency is given by,

$$\alpha_{i,j} = \frac{2}{3}\frac{RT}{W_{i,j}\mu_m}\frac{\left(d_i+d_j\right)^2}{d_i d_j} \tag{4.39}$$

The enhancement factor is included the denominator of the collision efficiency because for negative potentials (attraction), the value of the integral is less than unity and will increase the collision frequency. The effective Hamaker constant is determined as follows (Wang *et al.*, 2010),

$$A_{eff} = \left(\sqrt{A_{med}} - \sqrt{A_{asph}}\right)^2 \tag{4.40}$$

The Hamaker constant for the medium, A_{med}, was estimated as the volume average of the Hamaker constants of oil and precipitant, $A_{med} = \Sigma\varphi_i A_i$, where φ_i is the volume fraction of the components. In this study, the Hamaker constants were set to 4.5×10^{-20} J for *n*-heptane (Israelachvili, 2011), 6×10^{-20} J for asphaltenes (Fotland and Askvik, 2008), 6×10^{-20} J for bitumens (Liu *et al.*, 2004), and 5×10^{-20} J for other oils (Vincent, 1973). All these values were originally reported in air at 20ºC.

Collision Efficiency (or the Stickiness of Asphaltene Aggregates)

In the preliminary population balance model, the collision efficiency was assumed to be invariant with time. However, the adhesion forces between asphaltene surfaces decreases significantly over time as shown in Section 3.6 and also reported by Wang *et al*. (2010) and Natarajan *et al.* (2014). These studies used a Surface Force Apparatus (SFA) to investigate the adhesion between

asphaltene layers adsorbed on mica surfaces. In Section 3.6 it was shown that the attraction forces in a precipitant such as *n*-heptane decreased significantly within minutes and disappeared almost completely within 90 min. Atomic force microscopy indicated that the polar branches of the asphaltene molecules reorient away from the fluid reducing the interparticle interactive forces. In colloquial terms, the asphaltene particles lose their stickiness over time.

This observation is consistent with the data collected for the WC-B-B2 and MX-B-A1 where aggregate sizes reach large diameters within few seconds but later diameters remained unchanged. High collision efficiencies at early times may explain the initial rapid increase in aggregate size. To incorporate the decrease in stickiness over time into the population balance model, a time-dependent expression for the collision efficiency was introduced, as follows

$$\beta = \beta_E \exp(-k_s t) + \beta_{res} \tag{4.41}$$

where β_E and β_{res} are the initial and residual collision efficiencies and k_s the rate of decay of the adhesion force (stickiness). Although the surface force measurements suggest the particles lose all of their stickiness over time, a residual stickiness was required because new particles are nucleating over time maintaining some stickiness in the mixture of aggregates.

4.3.5 Performance of the Modified Population Balance Model

The modified population balance model was implemented following an algorithm similar to Figure 4.1. As before, the temperature and precipitant content must be specified. The other model inputs are the:

- medium properties (density, viscosity, and Hamaker constant)
- asphaltene density, ρ_A
- asphaltene fractal dimension, D_f
- equilibrium yield, $Y_{A,eq}$ and immediate yield fraction, f
- centrifugation conditions (r_c, L, t_c)
- primary particle diameter, d_p
- nucleation rate, k_N
- collision efficiency parameters (β_E, k_s, and β_{res}).

The density and viscosity of the medium, the asphaltene density, and the fractal dimension were determined as described for the original model. The Hamaker constant was determined as described in Section 4.3.4. The equilibrium yields and fractional slow yields were obtained from the measured yield curves and are provided in Appendix D. The primary particle diameters were set from the diffusion calculations as described in Section 4.3.4. The remaining parameters (k_N, β_E, k_s, and β_{res}) were simultaneously adjusted to fit the measured yield and aggregate diameter data. The new objective function is given by,

$$OF = \min_{k_N,\beta_E,k_s,\beta_{res}} \left[\frac{1}{n_y}\sum_{j=1}^{n_y}\left(Y_{j,\text{exp}} - Y_{j,\text{ model}}\right)^2 + \frac{1}{n_d}\sum_{k=1}^{n_d}\left(d_{4,3_{k,\text{exp}}} - d_{4,3_{k,model}}\right)^2\right] \qquad (4.42)$$

The fitted parameters are listed in Table 4.5. The same constant nucleation rate was found for all four oils. The fitting of the collision efficiency for the oils with low asphaltene contents (MSB and EU-HO-A1) was relatively straightforward: the initial collision efficiency, β_E, was independent of the *n*-heptane content and a constant stickiness was sufficient to fit the data. For the bitumens (WC-B-B2 and MX-B-A1), the initial collision efficiency decreased exponentially as the *n*-heptane content increased (see Appendix E). In addition, a time dependent stickiness was required to fit the data. The adhesion decay rate, k_s, was similar for both bitumens, and was set to the average value of 1.5 s^{-1}. This decay rate is equivalent to a 95% loss in the collision efficiency (stickiness) after 5 minutes of contact time. Similarly, a constant value for the residual collision efficiency, β_{res}, was sufficient to fit the data for both oils. The fitted model matched the yield with an AAD within 0.3 wt% and diameter data with average absolute relative deviations (AARD) below 25%, Table 4.6. The fitted yields are shown in Figure 4.5 (dashed lines) and the fitted aggregate diameters in Figure 4.7 and 4.8 (dashed lines).

The main difference between the oils is their collision efficiency. The collision efficiencies in the bitumens are initially very high but decrease significantly as the *n*-heptane content increases and over time. The collision efficiencies in the low asphaltene content oils may well decrease with increasing *n*-heptane content and time but the changes are too small to detect given the low initial collision efficiency. Interestingly, the residual collision efficiencies of the bitumens are in the same order of magnitude of those of the low asphaltene content oils. In other words, the asphaltenes

from bitumens are initially highly sticky but, after few minutes, behave similarly to asphaltenes from other oils.

The reason for the difference in the initial stickiness in the different oils is unknown. However, the atomic force data collected by Zeng's group (Wang *et al*., 2010) have shown that the adhesion force (stickiness) between asphaltene surfaces increases as the surrounding medium becomes a poorer solvent for the asphaltenes; that is, as the *n*-heptane content increases. For the diluted bitumens in this study, the apparent stickiness decreases at higher *n*-heptane content. Therefore, it is likely that the change in stickiness with dilution is related to the change in chemical composition of the precipitating asphaltenes. The least soluble asphaltenes appear to be stickier than the more soluble asphaltenes. The asphaltenes in the low asphaltene content oils may simply have a smaller fraction of "sticky" asphaltene components. To establish a relationship between asphaltene chemistry and stickiness, adhesion force measurements and chemical characterization would be required for whole and fractionated asphaltenes from a broad range of samples. Such an analysis is beyond the scope of this study.

Table 4.5. Fitted parameters for the modified population balance model.

Oil	*n*-Heptane Content, wt%	β_E	β_{res}	k_s (s^{-1})	k_N (s^{-1})
WC-B-B2	54.5	10.809	1.0×10^{-8}	1.5	7.80×10^{-6}
	57.5	1.586			
	59.5	0.289			
	64.5	0.186			
MX-B-A1	48.5	7.321			
	52.0	0.075			
	55.0	0.062			
MSB	38.5 - 55.0	8.21×10^{-8}	-	-	7.80×10^{-6}
EU-HO-A1	80.0 – 86.0	1.82×10^{-8}			

Table 4.6. Deviations of the fitted modified population balance model.

Oil	Yield AAD (wt%)	Diameter AARD (%)
WC-B-B2	0.16	24.1
MX-B-A1	0.30	6.4
MSB	0.01	15.7
EU-HO-A1	0.01	21.9

4.3.6 General Application of the Modified Population Balance Model

For a generally applicable model, the inputs must be specified either from measurements or correlations. The input parameters for the model were listed in Section 4.3.5. The medium properties can be determined from measurements or from existing correlations based on known or measured properties such as the oil density. Asphaltene densities vary within a narrow range and, if not measured, can be set to 1200 kg/m³. The equilibrium yields must be measured or calculated; for example, from a regular solution model (Akbarzadeh *et al.*, 2005) or an equation of state (Johnston *et al*., 2017; Punnapala and Vargas, 2013; Zhang *et al*., 2019). A nucleation rate (k_N) of 7.6×10^{-8} s^{-1} and a stickiness decay factor (k_S) of 1.5 s^{-1} are recommended. The remaining inputs are the primary particle diameter (d_p), the immediate yield fraction (f), and the collision efficiency parameters (β_E and β_{res}). Each are discussed below.

Primary Particle Diameter

The application of the growth model of Eq. 4.28 provides an approximation to the primary particle diameters. It depends mainly on the concentration of destabilized asphaltenes which is proportional to the asphaltene content of the oil. Hence, the primary particle diameters were correlated to the C5-asphaltene contents of the oils from Table 2.1 with the following expression

$$d_p = 54.532\, W_A \tag{4.43}$$

where d_p is in nm and W_A is the mass percent of *n*-pentane insoluble asphaltenes in the oil. Figure 4.13 shows that the linear expression fits the data with an AARD of 7.4%. In some of the examples from the literature, only an *n*-heptane insoluble asphaltene content is reported. In this case, the primary particle parameter is correlated as follows,

$$d_p = 57.57\, W_{A,C7} + 105.01 \qquad (4.44)$$

where $W_{A,C7}$ is the mass percent of *n*-heptane insoluble asphaltenes in the oil. This correlation has an AARD of 10.1%.

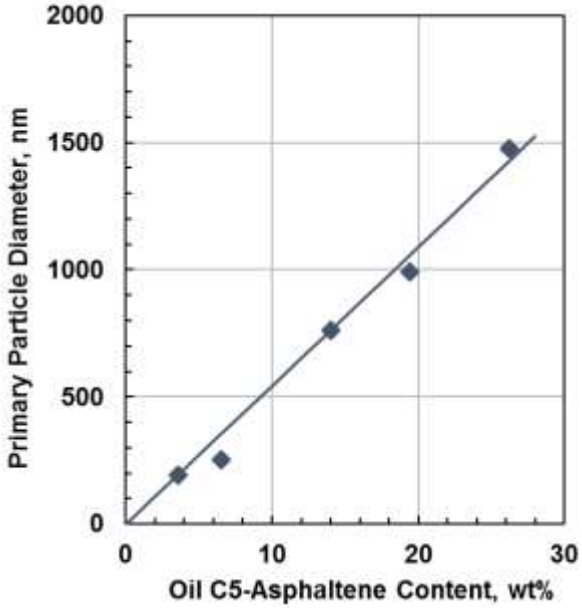

Figure 4.13. Correlation of the primary particle diameter to the C5-asphaltene content of the oil.

Immediate Precipitation Fraction (f)

The fraction of asphaltenes that precipitate immediately increased monotonically with the precipitant composition (see Appendix E). In theory, f could be correlated to the difference between the solubility parameters of the asphaltenes and the medium. However, solubility parameters for asphaltenes and oils are not easily determined. Instead, f was correlated to the degree of separation from the onset (w-w_{onset}) with following empirical expression,

$$f = \exp\{-B \exp[-C(w - w_{onset})]\} \qquad (4.45)$$

where w is the weight percent of precipitant in the mixture and w_{onset} is the equilibrium onset value. The onset can be obtained experimentally or from a thermodynamic equilibrium model (regular solution model or EoS tuned with long term equilibrium data). The parameter C was correlated to the ratio between the specific gravity of the oil (SG_o) and the equilibrium onset value as follows,

$$C = \frac{0.421 - 16.13(SG_o / w_{onset})}{1 - 34.83(SG_o / w_{onset})} \quad (4.46)$$

The parameter *B* was correlated to the asphaltene content (C5-asphaltenes) of the oil as follows,

$$B = 164.6C\ W_A^{-0.8453} \quad (4.47)$$

The correlated values of *f* are available in Appendix E. The AARD was 6.8% almost within the uncertainty of the fitted values.

Initial Collision Efficiency (β_E)

The initial collision efficiency was also correlated to the degree of separation from the equilibrium onset (w-w_{onset}) as follows,

$$\beta_E = k \exp\left[\frac{9.122 - 3.05(w - w_{onset})}{(w - w_{onset}) + 2.874}\right] \quad (4.48)$$

The pre-exponential factor *k* depends on the type of precipitant used and the specific gravity of the oil at 20ºC (SG_o), and is given by,

$$k = k_0 \exp(17.905\ SG_o - 31.63) \quad (4.49)$$

where k_0 is 5.55×10^4 for *n*-heptane diluted oil, and 2.32×10^6 for *n*-pentane. Eq. 4.48 was fitted to measured aggregate diameters from both the Development and Supplemental datasets. The correlation fit the collision efficiencies in *n*-heptane and in *n*-pentane with an AARD of 35% and 62%, respectively. The deviations result mainly from the scatter in the experimentally derived data. The comparison between the experimentally derived and correlated collision efficiencies is available in Appendix E.

Performance of the Model with Correlations

After including the above correlations, the only inputs to the model are the equilibrium yields (here taken from measurements), the temperature, and the precipitant content. The correlations were first tested on the Development Dataset. Table 4.7 summarizes the incremental deviations obtained for yields and aggregate diameters compared to the results of the model using measured immediate and equilibrium yields. For the MSB and EU-HO-A1 (low asphaltene content), β_E was independent of time, therefore the collision efficiency was fixed to 5×10^{-8}. This is the average value obtained for both oils reported in Table 4.5. The yields obtained over time were virtually unaffected by the use of the proposed correlations (about 0.01 wt% increment in AAD). The main differences were

observed in the estimation of aggregate diameters, in particular near the equilibrium onset composition. Because the correlation for β_E is an exponential function, small deviations in $(w-w_{onset})$ generate relatively large differences in the initial diameters. In this region, larger deviations were observed, however the model still captured the trend of the aggregate diameters to within 33%.

Table 4.7. Deviations of the modified population balance model using the proposed empirical correlations.

Oil	Yield ARD (wt%)	Diameter AARD (%)	Incremental* Yield, (wt%)	Incremental* Diameter, (%)
WC-B-B2	0.22	28.6	+0.06	+4.5
MX-B-A1	0.42	27.1	+0.11	+20.7
MSB	0.01	32.3	0	+16.6
EU-HO-A1	0.02	27.8	+0.01	+5.9

* Incremental errors obtained by using correlations instead of experimental values.

The performance of the model with the proposed correlations was then tested on the Supplemental Dataset (WC-B-A3 bitumen diluted with *n*-heptane and *n*-pentane). The input primary particle diameters were 790 nm in *n*-heptane (from Eq. 4.43) and 1400 nm in *n*-pentane (from Eq. 4.28). The rest of parameters were determined as described previously. The model results are shown in Figure 4.9. The yields over time in *n*-heptane, Figure 4.9b, were predicted to within 0.7 wt%, although the yield at intermediate times was slightly overestimated. The initial diameters of the asphaltene aggregates in *n*-heptane and *n*-pentane, Figure 4.9c, were matched with AARD of 9.1% and 13%, respectively. Figure 4.9d shows that the model matches the rapid increment in diameter and the nearly constant value observed at longer times. In *n*-heptane, the diameters are matched to within the experimental error ±5.6%. The aggregate diameters measured with the FBRM technique appear to decrease over time; however, this trend was attributed to asphaltene deposition in the laser probe or settling of the larger aggregates over time as discussed in Chapter 3. In *n*-pentane, the diameters were under-predicted near the onset but over-predicted at high dilutions with deviations up to 35%.

4.3.7 Testing the Modified Population Balance Model

Maqbool *et al*. (2009, 2011a, 2011b) reported yields of asphaltene precipitation over time for an Alaskan crude oil (k-1) and for a Gulf of Mexico crude oil (GM2) both diluted with *n*-heptane. Sufficient data were provided in these sources to test the model and compare the results in terms of yields and aggregate diameters. Properties of these oils are provided in Table 4.8.

Table 4.8. Properties of the crude oils used to test the model as reported in literature (Maqbool *et al*., 2009, 2011a, 2011b).

Sample	Density @ 20ºC kg/m^3	Viscosity @ 20ºC mPa·s	C7-Asph. wt%
k-1	923.8	160	10.9
GM2	867.8	15.7	3.6

Asphaltene yield data for the k-1 oil and GM2 oils were measured in air over 500 h and 1000 h, respectively. The solutions were centrifuged at 14000 rpm for 10 minutes (L_c = 0.03 m, r_c = 0.073 m) to recover the precipitated asphaltenes and gravimetrically determine the yields. Only data at 20ºC are considered here and are shown in Figure 4.14. For the k-1 oil, the asphaltene yields appear to reach a plateau value by 500 h, Figure 4.14a. The yield from the GM2 oil increased continuously over 1000 h, Figure 4.14b. The continuous increase in yield may be caused by oxygen which can affect the kinetics of precipitation at long contact times (Beck *et al*., 2005).

Only limited data on the size of the aggregates were available. Maqbool *et al.* (2009) reported aggregate diameters for the k-1 oil at 50 vol% *n*-heptane (approximately 43 wt%) in the range of 1-2 µm after 1.4 h of contact time, reaching 2 to 5 µm in diameter at 20 h. Maqbool *et al.* (2011b) analyzed micrographs of aggregates from the GM2 oil at 34% vol *n*-heptane (approximately 29 wt%). They found that the aggregate sizes were below 2 µm before 24 h and grew to 5 to 10 µm afterwards. In the same study, a population balance model was used to predict onset times of precipitation (as detection of 0.5 µm particles in the microscope). At 29 wt% *n*-heptane, particles of 0.5 µm were detected at 7.8 h. The above aggregate size data are shown in Figure 4.15.

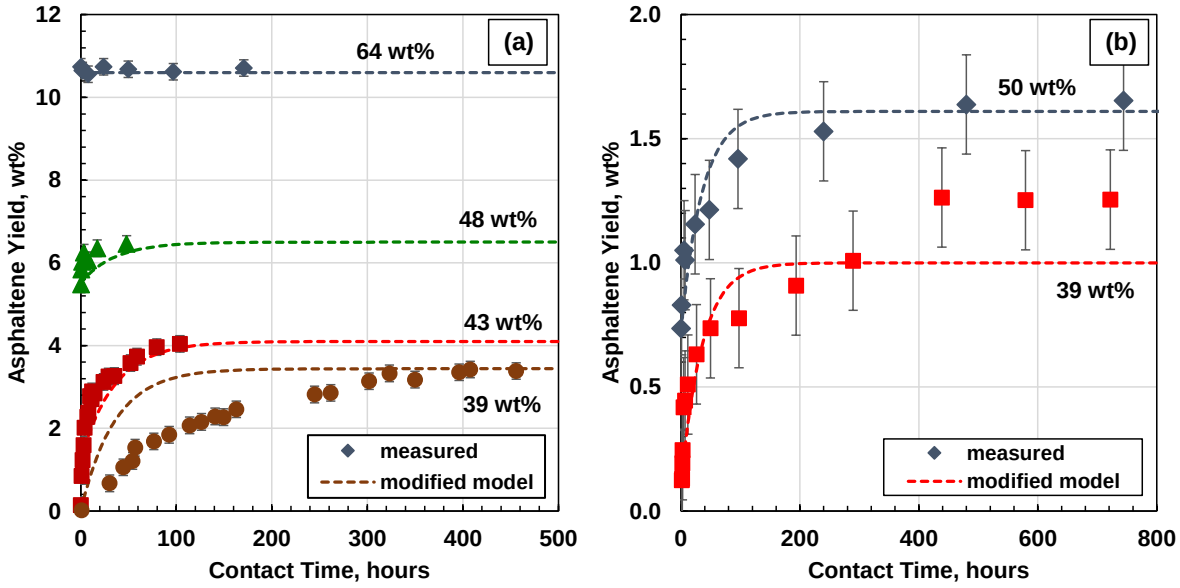

Figure 4.14. Measured and predicted (modified model) asphaltene yields over time at 20ºC for *n*-heptane diluted crude oils: a) k-1 oil; b) GM2 oil. Yields were collected in an air atmosphere and were originally reported by Maqbool *et al*. (2009, 2011a, 2011b).

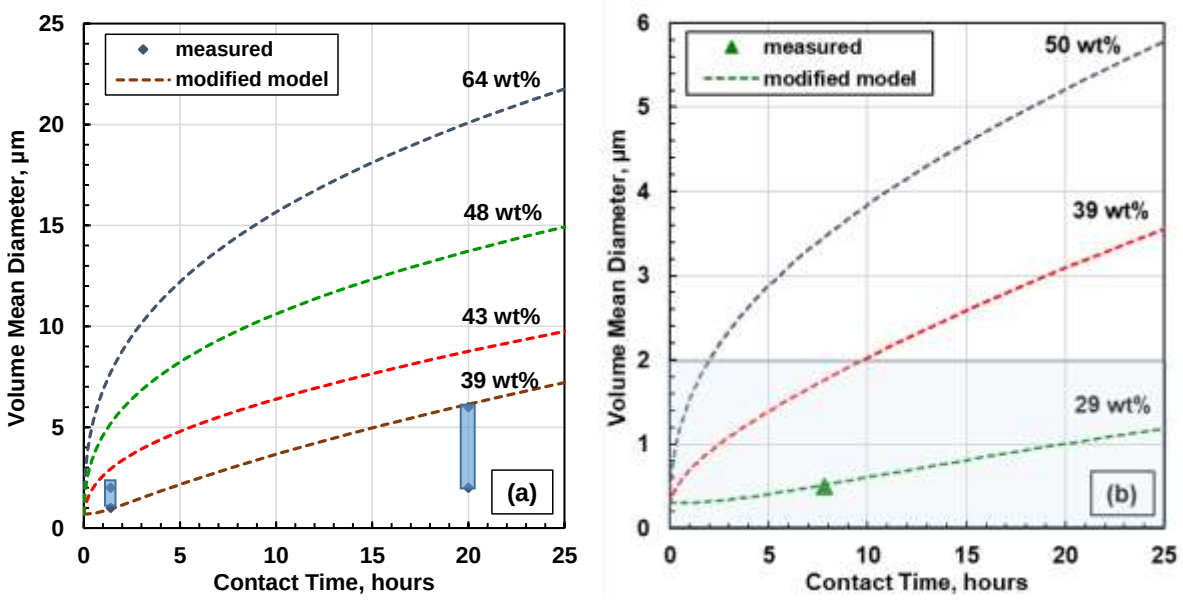

Figure 4.15. Asphaltene aggregate volume mean diameters as predicted by the modified population balance model for the *n*-heptane diluted crude oils reported by Maqbool *et al*. (2009, 2011a, 2011b). a) k-1 oil; b) GM2 oil. Shaded areas represent experimental observations made by Maqbool and coworkers; the shaded area in (b) applies at 29 wt% *n*-heptane.

The input parameters for the model were set as follows. The fraction of immediate precipitate, *f*, was set to the first measured yield data point. The equilibrium yields, $Y_{A,eq}$, were set to the experimental yield observed at 500 h. The nucleation rate was taken from Table 4.5. The collision efficiency of 5×10^{-8} was taken as the average for the low-asphaltene content oils (MSB and EU-HO-A1) from Table 4.5. The diameters of primary particles were calculated from Eq. 4.44 and were 700 nm for the k-1 oil and 300 nm for the GM2 oil. The aggregate fractal dimension was calculated with the correlation provided in Eq. 4.19. The density and viscosity of the mixtures were estimated following volume average and double log average mixing rules, respectively (Saryazdi *et al*., 2013; Yarranton *et al*., 2013).

As shown in Figure 4.14, the model predicted the yields of precipitation over the first 500 h with an AAD of 0.42 wt% for the k-1 oil and 0.11 wt% for the GM2 oil. Since the model was set to reach equilibrium yields based on the measured values at 500 h, it could not represent the increase in yield after 500 h. The model also over-predicted the k-1 yields at low solvent contents (near the equilibrium onset). It could be tuned to a better match by using a lower nucleation rate at this condition but considering all of the available data, there was not enough justification to correlate the nucleation rate to the proximity to the onset. Figure 4.15 shows that the model also predicted the aggregate diameters within the reported size ranges. It matched the slow increase of aggregate sizes over time and matched the onset detection times reported by Maqbool *et al.* (2009, 2011a, 2011b).

4.4 Conclusions

The onset and yield of asphaltene precipitation from four *n*-heptane diluted crude oils were initially time-dependent but each reached a plateau value after approximately 100 to 150 h of contact time. It appears that asphaltene precipitation reaches an equilibrium condition, supporting the hypothesis that asphaltene precipitation is a phase transition process.

At *n*-heptane contents just above the equilibrium onset, the yields increased slowly and reached equilibrium within 50 to 150 h. In contrast, at *n*-heptane contents well above the onset, high yields were obtained almost instantaneously. The yields then increased slowly over tens of hours until

equilibrium was attained. The time to obtain equilibrium yields decreased at higher *n*-heptane contents.

The kinetics of precipitation was first modeled with the population balance proposed by Maqbool *et al*. (2011a) modified to include the fractal dimension with the measurements presented in Chapter 3. The model was tuned to match the measured yields by tuning a constant collision efficiency for each oil. The model approximately matched the yield data over time at all *n*-heptane contents (AAD of 0.5 wt%); however, it failed to predict the size of the asphaltene aggregates. For the oils with low asphaltene content (MSB and EU-HO-A1), the model underpredicted the diameters by up to 50%. For the bitumen samples (WC-B-B2 and MX-B-A1), the predicted diameters were two orders of magnitude too low.

The rapid precipitation observed at early times and the sharp increase in aggregate size observed almost immediately upon contact with the precipitant was not accurately captured by the original model. This behavior was more consistent with a simultaneous nucleation/growth/aggregation process and these mechanisms were incorporated into the model by including: 1) a generation term for the nucleation of primary particles; 2) increasing the primary particle size to the micrometer scale as a result of the growth process; 3) including the interparticle attraction forces resulting from van der Waals interactions in the collision frequency term; 4) making the collision efficiency a function of time to account for the loss of adhesion observed in the asphaltene particles over time. The modified model adjusted the experimental yields with slightly better accuracy as the original model (AAD = 0.30 wt%) but also captured the change on the aggregate size to within 25% of the experimental values. The collision efficiency was higher for the bitumens than for the light oils but the reason for the difference is not known.

To generalize a model, a set of correlations were proposed for the model parameters. The remaining inputs for the model are the viscosity and density of the oil and of the precipitant at the given temperature, the asphaltene content of the oil, and equilibrium yield values that can be obtained either experimentally or from an equilibrium calculation (*e.g.* regular solution model or EoS). The modified model and the correlations were tested against data for a bitumen sample in

n-heptane and *n*-pentane, and data for two oils from the literature in *n*-heptane. The modified model predicted the yields within 0.55 wt% and aggregate diameters both with deviations less than 35%. If any kinetic data are available, the model could be tuned by adjusting the nucleation rate k_N (if only yield data are available) and also by adjusting β_E if also initial aggregate diameters are available.

4.5 Chapter References

Agrawal, P.; Schoeggl, F.F.; Satyro, M.A.; Taylor, S.D.; Yarranton, H.W. (2012). Measurement and Modeling of the Phase Behavior of Solvent Diluted Bitumens. *Fluid Phase Equilib.*, 334, 51–64.

Akbarzadeh, K.; Alboudwarej, H.; Svrcek, W.Y.; Yarranton, H.W. (2005). A Generalized Regular Solution Model for the Prediction of Asphaltene Precipitation from *n*-Alkane Diluted Heavy Oils and Bitumens. *Fluid Phase Equilib.,* 232, 159-170.

Alam, M.K. (1987). The Effect of van der Waals and Viscous Forces on Aerosol Coagulation. *Aerosol Sci. Technol.,* 6 (1), 41-52.

Alboudwarej, H.; Akbarzadeh, K.; Beck, J.; Svrcek, W.Y.; Yarranton, H.W. (2003). Regular Solution Model for Asphaltene Precipitation from Bitumens and Solvents. *Energy Fuels*, 49 (11), 2948-2956.

Alboudwarej, H.; Beck, J.; Svrcek, W.Y.; Yarranton, H.W.; Akbarzadeh, K. (2002). Sensitivity of Asphaltene Properties to Separation Techniques. *Energy Fuels*, 16, 462-469.

Alhammadi, A.A.; Chen, Y.; Yen, A.; Wang, J.; Creek, J.L.; Vargas, F.M.; Chapman, W.G. (2017). Effect of the Gas Composition and Gas/oil Ratio on Asphaltene Deposition. *Energy Fuels,* 31, 3610-3619.

Andersen, S.I.; Birdi, K.S. (1990). Influence of Temperature and Solvent on the Precipitation of Asphaltenes. *Fuel Sci. Technol. Int.,* 8 (6), 593-615.

Andersen, S.I.; Lindeloff, N.; Stenby, E.H. (1998). Investigation of Asphaltene Precipitation at Elevated Temperature. *Petr. Sci. Technol*., 16 (3-4), 323-334.

Angle, C.W.; Long, Y.; Hamza, H.; Lue, L. (2006). Precipitation of Asphaltenes from Solvent-Diluted Heavy Oil and Thermodynamic Properties of Solvent-Diluted Heavy Oil Solutions. *Fuel*. 85 (4), 492-506.

Arya, A.; Liang, X.; Von Solms, N.; Kontogeorgis, G.M. (2017). Modeling of Asphaltene Precipitation from Crude Oil with the Cubic Plus Association Equation of State, *Energy Fuels*, 31 (2), 2063-2075.

Bäbler, M.A. (2008). A Collision Efficiency Model for Flow-induced Coagulation of Fractal Aggregates. *AIChE J.*, 54 (7), 1748-1760.

Balakin, B.V.; Hoffmann, A.C.; Kosinski, P. (2010). Population Balance Model for Nucleation, Growth, Aggregation, and Breakage of Hydrate Particles in Turbulent Flow. *AIChE J.* 56 (8), 2052- 2062.

Balakin, B.V.; Hoffmann, A.C.; Kosinski, P. (2012). The Collision Efficiency in a Shear Flow. *Chem Eng. Sci.*, 68, 305-312.

Barrera, D.M.; Ortiz, D.P.; Yarranton, H.W. (2013). Molecular Weight and Density Distributions of Asphaltenes from Crude Oils. *Energy Fuels,* 27 (5), 2474-2487.

Beck, J.; Svrcek, W.Y.; Yarranton, H.W. (2005). Hysteresis in Asphaltene Precipitation and Re-dissolution. *Energy Fuels*, 19 (3), 944-947.

Betancourt, S.S.; Ventura, G.T.; Pomerantz, A.E.; Viloria, O.; Dubost, F.X.; Zuo, J.; Monson, G.; Bustamante, D.; Purcell, J.M.; Nelson, R.K.; Rodgers, R.P.; Reddy, C.M.; Marshall, A.G.; Mullins, O.C. (2009). Nanoaggregates of Asphaltenes in a Reservoir Crude Oil and Reservoir Connectivity. *Energy Fuels*, 23 (3), 1178-1188.

Buckley, J.S. (1999). Predicting the Onset of Asphaltene Precipitation from Refractive Index Measurements. *Energy Fuels*,13 (2), 328-332.

Buenrostro-Gonzalez, E.; Lira-Galeana, C.; Gil-Villegas, A.; Wu, J. (2004). Asphaltene Precipitation in Crude Oils: Theory and Experiments. *AIChE J*., 50, 2552-2570.

Carnahan, N.F. (2000). Precipitation of Asphaltenes in Heavy Oil and Tar Sands, in *Asphaltenes and Asphalts*, 2, Volume 40B, First Edition. T.F. Yen, G.V. Chilingarian, Elsevier, Amsterdam, The Netherlands.

Chaisoontornyotin, W.; Bingham, A.W.; Hoepfner, M.P. (2017). Reversibility of Asphaltene Precipitation Using Temperature-Induced Aggregation. *Energy Fuels*, 31, 3392-3398.

Chaisoontornyotin, W.; Zhang, J.; Ng, S.; Hoepfner, M.P. (2018). Rapid Heterogeneous Asphaltene Precipitation with Dispersed Solids. *Energy Fuels*, 32, 7458-7466.

Chu, B. (1967). *Molecular Forces: Based on the Baker Lectures of Peter J. W. Debye*. Interscience Publishers, New York, NY.

Elimelech, M.; Gregory, J.; Jia, X.; Williams, R.A. (1995). *Particle Deposition and Aggregation: Measurement, Modeling and Simulation*. Butterworth-Heinemann Ltd., Oxford, UK.

Family, F.; Meakin, P.; Deutch, J.M. (1989). Kinetics of Coagulation with Fragmentation: Scaling Behavior and Fluctuations. *Phys. Rev. Lett.,* 57 (6), 727-730.

Feke, D.L.; Schowalter, W.R. (1983). The Effect of Brownian Diffusion on Shear-induced Coagulation of Colloidal Suspensions. *J. Fluid Mech.,* 133, 17-35.

Ferworn, K.A.; Svrcek, W.Y.; Mehrotra, A.K. (1993). Measurement of Asphaltene Particle Size Distribution in Crude Oils Diluted with *n*-Heptane. *Ind. Eng. Chem. Res*., 32, 955-959.

Fotland, P.; Askvik, K.M. (2008). Determination of Hamaker Constants for Asphaltenes in a Mixture of Pentane and Benzene. *Colloids Surf., A.,* 324, 22-27.

Friedlander, S.K. (2000). *Smoke, Dust, and Haze: Fundamentals of Aerosol Dynamics*, Second Edition, Oxford University Press, New York, NY.

Gray, M.R. (2015). *Upgrading Oilsands Bitumen and Heavy Oil*, First Edition. The University of Alberta Press, Edmonton, AB.

Grimaldos, F. (2018). Measurement of Liquid-Liquid Diffusion in Solvent-Bitumen Systems. *MSc.* Thesis, University of Calgary.

Haji-Akbari, N.; Masirisuk, P.; Hoepfner, M.P.; Fogler, H.S. (2013). A Unified Model for Aggregation of Asphaltenes. *Energy Fuels,* 27 (5), 2497-2505.

Haji-Akbari, N.; Teeraphapkul, P.; Balgoa, A.T.; Fogler, H.S. (2015). Effect of *n*-Alkane Precipitants on Aggregation Kinetics of Asphaltenes. *Energy Fuels.* 29 (4), 2190-2196.

Haji-Akbari, N.; Teeraphapkul, P.; Fogler, H.S. (2014). Effect of Asphaltene Concentration on the Aggregation and Precipitation Tendency of Asphaltenes. *Energy Fuels,* 28(2), 909-919.

Hamaker, H.C. (1937). The London-van der Waals Attraction Between Spherical Particles. *Physica IV,* 10, 1058-1072.

Hammami, A.; Phelps, C.H.; Monger-McClure, T.; Little, T.M. (2000). Asphaltene Precipitation from Live Oils: An Experimental Investigation of Onset Conditions and Reversibility. *Energy Fuels*, 14(1), 14-18.

Headen, T.F.; Boek, E.S.; Stellbrink, J.; Scheven, U.M. (2009). Small Angle Neutron Scattering (SANS and V-SANS) Study of Asphaltene Aggregates in Crude Oil. *Langmuir*, 5, 422-428.

Hirschberg, A.; deJong, N.J.; Schipper, B.A.; Meijer, J.G. (1984). Influence of Temperature and Pressure on Asphaltene Flocculation. *SPE J.*, 24, 283-291.

Hoepfner, M.P.; Vilas-Bôas Fávero, C.; Haji-Akbari, N.; Fogler, H.S. (2013). The Fractal Aggregation of Asphaltenes. *Langmuir*, 29, 8799-8808.

Islam, M.A. (2004). Einstein-Smoluchowski Diffusion Equation: A Discussion. *Phys. Scr.*, 70, 120-125.

Israelachvili, J.N. (2011). *Intermolecular and Surface Forces*, Third Edition. Academic Press, London, UK.

Jeldres, R.I.; Fawell, P.D.; Florio, B.J. (2018). Population Balance Modeling to Describe the Particle Aggregation Process: A Review. *Powder Technol.*, 326, 190-207.

Johnston, K.A.; Schoeggl, F.F.; Satyro, M.A.; Taylor, S.D.; Yarranton, H.W. (2017). Phase Behavior of Bitumen and *n*-Pentane. *Fluid Phase Equilib.*, 442, 1-19.

Khoshandam, A.; Alamdari, A. (2010). Kinetics of Asphaltene Precipitation in a Heptane-Toluene Mixture. *Energy Fuels*, 24 (3), 1917-1924.

Kusters, K.A.; Wijers, J.G.; Thoenes, D. (1997). Aggregation Kinetics of Small Particles in Agitated Vessels. *Chem. Eng. Sci.*, 52 (1), 107-121.

Leite, E.R.; Ribeiro, C. (2012). *Crystallization and Growth of Colloidal Nanocrystals*, Springer, Amsterdam, The Netherlands.

Liu, J.; Xu, Z.; Masliyah, J. (2004). Role of Fine Clays in Bitumen Extraction from Oil Sands. *AIChE J.*, 50 (8), 1917-1927.

Long, Y.; Dabros, T.; Hamza, H. (2004). Analysis of Solvent-Diluted Bitumen from Oil Sands Froth Treatment Using NIR Spectroscopy. *Can. J. Chem. Eng*., 82 (4), 776-781.

Maqbool, T.; Balgoa, A.T.; Fogler, H.S. (2009). Revisiting Asphaltene Precipitation from Crude Oils: A Case of Neglected Kinetic Effects. *Energy Fuels*, 23, 3681-3686.

Maqbool, T.; Raha, S.; Hoepfner, M.P.; Fogler, H.S. (2011a). Modeling the Aggregation of Asphaltene Nanoaggregates in Crude Oil-Precipitant Systems. *Energy Fuels*, 25 (4), 1585-1596.

Maqbool, T.; Srikiratiwong, P.; Fogler, H.S. (2011b). Effect of Temperature on the Precipitation Kinetics of Asphaltenes. *Energy Fuels,* 25, 694-700.

Markov, I.V. (2003). *Crystal Growth for Beginners: Fundamentals of Nucleation, Growth and Epitaxy*. World Scientific Publishing Co., Hackensack, NJ.

Mostowfi, F.; Indo, K.; Mullins, O.C.; McFarlane, R. (2009). Asphaltene Nanoaggregates Studied by Centrifugation. *Energy Fuels,* 23, 1194-1200.

Mousavi-Dehghani, S.; Riazi, M.; Vafaie-Sefti, M.; Mansoori, G. (2004). An Analysis of Methods for Determination of Onsets of Asphaltene Phase Separations. *J. Pet. Sci. Eng*., 42, 145-156.

Mullins, O.C.; Sheu, E.Y.; Hammami, A.; Marshall, A. (2007). *Asphaltenes, Heavy Oils, and Petroleomics*. Springer New York, NY.

Nassar, N.N.; Betancur, S.; Acevedo, S.; Franco, C.A.; Cortes, F.B. (2015). Development of a Population Balance Model to Describe the Influence of Shear and Nanoparticles on the Aggregation and Fragmentation of Asphaltenes Aggregates. *Ind. Eng. Chem. Res.* 54, 8201-8211.

Natarajan, A.; Kuznicki, N.; Harbottle, D.; Masliyah, J.; Zeng, H.; Xu, Z (2014). Understanding Mechanics of Asphaltene Adsorption from Organic Solvent on Mica. *Langmuir,* 30 (31), 9370-9377.

Nguyen, T.K.; Maclean, N.; Mahiddine, S. (2014). Mechanisms of Nucleation and Growth of Nanoparticles in Solution. *Chem. Rev.*, 114 (15), 7610-7630.

Punnapala, S.; Vargas, F.M. (2013). Revisiting the PC-SAFT Characterization Procedure for an Improved Asphaltene Precipitation Prediction. *Fuel*, 108, 417-429.

Rahimi, H.; Nazar, A.R.S. (2010). Asphaltene Aggregates Fractal Restructuring Model, A Population Balance Approach. *Energy Fuels,* 24, 1088-1093.

Rahmani, N.H.G.; Masliyah, J.H.; Dabros, T. (2003). Characterization of Asphaltene Aggregation and Fragmentation in a Shear Field. *AIChE J.,* 49 (7), 1645-1655.

Rahmani, N.; Dabros, T.; Masliyah, J.H. (2005). Fractal Structure of Asphaltene Aggregates. *J. Colloid Interface Sci.,* 285 (2), 599-608.

Ramos-Pallares, F.; Lin, H.; Yarranton, H.W.; Taylor, S.D. (2017). Prediction of the Liquid Viscosity of Characterized Crude Oils by Use of the Generalized Walther Model. *SPE J.*, 22 (5), 1487-1505.

Rastegari, K.; Svrcek, W.Y.; Yarranton, H.W. (2004). Kinetics of Asphaltene Flocculation. *Ind. Eng. Chem. Res*., 43, 6861-6870.

Rodgers, R.P.; McKenna, A.M. (2011). Petroleum Analysis. *Anal. Chem.* 83, 4665-4687.

Safaie, K.; Nazar, A.R.S. (2013). Monte Carlo Modeling of Asphaltene Aggregation Coupled with Sedimentation. *J. Dispersion Sci. Technol*., 34, 1173-1182.

Saryazdi, F.; Motahhari, H.; Schoeggl, F.F.; Taylor, S.D.; Yarranton, H.W. (2013). Density of Hydrocarbon Mixtures and Bitumen Diluted with Solvents and Dissolved Gases. *Energy Fuels*, 27, 3666-3678.

Shampine, L.F. (2008). Vectorized Adaptive Quadrature in MATLAB. *J. Comput. Appl. Math.*, 211 (2), 131-140.

Smoluchowski, M. (1917). Versuch einer Mathematischen Theorie der Koagulations Kinetis Kolloider Losungen. *Z. Physik. Chem.*, 92, 129-168.

Soleimani-Khormakala, H.; Torkaman, M.; Bahrami, M. (2018). The Effect of Shear Rate on Aggregation and Fragmentation of Asphaltene Aggregates. *J. Dispersion Sci. Technol*., 40 (6), 836-845.

Speight, J.G. (2006). *The Chemistry and Technology of Petroleum*, Fourth Edition. CRC Press, Boca Raton, FL.

Spicer, P.T.; Pratsinis, S.E. (1996). Coagulation and Fragmentation: Universal Steady-state Particle-size Distribution. *AIChE J*., 42 (6), 1612-1620.

Thomas, D.N.; Judd, S.J.; Fawcett, N. (1999). Flocculation Modeling: A Review. *Water Res.*, 33 (7), 1579-1592.

Torkaman, M.; Bahrami, M.; Dehghani, M. (2017). Influence of Temperature and Stability of Asphaltenes. I. Perikinetic Aggregation. *Energy Fuels*, 31, 11169-11180.

Torkaman, M.; Bahrami, M.; Dehghani, M. (2018). Influence of Temperature on Aggregation and Stability of Asphaltenes. II. Orthokinetic Aggregation. *Energy Fuels*, 32, 6144-6154.

Vanni, M.; Baldi, G. (2002). Coagulation Efficiency of Colloidal Particles in Shear Flow. *Adv. Colloid Interface Sci.*, 97, 151-177.

Vilas-Bôas Fávero, C.; Maqbool, T.; Hoepfner, M.; Haji-Akbari, N.; Fogler, H.S. (2017). Revisiting the Flocculation Kinetics of Destabilized Asphaltenes. *Adv. Colloid Interface Sci.*, 244, 267-280.

Vincent, B. (1973). The van der Waals Attraction Between Colloidal Particles Having Adsorbed Layers: II Calculation of Interaction Curves. *J. Colloid Interface Sci.,* 42 (2), 270-285.

Wang, S.; Liu, J.; Zhang, L.; Masliyah, J.; Xu, Z. (2010). Interaction Forces Between Asphaltene Surfaces in Organic Solvents. *Langmuir,* 26 (1), 183-190.

Wattana, P.; Wojciechowski, D.J.; Bolanos, G.; Fogler, H.S. (2003). Study of Asphaltene Precipitation Using Refractive Index Measurement. *Petr. Sci. Technol.*, 21 (3-4), 591-613.

Wiehe, I.A. (2008). *Process Chemistry of Petroleum Macromolecules,* CRC Press, Boca Raton, FL.

Yang, Y.; Chaisoontornyotin, W.; Hoepfner, M.P. (2018). Structure of Asphaltenes During Precipitation Investigated by Ultra-small-angle X-ray Scattering. *Langmuir,* 34, 10371-10380.

Yarranton, H.W.; Masliyah, J.H. (1996). Molar Mass Distribution and Solubility Modeling of Asphaltenes. *AIChE J.,* 42 (12), 3533-3543.

Yarranton, H.W.; van Dorp, J.J.; Verlaan, M.L.; Lastovka, V. (2013). Wanted Dead or Live: Crude-Cocktail Viscosity – A Pseudocomponent Method to Predict the Viscosity of Dead Oils, Live Oils, and Mixtures. *J. Can. Pet. Technol.,* 52 (3), 176-191.

Yudin, I.K.; Nikolaenko, G.L.; Gorodetski, E.E.; Markhashov, E.L.; Frot, D.; Briolant, Y.; Agayan, V.A.; Anisimov, M.A. (1998). Universal Behavior of Asphaltene Aggregation in Hydrocarbon Solutions. *Pet. Sci. Technol.*, 16 (3-4), 395-414.

Zahnow, J.C.; Maerz, J.; Feudel, U. (2011). Particle-based Modeling of Aggregation and Fragmentation Processes: Fractal-like Aggregates. *Physica D,* 240, 882-893.

Zawala, J.; Dabros, T.; Hamza, H.A. (2012). Settling Properties of Aggregates in Paraffinic Froth Treatment. *Energy Fuels.* 26, 5775-5781.

Zhang, Y.; Arya, A.; Kontogeorgis, G.; Yarranton, H.W. (2019). Modeling the Phase Behavior of Bitumen/*n*-Alkane Systems with Cubic Plus Association (CPA) Equation of State. *Fluid Phase Equilib.*, 486, 119-138.

Chapter 5: The Effect of Air on the Kinetics of Asphaltene Precipitation from Diluted Crude Oils

In this contribution[3], the kinetics of asphaltene precipitation was investigated for five crude oils diluted with *n*-heptane at 21ºC in air atmosphere. The onset of precipitation, defined as the precipitant (*n*-heptane) content at which detectable asphaltene particles first appear, was measured in air at different contact times using the methods described in Section 2.6. Asphaltene yields (mass asphaltene / mass oil) were measured in air over time gravimetrically. The data were compared with yields and onsets presented in Chapter 4 that were collected in a nitrogen atmosphere. In an air atmosphere, the yields and onsets were the same as in nitrogen for the first 50 hours but then the yields gradually increased for the duration of the experiments. The onsets shifted to lower values over time and there was no equilibrium onset condition. It is hypothesised that the oxygen in the air catalyzes or participates in reactions that alter the asphaltenes and other crude oil components over time so that they become less soluble. The modified population balance model described in Chapter 4 was adapted to account for the increase in yield over time due to oxygen by introducing a term for the generation of unstable asphaltene primary particles. The model proposed matched the precipitation yield data from this study and from the literature with an average absolute deviation of less than 2 wt%.

[3] This chapter is based on the following article in preparation for submission: Duran, J.A.; Schoeggl, F.F.; Yarranton, H.W.; Vilas Bôas-Fávero, C.; Fogler, H.S. (2019). The Effect of Air on the Kinetics of Asphaltene Precipitation from Diluted Crude Oils.

5.1 Introduction

Asphaltenes are a solubility-class of components defined as the crude oil fraction that precipitates upon addition of an *n*-alkane (such as *n*-pentane or *n*-heptane) but is completely soluble in aromatic solvents like toluene (Speight, 2006). Asphaltene precipitation can occur with changes in composition, temperature, pressure, and contact time (Hirshberg *et al*., 1984; Hammami *et al*., 2000; Andersen and Birdi, 1990; Andersen *et al.*, 1998, Maqbool *et al*., 2009). At near ambient conditions, asphaltenes precipitate are particles that are initially detected at submicron to approximately 1 micrometer diameters and that grow/aggregate gradually over time (Agrawal *et al.*, 2012; Ferworn *et al.*, 1993; Rastegari *et al.*, 2004; Angle *et al*., 2006). In processes at higher temperatures (>100ºC) asphaltenes appear as droplets that form a second liquid phase (Johnston *et al*., 2017; Mancilla-Polanco *et al*., 2019). In this work, precipitation was initiated by the addition of *n*-heptane (precipitant or poor solvent) at room conditions (21ºC and 1 atm), therefore this study focusses on the precipitation of particles.

Asphaltene precipitation can occur in several oilfield processes. In some cases, the precipitation is undesirable. For example, asphaltene precipitation initiated by the addition of a paraffinic diluent or a lighter oil can cause deposition and fouling in reservoirs, wellbores, surface facilities, and pipelines (Wiehe, 2008). Deposition and fouling results in lost production and their treatment can be costly. In other cases, asphaltene precipitation is part of the process design; for example in paraffinic froth treatment and deasphalting processes (Gray, 2015; Sie *et al.*, 2019). In either case, it is necessary to determine the conditions at which asphaltenes start to precipitate (the onset of precipitation) and the amount of precipitate if operating beyond the onset condition.

Most studies dealing with asphaltene precipitation triggered by the addition of a precipitant (a poor solvent) have focused on determining the composition at which asphaltenes are first detected (onset) and the amount of precipitate (Carnahan, 2000; Mousavi-Dehghani *et al.*, 2004; Beck *et al*., 2005; Vilas-Bôas Fávero *et al.*, 2017; Angle *et al.*, 2006; Haji-Akbari *et al*., 2015; Chaisoontornyotin *et al.*, 2018). The measurements are usually performed at a contact time of approximately 24 h and are assumed to be at equilibrium conditions. The data are used to tune thermodynamic equilibrium models such as equations of state (Agrawal *et al*., 2012; Arya *et al*.,

2017; Zhang *et al*., 2019) or models based on regular solution theory (Alboudwarej *et al*., 2003; Akbarzadeh *et al*., 2005; Yarranton *et al*., 2018). The kinetics of precipitation is not usually accounted for and therefore the models may not be accurate at real process times where residence times may only be a few minutes.

Maqbool *et al*. (2009, 2011a) studied the kinetics of asphaltene precipitation in air and found that yields (amount) of precipitate increase over time in *n*-heptane diluted crude oil systems. In most cases asphaltene yields increased rapidly for approximately the first 24 hours and then increased at a slow rate after 24 h. The amount of *n*-heptane required to initiate precipitation was also found to be time-dependent and was lower for longer contact times. They suggested that no single value could be considered as the onset of precipitation but instead the onset depends on contact time. However, their measurements were performed in air and oxygen is known to affect asphaltene precipitation.

At temperatures above 150°C, oxygen has been shown to catalyze reactions that form asphaltenes. For example, Taylor and Frankenfeld (1978) investigated the effect of oxygen and nitrogen on deposit formation at 150 to 450ºC from initially deoxygenated jet fuel. They proposed that free radical chain reactions involving molecular oxygen created high molar mass hydrocarbons that corresponded to the asphaltene solubility class. Wilson and Watkinson (1996) studied deposits of peroxide gum formed at 180 to 255ºC from a model compound (indene) diluted in an inert lube oil. They reported that oxygen dissolved in a liquid hydrocarbon formed polymeric peroxides through autocatalytic reactions. The peroxides underwent subsequent decomposition reactions and free radical reactions with hydrocarbons. These reactions led to the formation of "new asphaltenes" and contributed to organic fouling. Mushrush and Speight (1995) showed that hydroperoxides can initiate polymerization (oligomerization) reactions and dissolved oxygen acts as a propagator. Polymerization reactions lead to the formation of new molecules in the range of asphaltenes from lower components like aromatics and resins. Heavier and more polar structures are formed as a result of these chain reactions leading to higher asphaltene yields. Moschopedis and Speight (1977) investigated the effect of oxygen on an Athabasca bitumen aerated at temperatures between 150 to 300ºC and found that some constituents of the bitumen converted to heavier molecular weight

components that fall into the category of asphaltenes. It is possible that oxygen catalyzed reactions occur at lower temperatures albeit at lower rates.

At lower temperatures near ambient conditions, oxygen can affect asphaltenes in other ways. Herrington (2001), and Herrington and Wu (1999) studied the oxidation of toluene diluted bitumen at 50ºC and found that oxidation at low temperatures may not be caused by oligomerization of aromatic species but instead by intermolecular associations formed within the oxidized asphaltenes. Choi *et al*. (2016) investigated asphaltene oxidation with ozone at 40ºC in a model oil consisting of *n*-heptane Athabasca asphaltenes rediluted in toluene. Oxygen was incorporated into the asphaltene molecules after short contact times (about 15 min) and produced more hydrophilic and polarizable asphaltenes with an increased tendency to self-associate.

Beck *et al.* (2005) confirmed that oxygen can affect asphaltene precipitation from *n*-heptane diluted bitumen even at ambient temperatures. In nitrogen, they observed a rapid initial increase in yield reaching a plateau in approximately 24 hours. However, in air, the precipitation continued after 24 h at a reduced rate for the duration of the experiments (up to 2 months). Shafiee (2014) reported that the "instantaneous" onsets (detection of precipitate after 1 min) in an *n*-heptane diluted bitumen at ambient conditions shifted to lower precipitant content values over 2 days in both air and nitrogen atmospheres. In nitrogen, the onsets reached equilibrium after 2 days of contact while, in air, the onsets decreased continuously for the duration of the experiment. The yields and onset measured in nitrogen reported in Chapter 4 confirmed that while yields initially increased and the onsets initially decreased over time, they both reached a plateau after approximately 150 h. In other words, yields and onsets were time-dependent but, in contrast to experiments performed in air, equilibrium values were eventually established.

There is a need for a kinetic model for asphaltene precipitation that can be applied to field processes, which are generally anaerobic, and to lab measurements, which are typically performed in air. In this way, lab measurements can be more accurately translated to field conditions. Maqbool *et al.* (2011a) modeled asphaltene yield data in air over time at different precipitant contents with a population balance approach using one fitting parameter. This approach was

summarized in Chapter 4. The model successfully matched the time for 0.5 μm diameter particles to appear. The model was later expanded to include a variety of light oils and precipitants, and the onset time was correlated to the solubility parameter of the asphaltenes and the mixture (Haji-Akbari *et al.*, 2013; 2015). However, this model could not fit the rapid increase in aggregate size within the first few seconds of contact with the precipitant that is observed in diluted bitumens and heavy oils (Rastegari *et al*., 2004; Ferworn *et al.*, 1993; Duran *et al.*, 2019b) as proved in Section 4.3.3. In Section 4.3.4 the original model was modified to include the nucleation of asphaltene nanoaggregates and the large interparticle force experienced by the particles once they come out of solution. This model matched yields and asphaltene aggregate sizes measured in nitrogen over time in different crude oils and bitumens. The model was reduced to one tuning parameter, the initial collision efficiency; however, the model does not account for the effect of oxygen.

In this chapter, the effect of oxygen from air in asphaltene precipitation is assessed at ambient conditions. The onset and yields of precipitated asphaltenes were measured in air as a function of time after *n*-heptane addition to two Western Canadian bitumen samples (WC-B-B2, and WC-B-A3), a Mexican bitumen (MX-B-A1), a European heavy oil (EU-HO-A1), and an Alberta Mixed Sweet Blend (MSB). All of the oils were diluted with *n*-heptane at 21ºC. The onsets and yields in air were compared with onsets and yields in nitrogen reported in Chapter 4 for the same mixtures. In addition, yields were measured for bitumen aerated at 23ºC, 40ºC and 70ºC prior to dilution with *n*-heptane in order to confirm the effect of oxygen on asphaltene precipitation. Asphaltene yields were adjusted with the modified model in air for the same oils of Chapter 4. Data reported in literature by Beck *et al.* (2005) for the WC-B-A0 sample were also adjusted with the approach proposed in this chapter.

5.2 Modified Population Balance Model for Asphaltenes Yields in Air

The modified population balance model developed in Chapter 4 was used to model asphaltene yield data in air. A size domain was defined to model the aggregation process with a lower limit set equal to the primary particle diameter (see Section 4.3.4) and the upper size limit arbitrarily set to 500 μm. The domain is divided into bins using a scaling factor $R_s = 2$.

The initial population is assumed to consist of monodisperse primary particles. The initial concentration of primary particles (C_1 in kmol/m³) is given by,

$$C_1(t=0) = \frac{Y_{A,eq} f \varphi_0 \rho_0}{MW_A N_n} \tag{5.1}$$

where $Y_{A,eq}$ is the equilibrium asphaltene yield of unstable asphaltenes, f is the fraction of asphaltenes that precipitates within a few seconds, φ_0 is the volume fraction of precipitant in the mixture and ρ_o is the crude oil density. The denominator represents the molecular weight of the primary particle where MW_A is the molecular weight of an average asphaltene molecule (set to 750 g/mol) and N_n is the number of asphaltene molecules per primary particle (assuming spherical geometry and calculated based on its diameter, the asphaltene molecular weight, and an asphaltene density of 1.2 g/cm³ as reported by Yarranton and Masliyah (1996). The equilibrium yield can be obtained experimentally or from a thermodynamic equilibrium model, such as a regular solution model or equation of state tuned with long term equilibrium data.

The fractal dimension of the asphaltene aggregates can be determined experimentally or from the following correlation,

$$D_f = 2.899 - \exp(-0.0208 \frac{w_u}{\mu_m^{0.45}}) \tag{5.2}$$

where μ_m is the medium viscosity in mPa·s, and w_u is the precipitate concentration in wt% and is defined in Eq. 4.20. The development of Eq. 5.2 is discussed in detail in Section 6.3.4. This correlation had lower errors than the initial correlation reported in Chapter 4 (Eq. 4.19). All other features of the model (collision kernel, primary particle diameter, anaerobic nucleation, *etc.*) were not adjusted. The only modification was the introduction of a nucleation rate term to account for the appearance of new asphaltenes over time in air.

5.2.1 Nucleation Rate in Air

As will be discussed later, the population balance model was modified to include an oxidation rate as a generation term in the balance of the primary particles (Eq. 4.30) as follows,

$$\frac{dC_1}{dt} = -C_1 \sum_{j=i}^{N-1} K_{1,j} C_j + \dot{r}_N + \dot{r}_{ox} \tag{5.3}$$

where r_{ox} is the "oxidation" rate and is given in (mol/m³·s). The term oxidation is used here for convenience and is not intended to indicate a mechanism. The same oxidation rate could be

introduced into any population balance that correctly represents the asphaltene onsets and yields in nitrogen. The oxidation rate was set to a constant value for each crude oil/*n*-heptane system and will be discussed in more detail later.

5.2.2 Model Implementation

The experimental yields in air for the five systems investigated were modeled using an algorithm similar to that presented in Figure 4.1 and implemented in Matlab™. The model previously tuned to the anaerobic yield data was used without modification except that the oxidation rate was included and the input constant oxidation rate for each system was adjusted to best fit the yield data in air. For each crude oil system and at each precipitant content, the oxidation rate, r_{ox}, was iterated to minimize the following objective function,

$$OF = \min_{r_{ox}} \frac{1}{n} \sum_{j=1}^{n} \left(Y_{j,\text{experimental at t}} - Y_{j,\text{ model at t}} \right)^2 \tag{5.4}$$

where *n* is the number of experimental yield points. The function *fminsearch* in Matlab™ was used as minimization tool. The minimization tolerance was set to 1×10^{-8} (kg asphaltene/kg crude oil).

The collision efficiency parameters of Eq. 4.41 were taken directly from Table 4.5. For the bitumens (WC-B-B2, WC-B-A3, MX-B-A1, WC-B-A0), the residual collision efficiency (β_{res}) and the stickiness decay factor (k_s) were set to the recommended values of 1×10^{-8} and 1.5 s^{-1}, respectively. For the EU-HO-A1 and MSB oils, these parameters were set to zero. For the four bitumens, the initial collision efficiency (β_E) depended on the precipitant content and the values reported in Table 4.5 at each *n*-heptane content were used. For the EU-HO-A1 and MSB crude oils, β_E was independent of the precipitant content and a value of 5×10^{-8} was used, as recommended in Section 4.3.6.

The remaining inputs required to initialize the model are:

- the *n*-heptane content of the mixture,
- the properties of the medium (density, viscosity, and Hamaker constant),
- the initial and equilibrium asphaltene yields in nitrogen at each *n*-heptane content,
- the centrifugation conditions,

- the oxidation rate.

The *n*-heptane content must be specified. The density and viscosity of mixtures of crude oils and *n*-heptane were measured and fitted with existing mixing rules (Saryazdi *et al*., 2013; Ramos-Pallares *et al.*, 2017) and are reported in Section 6.3.2. The Hamaker constants for the fluids in this study in air at 20ºC are the same values used in Chapter 4: 4.5×10^{-20} J for *n*-heptane (Israelachvili, 2011), 6×10^{-20} J for asphaltenes (Fotland and Askvik, 2008), 6×10^{-20} J for bitumens (Liu *et al*., 2004), and 5×10^{-20} J for other oils (Vincent, 1973). The initial and equilibrium asphaltene yields in nitrogen for these mixtures are reported in Appendix D and E. The centrifugation conditions were summarized in Table 4.1. The constant oxidation rate was the fitting parameter and is discussed later.

5.3 Results and Discussion

Asphaltene precipitation onsets and yields were measured over time in air for the first five crude oils in Table 2.1, each diluted with *n*-heptane at 21°C and atmospheric pressure. The data measured in this study are provided in Appendix F. The data in air are compared with onset and yield data for the same mixtures collected in nitrogen and reported in Chapter 4. The effect of aeration on the asphaltene yield from the final bitumen in Table 2.1 (WC-B-A0) diluted with *n*-heptane is examined to further test the effect of oxygen on asphaltene precipitation. These data were measured in a previously unpublished study and are provided in the Appendix G. The population balance model is adapted and fitted to the data measured in air. Finally, the model is used to reexamine data collected in air from the literature.

5.3.1 Onsets of Precipitation in Air

Figure 5.1 presents a series of micrographs taken near the onset of precipitation from *n*-heptane diluted WC-B-B2 bitumen in air at 21°C and atmospheric pressure. The asphaltene particles first appear as a haze that is difficult to capture with a micrograph because the particles are smaller than 0.5 μm. At 57 wt% *n*-heptane, this haze appears in less than one minute and then clearly defined particles and aggregates appear gradually over tens of minutes. At higher *n*-heptane contents, clearly defined particles appear immediately (not shown here). The onset of precipitation at a

contact time of zero (immediately after addition of precipitant) for this system in air was determined to 57.3 ± 0.3 wt% *n*-heptane (Table 4.2).

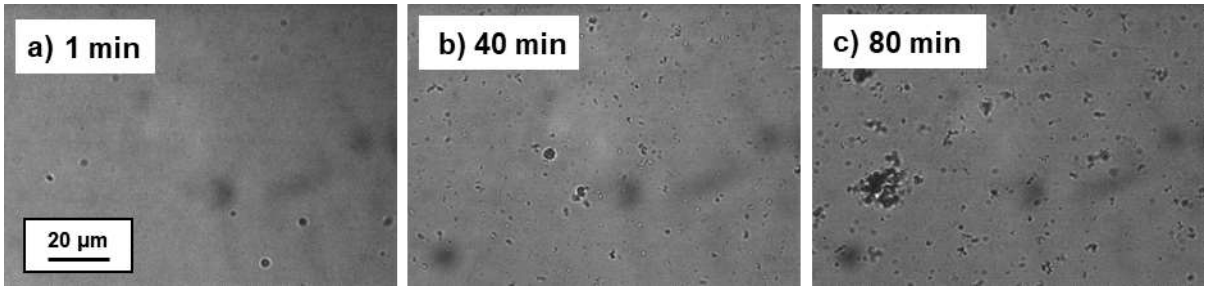

Figure 5.1. Micrographs showing the onset of asphaltene precipitation from the *n*-heptane diluted WC-B-B2 bitumen in air at 21ºC. Images correspond to a 57.0 wt% *n*-heptane mixture at a) 1 min; b) 40 min; and c) 80 min contact time. Note, the appearance of haze at this precipitant content occurs in less than 1 min.

The onsets of asphaltene precipitation from the WC-B-B2 bitumen diluted with *n*-heptane were also determined at various contact times from extrapolation of asphaltene yield data. Figure 5.2b shows that the onsets measured with the microscopic and extrapolated yield methods are consistent. Figure 5.2 also shows that the onsets shift to lower values over time; that is, the asphaltenes become less soluble over time. The shift to lower onsets and the gradual growth in the number of particles over time (Figure 5.2) confirm that asphaltene precipitation is a time dependent process.

Figure 5.2 shows that the extrapolated onsets in air and in nitrogen are identical within experimental error for about 48 h and then deviate. If only the data in air are considered, it appears that the onset of asphaltene precipitation migrates to lower solvent contents indefinitely for months or probably years as has been suggested elsewhere (Maqbool *et al*., 2009; Haji-Akbari *et al*., 2013). However, the data in nitrogen shows that a constant onset value is reached after approximately 100 hours. This constant value is interpreted as the equilibrium onset condition (See Section 4.3).

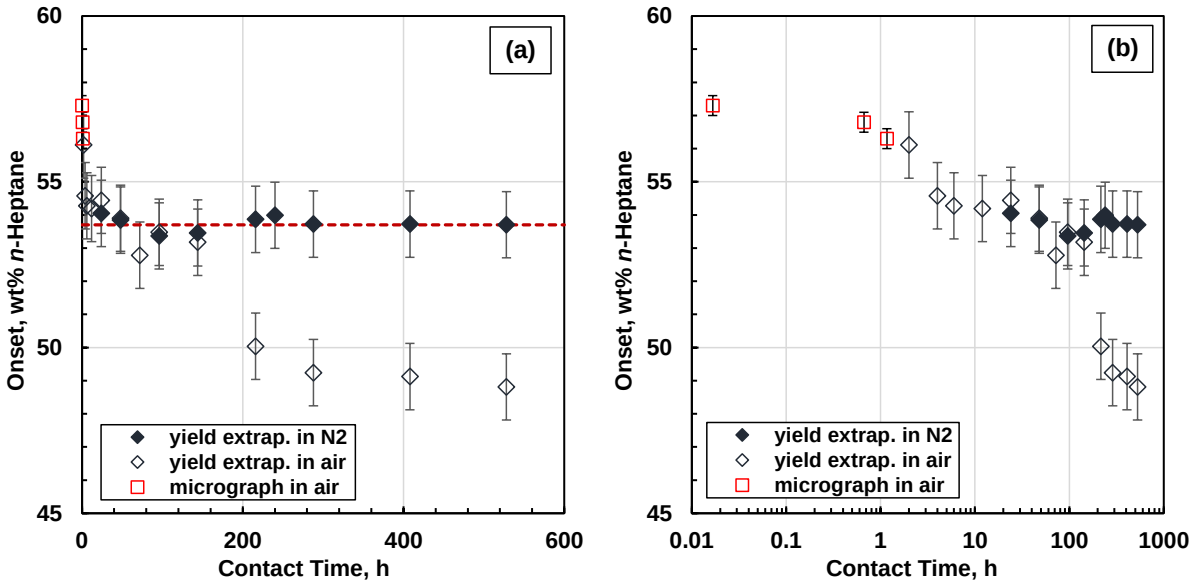

Figure 5.2. Comparison of gravimetric and micrographic onsets of precipitation in nitrogen and air atmospheres for *n*-heptane diluted WC-B-B2 bitumen at 21ºC: a) Cartesian coordinates; b) semi-log coordinates. Dashed line is the equilibrium onset in nitrogen, Table 4.3.

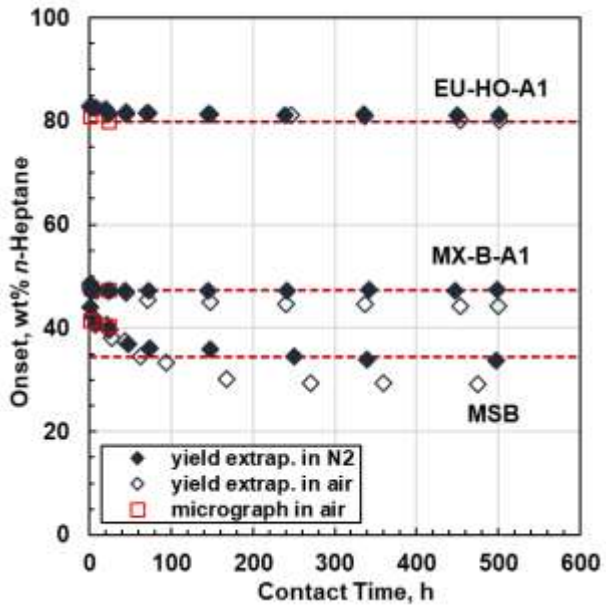

Figure 5.3. Comparison of gravimetric and micrographic onsets of precipitation in nitrogen and air atmospheres for *n*-heptane diluted EU-HO-A1, MX-B-A1, and MSB at 21ºC Dashed lines are the equilibrium onsets in nitrogen from Table 4.3.

Figure 5.3 shows the extrapolated onsets for the other oils in *n*-heptane. Insufficient onset data were measured for the WC-B-A3 bitumen (this oil was originally part of a separate study) and this oil is not included in the analysis. In the MX-B-A1 and MSB oils, the onsets decreased continuously over time in air but reached a plateau in nitrogen. In the EU-HO-A1 oil, it appears that the onsets in both air and nitrogen reached a plateau. It is not known why the onsets from this oil are almost unaffected by the presence of oxygen. In any case, it appears that an equilibrium onset condition is attained in nitrogen with all of the oils. The equilibrium onsets are reported in Table 4.3. The equilibrium onset for the *n*-heptane diluted WC-B-A3 at 21ºC was determined as part of this study and was 56.0 wt% *n*-heptane (± 1 wt%).

An equilibrium onset was not observed in air. Maqbool *et al*. (2009) suggested that asphaltene precipitation is a continuous aggregation process that takes long times at low precipitant concentrations. They hypothesized that the detection of particles after several months or even years is possible because of asphaltene nanoaggregates take longer to aggregate and reach detectable sizes. They defined a detection time as the time required to observe precipitate at a given solvent content. Their co-workers (Haji-Akbari *et al*., 2013; 2015; Vilas-Bôas Fávero *et al*., 2017) found that the detection time increased exponentially as the precipitant content decreased below the instantaneous onset (detection time = 0).

Figure 5.4 compares the extrapolated onsets of precipitation at different contact times in air and nitrogen environments. The contact time in this plot is equivalent to the detection time. In air, consistent with the previous studies, the detection time increased exponentially as the *n*-heptane content decreased below the instantaneous onset (detection time of zero). In contrast, in nitrogen, the detection time approached infinity at the equilibrium onset condition. No precipitation was detected at *n*-heptane contents below the equilibrium condition at any contact time considered in this study as shown in Figure 5.4 (details of the measurements are provided in Table 5.1). Therefore, it is more likely that an equilibrium onset is not observed in air because the presence of oxygen alters the asphaltenes and leads to a continuous decrease in the asphaltene solubility. The loss of solubility manifests as an increase in yields and a decrease in the *n*-heptane content required to initiate precipitation, this is, the onset decreases.

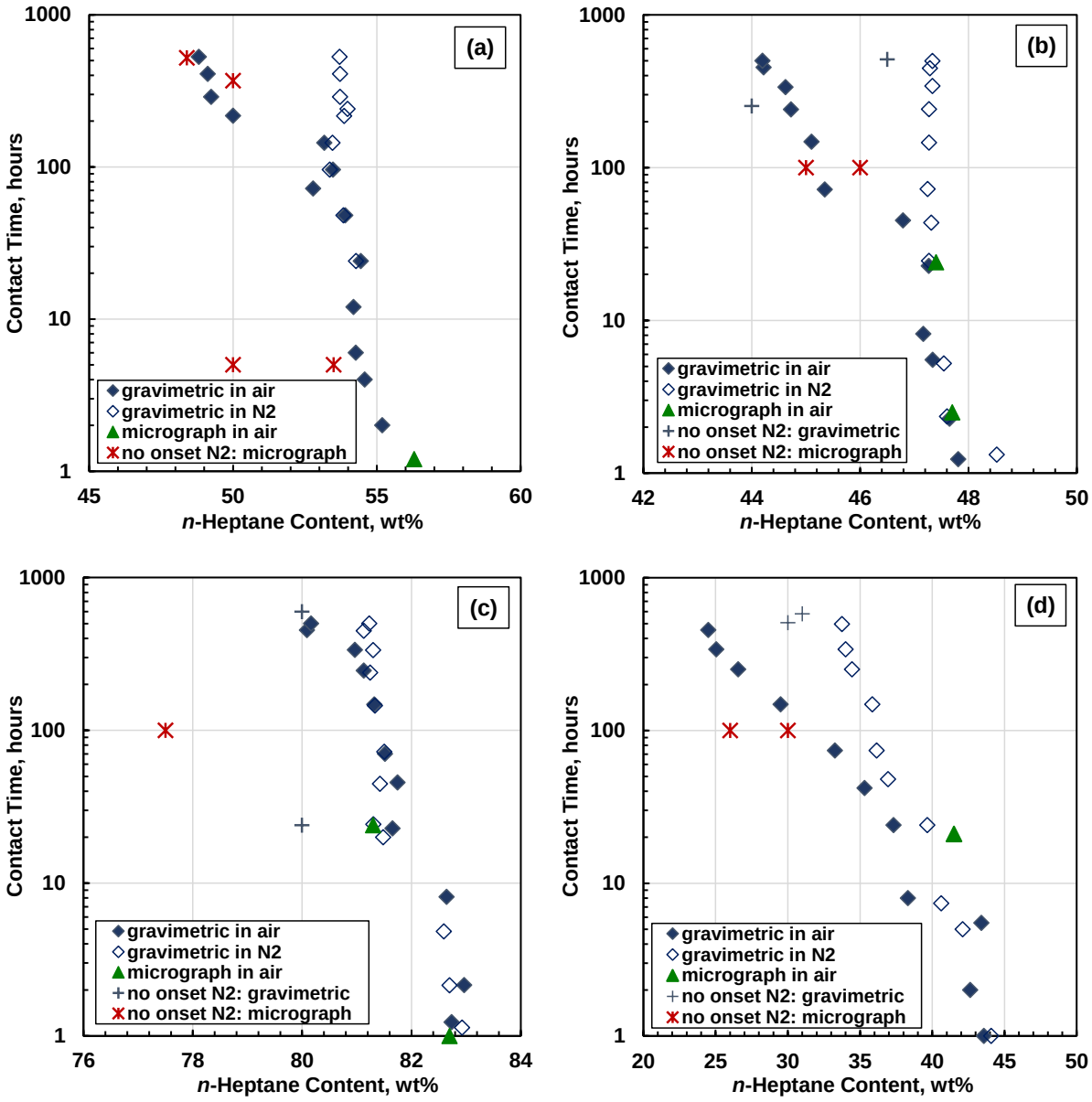

Figure 5.4. Extrapolated onsets of precipitation in air and nitrogen atmosphere interpreted as the time required to start detecting precipitated asphaltenes at a given solvent content: a) WC-B-B2; b) MX-B-A1; c) EU-HO-A1; d) MSB. Micrographic and gravimetric data where no asphaltene precipitation was detected in nitrogen are shown (+, *).

5.3.2 Asphaltene Precipitation Yields in Air

Figure 5.5 compares the asphaltene yields over time for the WC-B-B2 bitumen in air and nitrogen atmospheres. The yields in both atmospheres were similar for approximately the first 50 h but then

deviated. The yields in air increased gradually over time for the duration of the experiment (1000 h, not all data shown here). However, the yields in nitrogen reached a plateau or equilibrium yield after approximately 150 h. The time required to reach the equilibrium yield in nitrogen decreases with increased precipitant content. It is apparent that the oxygen in the air increased the long term asphaltene yield. The mechanism was not investigated in this study but, as discussed previously, oxidation of the asphaltenes can occur even at ambient conditions and tends to reduce their solubility (Choi *et al*., 2016).

Table 5.1. Experimental conditions at which no asphaltene precipitation was detected in nitrogen at 21 ºC and 1 atm.

Oil	Gravimetric Method		Microscopy	
	*n*C7 Content, wt%	Contact Time, h	*n*C7 Content, wt%	Contact Time, h
WB-B-B2	-	-	48 - 56.5	400
MX-B-A1	44, 46.5	500	45, 46	100
EU-HO-A1	80	500	77.5	100
MSB	30, 31	500	26, 30	100

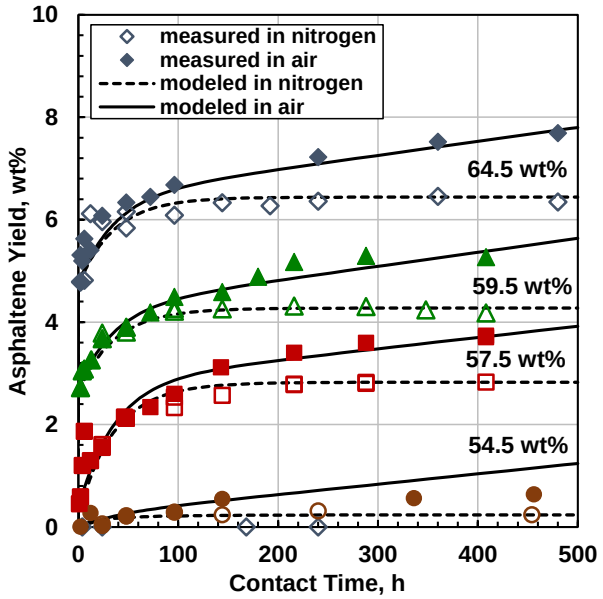

Figure 5.5. Comparison of asphaltene yields from *n*-heptane diluted WC-B-B2 bitumen over time in air (closed symbols) and nitrogen (open symbols) at 21ºC and 1 atm. Data in nitrogen were reported by Chapter 4. The uncertainty in the yields in nitrogen and air are ± 0.6 and ± 0.4 wt%, respectively.

Figure 5.6 compares the yields from WC-B-B2 bitumen with yields from two other Western Canadian bitumens all diluted with *n*-heptane at ambient conditions: 1) WC-B-A0, an Athabasca bitumen (Beck *et al*., 2005); 2) WC-B-A3 (this study). While the amount of precipitant required to obtain the same yield for each sample is different, the trends are the same for all three oils. In other words, the kinetics of asphaltene precipitation is similar for all three bitumens.

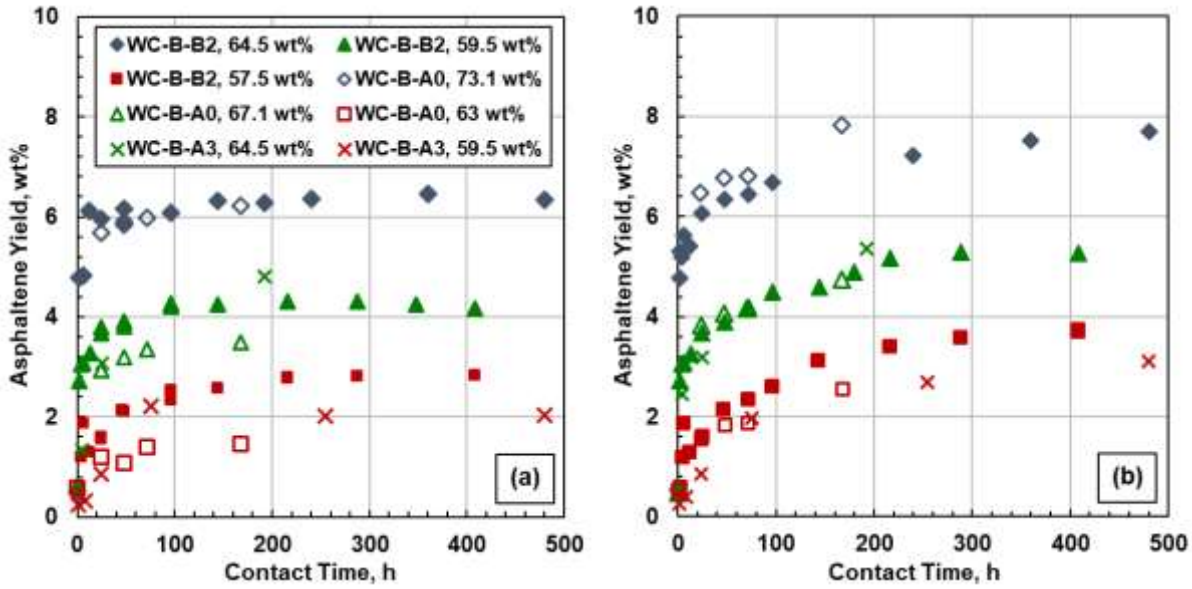

Figure 5.6. Comparison of asphaltene precipitation kinetics from *n*-heptane diluted WC-B-B2, WC-B-A3 (this study) and WC-B-A0 bitumen (Beck *et al*., 2005) at 21ºC and 1 atm: a) in nitrogen; b) in air atmosphere. Error bar in yields are ± 0.4 wt% in air ±0.6 wt% in nitrogen for the bitumens in this work and ±0.8 wt% for WC-B-A0. The data in nitrogen for WC-B-B2 and WC-B-A3 were originally reported in Chapter 4.

Figure 5.7 shows the asphaltene yields in air and nitrogen atmospheres for the remaining oils all diluted with *n*-heptane at 21°C and atmospheric pressure. In all cases except one, the yields were similar for approximately 50 hours and then deviated just as observed for the Western Canadian bitumens. The anomaly was the yields from MX-B-A1 at 52 wt% *n*-heptane where the yields in nitrogen and air deviated almost immediately. In this oil, the asphaltene aggregates formed in air were larger (approximately 10 μm) than in nitrogen (less than 4 μm). Therefore, the yields in nitrogen may have been underestimated because the aggregates could not be separated effectively

by centrifugation. This observation suggests that air may play a role not only in precipitation but in aggregation as well. In any case, it is apparent that air affects asphaltene precipitation in a wide range of crude oils even at ambient conditions.

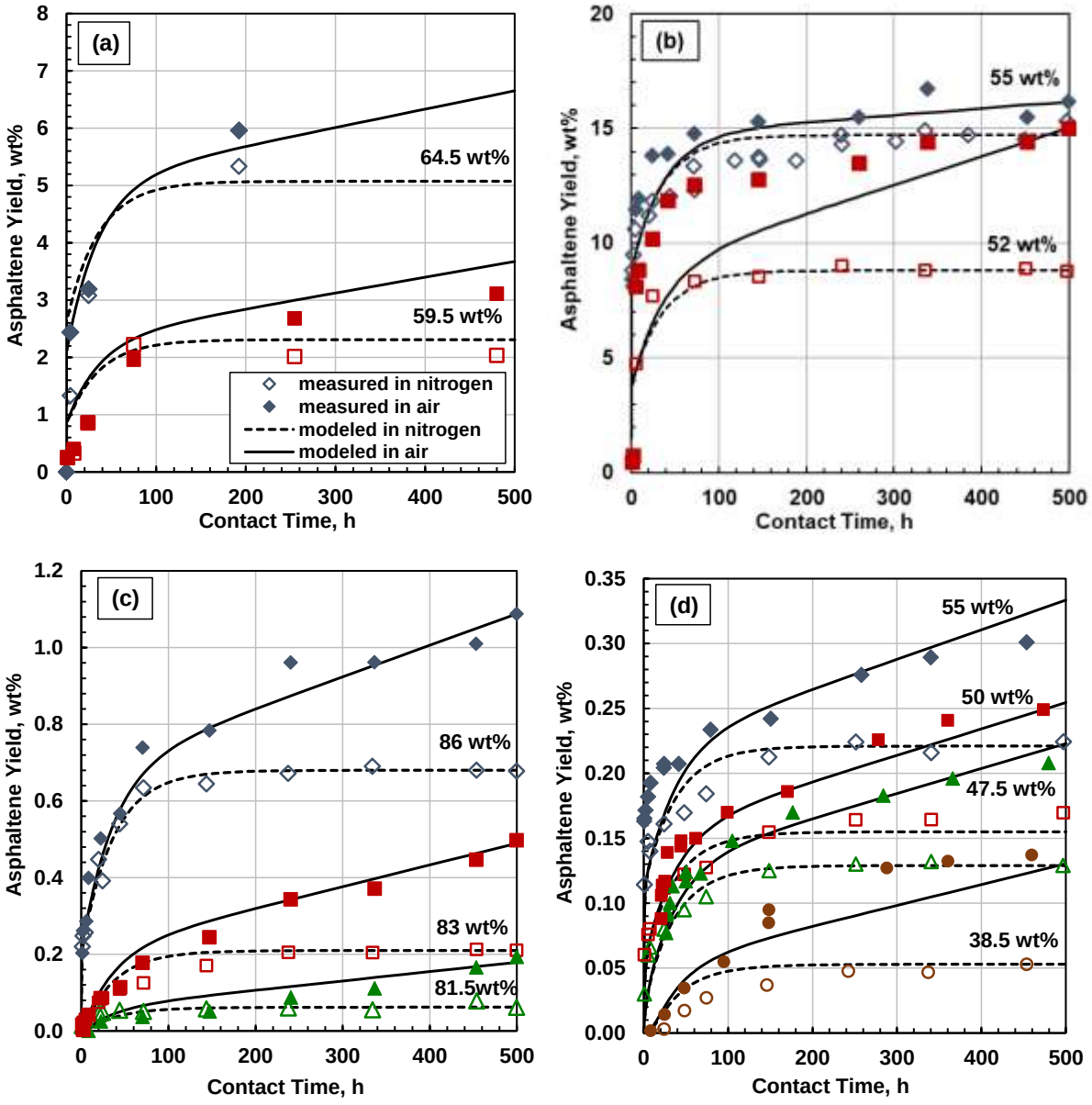

Figure 5.7. Kinetics of asphaltene precipitation in air (closed symbols) and nitrogen (open symbols) for crude oil diluted with *n*-heptane at 21ºC: a) WC-B-A3; b) MX-B-A1; c) EU-HO-A1; d) MSB. Error bars in the respective air and nitrogen atmosphere yields are ± 0.4 and ± 0.6 wt% for WC-B-A3; ± 0.29 and ± 0.58 wt% for MX-B-A1; ± 0.02 and ± 0.03 wt% for EU-HO-A1; ± 0.01 and ± 0.02 wt% for MSB. Data in nitrogen were reported in Chapter 4.

5.3.3 Effect of Aeration in Precipitation Yields

In order to verify the effect of oxygen on asphaltene yields, samples of the WC-B-A0 bitumen were aerated at 21, 40, and 70°C temperatures for 5 days[4]. A base case sample was also prepared where the bitumen was purged with nitrogen at 21°C (see Section 2.9) and not aerated. Yields were measured after 24 h contact time with *n*-heptane at 21°C and atmospheric pressure. Figure 5.8a shows that aeration of bitumen at 40 and 70°C increased the asphaltene yields relative to the base case sample. Aeration at 21ºC had little effect. To demonstrate that temperature alone was not responsible for the increased yield, a bitumen sample was pretreated in nitrogen at 70ºC and not aerated. The asphaltene yields from this sample were the same as the base case sample, within experimental error, Figure 5.8a.

The increase in asphaltene yield after aeration is consistent with the hypothesis that oxygen related reactions are generating components that fall into the asphaltene solubility class. The increased asphaltene yields at higher aeration temperatures could be the result of lower activation energies required to initiate these reactions as temperature increases. Another possibility is that, at higher temperatures, the reduction in bitumen viscosity allows the oxygen to diffuse more rapidly into the bitumen. While viscosity data at different temperatures were not available for the WC-B-A0 bitumen, the viscosity of a similar bitumen decreased from 66,000 to 425 mPa·s as the temperature increased from 21 to 70°C (Motahhari *et al*., 2013). The ineffectiveness of aeration at 21°C may be caused by the high viscosity of the bitumen at this temperature. Air bubbles appeared to coalesce rapidly substantially reducing the effective contact area between the air and bitumen. At higher temperatures, the air bubbles were much smaller and evenly distributed. Figure 5.8b indicates that simply exposing bitumen to air at 70ºC does not change the properties and composition of bitumen. This observation confirms that contact area of oxygen with the oil is an important factor and mass transfer is a limiting step for this process. It appears that diffusion limited oxidation reactions cause the extra asphaltene precipitation over time.

[4] Aeration experiments were performed as a part of an unpublished study by James Beck. The analysis of results is from this thesis.

Figure 5.8c compares the asphaltene yields over time for two aerated samples with the base case, both at an *n*-heptane content of 85 wt%. Although the yields from the aerated samples are consistently higher than the base case at a given *n*-heptane content, the change in yield over time is similar for all three samples. In other words, the initial aeration changes the amount of initially unstable asphaltenes but does not alter the subsequent precipitation kinetics.

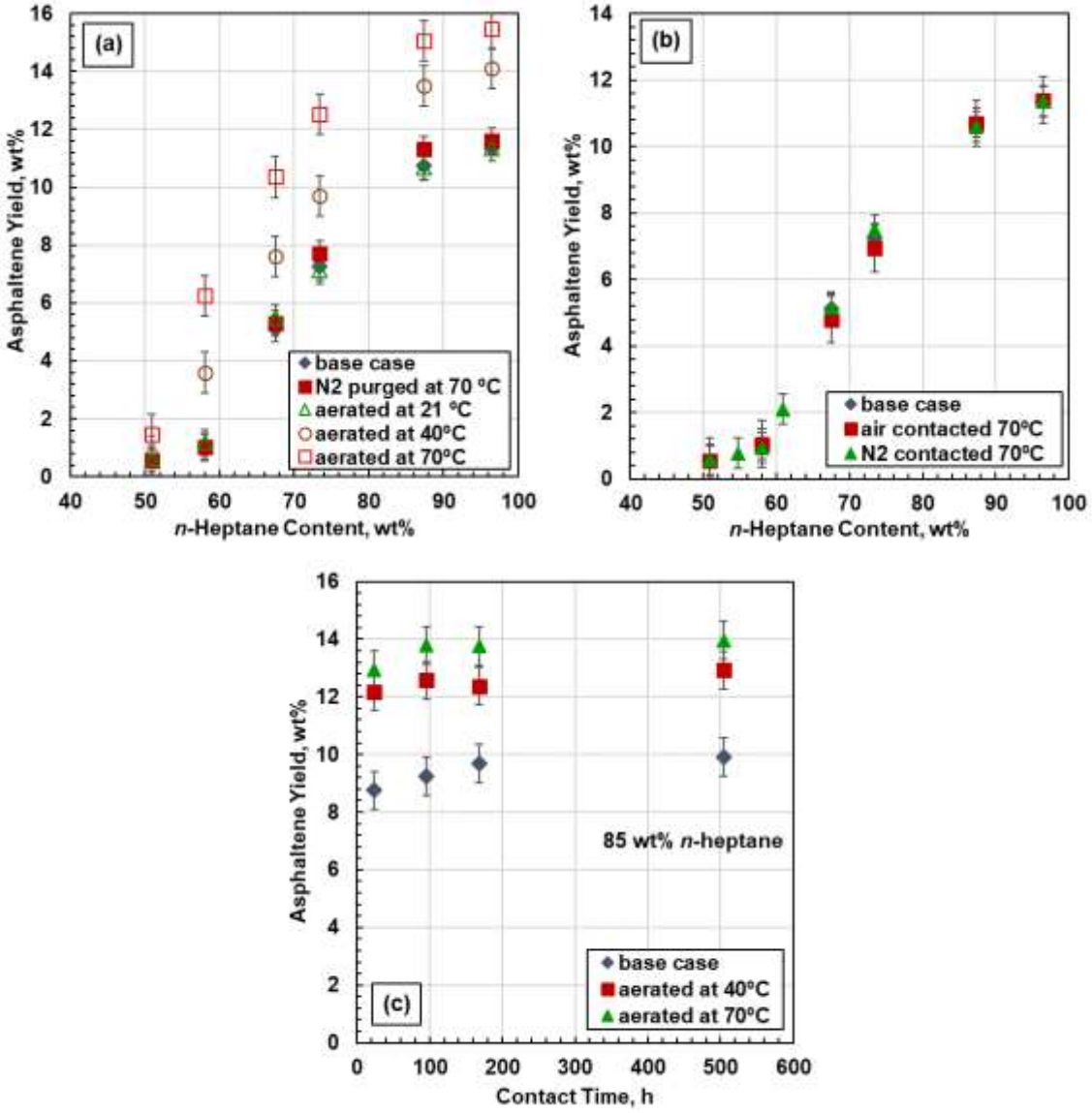

Figure 5.8. Effect of air on asphaltene yields from WC-B-A0 bitumen diluted with *n*-heptane at 21ºC and atmospheric pressure: a) effect of aeration prior to dilution, 24 hours of contact time with *n*-heptane; b) effect or air or nitrogen contact alone, 24 hours of contact time with *n*-heptane; c) effect of contact time at 85 wt% *n*-heptane.

5.3.4 Population Balance Modeling with Oxygen Effect

The population balance model was fitted to the yield data collected in air for the first five oils in Table 2.1 solely by adjusting the constant oxidation rate for each system. The modeled yields in air are shown in Figure 5.5 and 5.7. The fitted oxidation rates are listed in Table 5.2. The fitted model matched the yields in air for each system with an AAD less than 2 wt%.

Table 5.2. Oxidation rates obtained from fitting asphaltene yields with the population balance model.

Sample	r_{ox}, mol/m³·s	AAD, wt%
WC-B-B2	3.56×10^{-7}	0.29
WC-B-A3	3.63×10^{-7}	0.67
MX-B-A1	4.90×10^{-7}	1.71
EU-HO-A1	3.50×10^{-8}	0.02
MSB	3.63×10^{-8}	0.02

The oxidation rates for the bitumen samples were consistent within a factor of two. The oxidation rates for the lighter, less asphaltenic oils (EU-HO-A1 and MSB) were an order of magnitude lower than for the bitumen samples. The difference cannot be attributed to the solubility or diffusivity of the oxygen in the oils. First, once the oils are diluted with *n*-heptane, the differences in the mixture viscosities are relatively small. At 50 wt% *n*-heptane, the calculated mixture viscosity (see Section 6.3.2) with the most viscous oil (MX-B-A1) is 6.6 mPa·s compared with 1.1 mPa·s for the least viscous oil (MSB). Second, both solubility and diffusivity would be higher in the lower viscosity oils but these oils have a lower oxidation rate. Instead, the oxidation rate roughly correlates to the amount of asphaltenes in the oil as shown in Figure 5.9. It appears that the oxidation rate depends on both the availability of oxygen and on the amount of oxygen-reactive components in the oil. The amount and chemistry of these components and their reaction with oxygen likely varies from oil to oil and does not correspond exactly to the asphaltene content; however, an examination of the role of the oil chemistry is outside the scope of this study.

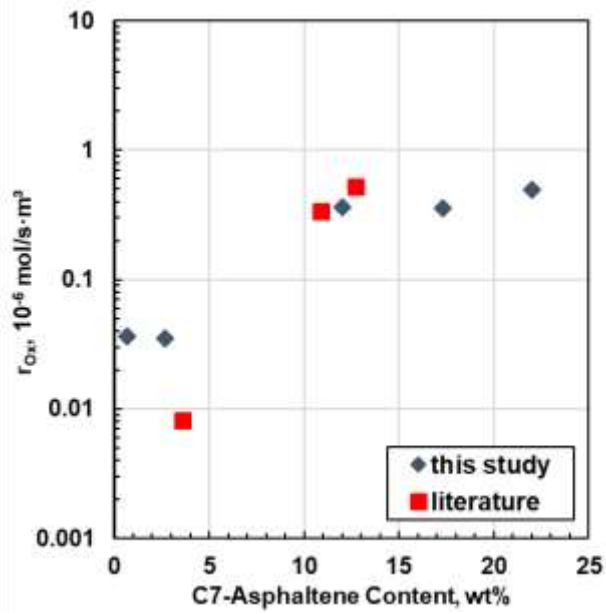

Figure 5.9. Oxidation rate versus the C7-asphaltene content of the oil.

5.3.5 Testing the Population Balance Model with Oxygen Effect

Three sources were found in the literature with sufficient data to test the model. Beck *et al*. (2005) reported yields in nitrogen and air atmospheres over time for the WC-B-A0 bitumen in Table 2.1 diluted with *n*-heptane at 21°C and atmospheric pressure. Maqbool *et al*. (2009; 2011a, 2011b) reported precipitate yields for an Alaskan crude oil (k-1) and Gulf of Mexico crude oil (GM2) at 20ºC and atmospheric pressure. Properties of these oils are provided in Table 4.8.

The model inputs for the three mixtures were determined as follows. The initial yield was taken as the first reported data point. The equilibrium yield at a given precipitant content was taken as the plateau value in nitrogen (WC-B-A0 bitumen) or, if nitrogen data were not available, the yield observed at 500 h in air (k-1 and GM2 oils). The density and viscosity of these mixtures were calculated as described in Section 4.3.7. For the WC-B-A0 bitumen sample, the collision efficiency parameters and primary particle diameter were determined from the recommended values and correlations from Section 4.3.6. For the k-1 and GM2 oils, the collision efficiency was set to 5×10^{-8} (the average value for the light oils reported in Table 4.5), and the primary particle diameters were set to 0.7 and 0.3 μm, respectively (see Section 4.3.7). All other model parameters were

calculated with the recommended values and correlations presented in Section 4.3.6. The model was tuned to match the yield data in air by adjusting the constant oxidation for each system.

Figure 5.10 shows the measured and modeled asphaltene yields from the *n*-heptane diluted WC-B-A0 bitumen. The model was adjusted to match the data in nitrogen and predicted the anaerobic asphaltene yields with an AAD of 0.16 wt%. The model fit the asphaltene yields in air with an AAD of 0.27 wt%. The fitted oxidation rate was 5.2×10^{-7} mol/m³·s.

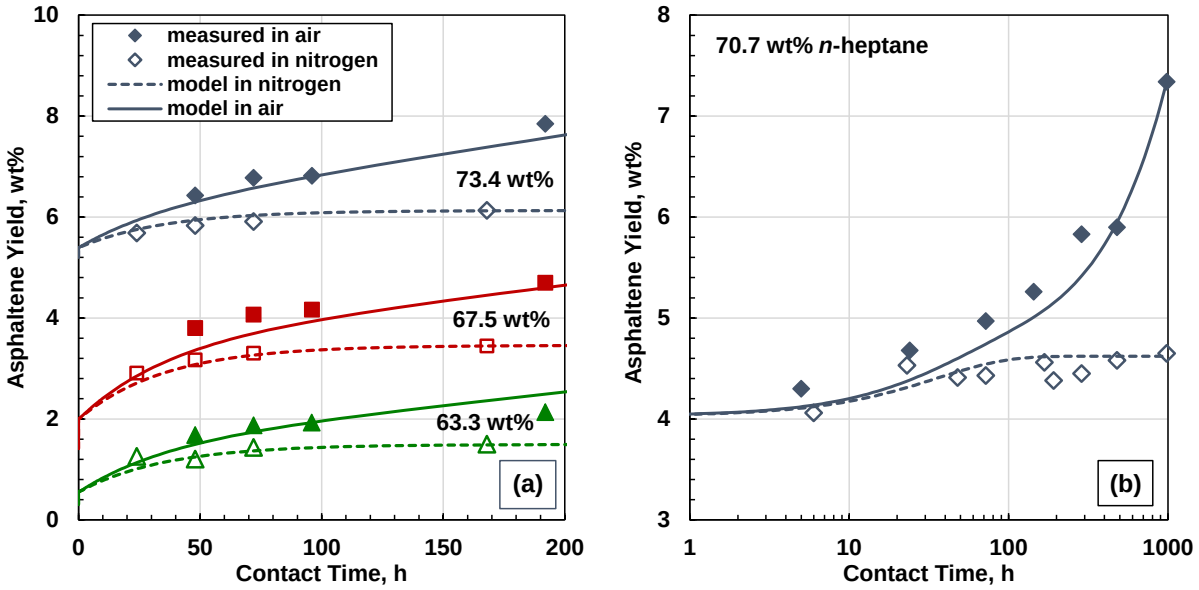

Figure 5.10. Asphaltene yields measured over time in air and nitrogen for the *n*-heptane diluted WC-B-A0 at 23ºC and 1 atm. a) short-term kinetics in Cartesian coordinates; b) long-term kinetics in semi-log coordinates. Yield data were reported by Beck *et al.* (2005) and model results are from this study. The repeatability of the measured yields was ±0.8 wt%.

Figures 5.11a and 5.11b show the measured and modeled yields from *n*-heptane diluted k-1 and GM2 oils, respectively. No yields were measured in nitrogen. The model fit the yields in air with an AAD of 0.41 wt% for the k-1 oil and 0.11 wt% for the GM2 oil. The fitted oxidation rates were 3.3×10^{-7} and 8.1×10^{-9} mol/m³·s, respectively. The higher deviation for the k-1 oil mainly resulted from the model overestimating the yields at the lower *n*-heptane contents at contact times below 100 h. The measured trends are different from all of the other oils in the study and could be an

experimental artifact. Alternatively, the oxidation rate may in fact depend on the mixture composition near the onset of precipitation. Unfortunately, there are insufficient data from which to draw a conclusion. Finally, the fitted oxidation rates for the three oils were generally consistent with the oxidation rates determined from the five oils from this study (Table 5.2) as shown in Figure 5.9.

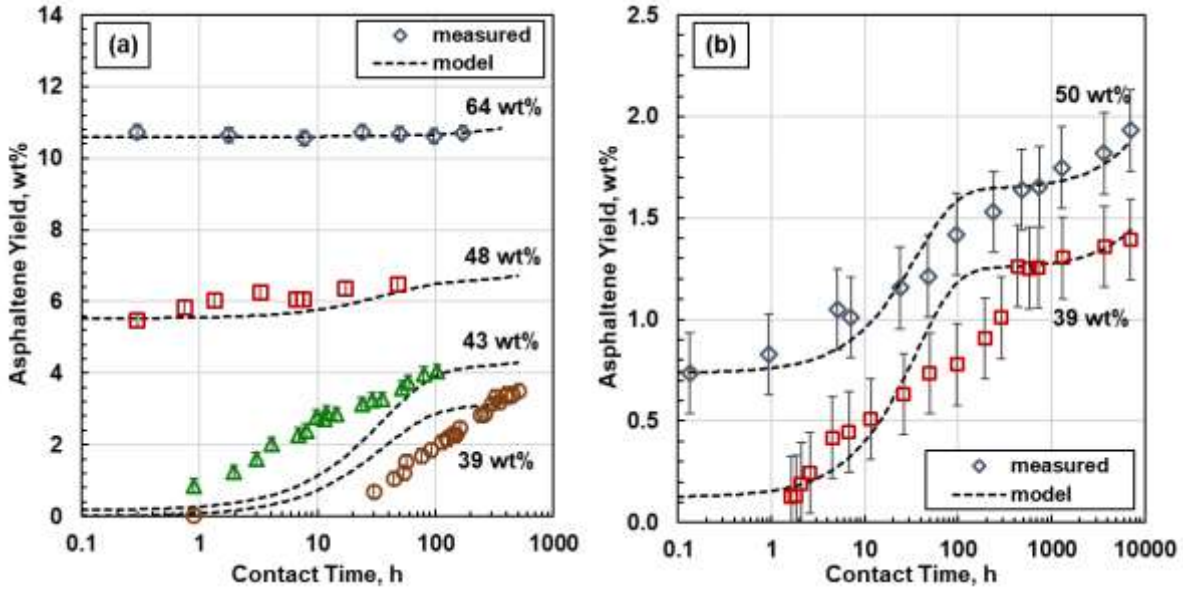

Figure 5.11. Measured and modeled asphaltene yields in air over time at 20ºC for *n*-heptane diluted crude oils: a) k-1 oil; b) GM2 oil. Data from Maqbool *et al.* (2009, 2011a, 2011b).

5.4 Conclusions

The kinetics of asphaltene precipitation was measured for a variety of bitumens and crude oils in an air atmosphere and compared with the data collected in nitrogen previously reported Chapter 4. In nitrogen, the onsets and yields became invariant after 50 to 150 h, consistent with reaching an equilibrium condition. In air, the onsets and precipitation yields followed the same trend over time as in nitrogen for approximately 50 h but then deviated; in particular, the onsets decreased and the yields increased gradually over time for the duration of the experiments, consistent with the observations of Maqbool *et al.* (2009; 2011a). The difference was attributed to oxygen which likely alters the composition and reduces the solubility of the asphaltenes. Aeration accelerated the

"oxidation" effect leading to a more rapid loss of asphaltene solubility and higher precipitation yields.

Considering that most industrial processes will be at anaerobic conditions, data collected after 50 hours in air may not be appropriate. For most oils diluted with *n*-heptane, the "real" kinetics appear to take place mainly within 50 hours. Therefore, the relevant short-term data can still be collected in air with negligible error.

Another consequence of the observed kinetics is that the onset and yields determined within the first few hours do not represent a thermodynamic equilibrium. For example, the instantaneous detection for the WC-B-B2 bitumen was 57.3 wt% while the apparent equilibrium onset is 53.7 wt%. Hence, some care is required in choosing methods and data for particular asphaltene precipitation issues. For example, if the target is data for a thermodynamic model, then data should be collected after 50-150 hours or early time data extrapolated to an equilibrium condition. Short term titration data, such as those often collected with near-IR and visual observations, will give misleading data for equilibrium models. On the other hand, if precipitation at process conditions and residence times is of interest, short term titrations are the appropriate choice. Equilibrium based models may give misleading results for short residence time processes. Also, although contact of diluted oil with air is not anticipated during normal operations, contact is possible during a process upset or in some storage circumstances. The models to predict asphaltene precipitation in these cases must account for the increased yield that is produced by the contact with oxygen.

The population balance model developed in Chapter 4 was adapted to account for the increased yields observed in air. An "oxidation" rate term was included in the primary particle balance equation to account for the generation of primary asphaltene particles formed from the additional insoluble asphaltenes generated from the oxidation (or oxygen catalyzed polymerization) of originally soluble oil components. The modified population balance model fit the yield data to within 2 wt%.

5.5 Chapter References

Agrawal, P., Schoeggl, F.F., Satyro, M.A., Taylor, S.D., Yarranton, H.W. (2012). Measurement and Modeling of the Phase Behavior of Solvent Diluted Bitumens, *Fluid Phase Equilib.*, 334, 51–64.

Akbarzadeh, K.; Alboudwarej, H.; Svrcek, W.Y.; Yarranton, H.W. (2005). A Generalized Regular Solution Model for the Prediction of Asphaltene Precipitation from *n*-Alkane Diluted Heavy Oils and Bitumens. *Fluid Phase Equilib.*, 232, 159-170.

Alboudwarej, H.; Akbarzadeh, K.; Beck, J.; Svrcek, W.Y.; Yarranton, H.W. (2003). Regular Solution Model for Asphaltene Precipitation from Bitumens and Solvents. *Energy Fuels*, 49 (11), 2948-2956.

Andersen, S.I., Birdi, K.S. (1990). Influence of Temperature and Solvent on the Precipitation of Asphaltenes, *Fuel Sci. Technol. Int.*, 8(6), 593-615.

Andersen, S.I., Lindeloff, N., Stenby, E.H. (1998). Investigation of Asphaltene Precipitation at Elevated Temperature, *Petr. Sci. Technol.*, 16(3-4), 323-334.

Angle, C.W.; Long, Y.; Hamza, H.; Lue, L. (2006). Precipitation of Asphaltenes from Solvent-Diluted Heavy Oil and Thermodynamic Properties of Solvent-Diluted Heavy Oil Solutions. *Fuel*, 85 (4), 492-506.

Arya, A.; Liang, X.; Von Solms, N.; Kontogeorgis, G.M. (2017). Modeling of Asphaltene Precipitation from Crude Oil with the Cubic Plus Association Equation of State, *Energy Fuels*, 31 (2), 2063-2075.

Beck, J., Svrcek, W.Y., Yarranton, H.W. (2005). Hysteresis in Asphaltene Precipitation and Re-dissolution, *Energy Fuels*, 19(3), 944-947.

Carnahan, N.F. (2000). Precipitation of Asphaltenes in Heavy Oil and Tar Sands, in *Asphaltenes and Asphalts*, 2, Volume 40B, First Edition. T.F. Yen, G.V. Chilingarian, Elsevier, Amsterdam, The Netherlands.

Chaisoontornyotin, W.; Zhang, J.; Ng, S.; Hoepfner, M.P. (2018). Rapid Heterogeneous Asphaltene Precipitation with Dispersed Solids. *Energy Fuels.* 32 (7), 7458-7466.

Choi, S.; Pyeon, W.; Kim, J.D.; Nho, N.S. (2016). Simple Functionalization of Asphaltene and its Application for Efficient Asphaltene Removal. *Energy Fuels,* 30 (9), 6991-7000.

Ferworn, K.A.; Svrcek, W.Y.; Mehrotra, A.K. (1993). Measurement of Asphaltene Particle Size Distribution in Crude Oils Diluted with n-heptane. *Ind. Eng. Chem. Res*., 32 (5), 955-959.

Fotland, P.; Askvik, K.M. (2008). Determination of Hamaker Constants for Asphaltenes in a Mixture of Pentane and Benzene. *Colloids Surf., A.*, 324 (1-3), 22-27.

Gray, M.R. (2005). *Upgrading Oilsands Bitumen and Heavy Oil*. First Edition. The University of Alberta Press, Edmonton, AB.

Haji-Akbari, N.; Masirisuk, P.; Hoepfner, M.P.; Fogler, H.S. (2013). A Unified Model for Aggregation of Asphaltenes. *Energy Fuels*, 27 (5), 2497-2505.

Haji-Akbari, N.; Teeraphapkul, P.; Balgoa, A.T.; Fogler, H.S. (2015). Effect of *n*-Alkane Precipitants on Aggregation Kinetics of Asphaltenes. *Energy Fuels*, 29 (4), 2190-2196.

Hammami, A.; Phelps, C. H.; Monger-McClure, T.; Little, T. M. (2000). Asphaltene Precipitation from Live Oils: An Experimental Investigation of Onset Conditions and Reversibility. *Energy Fuels*, 14(1), 14-18.

Herrington, P.R. (2001). The Role of Hydroaromatic Species in the Oxidation of Petroleum Bitumens. *Energy Fuels*, 15 (2), 444-448.

Herrington, P.R.; Wu, Y. (1999). Effect of Inter-Molecular Association on Bitumen Oxidation. *Pet. Sci. Technol.*, 17 (3), 291-318.

Hirschberg, A.; deJong, N.J.; Schipper, B.A.; Meijer, J.G. (1984). Influence of Temperature and Pressure on Asphaltene Flocculation. *Soc. Pet. Eng. J.* 24 (3), 283-291.

Israelachvili, J.N. (2011). *Intermolecular and Surface Forces*, Third Edition. Academic Press, New York, NY.

Johnston, K.A.; Schoeggl, F.F.; Satyro, M.A.; Taylor, S.D.; Yarranton, H.W. (2017). Phase Behavior of Bitumen and *n*-pentane. *Fluid Phase Equilib.*, 442, 1-19.

Liu, J.; Xu, Z.; Masliyah, J. (2004). Role of Fine Clays in Bitumen Extraction from Oil Sands. *AIChE J.*, 50 (8), 1917-1927.

Mancilla-Polanco, A.; Johnston, K.; Richardson, W.D.L.; Schoeggl, F.F.; Zhang, Y.; Yarranton, H.W.; Taylor, S.D. (2019). Phase Behavior of Heavy-Oil/Propane Mixtures. *SPE J.*, 24 (2), 596-617.

Maqbool, T.; Balgoa, A.T.; Fogler, H.S. (2009). Revisiting Asphaltene Precipitation from Crude Oils: a Case of Neglected Kinetic Effects. *Energy Fuels*, 23 (7), 3681-3686.

Maqbool, T.; Raha, S.; Hoepfner, M.P.; Fogler, H.S. (2011a). Modeling the aggregation of asphaltene nanoaggregates in crude oil-precipitant systems. *Energy Fuels*, 25 (4), 1585-1596.

Maqbool, T.; Srikiratiwong, P.; Fogler, H.S. (2011b). Effect of Temperature on the Precipitation Kinetics of Asphaltenes. *Energy Fuels*, 25 (2), 694-700.

Moschopedis, S.E., Speight, J.G. (1977). The Effect of Air Blowing on the Properties and Constitution of a Natural Bitumen. *J. Mater. Sci*., 12, 990-998.

Motahhari, H.; Schoeggl, F.F.; Satyro, M.A.; Yarranton, H.W. (2013). Viscosity Prediction for Solvent-Diluted Live Bitumen and Heavy Oil at Temperatures up to 175ºC. *J. Can. Petr. Technol.*, 52 (5), 376-390.

Mousavi-Dehghani, S.; Riazi, M.; Vafaie-Sefti, M.; Mansoori, G. (2004). An Analysis of Methods for Determination of Onsets of Asphaltene Phase Separations. *J. Pet. Sci. Eng*., 42 (2-4), 145–156.

Mushrush, G.W.; Speight, J.G. (1995). Instability and Incompatibility of Petroleum Products. First Edition, in *Petroleum Chemistry and Refining*, First Edition. Taylor & Francis, Washington D.C.

Ramos-Pallares, F.; Lin, H.; Yarranton, H.W.; Taylor, S.D. (2017). Prediction of the Liquid Viscosity of Characterized Crude Oils by Use of the Generalized Walther Model. *SPE J. (Soc. Pet. Eng.).* 22 (5), 1487-1505.

Rastegari, K.; Svrcek. W.Y.; Yarranton, H.W. (2004). Kinetics of Asphaltene Flocculation. *Ind. Eng. Chem. Res*., 43 (21), 6861-6870.

Saryazdi, F.; Motahhari, H.; Schoeggl, F.F.; Taylor, S.D.; Yarranton, H.W. (2013). Density of Hydrocarbon Mixtures and Bitumen Diluted with Solvents and Dissolved Gases. *Energy Fuels.* 27 (7), 3666-3678.

Shafiee, M. (2014). Kinetics of Asphaltene Precipitation and Flocculation from Diluted Bitumen. MSc. Thesis. University of Calgary.

Sie, C.; Nguyen, B.; Castellanos-Diaz, O.; Verlaan, M.; Nguyen, Q.P. (2019). Viscous Oil Recovery and in-situ Deasphalting in Fractured Reservoirs – Part 2: Effect of Solvent Type and Temperature. *Fuel,* 247 (1), 294-301.

Speight, J.G. (2006). *The Chemistry and Technology of Petroleum*, Fourth Edition. CRC Press, Boca Raton, FL.

Taylor, W.F.; Frankenfeld, J.W. (1978). Deposit Formation from Deoxygenated Hydrocarbons. 3. Effects of Trace Nitrogen and Oxygen Compounds. *Ing. Eng. Chem. Prod. Res. Dev.,* 17 (1), 86-90.

Vilas-Bôas Fávero, C.; Maqbool, T.; Hoepfner, M.; Haji-Akbari, N.; Fogler, H.S. (2017). Revisiting the Flocculation Kinetics of Destabilized Asphaltenes. *Adv. Colloid Interface Sci.*, 244, 267-280.

Vincent, B. (1973). The van der Waals Attraction between Colloidal Particles Having Adsorbed Layers: II Calculation of Interaction Curves. *J. Colloid Interface Sci.,* 42 (2), 270-285.

Wilson, D.I.; Watkinson, A.P. (1996). A Study of Autoxidation Reaction Fouling in Heat Exchangers. *Can. J. Chem. Eng.,* 74 (2), 236-246.

Wiehe, I.A. (2008). *Process Chemistry of Petroleum Macromolecules*, CRC Press, Boca Raton, FL.

Yarranton, H.W.; Powers, D.P.; Okafor, J.C.; van der Berg, F.G.A. (2018). Regular Solution Based Approach to Modeling Asphaltene Precipitation from Native and Reacted Oils: Part 2, Molecular Weight, Density, and Solubility Parameters of Saturates, Aromatics, and Resins. *Fuel*, 215, 766-777.

Zhang, Y.; Arya, A.; Kontogeorgis, G.; Yarranton, H.W. (2019). Modeling the Phase Behavior of Bitumen/n-Alkane Systems with the Cubic plus Association (CPA) Equation of State. *Fluid Phase Equilib.,* 486, 119-138.

Chapter 6: Settling Rates of Asphaltene Aggregates in *n*-Alkane Diluted Bitumen

In this contribution[5], the settling rates of asphaltene aggregates were measured in two Western Canadian bitumens diluted with *n*-heptane or *n*-pentane at 21°C and atmospheric pressure. The density and viscosity of the mixtures, the size distributions of the aggregates, and the fractal dimensions of the aggregates were also measured. The settling rates increased with increasing *n*-alkane content, reached a maximum at approximately 75 wt% *n*-alkane and then decreased at higher dilutions. The maximum settling rate corresponded to the maximum aggregate diameter and fractal dimension. The settling rate in *n*-pentane diluted bitumen was two orders of magnitude greater than in the same bitumen diluted with *n*-heptane. The difference was attributed to the lower density and viscosity of the medium, larger aggregates, and higher fractal dimensions in *n*-pentane versus *n*-heptane. The settling rates were modeled with Stokes' law without hindering and modified to include the fractal dimension of the aggregates. Since the aggregates were observed to settle as a zone, all aggregates were assigned the Sauter mean diameter from the measured size distributions. The model matched the measured settling rates to within 20% of the maximum settling rate.

6.1 Introduction

There are an estimated 165 billion barrels of recoverable heavy oil and bitumen in Western Canada, accounting for approximately 9.5% of the world's oil reserves (AER, 2019). For the sake of simplicity, the term bitumen will be used to describe both heavy oil and bitumen in this chapter. The dominant bitumen recovery methods are surface mining and *in situ* recovery (*e.g.*, cyclic steam stimulation or steam-assisted gravity drainage, SAGD) with mining operations accounting for over 50% of the bitumen extracted in Alberta. Some current and proposed bitumen recovery processes use solvent to reduce the density and viscosity of the bitumen; for example, solvent-assisted SAGD (Khaledi *et al.*, 2015), paraffinic froth treatment in mined oil sands processing (Tipman and

[5] This chapter is based on the following article submitted for publication in *Energy and Fuels*: Casas, Y.A., Duran, J.A.; Schoeggl, F.F.; Yarranton, H.W. (2019). Settling of Asphaltene Aggregates in *n*-Alkane Diluted Bitumen. The author of this thesis was a major contributor to this study although a significant portion of the experimental work was performed by Yoshinori Casas (2017). The discussion and modeling sections are the result of this thesis.

Sankey, 1993; Romanova *et al*., 2004; Feng and Qi, 2013), non-aqueous extraction of bitumen from mined oil sand (Hooshiar *et al*., 2012a, 2012b; Nikakhtari *et al*., 2013; Wang *et al*., 2013), and partial deasphalting processes (Brons and Yu, 1995; Gray, 2015; Northup and Sloan, 1996; Sie *et al*., 2019). Many of these processes involve the precipitation, aggregation, and settling of asphaltenes from solvent diluted bitumen, sometimes along with mineral solids and water droplets. In these processes, the solvent acts as a precipitant. This study focuses on the settling rates of asphaltene aggregates where asphaltenes is the dominant component of the aggregates; that is, settling with little or no water and solids.

Asphaltenes are the fraction of a crude oil with the highest molecular weight, density, aromaticity, polarity, heteroatom content, and metal content (Speight, 2006). By definition, they are a solubility-class consisting of the components that are insoluble in an *n*-alkane, typically *n*-pentane or *n*-heptane, but are completely soluble in an aromatic solvent, typically toluene. Hence, the addition of a paraffinic solvent to a crude oil can initiate asphaltene precipitation. Once precipitated, asphaltenes tend to aggregate into fractal structures with diameters ranging from 0.5 to several hundred micrometers (Ferworn *et al.*, 1993; Rahmani *et al*., 2005c; Angle *et al.*, 2006) and fractal dimension in the order of 1.6 to 3 (Long *et al*., 2013; Yang *et al*., 2018; Rastegari *et al*., 2004; Rahmani et al., 2005b). In this case, the fractal dimension is a scaling factor that relates the volume of the aggregate to the number of particles within the aggregate. The porosity of the aggregate is a function of its fractal dimension; the higher the fractal dimension, the lower the porosity. The size and fractal dimension of the aggregates are significant factors in settling and are reviewed first, followed by a review of settling rate data and models.

6.1.1 Asphaltene Aggregate Size and Fractal Dimension

The size of the asphaltene aggregates depends on the precipitant (poor solvent) type and content (Ferworn *et al.*, 1993; Rastegari *et al*., 2004; Angle *et al*., 2006; Rahmani *et al*., 2005c; Seifried *et al*., 2013), temperature (Long *et al.*, 2004a; Daneshvar, 2005; Torkaman *et al*., 2017; Kosior *et al.*, 2018), mixing rate (Rahmani *et al*., 2003; Shafiee, 2014; Zawala *et al*., 2012; Soleimani-Khormakala *et al*., 2018), and contact time (Maqbool *et al*., 2009, Nassar *et al.*, 2015). Asphaltene aggregate sizes were observed to increase continuously as the asphaltene and precipitant contents

increased (Ferworn *et al.*, 1993; Rastegari *et al*., 2004; Angle *et al*., 2006;), but remained almost unchanged above a threshold precipitant content as shown in Chapter 3. The aggregate sizes were also affected by the type of precipitant (Daneshvar, 2005; Calles *et al*., 2008; Seifried *et al*., 2013). In general, larger aggregates formed in stronger precipitants. For example, asphaltene aggregates were up to 5 times larger in *n*-pentane than in *n*-heptane (Daneshvar, 2005). The same results were obtained in Chapter 4. Asphaltenes aggregates were consistently larger in *i*-pentane than in *n*-pentane or in *n*-hexane (Kosior *et al*., 2016, 2018).

Temperature and mixing intensity have shown to have less impact on the size of asphaltene aggregates. In general, average diameters increased between 10 to 30% when the temperature increased between 30 to 100ºC (Daneshvar, 2005; Kosior *et al*., 2018). The effect of the mixing intensity in the size of asphaltene aggregates is less clear. For example, Shafiee (2014) and Rahmani *et al*. (2003) observed smaller aggregates with increasing mixing energy; however, in Chapter 3, no significant effect of mixing rates was found in the range investigated (195-330 rpm equivalent to a shear rate of 10-180 s^{-1}). More recently, the contact time between the precipitant and crude oil has also been found to impact the size of aggregates. In light oils, Maqbool *et al.* (2009, 2011) showed that aggregate diameters increased over time; however, in bitumens, steady-state sizes were reached within few minutes and remained unchanged over time as shown in Chapters 3 and 4.

These same variables also appear to impact the fractal dimensions of asphaltene aggregates although data on fractal dimensions are relatively scarce. Fractal dimensions of precipitated asphaltenes have been measured using settling tests supplemented with optical microscopy (Rahmani *et al*., 2005a, 2005b; Daneshvar, 2005) or using small or ultra-small x-ray scattering (Hoepfner *et al*., 2013; Long *et al*., 2013; Yang *et al*., 2018). Fractal dimensions were observed to increase continuously with precipitant content near the onset of precipitation (Long *et al*., 2013; Yang *et al*., 2018; Rahmani *et al*. 2005b). In Chapter 3 it was found that fractal dimensions of aggregates from diluted bitumen reached a maximum at intermediate precipitant contents (between 70 to 80 wt% *n*-heptane) and then decreased.

In Section 3.2.2 it was reported that mixing rate and time had minimal impact on the fractal dimensions of asphaltene aggregates. The effect of mixing intensity and temperature on the "compactness" of asphaltene aggregates containing mineral solids and water has also been assessed through measurements of the effective density or porosities of the aggregates but not directly related to the fractal dimensions (Long *et al*., 2002, 2004a, 2004b; Zawala *et al*., 2012; Kosior *et al*., 2016, 2018). Aggregates were denser and more compact at elevated temperatures and with higher mixing intensity applied during aggregation because more water droplets and solids were trapped within the aggregates. Since these measurements were made for aggregates containing significant amounts of mineral solids and water, it is not established if the same behavior also applies for aggregates containing asphaltenes alone. Nonetheless, it is clear that both aggregate size and fractal dimension are key factors affecting the settling rates of these aggregates (Long *et al*., 2004a; Rahmani *et al*., 2005a).

6.1.2 Settling Rates of Asphaltene Aggregates

No data were found for the settling rates of asphaltene aggregates in diluted bitumen; however, the settling rates of aggregates in diluted froth from paraffinic froth treatment processes has been studied extensively (Long *et al*., 2002, 2004a; 2004b; Long and Dabros, 2005; Valinasab, 2006; Zawala *et al*, 2012; Kosior *et al*., 2016, 2018). These aggregates consist of precipitated asphaltenes, mineral solids, and water droplets, and are expected to be qualitatively similar to asphaltene aggregates. Some data is also available for model oils (Rahmani *et al*., 2005a; Zahabi *et al*., 2010).

Long *et al.'s* (2004a) pioneering study investigated the settling of aggregates in an Athabasca bitumen froth diluted with *n*-heptane (C7) or a mixture of 50:50 *n*-pentane/*n*-hexane (C5/C6). The froth contained about 66 wt% bitumen, 24 wt% water and 10% solids. They observed that at solvent contents above the onset of asphaltene precipitation, asphaltene aggregates trap most of the emulsified water and inorganic solids. This result was critical for separation processes because it demonstrated that asphaltene precipitation is an effective method for removing water and solids from bitumen.

The settling rate of the froth aggregates is expected to increase as the density and viscosity of the medium decreases, as the aggregate size increases, and as the aggregate porosity decreases. Hence, the settling rate depends on the type of precipitant used as the diluent, the precipitant content in the diluted bitumen, the temperature, and the mixing conditions at which the aggregates formed. Long *et al.* (2004a) observed more rapid settling in the C5/C6 diluted bitumen (2.5 to 8.5 cm/min) than in the C7 diluted bitumen (0.4 to 2 cm/min), all at 30°C. The lower settling rates observed in *n*-heptane diluted froth occur because the aggregates were smaller and more porous in C7 versus C5/C6 (56 to 90 μm versus 115 μm and approximately 75% versus 40%, respectively), and also because C7 is denser and more viscous than C5/C6. Similarly, Kosior *et al.* (2016) found that settling rates were almost 50% higher in *i*-pentane than in *n*-pentane, and about one order magnitude lower in *n*-hexane (all at 62 wt% precipitant).

Kosior *et al.* (2016) found that the settling rates increased at higher precipitant contents by almost one order of magnitude between 60 and 75 wt% precipitant. The average aggregate diameters were similar for all the mixtures and temperatures investigated; therefore, the change in settling rate was likely related to the decrease in density and viscosity of the medium as the precipitant content of the mixture increased. Kosior *et al.* (2018) examined the effect of temperature and found that settling rates increased from 3 cm/min at 30ºC to 100 cm/min at 90ºC (both in *n*-pentane using a pressurized cell to conduct the experiments). They concluded that the increase in settling rates was caused not only by the reduced density and viscosity of the medium but mostly by the increase in density of the aggregates at higher temperatures.

The mixing intensity and temperature at which the froth aggregates form affect their structure and therefore their settling rate. Zawala *et al.* (2012) reported higher settling rates in a stationary fluid column after higher initial mixing intensities, for example increasing from 5 to 60 cm/min when the energy applied increased from 0.1 to 10 kJ/kg (measured at 80°C with *n*-pentane/toluene and *n*-heptane/toluene diluents). The size of the aggregates changed little with the mixing intensity and therefore the higher settling rates were attributed to the lower porosity (and higher density) of the aggregates formed at high mixing rates. Aggregate densities increased from 1300 up to 2000 kg/m³, indicating that asphaltenes trapped more inorganic solids as the mixing intensity increased.

Zahabi *et al.* (2010) confirmed this finding using Fourier transform infrared spectroscopy (FTIR) to measure the composition of aggregated asphaltenes. Long *et al.* (2004a) found that higher initial mixing temperatures produced larger aggregates that settled faster and could be rapidly removed from the diluted bitumen.

Similar results have been found for aggregates from model oils (Rahmani *et al*., 2005a; Zahabi *et al*., 2010). Rahmani *et al.* (2005a) examined settling rates from a model oil consisting of Athabasca asphaltenes rediluted in toluene (62.5 mg/L) and later mixed with *n*-heptane. They confirmed that settling rates increase with increased aggregate diameters and densities. Zahabi *et al.* (2010) examined settling rates of aggregates from a model oil (toluene diluted Athabasca bitumen) mixed with *n*-pentane. They observed that settling rates increased up to three times when 1 μm silica particles were added to the model oil at concentrations from 0 to 4 wt%. The aggregate diameters remained almost constant and it was concluded that settling rates increased because more compact (denser) aggregates were formed in the presence of silica particles.

6.1.3 Settling Models for Asphaltene Aggregates

Stokes' law-based hindered settling models have been used to model the settling rates of asphaltene aggregates from diluted froths (Long *et al.* 2002, 2004a; Kosior *et al*., 2016, 2018), and model oils (Rahmani *et al*., 2005a; Zahabi *et al.*, 2010). In these studies, the aggregate diameter was defined as the longest distance between any two edges of the aggregate. The density of the aggregate was calculated from the porosity of the aggregate, the density of the fluid medium, and the density of the material making up the aggregate structure. The porosity was calculated independently from the sediment volume of the settled aggregates (Long *et al.*, 2004a; Zahabi *et al.*, 2010). In most cases, either the settling rate of a single aggregate was modeled, or an average aggregate diameter and density were applied. Hindering was accounted for with a Richardson-Zaki correction factor empirically adjusted to fit the settling data at higher aggregate concentrations.

Long *et al.* (2004b) used this model to calculate asphaltene densities and porosities from experimental settling velocities of aggregates from a paraffin diluted froth. They reported

porosities in the range of 0.4 to 0.75, obtaining the lowest values for the strongest precipitants for asphaltenes (mixtures C5/C6). In model oils, Rahmani *et al*. (2005a, 2005b) found that the porosities of asphaltene aggregates increased with aggregate diameter and that highly porous aggregates (>80% porosity) had settling velocities higher that predicted by Stokes' equation. They reasoned that the surrounding fluid flowed through the porous structure and reduced the drag force exerted on the aggregate. They introduced a permeability function into the settling equation to account for the reduced drag. Kosior *et al*. (2016, 2018) introduced an additional correction factor for the transition regime at higher Reynolds numbers ($1<Re<20$).

To date, the settling of asphaltenes from diluted bitumen with little or no mineral solids and water droplets has not been investigated. Settling data and an appropriate model for these systems would be useful for designing and operating any process involving partial deasphalting of a bitumen with low water and solids content. In addition, since the aggregates consist only of asphaltenes, their matrix density is known reducing the uncertainty of the settling model input parameters. Hence, a more rigorous test of any proposed settling model is possible.

6.1.4 Objectives

The goal of this chapter is to measure and model the settling of asphaltenes from diluted bitumen. Settling rates of asphaltene aggregates precipitated from bitumen with *n*-heptane and *n*-pentane at 21°C and atmospheric pressure were measured. The following mixtures were investigated: WC-B-A3/*n*-pentane, WC-B-A3/*n*-heptane, and WC-B-B2(1)/*n*-heptane. Sample WC-B-B2 was used to verify the effect of the water + solids content on the settling rates and had lower water and solids content than WC-B-B(1) (see Table 2.1). The onset and amount of asphaltene precipitation for each system was measured in order to determine the aggregate concentrations. The size distribution and fractal dimension of the aggregates were also measured as well as the density and viscosity of the mixtures of precipitant and bitumen used in this study. The effects of the precipitant type and content on the fluid properties, aggregate size and fractal dimension, and ultimately in the settling velocities are discussed. A Stokes' Law based settling model is evaluated and the effect of using different definitions of the aggregate mean diameter is considered. A straightforward methodology is proposed to model settling rates for *n*-alkane diluted bitumens.

6.2 Settling Model

Stokes' Law-based models have been used to model the settling rates of asphaltene aggregates (Rahmani *et al.*, 2005a; Long *et al.*, 2004a; Kosior *et al.*, 2016, 2018). Stokes' Law gives the terminal velocity of a spherical and impermeable particle moving in creep flow as follows,

$$u_s = \frac{g(\rho_s - \rho_m)d^2}{18\mu_m} \tag{6.1}$$

where u_s is the terminal settling velocity, d is the particle diameter, ρ_s is the particle density, ρ_m is the density of the fluid (medium), and μ_m is the fluid viscosity. For a porous object (such as an aggregate), the density (ρ_{agg} instead of ρ_s) is defined in terms of the volume occupied by solid material within the aggregate and the volume occupied by fluid. The total volume is defined by a boundary inside which the solid and fluid material is assumed to have a common uniform velocity. Long *et al.*, (2004a) assumed that aggregates are made of smaller primary particles to obtain the following equation for the density difference between the aggregate and the fluid medium,

$$\rho_{agg} - \rho_m = (1 - \phi)(\rho_p - \rho_m) \tag{6.2}$$

where ϕ is the porosity of the aggregate and ρ_p is the primary particle density. It has been shown that asphaltene aggregates are fractal structures (Janardhan and Mansoori, 1993; Rahmani *et al.*, 2005b; Hoepfner *et al.*, 2013) and, therefore, the aggregate porosity depends on the size of the aggregate as follows,

$$1 - \phi = \left(\frac{d_{agg}}{d_p}\right)^{D_f - 3} \tag{6.3}$$

where d_{agg} and d_p are the aggregate and primary particle density respectively and D_f is the fractal dimension. Eqs. 6.2 and 6.3 are substituted into Eq. 6.1 to obtain the following expression for the settling rate of an aggregate in a dilute medium,

$$u = \frac{g(\rho_p - \rho_m)d_{agg}^2}{18\mu_m}\left(\frac{d_p}{d_{agg}}\right)^{3 - D_f} = \frac{g(\rho_p - \rho_m)}{18\mu_m}\left(\frac{d_{agg}^{D_f - 1}}{d_p^{D_f - 3}}\right) \tag{6.4}$$

For a non-dilute medium, where the motion of one particle can affect another, the Richardson-Zaki hindered settling correction (Richardson and Zaki, 1954) is introduced to obtain the following expression,

$$u = \frac{g(\rho_p - \rho_m)}{18\mu_m}\left(\frac{d_{agg}^{D_f - 1}}{d_p^{D_f - 3}}\right)\alpha_m^n \tag{6.5}$$

where α_m is the volume fraction of fluid in the suspension and n is the Richardson-Zaki exponent. Eq. 6.5 applies to a single aggregate. The asphaltene aggregates are polydisperse in size and, in isolation, would each settle at a different rate. However, as will be discussed later, the aggregates settled as a zone; that is, all at the same rate. Therefore, the settling was modeled with Eq. 6.5 assuming an average diameter to be discussed later. The inputs to the model are the density and viscosity of the medium, the primary particle density and diameter, the average aggregate diameter and fractal dimension, the fluid volume fraction, and the Richardson-Zaki exponent. Each input is discussed below.

Fluid Properties

The density and viscosity of the mixtures of bitumen and precipitant were measured and fitted with existing mixing rules (Saryazdi *et al.*, 2013; Ramos-Pallares *et al.*, 2017). The data and correlations are presented in Section 6.3.2 and summarized in Appendix B.

Primary Particles

The asphaltene particle density was taken as 1200 kg/m³ (Yarranton and Masliyah, 1996). The primary particle diameters were calculated following the methodology described in Section 4.3.4. Recall, this approach hypothesizes that asphaltenes undergo a process of simultaneous nucleation/growth/aggregation upon destabilization with a precipitant. Hence, asphaltene nanoaggregates (of few nanometers in diameter) grow immediately after nucleation to form micrometer-sized particles that later aggregate. Eq. 4.28 describes how an initial nucleus of radius r_0 grows over time.

The calculated primary particle diameters depend on concentration (a function of the asphaltene yield and precipitant content) and, for *n*-alkane diluted bitumens, have a maximum at *n*-alkane contents of approximately 75 wt% (see Figure 4.10). The primary particle diameter is set to this maximum value. Primary particle diameters were in the range of 0.4 to 1.6 μm for *n*-heptane and *n*-pentane diluted bitumen.

This approach was used to calculate the primary particle diameter for each system in this chapter. The concentration of destabilized asphaltenes was calculated from yields obtained at *1.5 h contact* and the diameters were calculated as a function of the asphaltene concentration. A radius of the starting nucleus of 2.5 nm and the growth time of 0.1 s were used as recommended in Chapter 4. The diffusivity coefficient of asphaltenes was calculated from Eq. 4.29 with $A_p = 2.35\times10^{-12}$ for *n*-heptane diluted bitumen, and 2.74×10^{-12} for *n*-pentane diluted bitumen (Grimaldos, 2018). The calculated maximum primary particle diameters are provided in Table 6.1.

Table 6.1. Asphaltene primary particle diameters used in the calculation of fractal dimension of asphaltene aggregates.

Sample	Precipitant	d_p, μm
WC-B-A3	*n*-pentane	1.4
WC-B-A3	*n*-heptane	0.8
WC-B-B2*	*n*-heptane	1.0

* refers to both WC-B-B2 and WC-B-B2(1).

Hindering

The hindering correction requires the fluid volume fraction and the Richardson-Zaki exponent. The volume fraction of fluid in the suspension is determined as follows,

$$\alpha_m = 1 - \alpha_{agg} = \frac{V_{agg,s}}{V_{susp}} \tag{6.6}$$

where α_{agg} is the volume fraction of aggregates in the suspension, $V_{agg,s}$ is the volume occupied by asphaltene aggregates in the suspension, and V_{susp} is the total suspension volume. The volume of the aggregates in the mixture is calculated from their mass and porosity, as follows,

$$V_{agg,s} = \frac{m_s}{\rho_p(1-\phi)} \tag{6.7}$$

where m_s is the mass of precipitated asphaltenes. All the precipitated asphaltenes are assumed to be suspended while the aggregation occurs. The aggregate porosity was calculated from Eq. 6.3 using the average diameter of the aggregates. The mass of precipitated asphaltenes is calculated from the asphaltene yield as follows,

$$m_s = Y_A(1 - w_{solv}) \tag{6.8}$$

where Y_A is the yield of precipitated asphaltenes (mass precipitate/mass bitumen) at a given dilution and w_{solv} is the mass fraction of precipitant in the mixture. Eqs. 6.7 and 6.8 are substituted into Eq. 6.6 to obtain the following expression,

$$\alpha_m = 1 - \frac{Y_A \rho_m (1 - w_{solv})}{\rho_p (1 - \phi)} \tag{6.9}$$

The yields are measured or can be predicted from an independent model. The porosity is obtained from Eq. 6.3. The Richardson-Zaki exponent depends on the Reynolds number (Richardson and Zaki, 1954). For Re<1, Richardson and Zaki (1954) recommended a value of 4.65 for the exponent. For the 1<Re<200 transition regime, Rahmani *et al*. (2005a) used the following correlation to calculate the exponent,

$$n = \left(4.45 + 18 \frac{d_{agg}}{D_c}\right) {Re_p}^{-0.1} \tag{6.10}$$

where D_c is the internal diameter of the graduated cylinder used in the experiments (3.5 cm). The Reynolds numbers for the *n*-heptane diluted mixtures were always lower than 0.1. The Reynolds numbers for the *n*-pentane diluted bitumen mixtures ranged from 0.4 up to 6 and the calculated values of *n* ranged from 4.5 to 5.08. Since the deviation from 4.65 was small, a value of 4.65 was used in all cases.

Aggregate Diameter

Since zone settling was assumed, only the average diameter of the aggregates was required. The size distributions of the aggregates were measured, and average diameters calculated from the distribution. The choice of average diameter (number mean, area mean, *etc*.) is discussed later.

Fractal Dimension

The fractal dimension could not be measured exactly. Instead, both compacted and uncompacted sediment volumes (see Section 2.5) were used to calculate the fractal dimension and an effective fractal dimension was defined as follows,

$$D_{f,eff} = (1 - x) D_{f,uc} + x D_{f,c} \tag{6.11}$$

where *x* is the weighting factor for the fractal dimension that ranges between 0 and 1. The model was tuned to match the measured settling rates by iterating the weighting factor to minimize the following objective function,

$$OF = \frac{1}{N}\sum\left(u_{exp} - u_{model}\right)^2 \quad (6.12)$$

where N is the number experimental data points, u_{exp}, is the experimental settling rate, and u_{model}, is the settling rate calculated from Eq. 6.5. The minimization tolerance for convergence was set to 1×10^{-8} m²/s².

6.3 Results and Discussion

The main factors that affect the settling rate are discussed including the density and viscosity of the medium and the size and fractal dimension of the aggregates. Asphaltene precipitation yields and precipitate concentrations are presented first because they are used as an aid in interpreting the aggregate properties and were required for some of the settling model input calculations. Finally, the settling process is described, the settling rates are presented, and the proposed settling model is adapted to fit the settling data. All of the measured data are provided in the Appendices H to K.

6.3.1 Yields and Onsets of Precipitation

The onset of asphaltene precipitation is defined as the precipitant content at which precipitation is first detected at a given contact time (see Chapter 4). The onset value was required to determine the precipitant content range at which asphaltenes precipitate and form aggregates and, therefore, at which settling experiments can be performed. The asphaltene yield is defined as the mass of precipitate obtained divided by the mass of original bitumen and is a required input for the settling model. Asphaltene onsets and yields depend on the length of time the precipitant has been in contact with the bitumen as described in Chapter 4. The contact time for the settling experiments was approximately 1.5 hours and therefore the onsets and yields were determined at this contact time.

Measured onsets and precipitation yields for mixtures of *n*-heptane and WC-B-A3 bitumen were reported elsewhere in Chapter 4. Onsets and yields for mixtures WC-B-B2(1) bitumen (the sample with higher water + TI content, Table 2.1) with *n*-pentane and *n*-heptane at 1.5 h contact time were measured in this study. Table 6.2 lists the onsets for the three mixtures and Figure 6.1a shows the yields all at 1.5 h of contact time. The onset of precipitation for the WC-B-A3 bitumen is lower and yields are higher in *n*-pentane because it is a stronger precipitant for asphaltenes (Wiehe, 2008;

Akbarzadeh *et al.*, 2005). The onset was lower for the WC-B-B2(1) bitumen than the WC-B-A3 bitumen indicating the WC-B-A3 asphaltenes were more soluble and the bitumen itself is a better solvent for asphaltenes. The yields for the WC-B-B2(1) bitumen were higher than for the WC-B-A3 bitumen because it contained more asphaltenes, Table 2.1.

Table 6.2. Onsets of asphaltene precipitation at 1.5 h contact time and 21ºC.

Mixture	Onset at 1.5 h wt% precipitant
n-pentane/WC-B-A3	47.6
n-heptane/WC-B-A3	56.3
n-heptane/WC-B-B2(1)	46.1

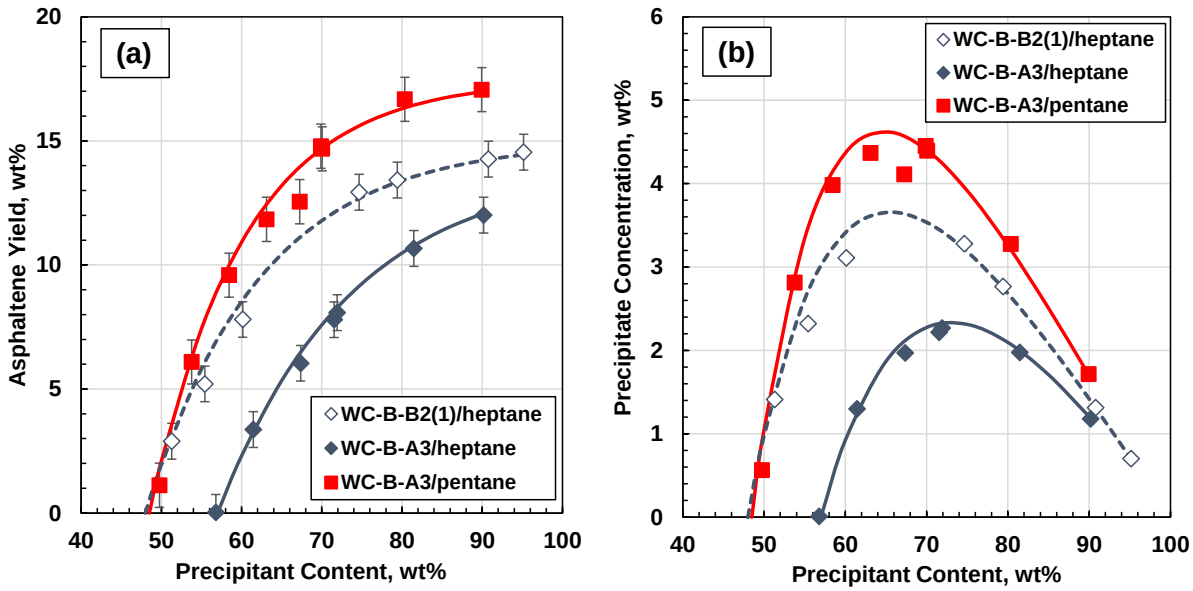

Figure 6.1. Asphaltene yields and precipitate concentration for the *n*-heptane and *n*-pentane diluted bitumen mixtures as a function of precipitant content at 21ºC and 1.5 h contact time. a) yields; b) asphaltene precipitate concentration. Solids lines correspond to correlated data with Eq. 6.13.

For input into the settling calculation, the yields at 1.5 h were fitted with the following empirical equation,

$$Y_A = w_A\{1 - exp[-b(w - w_{onset})]\} \quad (6.13)$$

where w_A is the asphaltene content (mass percent) of the oil reported in Table 2.1 (C5 or C7-asphaltenes, depending on the type of precipitant used), w is the precipitant content in wt%, and w_{onset} is the onset of precipitation from Table 6.2. The values obtained for the fitting parameter b, and the average absolute deviation (AAD) of the correlation are reported in Table 6.3.

Table 6.3. Parameters for the correlation to determine asphaltene yields at 1.5 h and 21ºC.

Mixture	b (1/wt%)	AARD (%)
n-pentane/WC-B-A3	0.085	0.43
n-heptane/WC-B-A3	0.060	0.21
n-heptane/WC-B-B2(1)	0.071	0.33

The concentration of precipitated asphaltenes will be used to help interpret the aggregate size data presented later. It was calculated from the yield data at different precipitant contents as follows,

$$w_u = \frac{Y_A}{100}(100 - w) \tag{6.14}$$

where w_u is the concentration of precipitate in wt% and w is mass percent of precipitant in the mixture. The calculated asphaltene concentrations for the three diluted bitumen mixtures are shown in Figure 6.1b. The precipitate concentration increased rapidly above the onset but reached a maximum when the yield reached a plateau (approximately 70 wt% precipitant). The precipitate concentration decreased at higher precipitant contents because the additional precipitant diluted the mixture without causing much more precipitation.

6.3.2 Effect of Fluid Properties on Settling Rates

Densities and viscosities for the continuous phase (no precipitated asphaltenes) of the three mixtures investigated in this study are shown in Figures 6.2a and 6.2b, respectively. The density and viscosity of the bitumen samples were provided in Table 2.1. The precipitant properties were obtained from Lindstrom and Mallard (2019). The measured mixture densities were fitted with the following excess volume mixing rule (Saryazdi *et al*., 2013),

$$\rho_m = \left[\frac{w_s}{\rho_s} + \frac{w_b}{\rho_b} - w_s w_b \left(\frac{1}{\rho_s} + \frac{1}{\rho_b}\right)\beta_{sb}\right]^{-1} \tag{6.15}$$

where ρ_m is the mixture density, w is the mass fraction, β is the binary interaction parameter, and subscripts s and b denote precipitant (solvent) and bitumen, respectively. The interaction parameter was adjusted with the least squares method to fit the experimental data (see Appendix B). The fitted interaction parameters are provided in Table 6.4. Eq. 6.15 fit the density data with an average absolute deviation (AAD) of 2.1 kg/m³. Some of the deviation likely occurs because some of the asphaltenes had precipitated at precipitant contents above the onset changing the composition of the residual bitumen. Nonetheless, the deviation is less than 0.3% and is not expected to significantly impact the settling calculations.

The measured viscosities were fitted with a mixing rule based on the modified Walther equation (Yarranton *et al*., 2013; Ramos-Pallares *et al*., 2017) and given by,

$$\log[\log \mu_m + 1] = w_s A_s + w_b A_b - w_s w_b A_S A_b \alpha_{sb} \tag{6.16}$$

where μ_m is the mixture viscosity and α_{sb} is the viscosity binary interaction parameter, and the parameter A is defined as follows,

$$A = \log[\log(\mu + 1)] \tag{6.17}$$

where μ is the viscosity of the component at the given pressure and temperature. The values for the interaction parameter of WC-B-B2 and WC-B-B2(1) bitumen mixtures were taken directly from Ramos-Pallares *et al.* (2017). The interaction parameter for the WC-B-A3 bitumen was obtained from fitting the viscosity data collected by Marquez (2019) for mixtures of this bitumen with *n*-heptane and *n*-pentane at 21ºC. The interaction parameters are provided in Table 6.4. Eq. 6.16 fit the experimental data with an AARD of 4.1%.

Table 6.4. Interaction parameters for the density and viscosity mixing rules for *n*-heptane or *n*-pentane diluted bitumens at 21ºC and 1 atm.

Sample	Precipitant	β_{12}	α_{12}
WC-B-A3	*n*-pentane	0.010	0.33
WC-B-A3	*n*-heptane	0.015	0.25
WC-B-B2*	*n*-heptane	0.015	0.25

* applies for both WC-B-B2 and WC-B-B2(1) samples.

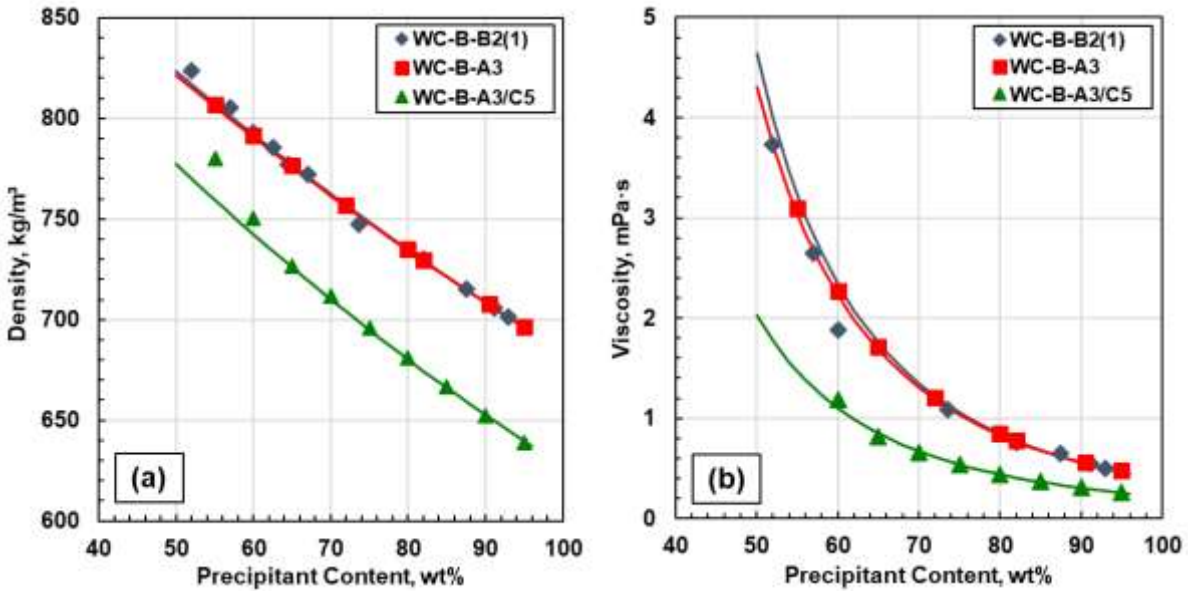

Figure 6.2. Correlated density (a) and viscosity (b) of *n*-heptane or *n*-pentane diluted bitumen samples at 21ºC and 1 atm. Error bars are ± 0.05 kg/m^3 for density and ± 5% for viscosity measurements but are not shown to avoid clutter.

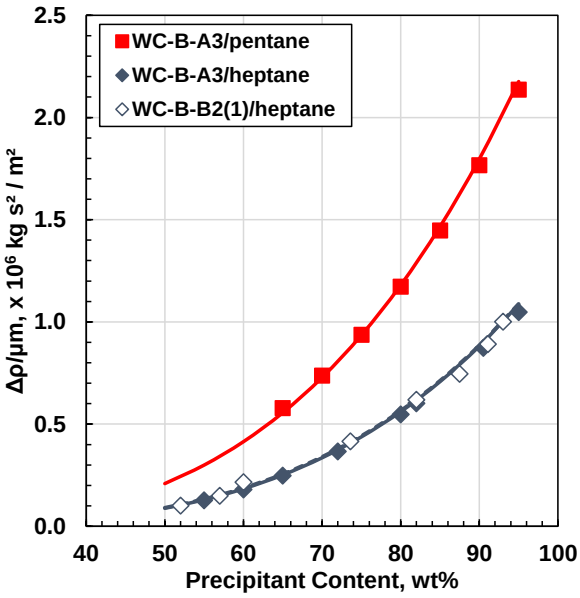

Figure 6.3. Driving force for the settling rates of asphaltene aggregates considering the properties (density and viscosity) of the fluid medium only. Properties of the fluid taken from the data reported in Figure 6.2 and ρ_A =1200 kg/m^3. Solid lines were calculated from the fitted densities and viscosities.

The density difference between the fluid medium and the asphaltenes divided by the viscosity of the fluid medium ($\Delta\rho/\mu_m$) is proportional to the driving force for settling over the resistance to settling. Figure 6.3 shows that this ratio increased with increasing precipitant content and was higher in *n*-pentane versus *n*-heptane at the same precipitant content. In other words, if all other factors were constant, the settling rate would be expected to increase with increasing precipitant content and to be significantly higher in *n*-pentane versus *n*-heptane.

6.3.3 Mean Diameters of Asphaltene Aggregates

The cumulative number frequency distributions of asphaltene aggregates from the diluted bitumen mixtures in this study are provided in Appendix H. For all the measured distributions, the five forms of aggregate mean diameter from Table 2.2 were calculated and are shown in Figure 6.4 for the three mixtures of bitumen and precipitant from this study. The results are in general agreement with mean diameter data for mixtures of bitumen and precipitant in the literature: volume moment diameters between 196 to 286 μm at *n*-heptane contents between 77 to 96 wt% (Ferworn *et al.*, 1993); volume mean diameters between 85 to 150 μm at *n*-heptane contents above 85 wt% (Daneshvar, 2005; Shafiee, 2014); volume mean diameters in the order of 300 μm at 95 wt% *n*-pentane content (Daneshvar, 2005).

The aggregate size increased as the precipitant content increased and reached a plateau at a precipitant content of approximately 80 wt%. As discussed in Chapter 4, the aggregate size increased above the onset because more asphaltenes precipitated increasing the concentration of the primary particles that form the aggregates. The aggregate size reached a plateau when the precipitate concentration reached a maximum but did not decrease when the particle concentration decreased above the maximum. It is possible that the driving force for aggregation increased as the precipitant content increased counteracting the effect of the reduced precipitate concentration. The outcome was more porous structures with a similar average size but fewer primary particles within the aggregate.

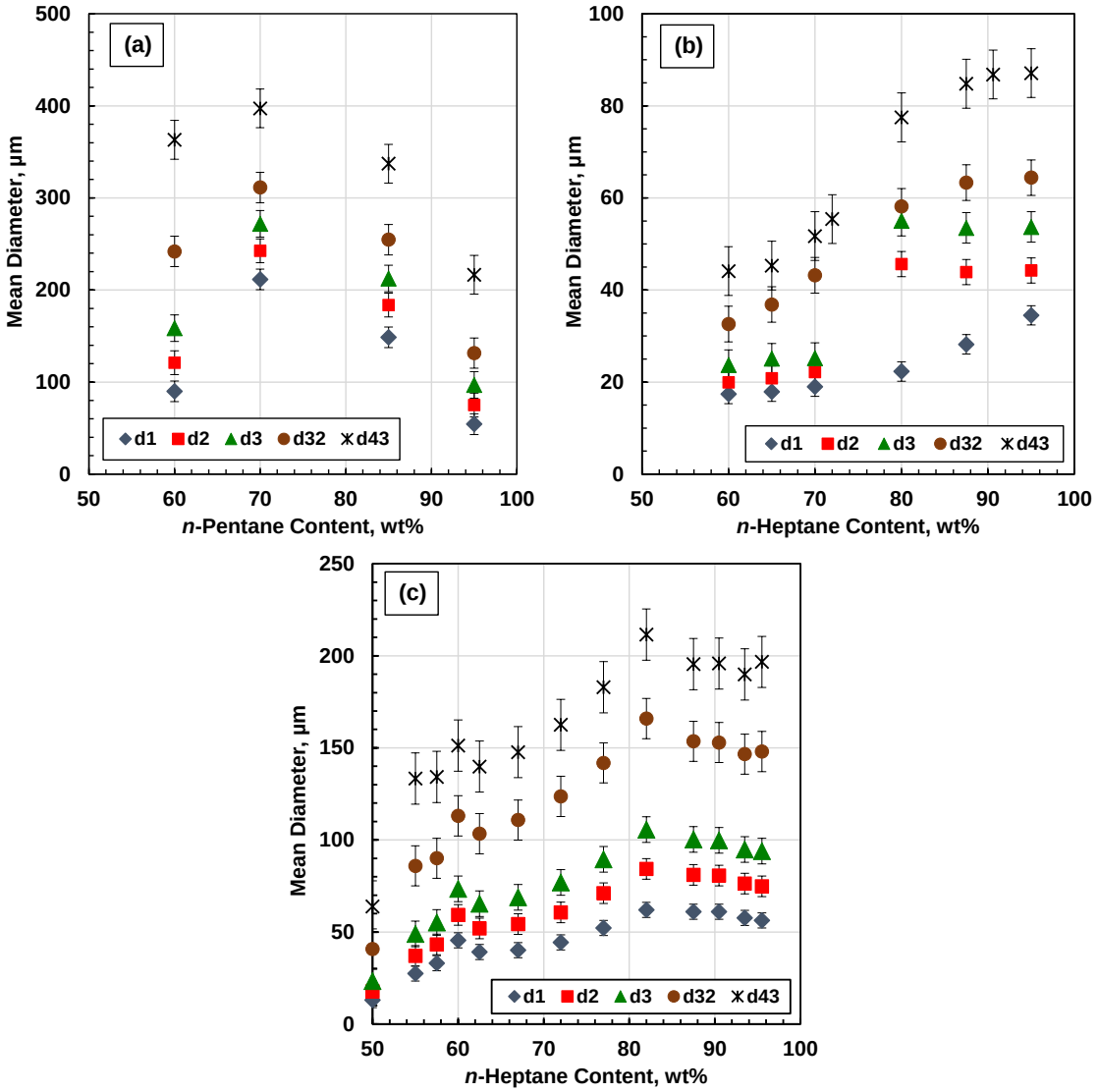

Figure 6.4. Asphaltene aggregate mean diameters for mixtures of bitumen and precipitant measured after 1 h of mixing at 195 rpm and 21ºC: a) *n*-pentane/WC-B-A3; b) *n*-heptane/WC-B-A3; c) *n*-heptane/WC-B-B2(1). Definitions of the mean diameters are provided in Table 2.2.

The aggregates formed in *n*-pentane were much larger than the aggregates formed in *n*-heptane, partly because the precipitate concentration was higher but more likely because *n*-pentane is a more effective precipitant giving a high driving force for aggregation. The aggregates formed in the WC-B-B2(1) bitumen were larger than those formed in the WC-B-A3 bitumen, likely because the precipitate concentration was higher. In general, the settling rates are expected to peak at the precipitant content corresponding the maximum aggregate diameter. The highest settling rates are

expected in *n*-pentane and higher settling rates are expected in the WC-B-B2(1) bitumen versus the WC-B-A3 bitumen.

6.3.4 Correlation for the Fractal Dimension

Figure 6.5 shows the fractal dimension of asphaltene aggregates from the *n*-pentane and *n*-heptane diluted bitumen samples as a function of the precipitant content. Both compacted and uncompacted fractal dimensions are reported. The fractal dimension from uncompacted volumes are smaller than the compacted volumes because the same aggregate mass occupies a larger space.

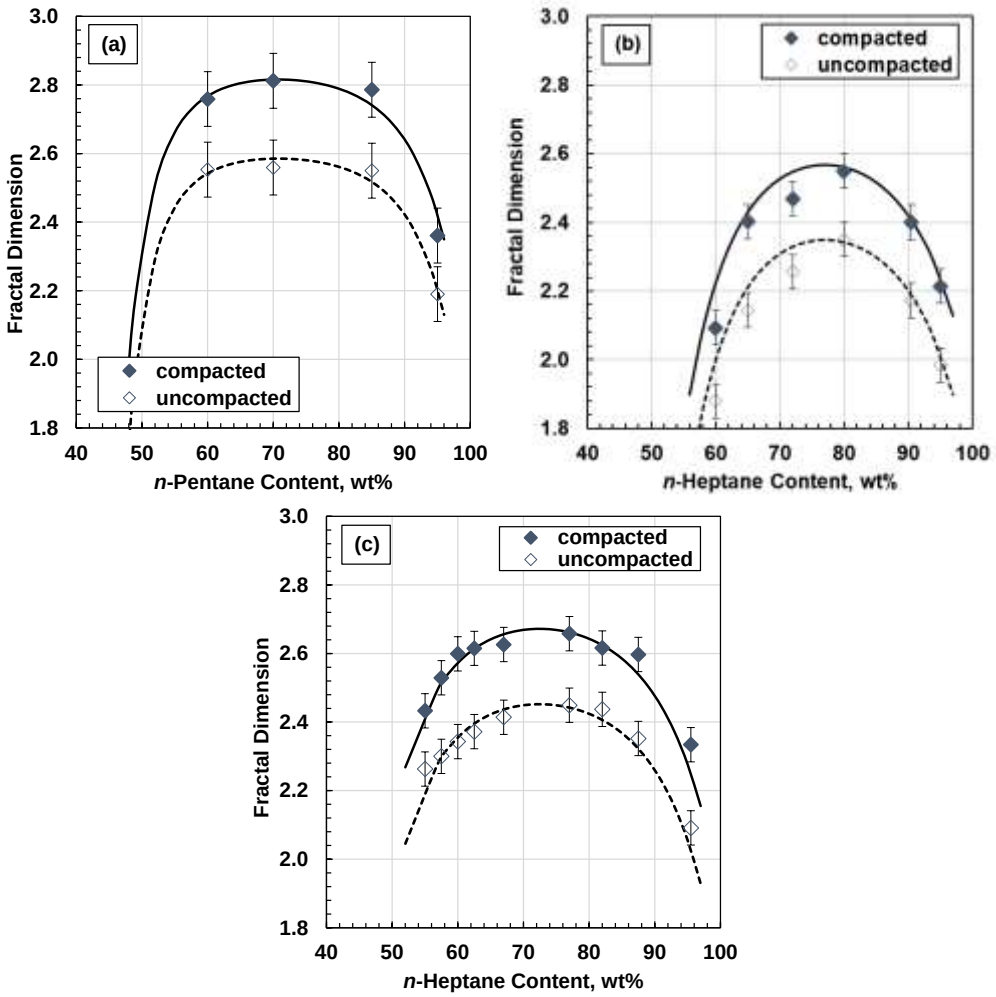

Figure 6.5. Fractal dimensions from sediment volumes for aggregates from *n*-pentane and *n*-heptane diluted bitumen mixtures at 21ºC: a) *n*-pentane/WC-B-A3; b) *n*-heptane/WC-B-A3; c) *n*-heptane/WC-B-B2(1). Symbols are data; solid lines are from Eq. 6.18 and dashed lines from Eq. 6.19.

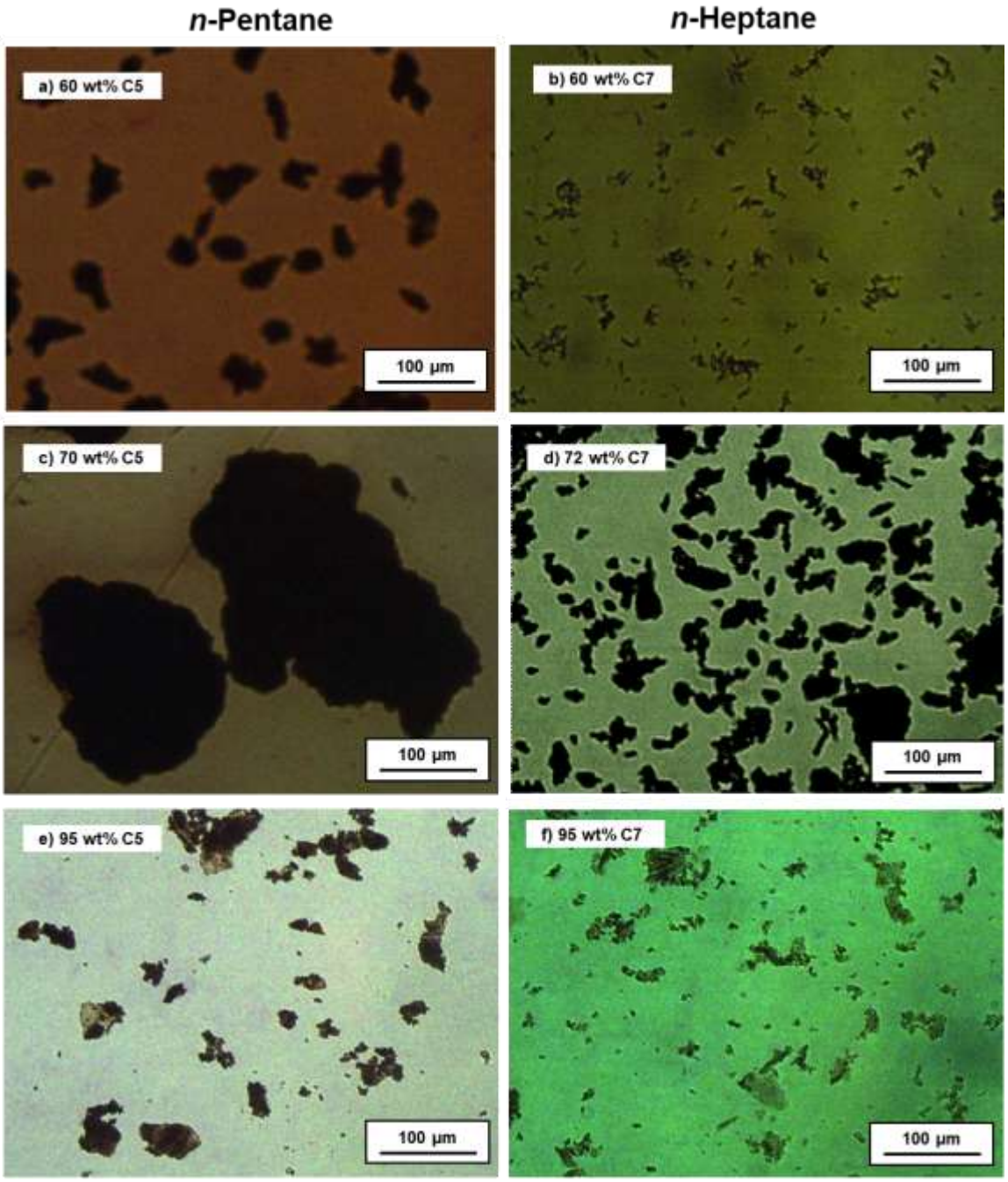

Figure 6.6. Micrographic images of asphaltene aggregates from WC-B-A3 bitumen diluted with *n*-pentane or *n*-heptane at precipitant contents from 60 to 95 wt% at 21ºC. a) 60 wt% *n*-pentane; b) 60 wt% *n*-heptane; c) 70 wt% *n*-pentane; d) 72 wt% *n*-heptane; e) 95 wt% *n*-pentane; f) 95 wt% *n*-heptane.

All the compacted fractal dimensions range from 2 to 2.8, in qualitative agreement with most previous studies for similar systems (Yang *et al.*, 2018; Daneshvar, 2005). In Chapter 3 values in the range of 2.3 to 2.85 were reported for diluted bitumen systems and fractal dimensions were correlated as a function of the precipitant content. On the other hand, Rahmani *et al.* (2005b) estimated fractal dimensions in the order of 1.3 to 1.6. However, the microscopic images of Figure 6.6 indicate that asphaltene aggregates, even at high dilutions are relatively compact three-dimensional structures rather than two-dimensional or very porous aggregates. Hence, the fractal dimensions above 2.3 correspond more closely to the microscopic images. Since the asphaltene aggregates have relatively high fractal dimensions and therefore low porosities (less than 16%), the effects of the aggregate permeability can be neglected in the settling calculations (Kosior *et al.*, 2016, 2018).

The fractal dimension increased with increasing precipitant contents reaching a maximum at a similar precipitant content as the maximum in the concentration of precipitated asphaltenes. The micrographs in Figure 6.6 confirm that the aggregate structures in *n*-heptane are more compact and more spherical (higher D_f) at approximately 75 wt% precipitant where the maximum occurs. Fractal dimensions in *n*-pentane were higher than those of the *n*-heptane diluted bitumen (about 0.2-0.3 units of difference) and the micrographs confirm this difference. The precipitate concentration is higher in *n*-pentane than in *n*-heptane at a given precipitant content. Hence, it appears that the fractal dimension depends on the precipitate concentration.

In Section 3.7.2 an empirical correlation was provided for the fractal dimension of the fully compacted sediment bed in terms of the concentration of precipitated asphaltenes. However, that correlation was not adapted for *n*-pentane data and tended to overestimate the fractal dimensions near the onset of precipitation. Instead, the fractal dimensions were found to correlate to both the concentration of primary particles and the mass transfer rate of asphaltenes in diluted bitumen. The mass transfer rate is related to diffusivity which in turn has a power law relationship with the inverse viscosity of the medium (Grimaldos, 2018). Hence, the proposed correlation parameter is $\frac{w_u}{{\mu_m}^k}$, where w_u is the concentration of precipitated asphaltenes in wt% and k is a fitted exponent.

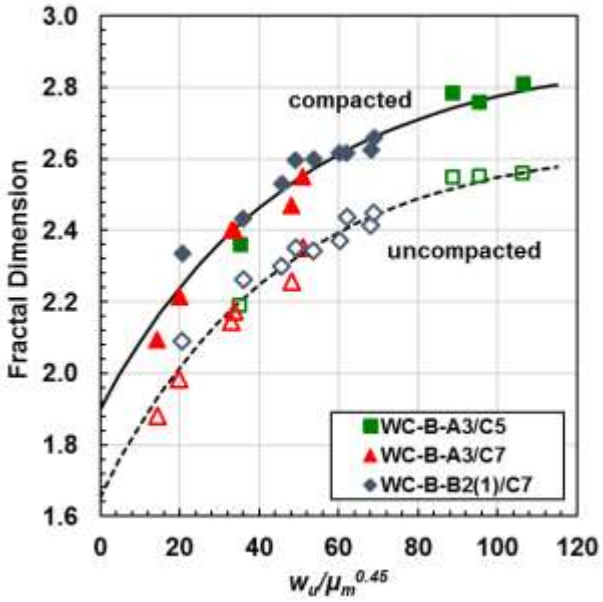

Figure 6.7. Uncompacted and compacted fractal dimensions of asphaltene aggregates from *n*-pentane and *n*-heptane diluted bitumens as a function of the concentration of precipitated asphaltenes and medium viscosity. Closed and open symbols are compacted and uncompacted fractal dimension data, respectively; solid line is from Eq. 6.18 and dashed line from Eq. 6.19.

Figure 6.7 shows the experimental fractal dimensions as a function of $w_u/\mu_m^{\,k}$ for the two systems. The value obtained for *k* that best fit the data using the least squares method was 0.45. The value of 0.45 is consistent with the values of 0.35 to 0.59 used by Grimaldos (2018) to correlate diffusivity to viscosity in bitumen diluted with toluene and *n*-alkanes. The compacted and uncompacted fractal dimensions from this study were each fitted to obtain the following correlations:

Compacted D_f $$D_{f,c} = 2.899 - \exp(-0.0208\frac{w_u}{\mu_m^{0.45}}) \quad (6.18)$$

Uncompacted D_f $$D_{f,uc} = 2.656 - \exp(-0.0225\frac{w_u}{\mu_m^{0.45}}) \quad (6.19)$$

The compacted and uncompacted D_f correlations fit the data with AARD of 2.4% and 3.2%, respectively. The solid lines in Figure 6.5 correspond to calculated fractal dimensions from the proposed correlations.

6.3.5 Settling Process

Type of Settling

The settling rate of an individual aggregate will depend on its size and porosity (fractal dimension) and can be modeled with Stokes' law (Rahmani *et al*., 2005a; Zawala *et al.*, 2012; Kosior *et al.*, 2018). The settling rate of an aggregate within a suspension of aggregates with a polydisperse distribution of diameters and porosities is not obvious. In this case, the settling rate of an individual aggregate may be hindered but remain different from other aggregates of different size and porosity, or the aggregates may settle as a zone (a particular case of hindering). Aggregates settling as a zone will settle at the same rate independently of their size and composition (Tiller, 1981; Bhargava and Rajagopal, 1990; Lin and Lohnes, 1984; Long *et al.*, 2002).

If the aggregates settle independently, a concentration gradient will develop as the largest, least porous aggregates settle more rapidly than the smaller or more porous aggregates. If the aggregates settle as a zone, there will be a settling front with no aggregates above the front and some average aggregate concentration below the front. Figures 6.8a and 6.8c show the concentration profiles of asphaltenes during a typical settling experiment. The aggregate concentration above the front is uniformly zero (for example above 12 cm at 20 minutes and above 3 cm at 45 minutes in Figure 6.8a). Micrographic observations (not shown here) confirmed that the fluid above the front was free of aggregates. Hence, the aggregates settled as a zone in the experiments in this study. Long *et al*. (2002) also observed zone settling for aggregates of asphaltenes, solids, and water from bitumen froth.

Co-settling of Toluene Insolubles

The settling rate of both asphaltene aggregates and toluene insolubles were measured for the WC-B-B2(1) bitumen since it had the highest content toluene insolubles, Table 2.1. The asphaltene and toluene insoluble profiles were measured with the sampling method at 55 wt% *n*-heptane at settling times of 20 and 45 minutes, Figure 6.8a and 6.8b. The height represented in both figures is the average height of the layer. Note that the volume fraction of asphaltenes is two orders of magnitude higher than the volume fraction of toluene insolubles. A similar dataset was obtained for the same mixture at 62.5 wt% *n*-heptane, Figure 6.8c and 6.8d.

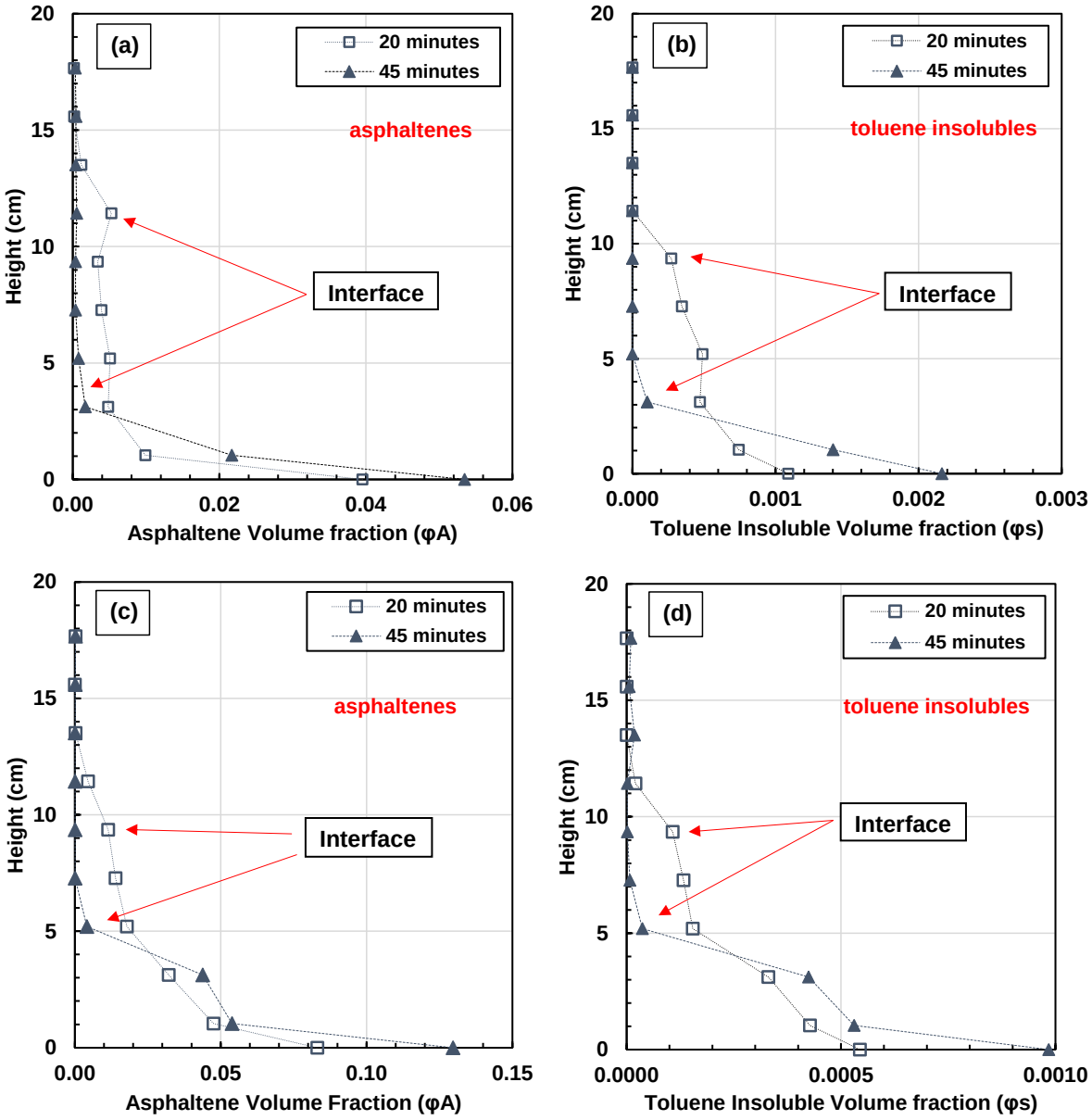

Figure 6.8. Gravimetric profiles after 20 and 45 minutes settling for *n*-heptane diluted WC-B-B2(1) bitumen at 55 and 62.5 wt% precipitant and 21ºC. a) asphaltene profile at 55 wt%; b) toluene insolubles profile at 55 wt%; c) asphaltene profile at 62.5 wt%; d) toluene insolubles profile at 62.5 wt%. Solid lines are provided as a visual aid. Data originally reported by Casas (2017).

Both volume fractions of asphaltenes and toluene insolubles above the settling front approached zero, indicating that all of the material was settling as a zone. The location of the front was almost identical for the asphaltenes and toluene insolubles at each time confirming that asphaltene aggregates and TI were settling at the same rate. The results are consistent with the incorporation

of toluene insolubles into the structures of the asphaltene aggregates, as reported in paraffinic froth treatment studies (Long *et al*., 2002; Zahabi *et al*., 2010). The incorporation of toluene insolubles is attributed to a relatively strong attraction between asphaltenes and mineral solids because solids are partially coated by organic compounds (Nikakhtari *et al.*, 2014; Pal *et al*., 2015).

6.3.6 Measured Settling Rates

Figure 6.9 shows the settling rates of asphaltene aggregates from the three mixtures in this study. In all cases, there was no settling below the onset of precipitation (vertical dashed lines in Figure 6.9); the null data are not shown here. Above the onset, the settling rates increased as the precipitant content increased reaching a maximum rate at intermediate dilutions (about 85% *n*-pentane or 80% *n*-heptane), and then decreased at higher dilutions. The settling rates in *n*-pentane were 2 orders of magnitude higher than in *n*-heptane for the WC-B-A3 bitumen. The data are in qualitative agreement with the available literature data. For example, Kosior *et al.* (2016) observed rates of about 30 cm/min for diluted bitumen froth at 30ºC and 60 wt% *n*-pentane. Figure 6.9 shows settling rates in the order of 10 to 40 cm/min for the *n*-pentane diluted system. Others have observed that settling rates are higher in lighter paraffinic precipitants and at increased precipitant contents (Long *et al*., 2004a, Kosior *et al*., 2016; 2018).

As discussed previously, the settling rate is determined by the density and viscosity of the mixture and the size and fractal dimension of the aggregates. For a given precipitant, the addition of precipitant decreased both the density and viscosity of the mixture tending to increase the settling rate. However, the effect of the aggregate size and fractal dimension appeared to dominate, particularly at higher precipitate contents. In all three systems, the settling rates reached a maximum that coincided with the maximum in the aggregate diameter and fractal dimension.

The higher settling rates in the *n*-pentane diluted bitumen can be attributed to the same three factors. Comparing *n*-pentane with *n*-heptane, the $\Delta\rho/\mu$ ratio was about 53% higher, the aggregate diameters were 3-6 times higher, and their fractal dimensions were 12% higher. All three factors contribute to the higher settling rates. Finally, while the *n*-heptane/WC-B-B2(1) and *n*-heptane/WC-B-A3 systems had similar fluid properties, the settling rates of the WC-B-B2(1)

aggregates were significantly higher than for the WC-B-A3 aggregates because the WC-B-B2(1) aggregates were bigger and denser. The WC-B-B2(1) aggregates had an approximately 50% larger diameter and 6% higher fractal dimension.

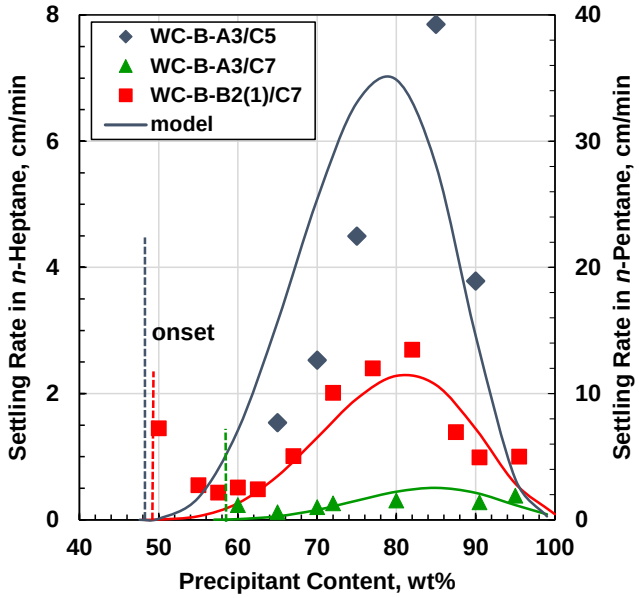

Figure 6.9. Measured settling rates of asphaltenes aggregates from *n*-pentane and *n*-heptane diluted WC-B-A3 and WB-B-B2(1) bitumen samples at 21ºC. Note, settling rates of the *n*-pentane diluted mixture are two orders of magnitude higher than in *n*-heptane (scale on the right). Solid lines are the non-hindered settling model. Error bars are not shown to avoid clutter but are 38.9% for WC-B-A3/C5, 23.0% for WC-B-A3/C7 and 18.5% for WC-B-B2(1)/C7.

Figure 6.9 also shows that there was also a local maximum in the settling rate in the *n*-heptane/WC-B-B2(1) system just above the onset of precipitation. This result was unexpected because, near the onset, the medium is denser and more viscous, and the aggregates are smaller with lower fractal dimension. The local maximum in the settling rate may be related to the presence of toluene insolubles and/or water in the aggregates. For example, Zahabi *et al*. (2010) reported increased settling rates for asphaltene aggregates when silica particles were present. They concluded that silica particles and water incorporate into the asphaltene structures and if the ratio of solids/water to asphaltenes is significant then settling rates would increase. Near the onset condition, the aggregates might have a large proportion of water and solids trapped into the structures leading to a higher matrix density and possibly fractal dimension for the aggregate than predicted.

This hypothesis was tested by comparing the settling rates for the *n*-heptane diluted WC-B-B2(1) and WC-B-B2 bitumens. Table 2.1 shows that the WC-B-B2(1) sample had a higher content of water and toluene insolubles than the WC-B-B2 sample. If the hypothesis is correct, there would be enhanced settling for WC-B-B2(1) but not for WC-B-B2. Figure 6.10 confirms that the settling rates were higher in the WC-B-B2(1) bitumen near the onset condition; however, at higher precipitant contents, the difference in settling rates between the two samples was negligible. The results are consistent with a relatively high proportion of water/solids to asphaltenes in the aggregates formed near the onset, giving higher than expected settling rates. At higher solvent contents, the proportion of precipitated asphaltenes is much higher and the water and solids have little effect on the aggregate properties and settling rates. Unfortunately, the aggregates at precipitant contents just above the onset of precipitation are small and could not be resolved with the microscope in sufficient detail to confirm their structure.

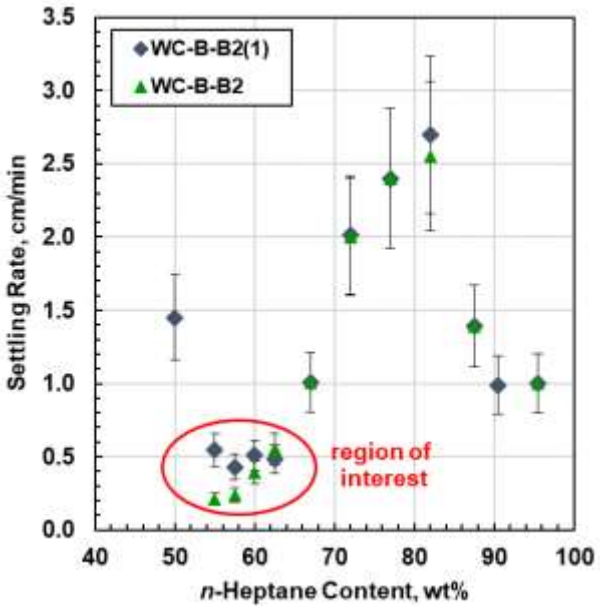

Figure 6.10. Comparison of settling rates of asphaltene aggregates from *n*-heptane diluted WC-B-B2(1) and WC-B-B2 bitumens at 21ºC.

6.3.7 Modeled Settling Rates

As was discussed in Section 6.2, the inputs to the settling model are the density and viscosity of the medium, the primary particle density and diameter, the average aggregate diameter and fractal dimension, the fluid volume fraction, and the Richardson-Zaki hindering equation exponent. All of the inputs have now been specified except for the choice of average diameter and the weighting factor between the compacted and uncompacted fractal dimension (x in Eq. 6.11). In addition, it is not clear if zone settling is better represented with a hindered or unhindered settling rate. To complete the specification of the inputs, the model was first fitted to the settling rate data for each diluted bitumen system at each choice of average diameter both with and without hindered settling. The fitted parameter was the scaling factor for the fractal dimension. The fitted weighting factors and the absolute average deviation (AAD) of the fitted settling rates are provided in Table 6.5.

Figure 6.11 shows that all five definitions of mean diameter can fit the settling data in the n-heptane/WC-B-B2(1) system with similar accuracy. Similar results were found for the other two systems (see Appendix K). However, the fractal dimension is expected to fall between the compacted and uncompacted values; that is, a scaling factor between zero and one. Only the volume mean diameter (d_3) and the Sauter mean diameter (d_{32}) came close to meeting this requirement for all of the systems in Table 6.5. The Sauter mean diameter was the most consistent with the expected range of scaling factors. In addition, it is the ratio of volume to surface area and better represents the ratio of buoyance to drag that governs settling. Therefore, the Sauter mean diameter was selected as the average diameter for all further modeling.

Figure 6.11 also shows that similar results are obtained with and without hindered settling although different weighting factors are required to fit the data in each case. When the hindering correction is neglected, the model deviations are slightly higher for the *n*-pentane diluted systems but are lower for both *n*-heptane diluted mixtures. The model deviations of the hindered model were slightly lower above 80 wt% precipitant (not shown here), indicating that hindering might be present at intermediate and high precipitant contents. Nevertheless, the predictions of the non-hindered model generally fall within the experimental error of the settling rates. It is recommended to use the unhindered settling model because this model is simpler and requires fewer input data.

Table 6.5. Adjusted weighting factors for the fractal dimension using different definitions of aggregate mean diameter in the modified Stokes' settling model.

With Hindering						
	n-pentane/WC-B-A3		*n*-heptane/WC-B-A3		*n*-heptane/WC-B-B2(1)	
Diameter	*x*	AAD, cm/min	*x*	AAD, cm/min	*x*	AAD, cm/min
d_1	0.92	7.39	1.37	0.11	1.86	0.46
d_2	0.72	6.83	0.88	0.12	1.41	0.45
d_3	0.57	6.43	0.69	0.12	1.07	0.44
d_{32}	**0.40**	**6.03**	**0.54**	**0.12**	**0.62**	**0.42**
d_{43}	0.23	5.04	0.40	0.12	0.46	0.40
Without Hindering						
	n-pentane/WC-B-A3		*n*-heptane/WC-B-A3		*n*-heptane/WC-B-B2(1)	
Diameter	*x*	AAD, cm/min	*x*	AAD, cm/min	*x*	AAD, cm/min
d_1	0.65	8.01	1.11	0.11	1.68	0.45
d_2	0.37	7.68	0.45	0.11	1.13	0.44
d_3	0.15	7.50	0.14	0.11	0.74	0.42
d_{32}	**-0.01**	**7.46**	**-0.02**	**0.11**	**0.07**	**0.39**
d_{43}	-0.50	7.00	-0.50	0.11	-0.29	0.38

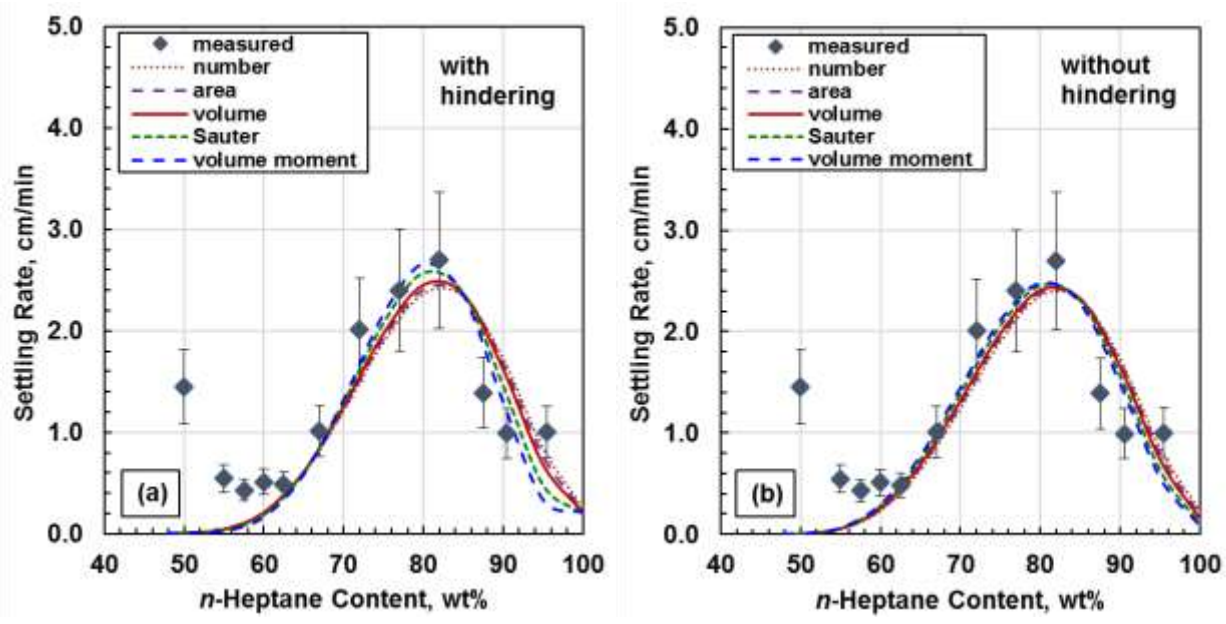

Figure 6.11. Adjusted settling rates with the modified Stokes' model for asphaltene aggregates from *n*-heptane diluted WC-B-B2(1) bitumen mixtures using different definitions of mean diameter. a) model with hindering effect; b) model without hindering. The values obtained for the weighting factor *x* for each curve are provided in Table 6.5.

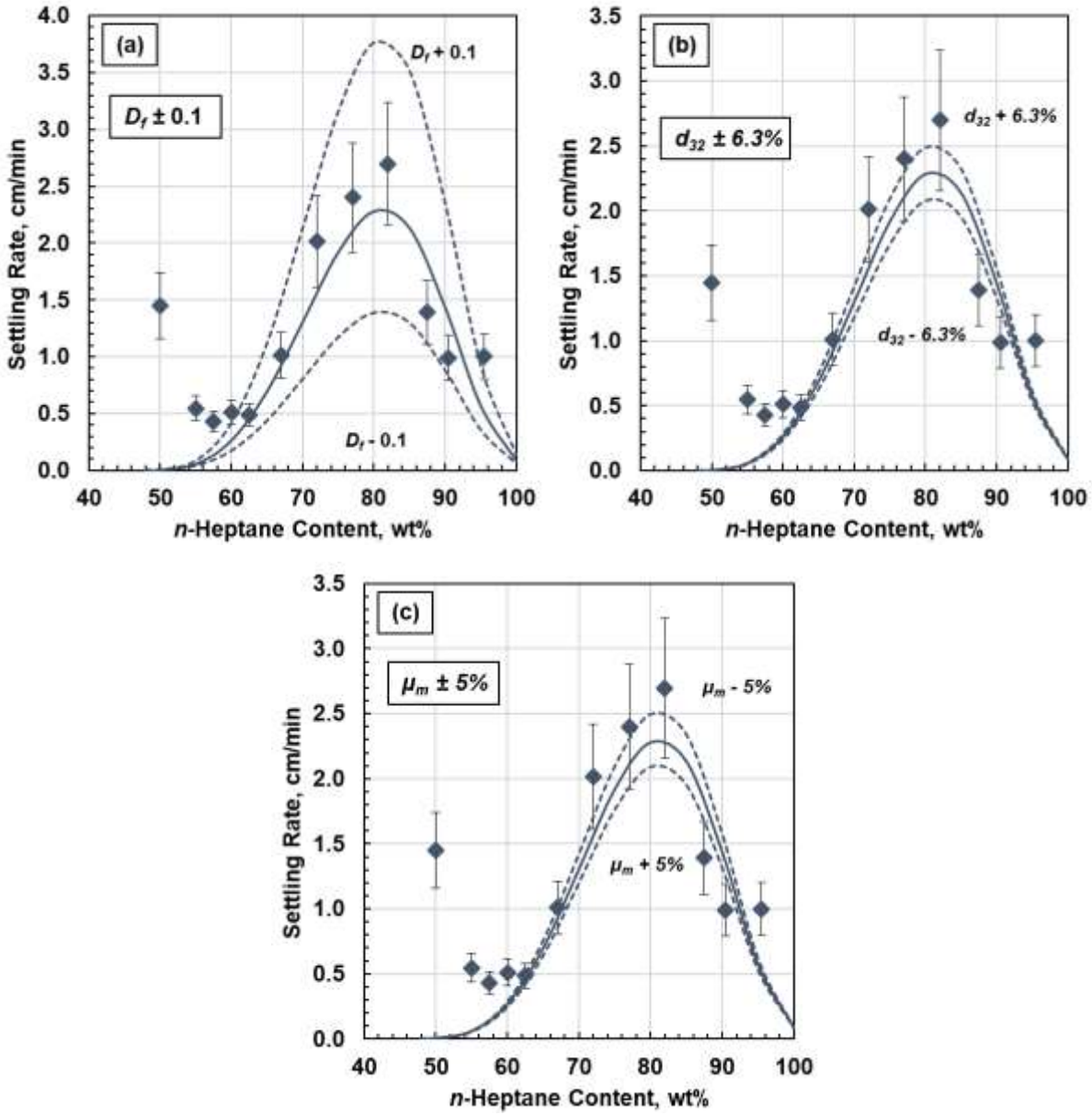

Figure 6.12. Sensitivity analysis for the variables with larger source of error on the modified Stokes' model (non-hindered settling) describing settling rates of asphaltene aggregates. Data shown correspond to the mixture *n*-heptane/WC-B-B2(1) at 21ºC.

Finally, in order to fully specify the model, a single weighting factor of zero was applied in Eq. 6.11 in all cases. In other words, the uncompacted fractal dimension was used with the Sauter mean diameter and no hindering. Figure 6.9 shows the fitted model. The AAD were 8.6, 0.1, and

0.4 cm/min for the *n*-pentane/WC-B-A3, *n*-heptane/WC-B-A3, and *n*-heptane/WC-B-B2(1) systems, respectively. The deviations were all less than 20% of the maximum settling rate.

Figure 6.12 shows the sensitivity of the model to the most impactful input parameters for the *n*-heptane diluted WC-B-B2(1) bitumen. The sensitivities were calculated using the uncertainties of the inputs: ±0.1 for the fractal dimension (half the difference between the compacted and uncompacted fractal dimension), ±6.3% for diameter and ±5% for viscosity. In each case, all other inputs were held constant. When an error equivalent to the uncertainty of diameter or viscosity is introduced, the maximum error in the settling rate was approximately 23%. The model was far more sensitive to the fractal dimension where an error of 0.1 in the fractal dimension caused a 50% error in the settling rate. The model is sensitive to the fractal dimension because at a fractal dimension above 2.5 the porosity changes significantly with a small change in the fractal dimension. For example, for an aggregate with a diameter of 100 μm and a fractal dimension of 2.8 (using d_p = 1 μm), a change of 0.1 in the fractal dimension corresponds to a 19% change in the porosity. Using correlations for the fractal dimension will add to the uncertainty of the fractal dimension and, therefore, it is recommended to use measured fractal dimensions when available. If data are not available, it is recommended to use the fractal dimension correlations and tune the weighting factor to the available settling rate data. If no settling data are available, then a weighting factor of zero is recommended.

6.4 Conclusions

Settling rates of asphaltene aggregates from *n*-pentane and *n*-heptane diluted bitumen mixtures were measured at different precipitant contents all at 21ºC. Zone settling was observed in all cases. Settling rates increased with precipitant content until approximately 75 wt% precipitant and then decreased at higher dilutions. Settling rates in *n*-pentane diluted bitumen were approximately 2 orders of magnitude higher than in the same bitumen diluted with *n*-heptane.

The settling rate was confirmed to depend on a combination of the fluid density and viscosity and the aggregate diameter and fractal dimension. The maximum in the settling rate corresponded to the maximum in aggregate diameter and fractal dimension. These maxima corresponded to the

maximum in the concentration of precipitated asphaltenes. The fractal dimension was correlated to the precipitate concentration and the fluid viscosity. The higher settling rates in *n*-pentane were attributed to all three factors: lower fluid density and viscosity, larger aggregates, and higher fractal dimension.

Settling rates were modeled with Stokes' Law with no hindering and modified to include the fractal dimension of the aggregates. Since zone settling was observed, the Sauter mean diameter was assumed to apply to all of the aggregates. The fractal dimension was calculated from the uncompacted sediment volumes of the settled aggregates. The model matched the measured settling rates with average deviations less than 20% of the maximum settling rate for each system. If the correlation for the fractal dimension is employed and the fluid properties are known, the only measurement required for the model is the Sauter mean diameter of the aggregates. However, the model was most sensitive to the fractal dimension and it is recommended to use experimental fractal dimensions when data are available.

6.5 Chapter References

Akbarzadeh, K.; Alboudwarej, H.; Svrcek, W.Y.; Yarranton, H.W. (2005). A Generalized Regular Solution Model for the Prediction of Asphaltene Precipitation from *n*-Alkane Diluted Heavy Oils and Bitumens. *Fluid Phase Equilib.*, 232, 159-170.

Alberta Energy Regulator (AER). (2019). ST98: Alberta Energy Outlook. *Alberta Energy Regulator*, Calgary, AB.

Angle, C.W.; Long, Y.; Hamza, H.; Lue, L. (2006). Precipitation of Asphaltenes from Solvent-diluted Heavy Oil and Thermodynamic Properties of Solvent-diluted Heavy Oil Solutions. *Fuel*, 85, 492-506.

Bhargava, D.S.; Rajagopal, K. (1990). Modelling in Zone Settling for Different Types of Suspended Materials. *Water Res.*, 24 (6), 675-683.

Bowman, C.W. (1963). *Molecular and Interfacial Properties of Athabasca Tar Sands*. No. 13 in Proceedings of the 7th World Petroleum Congress, Vol. 3, Elsevier Publishing Co., 583-603.

Brons, G.; Yu, J.M. (1995). Solvent Deasphalting Effects on Whole Cold Lake Bitumen. *Energy Fuels,* 9 (4), 641-647.

Calles, J. A.; Dufour, J.; Marugán, J.; Peña, J. L.; Giménez-Aguirre, R.; Merino-García, D. (2008). Properties of Asphaltenes Precipitated with Different *n*-Alkanes. A Study to Assess the Most Representative Species for Modeling. *Energy Fuels*, 2(22), 763-769.

Casas, Y. (2017). Settling Rate of Asphaltenes and Solids from Diluted Bitumen. MSc. Thesis. University of Calgary.

Daneshvar, S. (2005). Asphaltene Flocculation in Diluted Bitumen Systems. MSc. Thesis. University of Calgary.

Feng, R.; Qi, L. (2013). Froth Treatment in Athabasca Oil Sands Bitumen Recovery Process: A Review. *Energy Fuels,* 27 (12), 7199-7207.

Ferworn, K.A.; Svrcek, W.Y.; Mehrotra, A.K. (1993). Measurement of Asphaltene Particle Size Distributions in Crude Oils Diluted with *n*-Heptane. *Ind. Eng. Chem. Res.*, 32, 955-959.

Gray, M.R. (2015). *Upgrading Oilsands Bitumen and Heavy Oil*. First Edition. The University of Alberta Press, Edmonton, AB.

Grimaldos, F. (2018). Measurement of Liquid-Liquid Diffusion in Solvent-Bitumen Systems, M.Sc. Thesis. University of Calgary.

Hoepfner, M.; Vilas-Bôas Fávero C.; Haji-Akbari, N.; Fogler, H.S. (2013). The Fractal Aggregation of Asphaltenes. *Langmuir*, 29, 8799-8808.

Hooshiar, A.; Uhlik, P.; Ivey, D.G.; Liu, Q.; Etsell, T.H. (2012a). Clay Minerals in Nonaqueous Extraction of Bitumen from Alberta Oil Sands: Part 1. Nonaqueous Extraction Procedure. *Fuel Process. Technol.*, 94 (1), 80-85.

Hooshiar, A.; Uhlik, P.; Liu, Q.; Etsell, T.H.; Ivey, D.G. (2012b). Clay Minerals in Nonaqueous Extraction of Bitumen from Alberta Oil Sands: Part 2. Characterization of Clay Minerals. *Fuel Process. Technol.*, 96, 183-194.

Janardhan, A.S.; Mansoori, G.A. (1993). Fractal Nature of Asphaltene Aggregation. *J. Pet. Sci. Eng.*, 9 (1), 17-27.

Khaledi, R.; Boone, T.J.; Motahhari, H.R.; Subramanian, G. (2015). Optimized Solvent for Solvent Assisted-Steam Assisted Gravity Drainage (SA-SAGD) Recovery Process. In *Proceedings of the SPE Canada Heavy Oil Technical Conference*, Calgary, AB.

Kosior, D.; Ngo, E.; Dabros, T. (2016). Determination of the Settling Rate of Aggregates Using the Ultrasound Method During Paraffinic Froth Treatment. *Energy Fuels*, 30 (10), 8192-8199.

Kosior, D.; Ngo, E.; Xu, Y. (2018). Aggregates in Paraffinic Froth Treatment: Settling Properties and Structure. *Energy Fuels,* 32, 8268-8276.

Lin, T.W.; Lohnes, R.A. (1984). Zone Settling Explained as Self Weight Consolidation. *J. Powder Bulk Solids Technol.,* 8(2), 29-36.

Linstrom, P.J.; Mallard, W.G., Eds. (2019). NIST Chemistry WebBook, NIST Standard Reference Database Number 69, National Institute of Standards and Technology, Gaithersburg, MD.

Long, B.; Chodakowski, M.; Shaw, J.M. (2013). Impact of Liquid-Vapor to Liquid-Liquid-Vapor Phase Transitions on Asphaltene-Rich Nanoaggregate Behavior in Athabasca Vacuum Residue + Pentane Mixtures. *Energy Fuels*, 27 (4), 1779-1790.

Long, Y.; Dabros T. (2005). Monitoring the Settling of Water-Solids-Asphaltenes Aggregates Using In-line Probe Coupled with a Near-Infrared Spectrophotometer. *Energy Fuels.* 19 (4), 1542-1547.

Long, Y.; Dabros, T.; Hamza, H. (2002). Stability and Settling Characteristics of Solvent-diluted Bitumen Emulsions. *Fuel*, 81 (15), 1945-1952.

Long, Y.; Dabros, T.; Hamza, H. (2004a). Structure of Water/Solids/Asphaltenes Aggregates and Effect of Mixing Temperature on Settling Rate in Solvent-Diluted Bitumen. *Fuel*, 83 (7-8), 823-832.

Long, Y.; Dabros, T.; Hamza, H. (2004b). Analysis of Solvent-Diluted Bitumen from Oil Sands Froth Treatment Using NIR Spectroscopy. *Can. J. Chem. Eng*., 82 (4), 776-781.

Maqbool, T.; Balgoa, A.T.; Fogler, H.S. (2009). Revisiting Asphaltene Precipitation from Crude Oils: a Case of Neglected Kinetic Effects. *Energy Fuels*, 23, 3681-3686.

Maqbool, T.; Raha, S.; Hoepfner, M.P.; Fogler, H.S. (2011). Modeling the Aggregation of Asphaltene Nanoaggregates in Crude Oil-Precipitant Systems. *Energy Fuels*. 25 (4), 1585-1596.

Marquez, A.A. (2019). Viscosity of Characterized Visbroken Heavy Oils. MSc. Thesis. University of Calgary.

Nassar, N.N.; Betancur, S.; Acevedo, S.; Franco, C.A.; Cortes, F.B. (2015). Development of a Population Balance Model to Describe the Influence of Shear and Nanoparticles on the Aggregation and Fragmentation of Asphaltene Aggregates. *Ind. Eng. Chem. Res.*, 54, 8201-8211.

Nikakhtari, H.; Vagi, L.; Choi, P.; Liu, Q.; Gray, M. R. (2013). Solvent Screening for Non-Aqueous Extraction of Alberta Oil Sands. *Can. J. Chem. Eng.*, 91 (6), 1153–1160.

Nikakhtari, H.; Wolf, S.; Choi, P.; Liu, Q.; Gray, M. (2014). Migration of Fine Solids into Product Bitumen from Solvent Extraction of Alberta Oil Sands. *Energy Fuels*, 28, 2925–2932.

Northup, A.H.; Sloan, H.D. (1996). Advances in Solvent Deasphalting Technology. AM-96-55. NPRA Annual Meeting, San Antonio, TX.

Pal, K.; Nogueira Branco, L. D. P.; Heintz, A.; Choi, P.; Liu, Q.; Seidl, P. R.; Gray, M. R. (2015). Performance of Solvent Mixtures for Non-Aqueous Extraction of Alberta Oil Sands. *Energy Fuels*, 29 (4), 2261–2267.

Rahmani, N.; Dabros, T.; Masliyah, J.H. (2005a). Settling Properties of Asphaltene Aggregates. *Energy Fuels*, 19 (3), 1099-1108.

Rahmani, N.; Dabros, T.; Masliyah, J.H. (2005b). Fractal Structure of Asphaltene Aggregates. *J. Colloid Interface Sci.*, 285 (2), 599-608.

Rahmani, N.; Dabros, T.; Masliyah, J.H. (2005c). Online Optical Monitoring of Asphaltene Aggregation. *Ind. Eng. Chem. Res.*, 44(1), 75-84.

Rahmani, H.; Masliyah, J.H.; Dabros, T. (2003). Characterization of Asphaltene Aggregation and Fragmentation in a Shear Field. *AIChE J.*, 49 (7), 1645-1655.

Ramos-Pallares, F.; Lin, H.; Yarranton, H.W.; Taylor, S.D. (2017). Prediction of the Liquid Viscosity of Characterized Crude Oils by Use of the Generalized Walther Model. *SPE J. (Soc. Pet. Eng.).* 22 (5), 1487-1505.

Rastegari, K.; Svrcek, W.Y.; Yarranton, H.W. (2004). Kinetics of Asphaltene Flocculation. *Ind. Eng. Chem. Res*., 43 (21), 6861-6870.

Richardson, J. F.; Zaki, W. N. (1954). Sedimentation and Fluidisation: Part I. *Trans. Inst. Chem. Eng.*, 32, 35-53.

Romanova, U.G.; Yarranton, H.W.; Schramm, L.L.; Shelfantook, W.E. (2004). Investigation of Oil Sands Froth Treatment. *Can. J. Chem. Eng.*, 82 (4), 710-721.

Saryazdi, F.; Motahhari, H.; Schoeggl, F.F.; Taylor, S.D.; Yarranton, H.W. (2013). Density of Hydrocarbon Mixtures and Bitumen Diluted with Solvents and Dissolved Gases. *Energy Fuels.* 27, 3666-3678.

Seifried, C.M.; Crawshaw, J.; Boek, E.S. (2013). Kinetics of Asphaltene Aggregation in Crude Oil Studied by Confocal Laser-Scanning Microscopy. *Energy Fuels,* 27 (4), 1865-1872.

Shafiee, M. (2014). Kinetics of Asphaltene Precipitation and Flocculation from Diluted Bitumen. MSc. Thesis. University of Calgary.

Sie, C.; Nguyen, B.; Castellanos-Diaz, O.; Verlaan, M.; Nguyen, Q.P. (2019). Viscous Oil Recovery and in-situ Deasphalting in Fractured Reservoirs – Part 2: Effect of Solvent Type and Temperature. *Fuel,* 247 (1), 294-301.

Soleimani-Khormakala, H.; Torkaman, M.; Bahrami, M. (2018). The Effect of Shear Rate on Aggregation and Fragmentation of Asphaltene Aggregates. *J. Dispension Sci. Technol.,* 40 (6), 836-845.

Speight, J.G. (2006). The Chemistry and Technology of Petroleum. Fourth Edition. CRC Press, Boca Raton, FL.

Tiller, F.M. (1981). Revision of Kynch Sedimentation Theory. *AIChE J.*, 27 (4), 823-829.

Tipman, R.N.; Sankey, B.M. (1993). Process for Separation of Hydrocarbon from Tar Sands Froth. United States Patent US 5,236,577.

Torkaman, M.: Bahrami, M.; Dehghani, M. (2017). Influence of Temperature and Stability of Asphaltenes. I. Perikinetic Aggregation. *Energy Fuels,* 31, 11169-11180.

Valinasab, M. (2006). The Effect of Bitumen Extraction Conditions on Froth Treatment Effectiveness. MSc. Thesis, University of Calgary.

Van, A.L.; Bang, D.P.V. (2013). Hindered Settling of Sand/mud Flocs Mixtures: From Model Formulation to Numerical Validation. *Adv. Water Resour.*, 53, 1-11.

Vilas-Bôas Fávero, C.; Maqbool, T.; Hoepfner, M.; Haji-Akbari, N.; Fogler, H.S. (2017). Revisiting the Flocculation Kinetics of Destabilized Asphaltenes. *Adv. Colloid Interface Sci.*, 244, 267-280.

Wang, S.; Liu, Q.; Tan, X.; Xu, C.; Gray, M. R. (2013). Study of Asphaltene Adsorption on Kaolinite by X-ray Photoelectron Spectroscopy and Time-of-Flight Secondary Ion Mass Spectroscopy. *Energy Fuels,* 27 (5), 2465–2473.

Wiehe, I.A. (2008). *Process Chemistry of Petroleum Macromolecules*, CRC Press, Boca Raton, FL.

Yang, Y.; Chaisoontornyotin, W.; Hoepfner, M.P. (2018). Structure of Asphaltenes during Precipitation Investigated by Ultra-Small-Angle X-ray Scattering. *Langmuir*, 34 (35), 10371-10380.

Yarranton, H.W.; Masliyah, J.H. (1996). Molar Mass Distribution and Solubility Modeling of Asphaltenes. *AIChE J.*, 42 (12), 3533-3543.

Yarranton, H.W.; van Dorp, J.J.; Verlaan, M.L.; Lastovka, V. (2013). Wanted Dead or Live: Crude-Cocktail Viscosity – A Pseudocomponent Method to Predict the Viscosity of Dead Oils, Live Oils, and Mixtures. *J. Can. Pet. Technol.*, 52 (3), 176-191.

Zahabi, A.; Gray, M.R.; Czarnecki, J.; Dabros, T. (2010). Flocculation of Silica Particles from a Model Oil Solution: Effect of Adsorbed Asphaltenes. *Energy Fuels.* 24 (6), 3616-3623.

Zawala, J.; Dabros, T.; Hamza, H.A. (2012). Settling Properties of Aggregates in Paraffinic Froth Treatment. *Energy Fuels.* 26, 5775-5781.

Chapter 7: Conclusions and Recommendations

In this thesis, the precipitation, aggregation, and settling of asphaltenes from *n*-alkane diluted bitumen was investigated at ambient conditions. Models to predict asphaltene yields and aggregate diameters (in anaerobic conditions and in air), and settling rates were proposed. The application of the models is discussed below and then the overall contributions, conclusions, and recommendations are summarized.

7.1 Application of Models

The asphaltene precipitation/aggregation and settling models proposed in this thesis are intended for use in operations dealing with asphaltenes precipitated from *n*-pentane or *n*-heptane diluted bitumen mixtures at 21ºC and 1 atm with neglibible water and inorganic solid content (less than 5 wt%). The target operations are any process where the asphaltenes precipitate as glassy particles such as solids removal from the bitumen product of potential non-aqueous extraction processes and partial deasphalting upgrading processs.

Precipitation/Aggregation Model:

The precipitation/aggregation model provides asphaltene yields and aggregate size distributions over time in *n*-pentane or *n*-heptane diluted bitumen in anaerobic conditions or in the presence of air at 21ºC and 1 atm. To determine the size distribution in an anaerobic process, the inputs for the model are the density and viscosity of the medium, the asphaltene density, equilibrium yields, the fractal dimension of the precipitated asphaltene aggregates, the primary particle diameter, and the nucleation and collision efficiency parameters described in Section 4.3.4. Correlations are provided for the fluid properties as a function of temperature and pressure. A value of 1200 kg/m^3 is recommended for the asphaltene density (Yarranton and Masliyah, 1996). The equilibrium yields can be determined from yields measured over time or calculated from an equilibrium model such as regular solution theory. The nucleation and collision efficiency parameters can be obtained from the correlations provided in Section 4.3.6 that are valid for *n*-pentane or *n*-heptane diluted crude oils at 21ºC. A correlation for the primary particle diameter is provided in Section 4.3.6.

The yield is determined as the amount of aggregated asphaltenes that can be separated and detected. If the application is a centriguge, the separation efficiency can be determined from the centrifuge dimensions, rotational speed, and time using Eq. 4.17. If the application is gravity settling, the settling model can be used to predict the sediment accumulation (equivalent to yield). If the application is a filtering process, the separation efficiency can be estimated by defining a threshold aggregate size such that aggregates below that size are not expected to be detected as precipitate at the given residence time. For example, aggregates with diameters < 1 μm are assigned a separation of efficiency of 0 and larger aggregates a separation efficiency of 1.

For asphaltene precipitation/aggregation in air, the model is applied in the same way except that an oxidation rate is included (as shown in Section 5.2.1). The oxidation rate parameter approximately depends on the asphaltene content of the bitumen (Figure 5.9). For Western Canadian bitumens an average value of 3.6×10^{-7} mol/m^3·s can be used if no yield data in oxygen are available (see Table 5.2) to tune the model.

Settling Model:

The settling model provides the average settling rate of precipitated asphaltenes in *n*-pentane or *n*-heptane diluted bitumen at 21ºC and 1 atm. The inputs to the model are the density and viscosity of the diluted bitumen, the asphaltene density, the primary particle diameter, and the aggregate diameter, and fractal dimension. The fluid properties, asphaltene density, and primary particle diameter are determined as described for the precipitation/aggregation model. The average aggregate diameter can be measured or calculated using the precipitation/aggregation model. The fractal dimension can be determined experimentally from the compacted and uncompacted sediment volumes of settled aggregates. If data are not available, correlations are provided for the compacted and uncompacted fractal dimension at 21°C and 1 atm. The model is tuned with a single parameter that scales the fractal dimension between the uncompacted and compacted values.

Industrial applications for solvent-based extraction and partial upgrading of bitumen using solvent deasphalting operate at temperatures higher than 21ºC; for example, commercial paraffinic froth treatment processes operate at 40 to 90°C (Tipman and Sankey, 1993; Feng and Qi, 2013). These

processes may also use solvents other than *n*-pentane or *n*-heptane or mixed solvents. To apply the models at these conditions, almost all of the model parameters must be redetermined. The correlations for fluid properties are available for many solvents at a wide range of temperatures and pressures. In addition, mixing rules are available to determine mixture properties (Ramos-Pallares *et al*., 2017; Saryazdi *et al*., 2013). The asphaltene density can be determined using the following temperature dependence: 0.727 kg/m³/°C between 16 and 90ºC (Ramos-Pallares, 2017). Asphaltene density is insensitive to pressure. Measurements are required to determine most of the other parameters.

For the precipitation/aggregation model, the equilibrium yields, nucleation and collision efficiency parameters, and the primary particle diameter must be redetermined. The equilibrium yields can be determined from yields measurements at the specified conditions or calculated from an equilibrium model such as regular solution theory. Aggregate size distributions can be measured and modeled to determine the nucleation and collision efficiency parameters. Primary particle diameters can be estimated from the maximum size predicted from a diffusion-limited growth model (Eq. 4.25). In this model, the asphaltene density and diffusivity of the medium are a function of temperature.

For the settling model, the aggregate diameter and fractal dimensions must be redetermined. The aggregate diameter can be measured or calculated with the precipitation/aggregation model. The fractal dimensions can be measured as a function of temperature using the sediment volume method. Settling data are recommended to tune the fractal dimension scaling parameter.

Application of the Models at Other Systems:

The physics in both precipitation/aggregation and settling models are applicable to other systems that involve the nucleation and aggregation of particles into aggregates that scale as fractals and settle as a zone. The model inputs would have to be determined experimentally as discussed above for asphaltene precipitation/aggregation and settling at other conditions.

7.2 Contributions

The other main contributions from the thesis are as follows:

- A comprehensive dataset of asphaltene precipitation yields, aggregate size distributions, and settling rates was measured. Data was collected at 21ºC in *n*-pentane or *n*-heptane above the onset the equilibrium onset of precipitation (48 to 95 wt% precipitant). Aggregate sizes were measured in an agitated vessel at Reynolds numbers between 0 and 22,000.
- It was demonstrated that the precipitated aggregates have fused structures that form through a simultaneous nucleation, growth, and flocculation process. Within a few seconds, the aggregates cease to flocculate. If shattered, they will not reform. These observations led to a new model for the kinetics of asphaltene precipitation. They also demonstrate that aggregate sizes are insensitive to shear, an important consideration for process design.
- A population balance model was developed to account for the evolution of asphaltene precipitation yields and aggregate sizes over time. The inputs of the model are the fluid properties, the asphaltene primary particle density and diameter, the fractal dimension of the aggregates, the equilibrium yields, and the nucleation and collision efficiency parameters. The fractal dimension can be obtained experimentally or from a correlation developed in this thesis. The equilibrium yields can be calculated from thermodynamic equilibrium models. The model provides the size distribution of aggregates and asphaltene yields over time (at given centrifugation conditions). Correlations are provided for the remaining model parameters. The model is applicable to Western Canadian bitumen diluted with *n*-pentane or *n*-heptane. The aggregate diameters from the model can be used directly as an input for the settling model. The model is tuned for anaerobic conditions which are typically found during *in situ* extraction and partial upgrading of bitumen.
- It was confirmed that oxygen from air alters the observed kinetics of asphaltene precipitation. Yields and onsets in air increased continuously and equilibrium conditions were not attained within the time of the observations (up to about 1000 h). The population balance model was adapted to account for the increased yields observed in air. An additional generation rate term for the primary particles describes the appearance of new asphaltenes over time formed by reaction of soluble asphaltenes or lower molecules with

oxygen from air. The input parameters are the same as for the model in anaerobic conditions, but the model can be tuned using the oxidation rate to predict yields in air. The effect of air on asphaltene precipitation was negligible at short contact times (<50 h), and therefore is not expected to affect precipitation yields and aggregate sizes in processes with residence times in the order of minutes to few hours.

- A model to predict settling rates of asphaltene aggregates from *n*-alkane diluted bitumens was developed. The inputs for the model were the fluid properties (density and viscosity) and the aggregate size and fractal dimension. Existing correlations were available for the fluid properties. A new correlation was developed for the fractal dimension. The aggregate size can be measured or obtained from the precipitation/aggregation model. The settling model is predictive but can be tuned by adjusting the fractal dimension. This model can be used directly in the design of asphaltene settling processes.

The main conclusions from the thesis and recommendations for future research are presented below.

7.3 Conclusions

Asphaltene Aggregation

Asphaltene aggregates precipitated from *n*-alkane diluted bitumen appeared to form from three simultaneous processes: nucleation, growth, and flocculation. The precipitating asphaltenes were hypothesized to nucleate from the stable nanoaggregates present in the oil (Mostowfi *et al*., 2008; Hoepfner *et al*., 2013) and to grow almost instantaneously to form larger particles in the order of 200 to 1500 nm. These larger particles act as primary units for the subsequent flocculation process. The final aggregates range in size up to several hundred micrometers.

The aggregates did not reach a dynamic equilibrium between flocculation and disintegration but rather had fused structures. It was hypothesized that the adhesive forces between asphaltene surfaces were initially strong enough to fuse the precipitating primary particles but that the adhesive force diminished over time so that the particles and aggregates no longer fused. Without the adhesive forces, collisions did not result in further flocculation and shattered flocs did not reform. The loss of adhesive forces was confirmed with surface force apparatus measurements.

From the onset of precipitation to approximately 75 to 80 wt% *n*-alkane, the average size of the aggregates increased with increased *n*-alkane contents because more precipitated asphaltenes (and therefore more primary particles) were available to participate in the aggregation process. Above 75-80 wt% n-alkane, the concentration of precipitate decreases but the aggregate sizes remain constant. This maximum is contrary the conceptual view of a pure flocculation process, in which the size is primarily driven by the concentration of primary particles (Rahmani *et al*., 2003; Rastegari *et al*., 2004). In a poor solvent environment for asphaltenes, the increase in inter-particle forces (asphaltene-asphaltene) with *n*-alkane content appears to be a significant factor and to dominate the concentration effect at high *n*-alkane contents.

The asphaltene aggregates were fractal structures at all the conditions investigated in this thesis. The fractal dimension provides a relationship between the number of particles in an aggregate and the aggregate diameter and density making it a useful tool to characterize the aggregates (Rahmani *et al*., 2005). The fractal dimension was found to depend on the *n*-alkane content. In other words, the aggregate morphology is a function of the affinity of the asphaltenes with the solvent medium. Near the onset, the asphaltene aggregates had planar or linear structures corresponding to fractal dimensions close to 2. At higher particle concentrations and increasing precipitant content (poorer solvency), the aggregates become more compact and three dimensional with fractal dimensions close to 3. Above approximately 75-80 wt% *n*-alkane, the aggregates became more porous and dendritic and the fractal dimension decreased. The looser aggregates formed at high dilution were more easily shattered when the shear rate was increased than the compact aggregates formed at intermediate *n*-alkane contents. A correlation for the fractal dimension was proposed for input to a proposed precipitation/aggregation model and a proposed settling model.

Shear affected the flocculation of asphaltene aggregates only during their formation. At this early stage (a few seconds at most), increased mixing speed appeared to counteract the nucleation step or to break the aggregates before they could reach larger sizes. After a few seconds, the aggregates were virtually unaffected by shear, except for shattering at high dilutions. The lack of shear sensitivity was the key evidence that the aggregates were fused structures. As a result, shear is

anticipated to have minimum impact in industrial processes dealing with asphaltene aggregates, except at the early stages (in the order of seconds) of aggregation formation.

Asphaltene Precipitation

In anaerobic conditions, yields and onsets of precipitation reached constant values after tens of hours of contact with the precipitant. No precipitate was detected below the equilibrium onset of precipitation for the duration of the experiments (>500 hours). The results are consistent with equilibrium phase behavior with a slow kinetic step before reaching equilibrium. They are also consistent with previous observations of reversible asphaltene precipitation with a hysteresis (Beck *et al*., 2005). The kinetic behavior may be related to the polydispersity of the asphaltenes. At lower precipitant contents and early times, the least soluble fraction comes out of solution within a few seconds. Asphaltenes with slightly higher solubility in the medium must overcome a greater thermodynamic barrier to nucleate and come out of solution gradually over time. Asphaltenes with even greater solubility remain in solution. Eventually, an equilibrium is achieved.

Oxygen from air appears to alter the nucleation step in the precipitation process. Even at ambient temperature, oxygen diffuses through the low viscosity medium and perhaps reacts (or catalyzes reactions) with oil constituents (most likely resins and asphaltenes) that would be otherwise stable in the medium. The reactions create new molecules (or even molecular aggregates) that fall into the category of asphaltenes. In turn, these "new asphaltenes" precipitate over time and contribute to the continuous increase of yields in air and the shifting to lower and lower onsets. Hence, in air, no equilibrium is observed.

The kinetics in air is virtually identical to the kinetics in anaerobic environment for the first 48 h after contact with a precipitant because the effect of air is negligible in this time frame. After 48 h, the yields in air and nitrogen diverge. The negligible air effect at early contact times means that precipitation data collected in air (which is easier to obtain than data in nitrogen) can be used to make predictions of industrial processes occurring in this timespan (less than 48 h). For processes where equilibrium conditions are expected or to tune thermodynamic equilibrium models, long term data must be collected in anaerobic conditions.

A population balance model from literature (Maqbool *et al*., 2011) was adapted to include the nucleation of unstable asphaltenes, the growth nuclei to form primary particles, and the flocculation of these particles to form larger flocs. In addition, the loss of stickiness over time that was observed in the aggregation experiments was accounted for in the model proposed. The inputs of the model are the fluid properties, the asphaltene primary particle density and size, the fractal dimension of the aggregates, the equilibrium yields, and the nucleation and collision efficiency parameters. The model was adjusted to experimental yields and aggregate sizes and correlations were provided to generalize the model for different oils (ranging from light oils to bitumens) and precipitants. Data from literature was used to test the robustness and accuracy of the model in both nitrogen and air atmospheres. The outputs of this combined model can be used directly as an input of the proposed settling model.

Settling of Asphaltene Aggregates

Zone settling was identified as the dominant mechanism for the systems investigated in this thesis. Also, it was confirmed that asphaltenes trap mineral solids and water droplets that can be separated at the same time with the asphaltenes (Long *et al*., 2004; Nikakhtari *et al*., 2014).

A Stokes' law-based model was developed for the zone settling; that is, an average diameter (the Sauter mean diameter) was assumed for all of the aggregates because they all settled at the same rate. The model inputs are the precipitant content, the density and viscosity of the medium, the Sauter mean diameter of the aggregates, and the fractal dimension of the aggregates (used to determine the density of the aggregates). The properties of the fluid medium were correlated using existing methods. The Sauter mean diameter was obtained from experimental values but could also be calculated from the precipitation/aggregation model. The fractal dimension was calculated from a correlation developed in this thesis. The model is predictive but can be tuned by adjusting the fractal dimension. The sensitivity of the model to the uncertainties on the inputs parameters (fractal dimension, medium viscosity and aggregate mean diameter) was tested and the errors were less than 20% in the prediction of settling rates. The proposed model can be used to predict settling rates for asphaltene aggregates from *n*-alkane diluted bitumen systems at room temperature.

7.4 Recommendations for Future Work

It is recommended to:

- expand the aggregate size and settling rate database and retune the aggregation model for higher temperature. Settling processes dealing with asphaltene aggregates (for example PFT or the non-aqueous extraction process) operate at temperatures in the range of 40 to 80ºC (Tipman and Sankey, 1993; Hooshiar *et al*., 2012). Other studies dealing with diluted bitumen froth have found that asphaltenes aggregate size increase with temperature (Torkaman *et al*., 2017; Kosior *et al*., 2018). In some cases, this increment is continuous (Torkaman *et al*., 2017) but in others, the aggregates size reached at maximum and then decrease (Kosior *et al*., 2018; Daneshvar, 2005). If it is assumed that aggregates consisting only of asphaltenes (no mineral solids or water) behave similarly to the systems investigated by those authors, an increase of temperature will favour the formation of larger flocs, reduce the density and viscosity of the medium, and will increase the settling rates. To perform these measurements, a new apparatus such as an autoclave with a sight glass will be required to control precipitant evaporation. Aggregate sizes can be measured with an optical or a light back scattering method with the measurement probe located inside the autoclave. Calibration of the size measurements prior to the settling test is recommended.
- measure the fractal dimension of asphaltene aggregates from *n*-alkane diluted bitumen at different temperatures. The autoclave proposed above could be used for this purpose as long as the sediment volumes could be measured. The effect of temperature during formation and over time in the structure of asphaltene aggregates has not been reported in literature; however, studies on PFT show that aggregates are denser at higher temperatures (Kosior *et al*., 2018; Zawala *et al*., 2012). A higher density indicates that the fractal dimension is higher at higher temperatures. Hence, increasing the temperature would again favor faster settling because more compact aggregates settle faster.
- measure the fractal dimension of asphaltene aggregates from lighter oils. Fractal dimensions were obtained experimentally only for aggregates from diluted bitumen systems. The correlation provided in Chapter 6 for the fractal dimension in terms of the medium viscosity and the concentration of precipitated asphaltenes is applicable for these

systems. However, the predictions of this correlation were not verified experimentally for lighter oils with lower asphaltene contents. The correlation predicts lower fractal dimensions for lighter oils than for diluted bitumens (in the range of 1.8 to 2.2). The consistency of the aggregate masses and the observed aggregates sizes obtained for different oils hints that the fractal dimensions are at least close to the predictions of the correlation, but still experimental validation with the sediment volume method is necessary.

- investigate asphaltene precipitation/aggregation and settling in bitumen diluted with other precipitants such as cycloalkanes. Paraffinic solvents used in industry are a mixture of components with a boiling range that lies between that of *n*-pentane (36.1ºC) and *n*-hexane (68ºC) (Gray, 2015; Lindstrom and Mallard, 2019). *n*-Heptane is selected in lab studies because it has lower volatility and still resembles the properties of the solvents used in industry. Nonetheless, it would better to tune models with mixtures more similar to the ones encountered in industrial applications. In recent years, cyclic alkanes, like cyclopentane or cyclohexane have been evaluated as potential candidates for the non-aqueous extraction process (Nikakhtari *et al*., 2013; Fan *et al*., 2012). These solvents have similar solvent power as *n*-pentane but have lower volatilities (NBP of 46ºC and 81ºC, respectively). A less volatile solvent implies lower solvent losses by evaporation in tailings and is still easily recoverable by distillation.
- investigate the loss of stickiness over time of precipitated asphaltenes. A compositional analysis and characterization (heteroatom content, double bond equivalent, molecular weight, *etc*.) of asphaltenes precipitated at different times and at different precipitant contents would provide insights on the origin of the stickiness of asphaltenes at different conditions and to understand how and why the stickiness is lost over time. Once this effect is better understood, the use of additives or better control of operational variables could help to increase the magnitude and timespan for sticky particles and promote the formation of larger aggregates that settle faster.
- investigate the nucleation of asphaltenes; that is, the growth of particles from nanoaggregates to micrometer scale particles. Typically, SANS or SAXS are used to investigate soluble asphaltenes (in the nanometer scale) (Hoepfner *et al*., 2013; Eyssautier

et al., 2012). These techniques are not capable of capturing the scattering properties of particles larger than 50-100 nm. Optical microscopy, ultrafiltration, or gravimetric methods are used to investigate asphaltene particles/aggregates in the micrometer scale. The gap in the understanding of asphaltenes in the mesoscale (50-500 nm) has not been covered to date. Yang *et al*. (2018) recently proposed the use of ultra-small angle x-ray scattering to investigate asphaltenes in the mesoscale. In future work, validation of the growth mechanism proposed in this thesis can be done with USAXS and similar techniques. Also, an investigation on the aggregation tendency of asphaltenes with different oils and solvents can be carried out focusing the attention in aggregates sizes in the range of 50 to 500 nm.

- investigate the chemistry behind the effect of oxygen on asphaltene precipitation. Perform oxidation experiments under controlled conditions and to use chemical markers to follow reaction paths is recommended. A better understanding of the mechanisms of asphaltene oxidation or oxygen catalyzed polymerization of asphaltenes or maltenes can help to design alternatives to mitigate this issue. On the other hand, opportunities and benefits can be found for oxidized asphaltenes, such as the study performed by Choi *et al.* (2016). In that work, asphaltenes were intentionally oxidized and later used as additives to promote asphaltene aggregation for bitumen extraction and finishing.
- measure the composition of asphaltene aggregates as a function of precipitant content and temperature. It is challenging to measure the composition of a dispersed phase but the sediment could be separated and the maltene and asphaltene contents determined with reasonable accuracy. The maximum settling rates of asphaltene aggregates were found at intermediate precipitant contents (75-80 wt% precipitant) that corresponded to the maximum aggregate diameter and fractal dimension. Studies in asphaltene phase equilibrium have shown that upon addition of precipitant, the heavy phase does not consist solely of asphaltenes and is better described as an asphaltene-rich phase (Johnston *et al*., 2017; Mancilla-Polanco *et al*., 2019). This "pitch" phase contains mainly asphaltenes but also contains a significant amount of maltenes and precipitant. The maximum yield (mass of asphaltene-rich phase divided by the mass of original oil) was obtained at a precipitant content that roughly corresponded to the maximum aggregate diameter, fractal dimension, and settling rate. It is possible that asphaltene aggregates even at ambient conditions

contain significant amounts of maltenes within the structures. Hence, another factor contributing to the higher fractal dimension and density of the aggregates observed in this concentration range may be the composition of asphaltene aggregates.

7.5 Chapter References

Beck, J.; Svrcek, W.Y.; Yarranton, H.W. (2005). Hysteresis in Asphaltene Precipitation and Re-dissolution. *Energy Fuels*, 19 (3), 944-947.

Choi, S.; Pyeon, W.; Kim, J.D.; Nho, N.S. (2016). Simple Functionalization of Asphaltene and its Application for Efficient Asphaltene Removal. *Energy Fuels*, 30 (9), 6991-7000.

Daneshvar, S. (2005). Asphaltene Flocculation in Diluted Bitumen Systems. MSc. Thesis. University of Calgary.

Eyssautier, J.; Frot, D.; Barré, L. (2012). Structure and Dynamics Properties of Colloidal Asphaltene Aggregates. *Langmuir*, 28 (33), 11997-12004.

Fan, M.; Sun, X.; Zhao, S.; Xu, Z. (2012). Solvent Selection for Asphalt Particles Production of Canadian Oil Sands Bitumen. *Acta Petrol. Sin.*, 28 (5), 783-790.

Feng, R.; Qi, L. (2013). Froth Treatment in Athabasca Oil Sands Bitumen Recovery Process: A Review. *Energy Fuels*, 27 (12), 7199-7207.

Gray, M.R. (2015). *Upgrading Oilsands Bitumen and Heavy Oil*. First Edition. The University of Alberta Press, Edmonton, AB.

Hoepfner, M.P.; Vilas-Bôas Fávero, C.; Haji-Akbari, N.; Fogler, H.S. (2013). The Fractal Aggregation of Asphaltenes. *Langmuir*, 29, 8799-8808.

Hooshiar, A.; Uhlik, P.; Ivey, D.G.; Liu, Q.; Etsell, T.H. (2012). Clay Minerals in Nonaqueous Extraction of Bitumen from Alberta Oil Sands: Part 1. Nonaqueous Extraction Procedure. *Fuel Process. Technol.*, 94 (1), 80-85.

Johnston, K.A.; Schoeggl, F.F.; Satyro, M.A.; Taylor, S.D.; Yarranton, H.W. (2017). Phase Behavior of Bitumen and *n*-pentane. *Fluid Phase Equil*. 442, 1-19.

Kosior, D.; Ngo, E.; Xu, Y. (2018). Aggregates in Paraffinic Froth Treatment: Settling Properties and Structure. *Energy Fuels*, 32, 8268-8276.

Linstrom, P.J.; Mallard, W.G., Eds. (2019). NIST Chemistry WebBook, NIST Standard Reference Database Number 69, National Institute of Standards and Technology, Gaithersburg, MD.

Long, Y.; Dabros, T.; Hamza, H. (2004). Structure of Water/Solids/Asphaltenes Aggregates and Effect of Mixing Temperature on Settling Rate in Solvent-Diluted Bitumen. *Fuel*, 83 (7-8), 823-832.

Mancilla-Polanco, A.; Johnston, K.; Richardson, W.D.L.; Schoeggl, F.F.; Zhang, Y.; Yarranton, H.W.; Taylor, S.D. (2019). Phase Behavior of Heavy-Oil/Propane Mixtures. *SPE J.*, 24 (2), 596-617.

Maqbool, T.; Raha, S.; Hoepfner, M.P.; Fogler, H.S. (2011). Modeling the Aggregation of Asphaltene Nanoaggregates in Crude Oil-Precipitant Systems. *Energy Fuels*, 25 (4), 1585-1596.

Mostowfi, F.; Indo, K.; Mullins, O.C.; McFarlane, R. (2008). Asphaltene Nanoaggregates Studied by Centrifugation. *Energy Fuels,* 23, 1194-1200.

Nikakhtari, H.; Vagi, L.; Choi, P.; Liu, Q.; Gray, M. R. (2013). Solvent Screening for Non-Aqueous Extraction of Alberta Oil Sands. *Can. J. Chem. Eng.*, 91 (6), 1153–1160.

Nikakhtari, H.; Wolf, S.; Choi, P.; Liu, Q.; Gray, M. (2014). Migration of Fine Solids into Product Bitumen from Solvent Extraction of Alberta Oil Sands. *Energy Fuels*, 28, 2925–2932.

Rahmani, H.; Masliyah, J.H.; Dabros, T. (2003). Characterization of Asphaltene Aggregation and Fragmentation in a Shear Field. *AIChE J.*, 49 (7), 1645-1655.

Ramos-Pallares, F. (2017). The Viscosity and Thermal Conductivity of Heavy Oils and Solvents. PhD. Dissertation. University of Calgary.

Ramos-Pallares, F.; Lin, H.; Yarranton, H.W.; Taylor, S.D. (2017). Prediction of the Liquid Viscosity of Characterized Crude Oils by Use of the Generalized Walther Model. *SPE J.*, 22 (5), 1487-1505.

Rastegari, K.; Svrcek, W.Y.; Yarranton, H.W. (2004). Kinetics of Asphaltene Flocculation. *Ind. Eng. Chem. Res*., 43, 6861-6870.

Saryazdi, F.; Motahhari, H.; Schoeggl, F.F.; Taylor, S.D.; Yarranton, H.W. (2013). Density of Hydrocarbon Mixtures and Bitumen Diluted with Solvents and Dissolved Gases. *Energy Fuels.* 27, 3666-3678.

Tipman, R.N.; Sankey, B.M. (1993). Process for Separation of Hydrocarbon from Tar Sands Froth. United States Patent US 5,236,577.

Torkaman, M.: Bahrami, M.; Dehghani, M. (2017). Influence of Temperature and Stability of Asphaltenes. I. Perikinetic Aggregation. *Energy Fuels*, 31, 11169-11180.

Yang, Y.; Chaisoontornyotin, W.; Hoepfner, M.P. (2018). Structure of Asphaltenes during Precipitated Investigated by Ultra-Small-Angle-X-ray Scattering. *Langmuir,* 34 (35), 10371-10380.

Yarranton, H.W.; Masliyah, J.H. (1996). Molar Mass Distribution and Solubility Modeling of Asphaltenes. *AIChE J*. 42(12), 3533-3543.

Zawala, J.; Dabros, T.; Hamza, H.A. (2012). Settling Properties of Aggregates in Paraffinic Froth Treatment. *Energy Fuels.* 26, 5775-5781.

References

Agrawal, P., Schoeggl, F.F., Satyro, M.A., Taylor, S.D., Yarranton, H.W. (2012). Measurement and Modeling of the Phase Behavior of Solvent Diluted Bitumens, *Fluid Phase Equilib.*, 334, 51–64.

Agrawala, M.; Yarranton, H.W. (2001). An Asphaltene Association Model Analogous to Linear Polymerization. *Ind. Eng. Chem. Res*., 40 (21), 4664-4672.

Akbarzadeh, K.; Alboudwarej, H.; Svrcek, W.Y.; Yarranton, H.W. (2005). A Generalized Regular Solution Model for Asphaltene Precipitation from *n*-Alkane Diluted Heavy Oils and Bitumens. *Fluid Phase Equil*., 232, 159-170.

Akbarzadeh, K.; Dhillon, A.; Svreck, W.Y.; Yarranton, H.W. (2004). Methodology for the Characterization and Modeling of Asphaltene Precipitation from Heavy Oils Diluted *n*-Alkanes. *Energy Fuels,* 18, 1434-1441.

Alam, M.K. (1987). The Effect of van der Waals and Viscous Forces on Aerosol Coagulation. *Aerosol Sci. Technol.*, 6 (1), 41-52.

Alberta Energy Regulator (AER). (2019). ST98: Alberta Energy Outlook. Alberta Energy Regulator, Calgary, AB.

Alboudwarej, H.; Akbarzadeh, K.; Beck, J.; Svrcek, W.Y.; Yarranton, H.W. (2003). Regular Solution Model for Asphaltene Precipitation from Bitumens and Solvents. *Energy Fuels,* 49 (11), 2948-2956.

Alboudwarej, H.; Beck, J.; Svrcek, W.Y.; Yarranton, H.W. (2002). Sensitivity of Asphaltene Properties to Separation Techniques. *Energy Fuels*, 16(2), 462-469.

Alhammadi, A.A.; Chen, Y.; Yen, A.; Wang, J.; Creek, J.L.; Vargas, F.M.; Chapman, W.G. (2017). Effect of the Gas Composition and Gas/oil Ratio on Asphaltene Deposition. *Energy Fuels,* 31, 3610-3619.

Allen, T. (2003). *Powder Sampling and Particle Size Determination*, Elsevier, Amsterdam, The Netherlands.

Andersen, S.I., Birdi, K.S. (1990). Influence of Temperature and Solvent on the Precipitation of Asphaltenes, *Fuel Sci. Technol. Int.*, 8(6), 593-615.

Andersen, S.I., Lindeloff, N., Stenby, E.H. (1998). Investigation of Asphaltene Precipitation at Elevated Temperature, *Petr. Sci. Technol.*, 16(3-4), 323-334.

Angle, C.W.; Long, Y.; Hamza, H.; Lue, L. (2006). Precipitation of Asphaltenes from Solvent-Diluted Heavy Oil and Thermodynamic Properties of Solvent-Diluted Heavy Oil Solutions. *Fuel*, 85 (4), 492-506.

Arnaud, C.H. (2009). Digging into Asphaltenes. *Chem Eng. News,* 87 (38), 12-17.

Arya, A.; Liang, X.; Von Solms, N.; Kontogeorgis, G.M. (2017). Modeling of Asphaltene Precipitation from Crude Oil with the Cubic Plus Association Equation of State, *Energy Fuels*, 31 (2), 2063-2075.

Bäbler, M.A. (2008). A Collision Efficiency Model for Flow-induced Coagulation of Fractal Aggregates. *AIChE J.,* 54 (7), 1748-1760.

Balakin, B.V.; Hoffmann, A.C.; Kosinski, P. (2010). Population Balance Model for Nucleation, Growth, Aggregation, and Breakage of Hydrate Particles in Turbulent Flow. *AIChE J.* 56 (8), 2052- 2062.

Balakin, B.V.; Hoffmann, A.C.; Kosinski, P. (2012). The Collision Efficiency in a Shear Flow. *Chem Eng. Sci.,* 68, 305-312.

Barrera, D.M.; Ortiz, D.P.; Yarranton, H.W. (2013). Molecular Weight and Density Distributions of Asphaltenes from Crude Oils. *Energy Fuels,* 27 (5), 2474-2487.

Beck, J., Svrcek, W.Y., Yarranton, H.W. (2005). Hysteresis in Asphaltene Precipitation and Re-dissolution, *Energy Fuels*, 19 (3), 944-947.

Betancourt, S.S.; Ventura, G.T.; Pomerantz, A.E.; Viloria, O.; Dubost, F.X.; Zuo, J.; Monson, G.; Bustamante, D.; Purcell, J.M.; Nelson, R.K.; Rodgers, R.P.; Reddy, C.M.; Marshall, A.G.; Mullins, O.C. (2009). Nanoaggregates of Asphaltenes in a Reservoir Crude Oil and Reservoir Connectivity. *Energy Fuels*, 23 (3), 1178-1188.

Bhargava, D.S.; Rajagopal, K. (1990). Modelling in Zone Settling for Different Types of Suspended Materials. *Water Res.,* 24 (6), 675-683.

Bowman, C.W. (1963). *Molecular and Interfacial Properties of Athabasca Tar Sands*. No. 13 in Proceedings of the 7th World Petroleum Congress, Vol. 3, Elsevier Publishing Co., 583-603.

Boxall, J.A.; Koh, C.A.; Sloan, E.D.; Sum, A.K.; Wu, D.T. (2010). Measurement and Calibration of Droplet Size Distributions in Water-in-Oil Emulsions by Particle Video Microscope and a Focused Beam Reflectance Method. *Ind. Chem. Res.,* 49 (3), 1412-1418.

Broeke, J.; Mateos-Perez, J.M.; Pascau, J. (2015). *Image Processing with ImageJ*. Packt Publishing, Birmingham, UK.

Brons, G.; Yu, J.M. (1995). Solvent Deasphalting Effects on Whole Cold Lake Bitumen. *Energy Fuels,* 9 (4), 641-647.

Buckley, J.S. (1999). Predicting the Onset of Asphaltene Precipitation from Refractive Index Measurements. *Energy Fuels*,13 (2), 328-332.

Buenrostro-Gonzalez, E.; Lira-Galeana, C.; Gil-Villegas, A.; Wu, J. (2004). Asphaltene Precipitation in Crude Oils: Theory and Experiments. *AIChE J*., 50, 2552-2570.

Calles, J. A.; Dufour, J.; Marugán, J.; Peña, J. L.; Giménez-Aguirre, R.; Merino-García, D. (2008). Properties of Asphaltenes Precipitated with Different *n*-Alkanes. A Study to Assess the Most Representative Species for Modeling. *Energy Fuels*, 2 (22), 763-769.

Carnahan, N.F. (2000). Precipitation of Asphaltenes in Heavy Oil and Tar Sands, in *Asphaltenes and Asphalts*, 2, Volume 40B, First Edition. T.F. Yen, G.V. Chilingarian, Elsevier, Amsterdam, The Netherlands.

Casas, Y. (2017). Settling Rate of Asphaltenes and Solids from Diluted Bitumen. MSc. Thesis. University of Calgary.

Castellanos-Diaz, O.; Sánchez, M.C.; Schoeggl, F.F.; Satyro, M.A.; Taylor, S.D.; Yarranton, H.W. (2014). Deep Vacuum Fractionation of Heavy Oil and Bitumen: Part 1. Apparatus and Standardized Procedure. *Energy Fuels*, 28 (5), 2857-2865.

Chacon-Patiño, M.L.; Rowland, S.M.; Rodgers, R.P. (2017). Advances in Asphaltene Petroleomics. Part 1: Asphaltenes are Composed of Abundant Island and Archipelago Structural Motifs. *Energy Fuels,* 31 (12), 13509-13518.

Chacon-Patiño, M.L; Rowland, S.M.; Rodgers, R.P. (2018). Advances in Asphaltene Petroleomics. Part 3. Dominance of Island or Archipelago Structural Motif is Sample Dependent. *Energy Fuels*, 32 (9), 9106-9120.

Chaisoontornyotin, W.; Bingham, A.W.; Hoepfner, M.P. (2017). Reversibility of Asphaltene Precipitation Using Temperature-Induced Aggregation. *Energy Fuels*, 31, 3392-3398.

Chaisoontornyotin, W.; Zhang, J.; Ng, S.; Hoepfner, M.P. (2018). Rapid Heterogeneous Asphaltene Precipitation with Dispersed Solids. *Energy Fuels,* 32, 7458-7466.

Choi, S.; Pyeon, W.; Kim, J.D.; Nho, N.S. (2016). Simple Functionalization of Asphaltene and its Application for Efficient Asphaltene Removal. *Energy Fuels,* 30 (9), 6991-7000.

Chu, B. (1967). *Molecular Forces: Based on the Baker Lectures of Peter J. W. Debye*. Interscience Publishers, New York, NY.

Clain, P.; Ndoye, F.T.; Delahaye, A.; Fournaison, L.; Lin, W.; Dalmazzone, D. (2015). Particle Size Distribution of TBPB Hydrates by Focused Beam Reflectance Measurement (FBRM) for Secondary Refrigeration Application. *Int. J. Refrig*., 50, 19-31.

Daneshvar, S. (2005). Asphaltene Flocculation in Diluted Bitumen Systems. MSc. Thesis. University of Calgary.

Dickie, J.P.; Yen, T.F. (1967). Macrostructures of Asphaltic Fractions by Various Instrumental Methods. *Anal. Chem.,* 39, 1847-1852.

Elimelech, M.; Gregory, J.; Jia, X.; Williams, R.A. (1995). *Particle Deposition and Aggregation: Measurement, Modeling and Simulation*. Butterworth-Heinemann Ltd., Oxford, UK.

Ellaban, O.; Abu-Rub, H.; Blaabjerg, F. (2014). Renewable Energy Resources: Current Status, Future Prospects and their Enabling Technology. *Renew. Sust. Energ. Rev.,* 39, 748-764.

Eyssautier, J.; Frot, D.; Barré, L. (2012). Structure and Dynamics Properties of Colloidal Asphaltene Aggregates. *Langmuir*, 28 (33), 11997-12004.

Eyssautier, J.; Levitz, P.; Espinat, D.; Jestin, J.; Gummbel, J.; Grillo, I.; Barré, L. (2011). Insight into Asphaltene Nanoaggregate Structure Inferred by Small Angle Neutron and X-ray Scattering. *J. Phys. Chem. B.*, 115 (21), 6827-6837.

Family, F.; Meakin, P.; Deutch, J.M. (1989). Kinetics of Coagulation with Fragmentation: Scaling Behavior and Fluctuations. *Phys. Rev. Lett.,* 57 (6), 727-730.

Fan, M.; Sun, X.; Zhao, S.; Xu, Z. (2012). Solvent Selection for Asphalt Particles Production of Canadian Oil Sands Bitumen. *Acta Petrol. Sin.,* 28 (5), 783-790.

Fan, T.; Buckley, J.S. (2002). Rapid and Accurate SARA Analysis of Medium Gravity Crude Oils. *Energy Fuels,* 16, 1571-1575.

Feke, D.L.; Schowalter, W.R. (1983). The Effect of Brownian Diffusion on Shear-induced Coagulation of Colloidal Suspensions. *J. Fluid Mech.*, 133, 17-35.

Feng, R.; Qi, L. (2013). Froth Treatment in Athabasca Oil Sands Bitumen Recovery Process: A Review. *Energy Fuels,* 27 (12), 7199-7207.

Ferworn, K.A.; Svrcek, W.Y.; Mehrotra, A.K. (1993). Measurement of Asphaltene Particle Size Distributions in Crude Oils Diluted with *n*-Heptane. *Ind. Eng. Chem. Res*., 32, 955-959.

Fotland, P.; Askvik, K.M. (2008). Determination of Hamaker Constants for Asphaltenes in a Mixture of Pentane and Benzene. *Colloids Surf., A.*, 324 (1-3), 22-27.

Friedlander, S.K. (2000). *Smoke, Dust, and Haze: Fundamentals of Aerosol Dynamics*, Second Edition, Oxford University Press, New York, NY.

Gray, M.R. (1994). *Upgrading Petroleum Residues and Heavy Oils*. Marcel Dekker, Inc., New York, NY.

Gray, M.R. (2015). *Upgrading Oilsands Bitumen and Heavy Oil*, First Edition. The University of Alberta Press, Edmonton, AB.

Gray, M.R.; Tykwinski, R.R.; Stryker, J.M.; Tan, X. (2011). Supramolecular Assembly Model for Aggregation of Petroleum Asphaltenes. *Energy Fuels*, 25 (7), 3125-3134.

Greaves, D.; Boxall, J.; Mulligan, J.; Montesi, A.; Creek, J.; Sloan, D.E.; Koh, C.A. (2008). Measuring the Particle Size of a Known Distribution Using the Focused Beam Reflectance Measurement Technique. *Chem. Eng. Sci*., 63(22), 5410-5419.

Grimaldos, F. (2018). Measurement of Liquid-Liquid Diffusion in Solvent-Bitumen Systems, *M.Sc*. Thesis. University of Calgary.

Haji-Akbari, N.; Masirisuk, P.; Hoepfner, M.P.; Fogler, H.S. (2013). A Unified Model for Aggregation of Asphaltenes. *Energy Fuels*, 27 (5), 2497-2505.

Haji-Akbari, N.; Teeraphapkul, P.; Balgoa, A.T.; Fogler, H.S. (2015). Effect of *n*-Alkane Precipitants on Aggregation Kinetics of Asphaltenes. *Energy Fuels.* 29 (4), 2190-2196.

Haji-Akbari, N.; Teeraphapkul, P.; Fogler, H.S. (2014). Effect of Asphaltene Concentration on the Aggregation and Precipitation Tendency of Asphaltenes. *Energy Fuels*, 28(2), 909-919.

Hamaker, H.C. (1937). The London-van der Waals Attraction Between Spherical Particles. *Physica IV*, 10, 1058-1072.

Hammami, A.; Phelps, C.H.; Monger-McClure, T.; Little, T.M. (2000). Asphaltene Precipitation from Live Oils: An Experimental Investigation of Onset Conditions and Reversibility. *Energy Fuels*, 14(1), 14-18.

Headen, T.F.; Boek, E.S.; Stellbrink, J.; Scheven, U.M. (2009). Small Angle Neutron Scattering (SANS and V-SANS) Study of Asphaltene Aggregates in Crude Oil. *Langmuir*, 5, 422-428.

Herrington, P.R. (2001). The Role of Hydroaromatic Species in the Oxidation of Petroleum Bitumens. *Energy Fuels*, 15 (2), 444-448.

Herrington, P.R.; Wu, Y. (1999). Effect of Inter-Molecular Association on Bitumen Oxidation. *Pet. Sci. Technol.*, 17 (3), 291-318.

Hewett, T.A. (1994). Fractal Methods for Fracture Characterization. In *Stochastic Modeling and Geostatistics.* Yarus, J.M. and Chambers R.L. (Eds.), AAPG Publications, Tulsa, OK.

Hirschberg, A.; deJong, N.J.; Schipper, B.A.; Meijer, J.G. (1984). Influence of Temperature and Pressure on Asphaltene Flocculation. *SPE J.* (24), 283-291.

Hoepfner, M.P.; Fogler, H.S. (2013). Multiscale Scattering Investigations of Asphaltene Cluster Breakup, Nanoaggregate Dissociation, and Molecular Ordering. *Langmuir*, 29 (49), 15423-15432.

Hoepfner, M.; Vilas-Bôas Fávero C.; Haji-Akbari, N.; Fogler, H.S. (2013) The Fractal Aggregation of Asphaltenes. *Langmuir*, 29, 8799-8808.

Hooshiar, A.; Uhlik, P.; Ivey, D.G.; Liu, Q.; Etsell, T.H. (2012). Clay Minerals in Nonaqueous Extraction of Bitumen from Alberta Oil Sands: Part 1. Nonaqueous Extraction Procedure. *Fuel Process. Technol.*, 94 (1), 80-85.

Hu, Y.-F.; Guo, T.-M. (2005). Effect of Temperature and Molecular Weight of *n*-Alkane Precipitants on Asphaltene Precipitation. *Fluid Phase Equilib.*, 192, 13-25.

Huang, J.; Liu, X.; Qiu, X.; Xie, L.; Yan, B.; Wang, X.; Huang, Q.; Zeng, H. (2017). Octadecyltrichlorosilane Deposition on Mica Surfaces: Insights into the Interface Interaction Mechanism. *J. Phys. Chem. B*, 121 (14), 3151-3161.

Hurtado, J.L.A.; Chodakowski, M.; Long, B.; Shaw, J.M. (2011). Characterization of Physically and Chemically Separated Athabasca Asphaltenes Using Small-Angle X-ray Scattering. *Energy Fuels*, 25 (11), 5100-5112.

Hwang, D.S.; Harrington, M.J.; Lu, Q.; Masic, A.; Zeng, H.; Waite, J.H. (2012). Mussel Foot Protein-1 (mcfp-1) Interaction with Titania Surfaces. *J. Materials Chem.*, 22 (31), 15530-15533.

Islam, M.A. (2004). Einstein-Smoluchowski Diffusion Equation: A Discussion. *Phys. Scr.*, 70, 120-125.

Israelachvili, J. N. (2011). *Intermolecular and Surface Forces*. Academic Press, Amsterdam, The Netherlands.

Israelachvili, J.; Min, Y.; Akbulut, M.; Alig, A.; Carver, G.; Greene, W.; Kristaiansen, K.; Meyer, E.; Pesika, N.; Rosenberg, K.; Zeng, H. (2010). Recent Advances in the Surface Forces Apparatus (SFA) Technique. *Rep. Prog. Phys*., 73 (3), 036601.

Janardhan, A.S.; Mansoori, G.A. (1993). Fractal Nature of Asphaltene Aggregation. *J. Pet. Sci. Eng.*, 9 (1), 17-27.

Jeldres, R.I.; Fawell, P.D.; Florio, B.J. (2018). Population Balance Modeling to Describe the Particle Aggregation Process: A Review. *Powder Technol.*, 326, 190-207.

Johnston, K.A.; Schoeggl, F.F.; Satyro, M.A.; Taylor, S.D.; Yarranton, H.W. (2017). Phase Behavior of Bitumen and *n*-pentane. *Fluid Phase Equil*. 442, 1-19.

Kelland, M.A. (2014). *Production Chemicals for the Oils and Gas Industry*. Second Edition. CRC Press, Boca Raton, FL.

Kempkes, M.; Eggers, J.; Mazzotti, M. (2008). Measurement of Particle Size and Shape by FBRM and in situ Microscopy. *Chem. Eng. Sci*., 63 (19), 4656-4675.

Khaledi, R.; Boone, T.J.; Motahhari, H.R.; Subramanian, G. (2015). Optimized Solvent for Solvent Assisted-Steam Assisted Gravity Drainage (SA-SAGD) Recovery Process. In *Proceedings of the SPE Canada Heavy Oil Technical Conference*, Calgary, AB.

Khayan, M. (1982). Proposed Classification and Definitions of Heavy Crude Oils and Tar Sands. In *The Future of Heavy Crude and Tar Sands*. R.F. Meyer, J.C. Wynn, and J.C. Olson (Eds.) UNITAR, New York, NY.

Khoshandam, A.; Alamdari, A. (2010). Kinetics of Asphaltene Precipitation in a Heptane-Toluene Mixture. *Energy Fuels,* 24 (3), 1917-1924.

Kosior, D.; Ngo, E.; Dabros, T. (2016). Determination of the Settling Rate of Aggregates Using the Ultrasound Method During Paraffinic Froth Treatment. *Energy Fuels*, 30 (10), 8192-8199.

Kosior, D.; Ngo, E.; Xu, Y. (2018). Aggregates in Paraffinic Froth Treatment: Settling Properties and Structure. *Energy Fuels,* 32, 8268-8276.

Kusters, K.A.; Wijers, J.G.; Thoenes, D. (1997). Aggregation Kinetics of Small Particles in Agitated Vessels. *Chem. Eng. Sci.*, 52 (1), 107-121.

Lasentec. (2002). *FBRM Control Interface Version 6.0 User Manual*. Lasentec Inc.

Leite, E.R.; Ribeiro, C. (2012). *Crystallization and Growth of Colloidal Nanocrystals*, Springer, Amsterdam, The Netherlands.

Lin, T.W.; Lohnes, R.A. (1984). Zone Settling Explained as Self Weight Consolidation. *J. Powder Bulk Solids Technol.,* 8(2), 29-36.

Linstrom, P.J.; Mallard, W.G., Eds. (2019). NIST Chemistry WebBook, NIST Standard Reference Database Number 69, National Institute of Standards and Technology, Gaithersburg, MD.

Liu, J.; Xu, Z.; Masliyah, J. (2004). Role of Fine Clays in Bitumen Extraction from Oil Sands. *AIChE J.,* 50 (8), 1917-1927.

Long, B.; Chodakowski, M.; Shaw, J.M. (2013). Impact of Liquid-Vapor to Liquid-Liquid-Vapor Phase Transitions on Asphaltene-Rich Nanoaggregate Behavior in Athabasca Vacuum Residue + Pentane Mixtures. *Energy Fuels*, 27, 1779-1790.

Long, Y.; Dabros T. (2005). Monitoring the Settling of Water-Solids-Asphaltenes Aggregates Using In-line Probe Coupled with a Near-Infrared Spectrophotometer. *Energy Fuels*. 19 (4), 1542-1547.

Long, Y.; Dabros, T.; Hamza, H. (2002). Stability and Settling Characteristics of Solvent-diluted Bitumen Emulsions. *Fuel*, 81 (15), 1945-1952.

Long, Y.; Dabros, T.; Hamza, H. (2004). Analysis of Solvent-Diluted Bitumen from Oil Sands Froth Treatment Using NIR Spectroscopy. *Can. J. Chem. Eng*., 82 (4), 776-781.

Long, Y.; Dabros, T.; Hamza, H. (2004). Structure of Water/Solids/Asphaltenes Aggregates and Effect of Mixing Temperature on Settling Rate in Solvent-Diluted Bitumen. *Fuel*, 83 (7-8), 823-832.

Long, Y.; Dabros, T.; Hamza, H. (2004). Analysis of Solvent-Diluted Bitumen from Oil Sands Froth Treatment Using NIR Spectroscopy. *Can. J. Chem. Eng*., 82 (4), 776-781.

Mancilla-Polanco, A.; Johnston, K.; Richardson, W.D.L.; Schoeggl, F.F.; Zhang, Y.; Yarranton, H.W.; Taylor, S.D. (2019). Phase Behavior of Heavy-Oil/Propane Mixtures. *SPE J*., 24 (2), 596-617.

Mandelbrot, B. (1982). *The Fractal Geometry of Nature*. W.H. Freeman and Co., New York, NY.

Maqbool, T.; Balgoa, A.T.; Fogler, H.S. (2009). Revisiting Asphaltene Precipitation from Crude oils: A Case of Neglected Kinetic Effects. *Energy Fuels*, 23, 3681-3686.

Maqbool, T.; Raha, S.; Hoepfner, M.P.; Fogler, H.S. (2011). Modeling the Aggregation of Asphaltene Nanoaggregates in Crude Oil-precipitant Systems. *Energy Fuels*. 25(4), 1585-1596.

Maqbool, T.; Srikiratiwong, P.; Fogler, H.S. (2011). Effect of Temperature on the Precipitation Kinetics of Asphaltenes. *Energy Fuels*, 25 (2), 694-700.

Markov, I.V. (2003). *Crystal Growth for Beginners: Fundamentals of Nucleation, Growth and Epitaxy*. World Scientific Publishing Co., Hackensack, NJ.

Marquez, A.A. (2019). Viscosity of Characterized Visbroken Heavy Oils. MSc. Thesis. University of Calgary.

Masliyah, J.H.; Czarnecki, J.; Xu, Z. (2011). *Handbook of Theory and Practice of Bitumen Recovery from Athabasca Oil Sands. Volume 1: Theoretical Basis.* First Edition. Kingsley Publishing Services, Edmonton, AB.

McKenna, A.M.; Chacon-Patiño, M.L.; Weisbrod, C.R.; Blakney, G.T.; Rodgers, R.P. (2019). Molecular-Level Characterization of Asphaltenes Isolated from Distillation Cuts. *Energy Fuels*, 33 (3), 2018-2029.

McKenna, A.M.; Donald, L.J.; Fitzsimmons, J.E.; Juyal, P.; Spicer, V.; Standing, K.G.; Marshall, A.G.; Rodgers, R.P. (2013). Heavy Petroleum Composition. 3. Asphaltene Aggregation. *Energy Fuels*, 27 (3), 1246-1256.

McKenna, A.M.; Marshall, A.G.; Rodgers, R.P. (2013). Heavy Petroleum Composition. 4. Asphaltene Compositional Space. *Energy Fuels*, 27 (3), 1257-1267.

Meyers, R.A. (2004). *Handbook of Petroleum Refining Processes.* Third Edition. McGraw Hill, New York, NY.

Moir, M.E. (2018). Asphaltenes, What Art Thou?: Asphaltenes and the Boduszynski Continuum. *ACS Symp. Ser. Am. Chem. Soc.*, 1282, 3-24.

Moschopedis, S.E., Speight, J.G. (1977). The Effect of Air Blowing on the Properties and Constitution of a Natural Bitumen. *J. Mater. Sci*., 12, 990-998.

Mostowfi, F.; Indo, K.; Mullins, O.C.; McFarlane, R. (2009). Asphaltene Nanoaggregates Studied by Centrifugation. *Energy Fuels*, 23, 1194-1200.

Motahhari, H.; Schoeggl, F.F.; Satyro, M.A.; Yarranton, H.W. (2013). Viscosity Prediction for Solvent-Diluted Live Bitumen and Heavy Oil at Temperatures up to 175ºC. *J. Can. Petr. Technol.,* 52 (5), 376-390.

Mousavi-Dehghani, S.; Riazi, M.; Vafaie-Sefti, M.; Mansoori, G. (2004). An Analysis of Methods for Determination of Onsets of Asphaltene Phase Separations. *J. Pet. Sci. Eng*., 42, 145-156.

Mullins, O.C.; Martinez-Haya, B.; Marshall, A.G. (2008). Contrasting Perspective on Asphaltene Molecular Weight. This Comment vs the Overview of A.A. Herod, K.D. Bartle, and R. Kandiyoti. *Energy Fuels,* 22 (3), 1765-1773.

Mullins, O.C.; Sabbah, H.; Eyssautier, J.; Pomerantz, A.E.; Barre, L.; Andrews, A.B.; Ruiz-Morales, Y.; Mostowfi, F.; McFarlane, R.; Goual, L.; Lepkowicz, R.; Cooper, T.; Orbulescu, J.; Leblanc, R.M.; Edwards, J.; Zare, R.N. (2012). Advances in Asphaltene Science and the Yen-Mullins Model. *Energy Fuels,* 26 (7), 3986-4003.

Mullins, O.C.; Sheu, E.Y.; Hammami, A., Marshall, A. (Eds.). (2007). *Asphaltenes, Heavy Oils, and Petroleomics*. Springer, New York, NY.

Mushrush, G.W.; Speight, J.G. (1995). Instability and Incompatibility of Petroleum Products. First Edition, in *Petroleum Chemistry and Refining*, First Edition. Taylor & Francis, Washington D.C.

Nassar, N.N.; Betancur, S.; Acevedo, S.; Franco, C.A.; Cortes, F.B. (2015). Development of a Population Balance Model to Describe the Influence of Shear and Nanoparticles on the Aggregation and Fragmentation of Asphaltene Aggregates. *Ind. Eng. Chem. Res.,* 54, 8201-8211.

Natarajan, A.; Kuznicki, N.; Harbottle, D.; Masliyah, J.; Zeng, H.; Xu, Z (2014). Understanding Mechanics of Asphaltene Adsorption from Organic Solvent on Mica. *Langmuir,* 30 (31), 9370-9377.

Natural Resources Canada (NRC). (July 2018). Energy Fact Book 2018-2019. Available from: https://www.nrcan.gc.ca/energy-facts/20061.

Nguyen, T.K.; Maclean, N.; Mahiddine, S. (2014). Mechanisms of Nucleation and Growth of Nanoparticles in Solution. *Chem. Rev.,* 114 (15), 7610-7630.

Nikakhtari, H.; Vagi, L.; Choi, P.; Liu, Q.; Gray, M. R. (2013). Solvent Screening for Non-Aqueous Extraction of Alberta Oil Sands. *Can. J. Chem. Eng*., 91 (6), 1153–1160.

Nikakhtari, H.; Wolf, S.; Choi, P.; Liu, Q.; Gray, M. (2014). Migration of Fine Solids into Product Bitumen from Solvent Extraction of Alberta Oil Sands. *Energy Fuels*, 28, 2925–2932.

Norwood, K.W.; Metzner, A.B. (1960). Flow Patterns and Mixing Rates in Agitated Vessels. *AIChE J.*, 6 (3), 432-437.

Northup, A.H.; Sloan, H.D. (1996). Advances in Solvent Deasphalting Technology. AM-96-55. NPRA Annual Meeting, San Antonio, TX.

Organization of the Petroleum Exporting Countries (OPEC). (September 2018). 2018 World Oil Outlook 2040. Available from: http://woo.opec.org.

Pal, K.; Nogueira Branco, L. D. P.; Heintz, A.; Choi, P.; Liu, Q.; Seidl, P. R.; Gray, M. R. (2015). Performance of Solvent Mixtures for Non-Aqueous Extraction of Alberta Oil Sands. *Energy Fuels*, 29 (4), 2261–2267.

Panuganti, S.R.; Vargas, F.M.; Gonzalez, D.L.; Kurup, A.S.; Chapman, W.G. (2012). PC-SAFT Characterization of Crude Oils and Modeling of Asphaltene Phase Behavior. *Fuel,* 93, 658-669.

Park, S.J.; Mansoori, G.A. (1988). Aggregation and Deposition of Heavy Organics in Petroleum Crudes, *Energy Sources*, 10 (2), 109-125.

Peramanu, S.; Singh, C.; Agrawala, M.; Yarranton, H.W. (2001). Investigation of the Reversibility of Asphaltene Precipitation. *Energy Fuels*, 15 (4), 910-917.

Punnapala, S.; Vargas, F.M. (2013). Revisiting the PC-SAFT Characterization Procedure for an Improved Asphaltene Precipitation Prediction. *Fuel*, 108, 417-429.

Rahimi, H.; Nazar, A.R.S. (2010). Asphaltene Aggregates Fractal Restructuring Model, A Population Balance Approach. *Energy Fuels*, 24, 1088-1093.

Rahmani, H.; Masliyah, J.H.; Dabros, T. (2003). Characterization of Asphaltene Aggregation and Fragmentation in a Shear Field. *AIChE J.*, 49 (7), 1645-1655.

Rahmani, N.; Dabros, T.; Masliyah, J.H. (2005). Fractal Structure of Asphaltene Aggregates. *J. Colloid Interface Sci*., 285 (2), 599-608.

Rahmani, N.; Dabros, T.; Masliyah, J.H. (2005). Online Optical Monitoring of Asphaltene Aggregation. *Ind. Eng. Chem. Res*., 44(1), 2005, 75-84.

Rahmani, N.; Dabros, T.; Masliyah, J.H. (2005). Settling Properties of Asphaltene Aggregates. *Energy Fuels*, 19 (3), 1099-1108.

Ramos-Pallares, F. (2017). The Viscosity and Thermal Conductivity of Heavy Oils and Solvents. PhD. Dissertation. University of Calgary.

Ramos-Pallares, F.; Lin, H.; Yarranton, H.W.; Taylor, S.D. (2017). Prediction of the Liquid Viscosity of Characterized Crude Oils by Use of the Generalized Walther Model. *SPE J*., 22 (5), 1487-1505.

Ramos-Pallares, F.; Schoeggl, F.F.; Taylor, S.D.; Satyro, M.A. Yarranton, H. W. (2016). Predicting the Viscosity of Hydrocarbon Mixtures and Diluted Heavy Oils Using the Expanded Fluid Model. Energy Fuels, 30(5), 3575-3595.

Rassandama, H.; Sahimi, M. (1996). Asphalt Flocculation and Deposition: II. Formation and Growth of Fractal Aggregates, *AIChE J*., 42 (12), 3319-3332.

Rastegari, K.; Svrcek, W.Y.; Yarranton, H.W. (2004). Kinetics of Asphaltene Flocculation. *Ind. Eng. Chem. Res*., 43, 6861-6870.

Read, J.; Whiteoak, D. (2003). Shell Bitumen Handbook. 5th edition. In *4.5. Bitumen Quality*. ICE Publishing, London, UK.

Riazi, M.R. (2005). *Characterization and Properties of Petroleum Fractions*. First Edition. ASTM International, Baltimore, MD.

Richardson, J. F.; Zaki, W. N. (1954). Sedimentation and Fluidisation: Part I. *Trans. Inst. Chem. Eng.*, 32, 35-53.

Rodgers, R.P.; McKenna, A.M. (2011). Petroleum Analysis. *Anal. Chem*., 83, 4665-4687.

Romanova, U.G.; Valinasab, M.; Stasiuk, E.N.; Yarranton, H.W. (2006). The Effect of Oil Sands Bitumen Extraction Conditions on Froth Treatment Performance. *J. Can. Pet. Technol*., 45 (9), 36-45.

Romanova, U.G.; Yarranton, H.W.; Schramm, L.L.; Shelfantook, W.E. (2004). Investigation of Oil Sands Froth Treatment. *Can. J. Chem. Eng.*, 82 (4), 710-721.

Safaie, K.; Nazar, A.R.S. (2013). Monte Carlo Modeling of Asphaltene Aggregation Coupled with Sedimentation. *J. Dispersion Sci. Technol*., 34, 1173-1182.

Saryazdi, F.; Motahhari, H.; Schoeggl, F.F.; Taylor, S.D.; Yarranton, H.W. (2013). Density of Hydrocarbon Mixtures and Bitumen Diluted with Solvents and Dissolved Gases. *Energy Fuels.* 27, 3666-3678.

Schümann, H.; Khatibi, M.; Tutkun, M. Pettersen, B.H.; Yang, Z.; Nydal, O.J. (2015). Droplet Size Measurements in Oil-Water Dispersions: A Comparison Study Using FBRM and PVM. *J. Dispersion Sci. Technol.,* 36 (10), 1432-1443.

Seifried, C. M.; Crawshaw, J.; Boek, E.S. (2013). Kinetics of Asphaltene Aggregation in Crude Oil Studied by Confocal Laser-Scanning Microscopy. *Energy Fuels*, 27 (4), 1865-1872.

Shafiee, M. (2014). Kinetics of Asphaltene Precipitation and Flocculation from Diluted Bitumen. MSc. Thesis. University of Calgary.

Shampine, L.F. (2008). Vectorized Adaptive Quadrature in MATLAB. *J. Comput. Appl. Math.*, 211 (2), 131-140.

Sie, C.; Nguyen, B.; Castellanos-Diaz, O.; Verlaan, M.; Nguyen, Q.P. (2019). Viscous Oil Recovery and in-situ Deasphalting in Fractured Reservoirs – Part 2: Effect of Solvent Type and Temperature. *Fuel*, 247 (1), 294-301.

Smoluchowski, M. (1917). Versuch Einer Mathematischen Theorie der Koagulations Kinetis Kolloider Losungen. *Z. Physik. Chem.*, 92, 129-168.

Soleimani-Khormakala, H.; Torkaman, M.; Bahrami, M. (2018). The Effect of Shear Rate on Aggregation and Fragmentation of Asphaltene Aggregates. *J. Dispension Sci. Technol.,* 40 (6), 836-845.

Speight, J.G. (2006). *The Chemistry and Technology of Petroleum*. Fourth Edition. CRC Press, Boca Raton, FL.

Spicer, P.T.; Pratsinis, S.E. (1996). Coagulation and Fragmentation: Universal Steady-state Particle-size Distribution. *AIChE J*., 42 (6), 1612-1620.

Strausz, O.P.; Lown, E,.M. (2003). *The Chemistry of Alberta Oil Sands, Bitumens, and Heavy Oils.* Alberta Energy Research Institute (AERI), Calgary, AB.

Tavakkoli, M.; Chen., A.; Sung, C.; Kidder, K.M.; Lee., J.J.; Alhassan, S.M.; Vargas, F.M. (2016). Effect of Emulsified Water on Asphaltene Instability in Crude Oils. *Energy Fuels*, 30 (5), 3676-3686.

Taylor, W.F.; Frankenfeld, J.W. (1978). Deposit Formation from Deoxygenated Hydrocarbons. 3. Effects of Trace Nitrogen and Oxygen Compounds. *Ing. Eng. Chem. Prod. Res. Dev.*, 17 (1), 86-90.

Thomas, D.N.; Judd, S.J.; Fawcett, N. (1999). Flocculation Modeling: A Review. *Water Res.*, 33 (7), 1579-1592.

Till, A. (2017). Measuring Technology Maturity: Theoretical Aspects. In *Measuring Technology Maturity: Operationalizing information from Patents, Scientific Publications, and the Web* (pp. 35-85). Berlin, Springer Gabler.

Tiller, F.M. (1981). Revision of Kynch Sedimentation Theory. *AIChE J.*, 27 (4), 823-829.

Tipman, R.N.; Long, Y. (1999). Solvent Process for Bitumen Separation from Oil Sands Froth. US Patent 5,876,592.

Tipman, R.N.; Sankey, B.M. (1993). Process for Separation of Hydrocarbon from Tar Sands Froth. United States Patent US 5,236,577.

Torkaman, M.; Bahrami, M.; Dehghani, M. (2017). Influence of Temperature and Stability of Asphaltenes. I. Perikinetic Aggregation. *Energy Fuels*, 31, 11169-11180.

Torkaman, M.; Bahrami, M.; Dehghani, M. (2018). Influence of Temperature on Aggregation and Stability of Asphaltenes. II. Orthokinetic Aggregation. *Energy Fuels*, 32, 6144-6154.

Valinasab, M. (2006). The Effect of Bitumen Extraction Conditions on Froth Treatment Effectiveness. MSc. Thesis, University of Calgary.

Van, A.L.; Bang, D.P.V. (2013). Hindered Settling of Sand/mud Flocs Mixtures: From Model Formulation to Numerical Validation. *Adv. Water Resour*., 53, 1-11.

Vanni, M.; Baldi, G. (2002). Coagulation Efficiency of Colloidal Particles in Shear Flow. *Adv. Colloid Interface Sci.*, 97, 151-177.

Vilas-Bôas Fávero, C.; Maqbool, T.; Hoepfner, M.; Haji-Akbari, N.; Fogler, H.S. (2017). Revisiting the Flocculation Kinetics of Destabilized Asphaltenes. *Adv. Colloid Interface Sci.*, 244, 267-280.

Vincent, B. (1973). The van der Waals Attraction Between Colloidal Particles Having Adsorbed Layers: II Calculation of Interaction Curves. *J. Colloid Interface Sci.*, 42 (2), 270-285.

Wang, J.; Lu, Q.; Harbottle, D.; Sjöblom, J.; Xu, Z.; Zeng, H. (2012). Molecular Interactions of a Polyaromatic Surfactant C5Pe in Aqueous Solutions Studied by a Surface Forces Apparatus. *J. Phys. Chem. B*, 116 (36), 11187-11196.

Wang, J.; Opedal, N.; Lu, Q.; Xu, Z.; Zeng, H.; Sjoblom, J. (2012). Probing Molecular Interactions of an Asphaltene Model Compound in Organic Solvents Using a Surface Forces Apparatus (SFA). *Energy Fuels*, 26 (5), 2591-2599.

Wang, S.; Liu, J.; Zhang, L.; Masliyah, J.; Xu, Z (2010). Interaction Forces between Asphaltene Surfaces in Organic Solvents. *Langmuir*, 26 (1), 183-190.

Wang, S.; Liu, Q.; Tan, X.; Xu, C.; Gray, M. R. (2013). Study of Asphaltene Adsorption on Kaolinite by X-ray Photoelectron Spectroscopy and Time-of-Flight Secondary Ion Mass Spectroscopy. *Energy Fuels*, 27 (5), 2465–2473.

Wattana, P.; Wojciechowski, D.J.; Bolanos, G.; Fogler, H.S. (2003). Study of Asphaltene Precipitation Using Refractive Index Measurement. *Petr. Sci. Technol*., 21 (3-4), 591-613.

Wiehe, I.A. (2008). *Process Chemistry of Petroleum Macromolecules*, CRC Press, Boca Raton, FL.

Wiehe, I.A.; Yarranton, H.W.; Akbarzadeh, K.; Rahimi, P.M.; Teclemariam, A. (2005). The Paradox of Asphaltene Precipitation with Normal Paraffins. *Energy Fuels*, 19, 1261-1267.

Wilson, D.I.; Watkinson, A.P. (1996). A Study of Autoxidation Reaction Fouling in Heat Exchangers. *Can. J. Chem. Eng.*, 74 (2), 236-246.

Wu, J.; Dabros, T. (2012). Process for Solvent Extraction from Oil Sand. *Energy Fuels*, 26 (2), 1002-1008.

Xu, R. (2000). *Particle Characterization: Light Scattering Methods*. Kluwer Academic Publishers, New York, NY.

Yang, Y.; Chaisoontornyotin, W.; Hoepfner, M.P. (2018). Structure of Asphaltenes During Precipitation Investigated by Ultra-small-angle X-ray Scattering. *Langmuir*, 34, 10371-10380.

Yarranton, H.W.; Fox, W.A.; Svrcek, W.Y. (2007). Effect of Resins on Asphaltene Self-association and Solubility. *Can. J. Chem. Eng.*, 85 (5), 635-642.

Yarranton, H.W.; Masliyah, J.H. (1996). Molar Mass Distribution and Solubility Modeling of Asphaltenes. *AIChE J*. 42(12), 3533-3543.

Yarranton, H.W.; Powers, D.P.; Okafor, J.C.; van der Berg, F.G.A. (2018). Regular Solution Based Approach to Modeling Asphaltene Precipitation from Native and Reacted Oils: Part 2, Molecular Weight, Density, and Solubility Parameters of Saturates, Aromatics, and Resins. *Fuel*, 215, 766-777.

Yarranton, H.W.; van Dorp, J.J.; Verlaan, M.L.; Lastovka, V. (2013). Wanted Dead or Live: Crude-Cocktail Viscosity – A Pseudocomponent Method to Predict the Viscosity of Dead Oils, Live Oils, and Mixtures. *J. Can. Pet. Technol*., 52 (3), 176-191.

Yudin, I.K.; Nikolaenko, G.L.; Gorodetski, E.E.; Markhashov, E.L.; Frot, D.; Briolant, Y.; Agayan, V.A.; Anisimov, M.A. (1998). Universal Behavior of Asphaltene Aggregation in Hydrocarbon Solutions. *Pet. Sci. Technol.*, 16 (3-4), 395-414.

Zahabi, A.; Gray, M.R.; Czarnecki, J.; Dabros, T. (2010). Flocculation of Silica Particles from a Model Oil Solution: Effect of Adsorbed Asphaltenes. *Energy Fuels*, 24 (6), 3616-3623.

Zahnow, J.C.; Maerz, J.; Feudel, U. (2011). Particle-based Modeling of Aggregation and Fragmentation Processes: Fractal-like Aggregates. *Physica D*, 240, 882-893.

Zawala, J.; Dabros, T.; Hamza, H.A. (2012). Settling Properties of Aggregates in Paraffinic Froth Treatment. *Energy Fuels*, 26, 5775-5781.

Zhang, L.; Shi, C.; Lu, Q.; Liu, Q.; Zeng, H. (2016). Probing Molecular Interactions of Asphaltenes in Heptol Using a Surface Forces Apparatus: Implications on Stability of Water-in-Oil Emulsions. *Langmuir*, 32 (19), 4886-4895.

Zhang, M. (2012). Role of Bitumen Viscosity in Bitumen Recovery from Athabasca Oil Sands. MSc. Thesis. University of Alberta.

Zhang, Y.; Arya, A.; Kontogeorgis, G.; Yarranton, H.W. (2019). Modeling the Phase Behavior of Bitumen/n-Alkane Systems with the Cubic plus Association (CPA) Equation of State. *Fluid Phase Equilib.*, 486, 119-138.

APPENDICES

APPENDIX A: CALIBRATION OF THE FBRM SIZE DISTRIBUTIONS

The FBRM method was used to measure aggregate size distributions over a wide range of *n*-heptane contents. The method is non-intrusive but there are several issues with obtaining representative diameter distributions:

- The FBRM method measures the primary chord size distribution which does not equal the diameter distribution, even for spherical particles. The chord length is the distance between two points on the edge of the particle traversed by the laser and will usually be less than the diameter of the sphere. Hence, this method will not produce a distribution of diameters skewed towards lower values even for perfect mono-disperse solids (Boxall *et al.,* 2010; Schümann *et al.,* 2015). In this study, the particles are irregular aggregates and the goal is to obtain a distribution of maximum diameters which increases the probability of obtaining a particle size distribution distant skewed to lower values. On the other hand, overlapping particles can be measured as a single larger particle skewing the distribution to larger values.
- The FBRM method gives misleading results if particle concentrations are too low to obtain a representative distribution or if a portion of the particles are below the detection threshold of 1-2 μm. The concentration of aggregates is too low (<100 counts/second) near the onset of precipitation and the particles are too small (< 2 μm) at short contact times (a few seconds of contact). The technique can also give misleading results at high particle concentrations. Figure A.1 shows that individual aggregates can be resolved if there is enough separation between them. However, if a high number of aggregates reaches the probe it is possible that the measured chord lengths do not correspond to individual aggregates but rather multiple overlapping structures. This source of error is most likely at the intermediate *n*-heptane contents (75-85 wt%) where the concentration of asphaltene precipitate reached a maximum.

Therefore, the measured primary chord length distributions must be calibrated to independently measured particle diameters; in this case, against micrographic measurements.

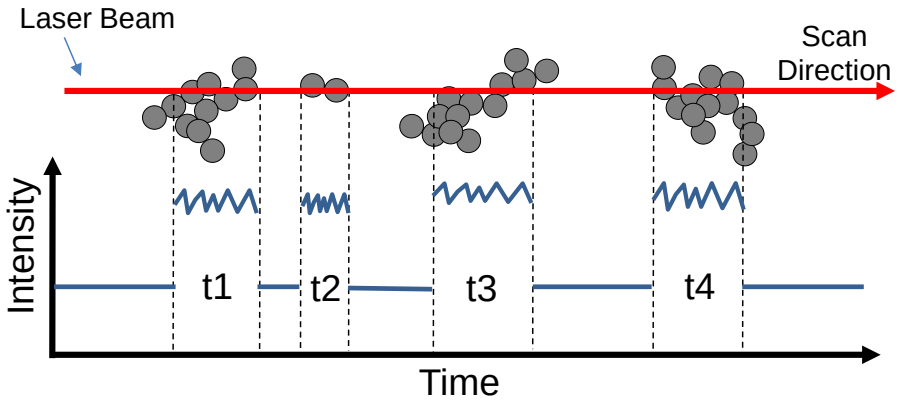

Figure A.1. Light scattering method used in this work to measure aggregate chord lengths Retrieved from Casas, 2017.

Micrographic distributions were measured on samples collected from the beaker at different *n*-heptane contents and times. The samples were placed on a microscope slide and observed at 10x and 40x magnifications (Figure A.2). The images were taken at random locations in the slide to avoid biases on small or large particles. The micrographic images were processed using ImageJ Software to estimate the number and diameter of particles (Broeke *et al*., 2015). The image was converted to black and white to increase the contrast between the aggregates and the surrounding fluid. The images were then processed to show the contour of the aggregates and their longest dimension (largest distance between any two points in the contour line) was recorded (Figure A.3). A number distribution was calculated from the measured diameters from sixteen images at 40x magnification (aggregates smaller than 40 µm) and one image at 10x (aggregates larger than 40 µm).

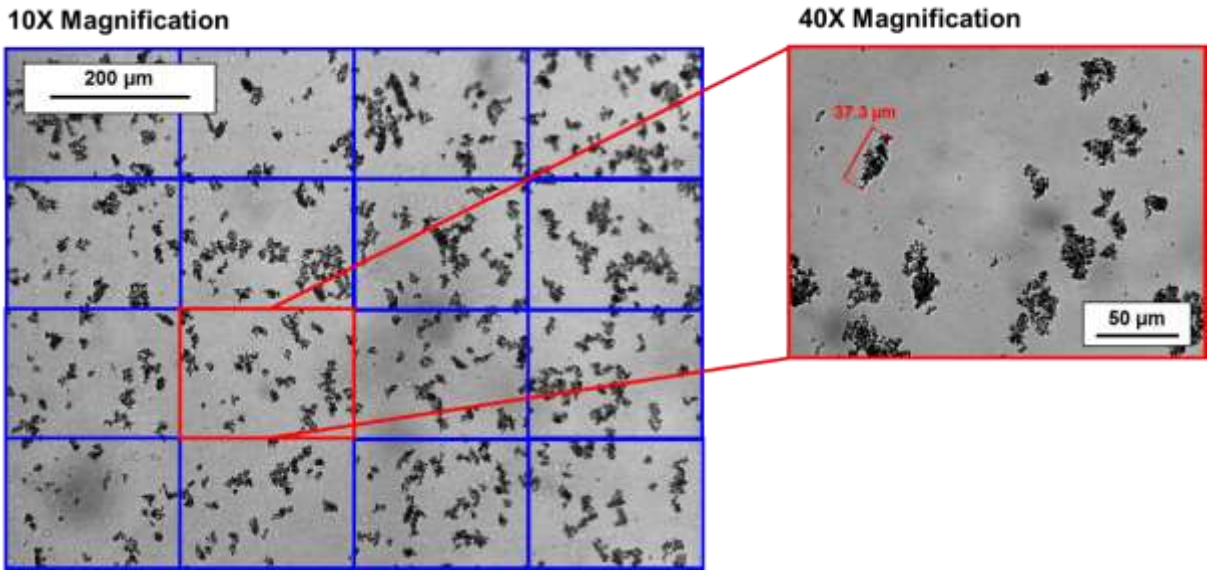

Figure A.2. Micrographics used for the determination of aggregate size distributions in a mixture of 87.5 wt% *n*-heptane and WC-B-A3 bitumen after 5 minutes mixing at 195 rpm. The 10X magnification image has the same area as 16 images at 40X magnification.

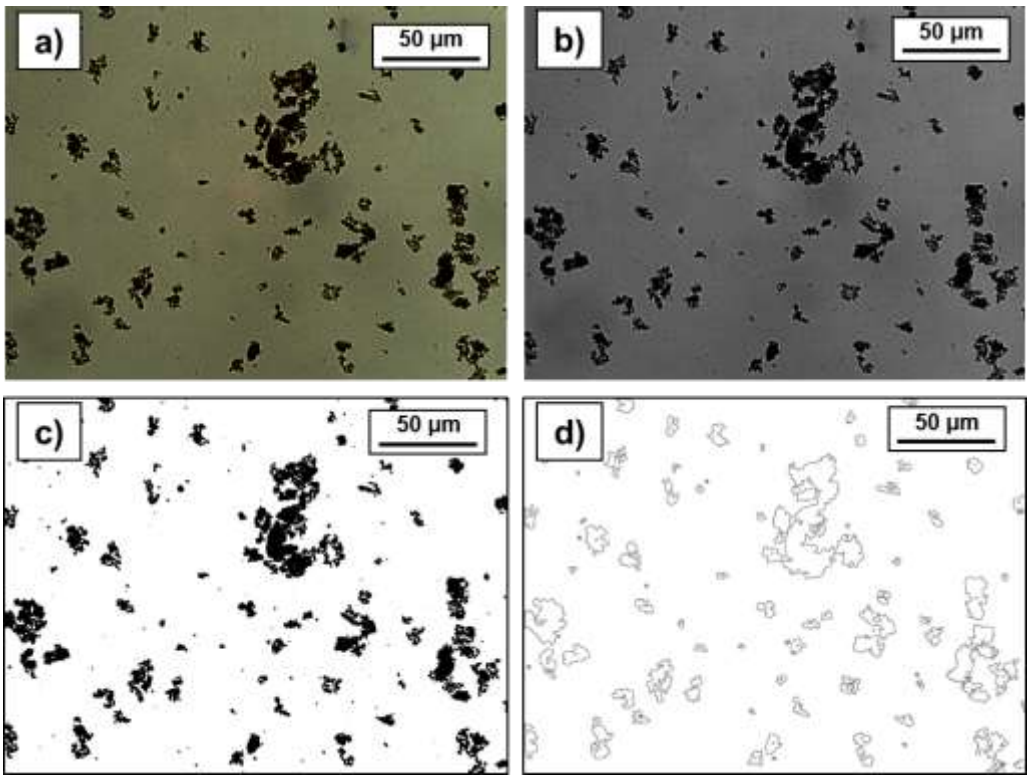

Figure A.3. Image processing for the determination of aggregate size distributions with the micrographic method in a mixture of 95 wt% *n*-heptane and WC-B-A3 bitumen after 1 minute mixing at 195 rpm: a) true color image; b) black and white (8 bits); c) binary image; d) contours.

The FBRM data were calibrated to the micrographic method distributions on a volume basis. For both datasets, the measured number frequencies, f_i, were transformed to volume frequencies, F_i, as follows:

$$F_i = \frac{f_i d_i^3}{\sum f_i d_i^3} \tag{A.1}$$

The experimental chord length volume distributions from the FBRM can be calibrated using a weighting factor, w_i, given by:

$$w_i = \frac{d_i^m}{\sum_{i=1}^{N} d_i^m} N \tag{A.2}$$

where N is the number of discrete bin sizes in the distribution and m is an exponent tuned for the calibration. The calibrated distribution is then given by:

$$F_i = \frac{f_i w_i d_i^3}{\sum f_i w_i d_i^3} \tag{A.3}$$

Figures A.4 and A.5 show that the uncalibrated volume moment chord length distributions from the FBRM match the micrographic volumetric distributions, except at *n*-heptane contents near the onset of precipitation (< 60 wt% *n*-heptane diluted WC-B-B2 bitumen and < 62 wt% *n*-heptane diluted WC-B-A3). At these low *n*-heptane contents, only micrographic data was used in this study. At all other conditions, no calibration was required; that is, the exponent *m* was set equal to zero. The mean deviation in the volume mean diameter obtained from the two methods for both diluted bitumen systems was ± 4.9 µm with a 90% confidence interval based on the analysis of 54 samples.

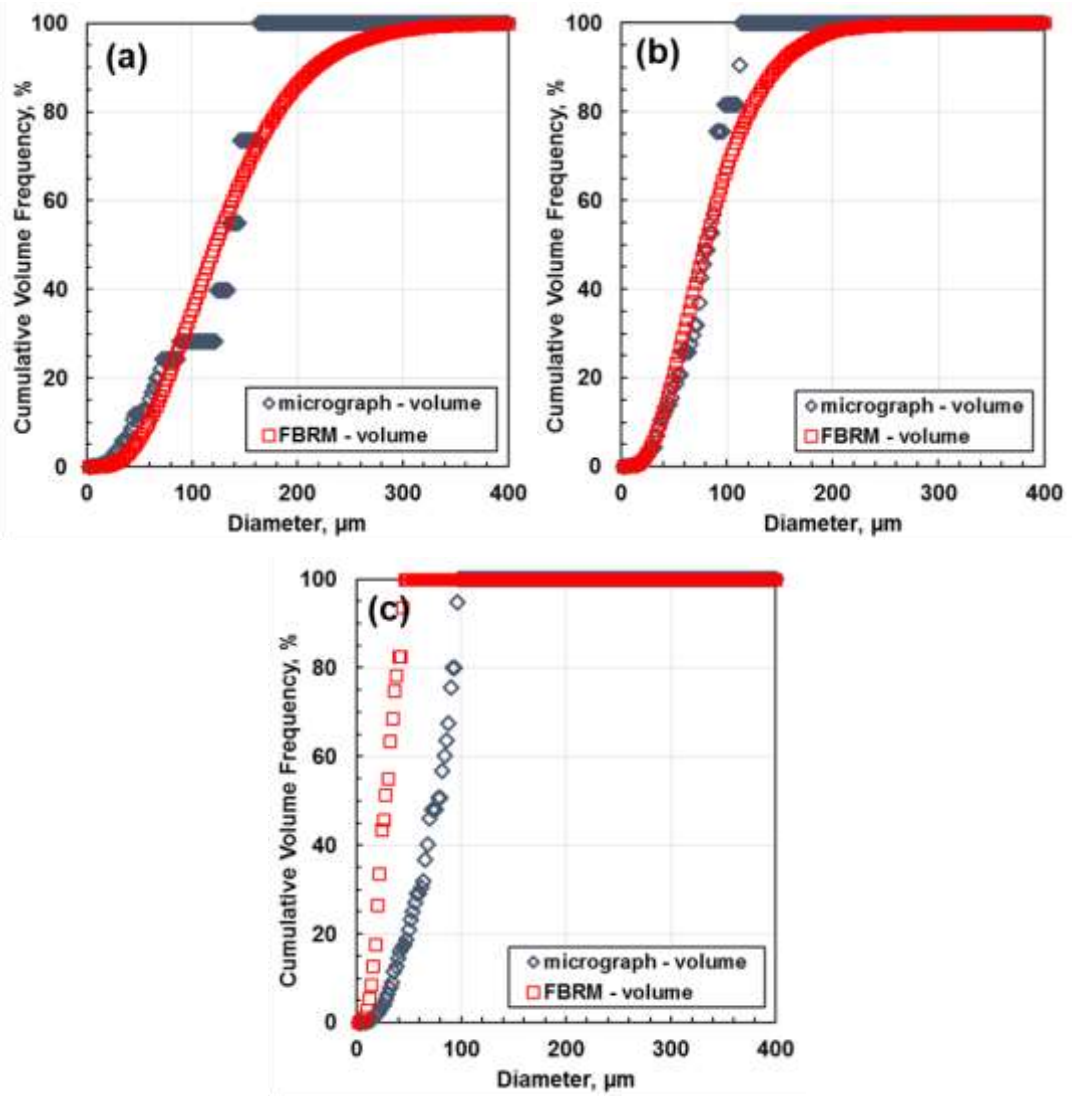

Figure A.4. Volume moment distributions from the micrographic and FBRM methods for mixtures of *n*-heptane and WC-B-B2 bitumen after 60 minutes mixing at 195 rpm and *n*-heptane contents of: a) 90.5 wt%; b) 82 wt%; c) 57.5 wt%.

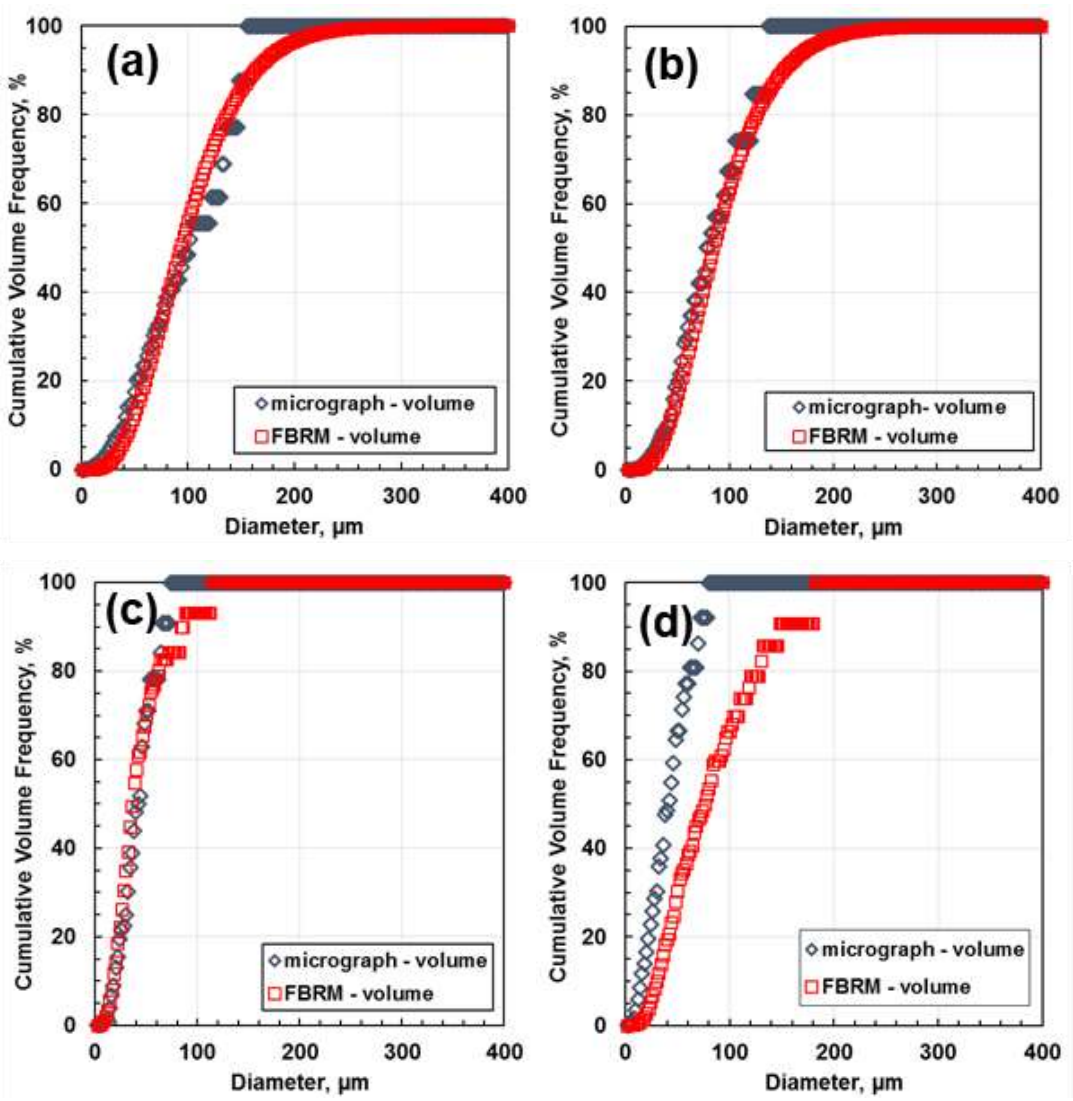

Figure A.5. Volume moment distributions from the micrographic and FBRM methods for mixtures of *n*-heptane and WC-B-A3 bitumen after 60 minutes mixing at 195 rpm and *n*-heptane contents of: a) 95 wt%; b) 80 wt%; c) 70 wt%; d) 59.5 wt%.

APPENDIX B: DENSITY AND VISCOSITY OF MIXTURES

B.1. Correlated Properties

Density of crude oil mixtures with *n*-heptane for the precipitation and settling studies were measured with and Anton Paar DMA 4500M density meter at 21ºC. The repeatability on the measurements was estimated at ± 0.05 kg/m^3 based on three repeats per sample analyzed. The densities of the crude oils (except WC-B-A3) were reported by Ramos-Pallares *et al.* (2016, 2017). For the WC-B-A3, the density and viscosity were measured by Marquez (2019). To measure the densities of the mixtures with *n*-heptane, samples were prepared at solvent contents ranging from 20 to 80 wt% *n*-heptane. In all cases, the sample was left to settle for 24 h after the addition of solvent to settle precipitated asphaltenes. Then, a sample of the supernatant was taken and analyzed in the density meter. The mixture density was calculated with the mixing rule proposed by Saryarzdi *et al.* (2013) as follows,

$$\rho_m = \left[\frac{w_1}{\rho_1} + \frac{w_2}{\rho_2} - w_1 w_2 \left(\frac{1}{\rho_1} + \frac{1}{\rho_2}\right)\beta_{12}\right]^{-1} \quad \text{(B.1)}$$

where ρ_m is the mixture density, and the subscripts 1 and 2 correspond to crude oil and *n*-heptane, respectively. The interaction parameter β_{12} was adjusted to fit the experimental data with the least squares method. The interaction parameters obtained in this work are reported in Table B.1. The measured and correlated densities are shown in Figure B.1.

Table B.1. Parameter used in the density and viscosity models.

Sample	Solvent	β_{12}	α_{12}
WC-B-B2	*n*-heptane	0.015	0.25
MSB	*n*-heptane	0.01295	0.3335
MX-B-A1	*n*-heptane	-0.00137	0.4241
EU-HO-A1	*n*-heptane	0.0029	0.3376
WC-B-A3	*n*-heptane	0.015	0.25
WC-B-A3	*n*-pentane	0.01	0.33

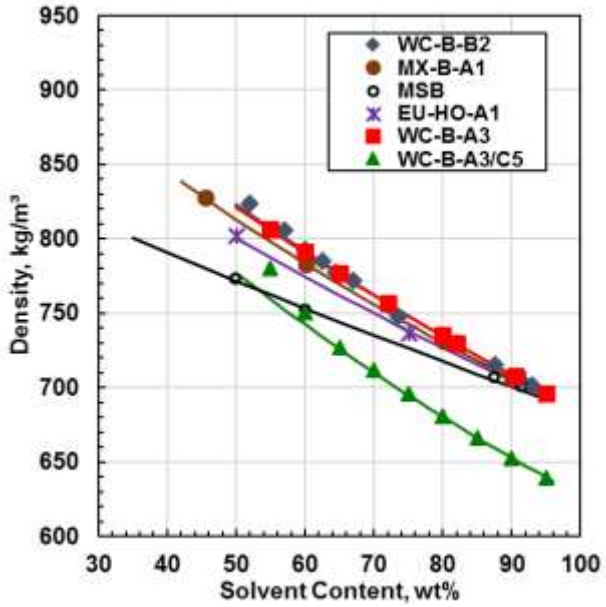

Figure B.1. Measured and correlated density of mixtures of crude oils diluted with *n*-heptane or *n*-pentane at 21ºC. Solids continuous lines correspond to the correlation of Eq. B.1.

Crude oil viscosity data was collected by Ramos-Pallares *et al.* (2016) and Marquez (2019) using an Anton Paar Model MCR-52 cone-and-plate rheometer. They collected data for crude oil viscosity at temperatures ranging from 20ºC to 100ºC, and for mixtures with different solvents. The data was correlated with the Walther equation (Yarranton *et al.*, 2013; Ramos-Pallares *et al.*, 2017), and for the binary system consisting on crude oil and *n*-heptane is presented as follows,

$$\log[\log \mu_m + 1] = w_1 A_1 + w_1 A_1 - w_1 w_2 A_1 A_2 \alpha_{12} \quad \text{(B.2)}$$

where μ_m is the mixture viscosity, and w is the mass fraction of crude oil (1) and *n*-heptane (2). The parameter A_i is defined as,

$$A_i = \log[\log(\mu_i + 1)] \quad \text{(B.3)}$$

where μ_i is the viscosity of the component i at the desired temperature. Values for the interaction parameter α_{12} were taken from Ramos-Pallares *et al.* (2017) for the same oils. For the WC-B-A3 bitumen, the interaction parameter was adjusted to the data collected by Marquez (2019). The value for the interaction parameters used in this work are presented in Table B.1.

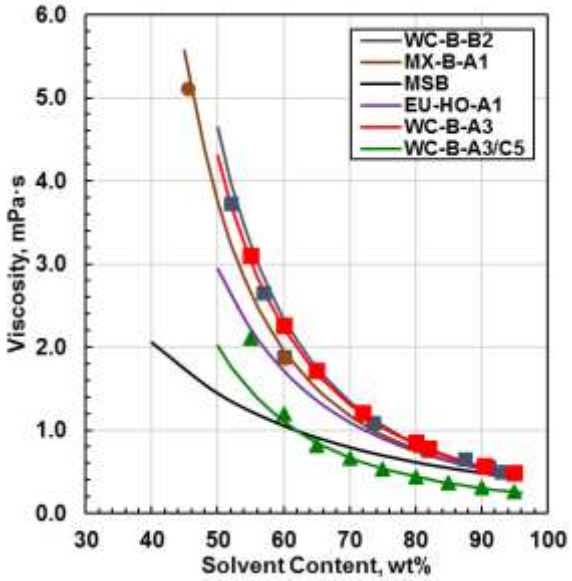

Figure B.2. Calculated viscosity of mixtures of crude oils diluted with *n*-heptane or *n*-pentane at 21ºC. Solids continuous lines correspond to the modified Walther model (Eq. B.2).

B.2. Density and Viscosity data for the Mixtures of the Settling Study

The density and viscosity of the diluted bitumen mixtures studied in Chapter 6 were measured for precipitate-free samples at 21ºC and 1 atm. Density of the mixtures are reported in Table B.2. The repeatability of the density measurements was ±0.05 kg/m³. Mixture viscosities are provided in Table B3. The repeatability on the viscosities was ± 5%.

Table B.2. Density of the diluted bitumen mixtures investigated in Chapter 6 at 21ºC and 1 atm.

***n*-pentane/WC-B-A3**		***n*-heptane/WC-B-A3**		***n*-heptane/WC-B-B2(1)**	
Solvent	Density	Solvent	Density	Solvent	Density
55.0	780.2	55.0	806.6	52.0	823.53
60.0	750.4	60.0	791.4	57.0	805.40
65.0	726.7	65.0	776.6	60.0	792.84
70.0	711.6	72.0	756.8	62.5	785.29
75.0	696.0	80.0	735.0	64.5	777.19
80.0	681.0	82.0	729.6	67.0	771.96
85.0	666.5	90.5	707.6	73.6	747.43
90.0	652.6	95.0	696.3	82.0	729.95
95.0	639.1			87.5	715.42
				91.1	705.83
				93.0	701.33

Table B.3. Viscosity of diluted bitumen mixtures of Chapter 6. Data collected at 21ºC and 1 atm.

***n*-pentane/WC-B-A3**		***n*-heptane/WC-B-A3**		***n*-heptane/WC-B-B2(1)**	
Solvent	Viscosity	Solvent	Viscosity	Solvent	Viscosity
60.0	1.19	55.0	3.10	52.0	3.73
65.0	0.82	60.0	2.27	57.0	2.65
70.0	0.66	65.0	1.71	60.0	1.89
75.0	0.54	72.0	1.21	73.6	1.09
80.0	0.44	80.0	0.85	82.0	0.76
85.0	0.37	82.0	0.78	87.5	0.65
90.0	0.31	90.5	0.56	91.1	0.55
95.0	0.26	95.0	0.48	93.0	0.50

APPENDIX C: YIELDS AND ONSET DATA OF ASPHALTENE PRECIPITATION IN ANAEROBIC CONDITIONS

C. 1. Asphaltene Yield Data and Onsets of Precipitation

Yield data collected in nitrogen atmosphere at 21ºC is presented in Table C.1 to C.5. Gravimetric onsets of precipitation are reported in Table C.6.

Table C.1. Yield data for WC-B-B2 in nitrogen at 21ºC.

WC-B-B2							
54.5 wt%		57.5 wt%		59.5 wt%		64.5 wt%	
Time, h	Yield, wt%	Time, h	Yield, wt%	Time, h	Yield, wt%	Time, h	Yield, wt%
24	0.06	1	0.45	2	2.72	2	4.77
48	0.21	2	0.59	4	3.05	2	5.31
96	0.29	4	1.20	6	3.08	4	5.19
144	0.24	6	1.87	13	3.26	6	5.63
240	0.31	12	1.29	24	3.67	12	5.40
454	0.24	24	1.55	48	3.90	24	6.07
		46	2.15	24	3.78	48	6.33
		24	1.60	96	4.27	2	4.79
		48	2.12	408	4.17	6	4.82
		96	2.33	48	3.80	12	6.12
		216	2.79	96	4.21	24	5.96
		288	2.80	144	4.26	48	5.83
		24	1.60	216	4.31	48	6.15
		48	2.12	288	4.30	96	6.09
		96	2.53	348	4.24	144	6.33
		144	2.57	528	4.38	192	6.27
		216	2.78			240	6.36
		288	2.82			360	6.45
		408	2.83			480	6.34

Table C.2. Yield data for MX-B-A1 in nitrogen at 21ºC.

MX-B-A1					
48.5 wt%		52 wt%		55 wt%	
Time, h	Yield, wt%	Time, h	Yield, wt%	Time, h	Yield, wt%
1.3	-0.03	5.2	4.75	1.3	8.83
2.5	0.01	24.7	7.72	2.4	9.50
5.3	0.01	72.8	8.32	5.2	10.59
20.1	0.00	145.4	8.53	20.0	11.20
24.7	0.01	241.0	9.04	24.6	11.84
43.9	0.02	335.9	8.81	43.8	12.04
72.8	0.05	449.9	8.89	72.7	12.31
145.5	0.18	497.1	8.79	145.4	13.75
241.1	0.20	2.2	3.74	241.0	14.32
337.0	0.17	40.9	7.40	335.9	14.92
454.1	0.22			449.8	14.50
498.7	0.24			497.0	15.30
				71.8	13.36
				118.6	13.59
				147.0	13.63
				188.8	13.60
				239.3	14.70
				384.2	14.72
				302.5	14.44

Table C.3. Yield data for MSB in nitrogen at 21ºC.

MSB							
45 wt%		47.5 wt%		50 wt%		55 wt%	
Time, h	Yield, wt%	Time, h	Yield, wt%	Time, h	Yield, wt%	Time, h	Yield, wt%
1.1	0.01	1.0	0.03	0.9	0.06	1.0	0.11
5.3	0.04	5.2	0.06	5.2	0.08	5.3	0.15
7.5	0.04	7.4	0.07	7.5	0.08	7.4	0.14
24.2	0.06	24.1	0.08	24.1	0.11	24.2	0.16
48.1	0.07	48.1	0.09	48.0	0.12	48.1	0.17
74.2	0.08	74.1	0.10	74.1	0.13	74.1	0.18
148.6	0.10	148.5	0.13	148.3	0.15	148.3	0.21
340.7	0.11	340.6	0.13	340.6	0.16	340.6	0.22
497.0	0.11	496.8	0.13	496.8	0.17	497.3	0.22
251.3	0.11	251.3	0.13	251.2	0.16	251.2	0.22

Table C.4. Yield data for EU-HO-A1 in nitrogen at 21ºC.

EU-HO-A1							
80 wt%		81.5 wt%		83 wt%		86 wt%	
Time, h	Yield, wt%	Time, h	Yield, wt%	Time, h	Yield, wt%	Time, h	Yield, wt%
1.0	0.00	1.2	0.01	1.2	0.01	1.1	0.22
2.0	0.01	2.3	0.02	2.2	0.02	2.1	0.25
5.0	0.01	4.9	0.03	4.8	0.03	4.7	0.26
7.6	0.01	20.0	0.05	20.0	0.07	19.9	0.45
24.2	0.01	24.4	0.05	24.3	0.09	24.3	0.39
46.9	0.01	44.1	0.05	44.0	0.11	44.0	0.54
75.8	0.01	71.5	0.05	71.4	0.13	71.4	0.63
149.9	0.01	143.7	0.06	143.6	0.17	143.6	0.64
243.9	0.01	237.6	0.06	237.6	0.21	237.5	0.67
339.3	0.01	334.4	0.06	334.3	0.20	334.2	0.69
435.6	0.03	453.8	0.08	453.8	0.21	453.7	0.68
504.6	0.04	499.8	0.06	499.8	0.21	499.7	0.68

Table C.5. Yield data for WC-B-A3 (supplemental data set) in nitrogen at 21ºC.

WC-B-A3			
59.5 wt%		64.5 wt%	
Time, h	Yield, wt%	Time, h	Yield, wt%
1.12	0.25	4.34	1.34
8.17	0.33	24.80	3.08
24.02	0.86	192.44	5.33
75.11	2.22		
254.54	2.02		
480.1	2.04		

Table C.6. Onsets of asphaltene precipitation measured in anaerobic conditions at 21ºC using the gravimetric method.

WC-B-B2		**MX-B-A1**		**MSB**		**EU-HO-A1**	
Time, h	Onset, wt%	Time, h	Onset, wt%	Time, h	Onset, wt%	Time, h	Onset, wt%
24	54.05	1.3	48.52	1.0	44.07	1.1	82.93
48	53.84	2.4	47.04	5.0	42.10	2.1	82.70
96	53.37	5.2	47.54	7.4	40.61	4.8	82.60
144	53.46	24.5	47.27	24.0	39.66	20.0	82.40
216	53.87	43.6	47.31	48.0	36.94	24.3	81.30
240	53.99	72.5	47.24	74.0	36.15	44.7	81.42
288	53.72	145.7	47.27	148.0	35.85	72.5	81.50
408	53.72	241.5	47.27	251.0	34.44	145.2	81.33
528	53.70	341.7	47.33	340.0	33.99	239.2	81.25
		447.5	47.29	497.0	33.74	335.5	81.30
		498.3	47.33			449.2	81.13
						501.0	81.23

C.2. Micrographic Determination of Onsets of Precipitation

The micrographic method was used to verify the onsets of asphaltene precipitation. Figure C.1 shows the micrographic onsets for the samples MSB, MX-B-A1, and EU-HO-A1.

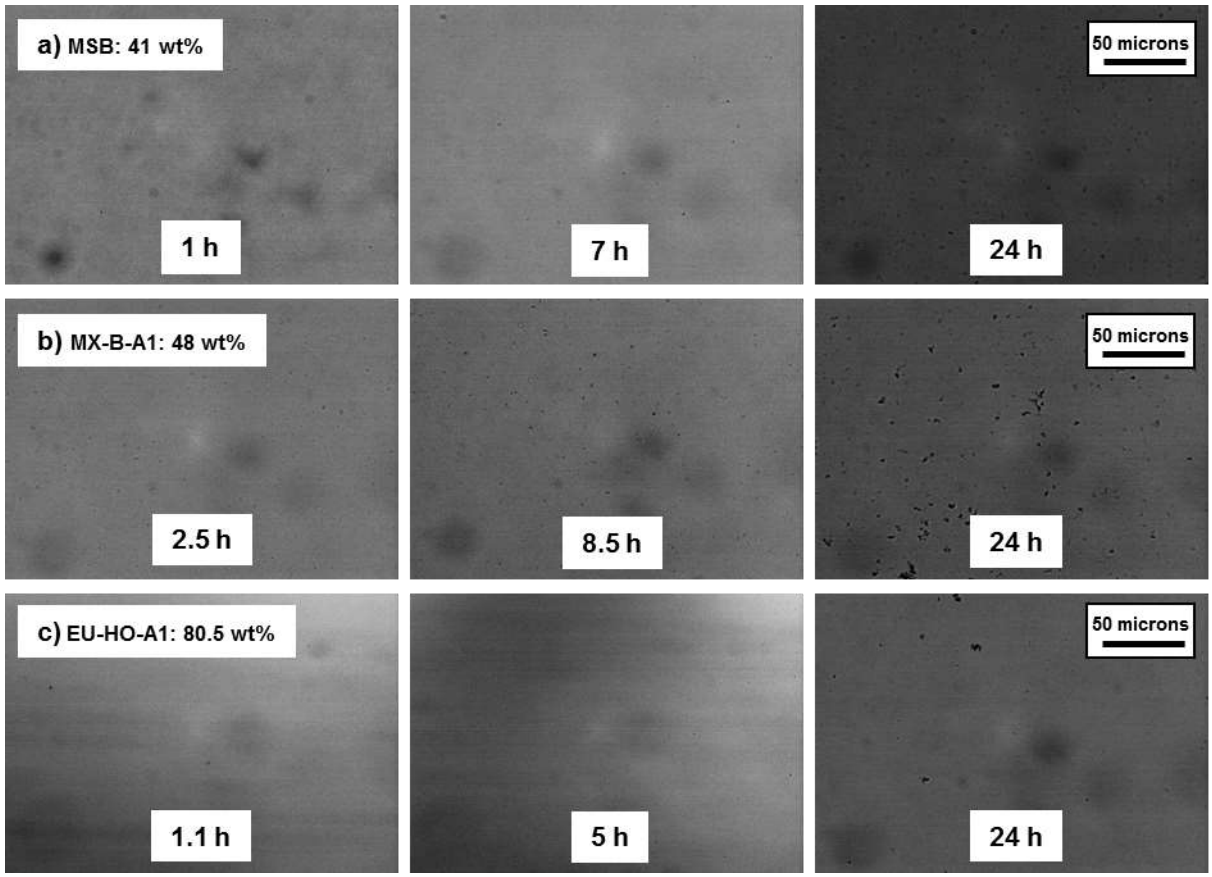

Figure C.1. Micrographs showing the onset of asphaltene precipitation from *n*-heptane diluted crude oils a) MSB at 41 wt%, b) MX-B-A1 at 48 wt%, and c) EU-HO-A1 at 80.5 wt% *n*-heptane in air at 21°C.

Table C.7. Gravimetric onset of asphaltene precipitation for crude oil samples diluted in *n*-heptane in air and nitrogen at 21ºC and 1 atm.

Crude Oil	Contact Time	Onset in Air	Onset in Nitrogen
WC-B-B2	2	56.5 ± 1.0	-
WC-B-B2	24	54.3 ± 1.3	-
MSB	2	41.7 ± 0.9	48.2 ± 0.7
MSB	24	38.6 ± 0.3	42.6 ± 0.2
MX-B-A1	2.5	47.8 ± 0.9	49.1 ± 1
MX-B-A1	24	47.6 ± 0.8	47.5 ± 0.9
EU-HO-A1	2	80.8 ± 1.1	84.6 ± 0.7
EU-HO-A1	24	80.6 ± 0.6	82.3 ± 0.7

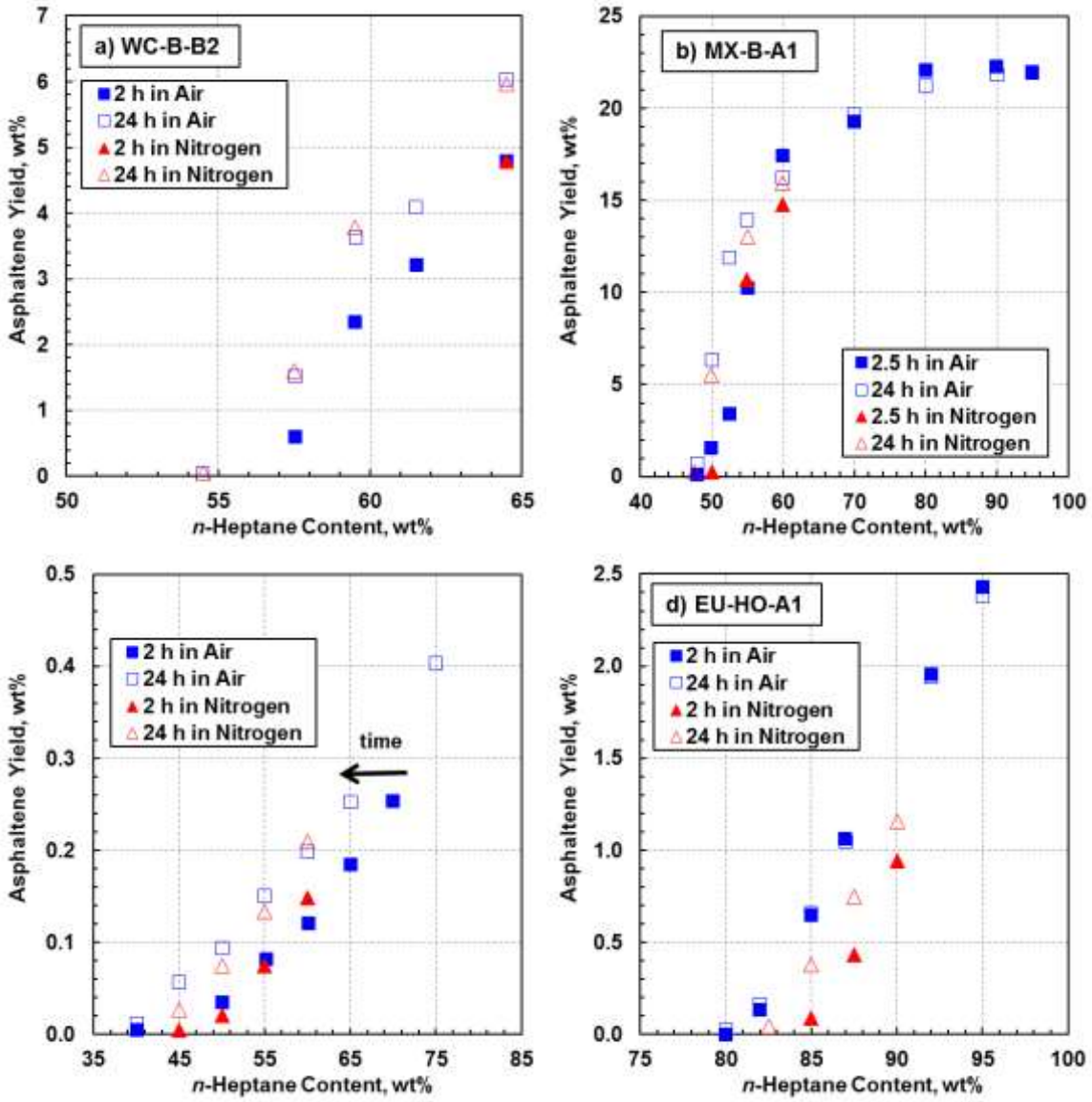

Figure C.2. Asphaltene yield curves showing the gravimetric onset of asphaltene precipitation from *n*-heptane diluted crude oils in air and nitrogen; a) WC-B-B2; b) MX-B-A1; c) MSB; b) MX-B-A1, and d) EU-HO-A1. Measurements done at 21°C. The repeatability of the yield measurement is ±0.41 wt% for WC-B-B2, ±0.49 wt% for MX-B-A1, ±0.02 wt% for MSB, and ±0.07 wt% for EU-HO-A1 but error bars are not shown to avoid clutter.

APPENDIX D: EXPERIMENTAL EQUILIBRIUM YIELDS AND IMMEDIATE YIELD FRACTIONS

The equilibrium yields ($Y_{A,eq}$) and immediate yield fractions (f) used in the solution of the population balance model of Chapter 4 were taken from the experimental data of Appendix C and are summarized in Table D.1.

Table D.1. Experimental equilibrium yields and immediate yield fractions for the systems studied in this work.

WC-B-B2			**MX-B-A1**		
n-heptane	$Y_{A,eq}$ (wt%)	f	*n*-heptane	$Y_{A,eq}$ (wt%)	f
54.5	0.238	0.05	48.5	0.239	0.03
57.5	2.826	0.15	52.0	8.810	0.425
59.5	4.275	0.64	55.0	14.710	0.60
64.5	6.440	0.74			
MSB			**EU-HO-A1**		
n-heptane	$Y_{A,eq}$ (wt%)	f	*n*-heptane	$Y_{A,eq}$ (wt%)	f
38.5	0.053	0.01	80.0	0.04	0.000
45.0	0.114	0.12	81.5	0.06	0.020
47.5	0.129	0.23	83.0	0.21	0.024
50.0	0.155	0.39	86.0	0.68	0.324
55.0	0.221	0.52			

APPENDIX E: CORRELATION FOR THE INPUTS OF THE PRECIPITATION AND AGGREGATION MODEL

E.1. Correlation for the Immediate Yield Fraction

The fraction of asphaltenes that precipitate immediately was correlated to the degree of separation from the onset (w-w_{onset}). Equation 4.45 depends on parameters B and C that are a function of the specific gravity of the oil, the C5-asphaltene content, and the equilibrium onset. Figure E.1 shows the experimental values for f (provided in Table D.1) and the correlated values. The AARD for the correlation was 6.8%.

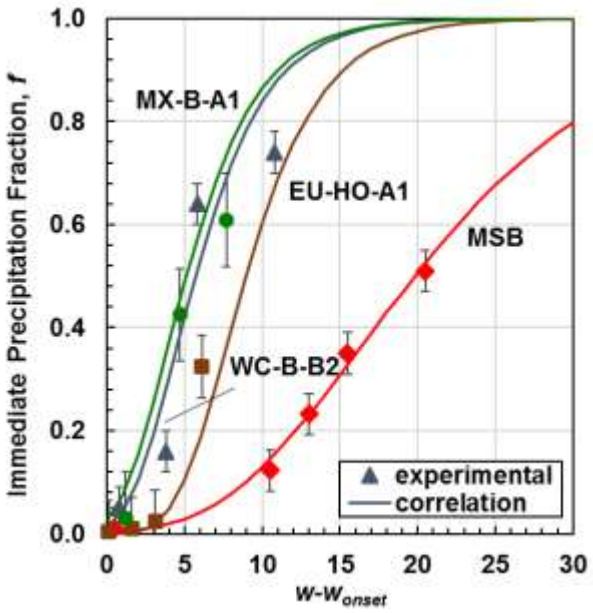

Figure E.1. Fitted and correlated immediate precipitation fraction.

E.2. Correlation for the Initial Collision Efficiency

The modified population balance model relies on the initial collision efficiency to account for the large aggregate diameters observed almost instantaneously upon precipitant addition. The initial collision efficiency was obtained from fitting the experimental diameters with the modified model. The values obtained for β_E at the different precipitant contents studied were correlated to the degree of separation from the onset. The supplemental data set was also introduced to improve the correlation and attempt to expand the predictions for *n*-pentane diluted oils. Figure E.2 shows the comparison between the values obtained from fitting the model to experimental diameters and the correlation proposed. The correlation has an AARD of 35% for the data in *n*-heptane and 62% for *n*-pentane diluted oils.

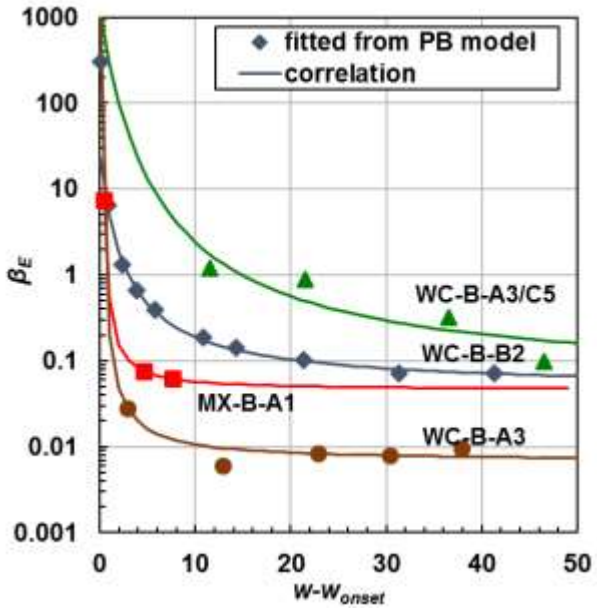

Figure E.2. Experimentally derived and correlated initial collision efficiency of the modified population balance model.

APPENDIX F: YIELDS AND ONSET DATA OF ASPHALTENE PRECIPITATION IN AIR ATMOSPHERE

F.1. Onsets of Asphaltene Precipitation in Air

Onset data for mixtures of crude oil and *n*-heptane were measured in air atmosphere at 21ºC and are presented in Table F.1. Onsets were obtained from extrapolation to zero yields from gravimetric yield data and confirmed with the micrographic method. Onsets are reported to ± 1 wt%.

Table F.1. Onsets of asphaltene precipitation from mixtures of crude oil and *n*-heptane measured in air atmosphere at 21ºC using the gravimetric method.

WC-B-B2		**MX-B-A1**		**MSB**		**EU-HO-A1**	
Time, h	Onset, wt%	Time, h	Onset, wt%	Time, h	Onset, wt%	Time, h	Onset, wt%
2.0	56.1	1.2	47.8	21.0	40.6	1.2	82.7
4.0	54.6	2.3	47.2	22.0	39.9	2.2	83.0
6.0	54.3	5.5	47.3	25.5	39.6	8.1	82.6
12.0	54.2	8.2	47.2	28.0	38.2	22.8	81.7
24.0	54.4	22.7	47.3	44.0	37.5	45.6	81.7
48.0	53.9	45.1	46.8	62.0	34.5	70.4	81.5
72.0	52.8	71.8	45.3	94.0	33.3	148.0	81.3
96.0	53.5	147.5	45.1	168.0	30.2	246.2	81.1
144.0	53.2	240.1	44.7	271.0	29.3	337.1	81.0
216.0	50.0	336.4	44.6	360.0	29.4	453.2	80.1
288.0	49.2	453.0	44.2	475.0	29.2	500.5	80.2
408.0	49.1	500.1	44.2				
528.0	48.8						

F.2. Asphaltene Yield Data in Air

Yield data for mixtures investigated in this work and collected under aerobic conditions at 21ºC are reported in Tables F.2 to F.5.

Table F.2. Asphaltene yields from mixtures of WC-B-B2 bitumen and *n*-heptane at 21°C and air atmosphere.

Yield at Specified *n*-Heptane Content							
54.5 wt%		57.5 wt%		59.5 wt%		64.5 wt%	
Time, h	Yield, wt%	Time, h	Yield, wt%	Time, h	Yield, wt%	Time, h	Yield, wt%
2.0	0.00	1.0	0.45	2.0	2.72	2.0	4.77
4.0	0.02	2.0	0.59	4.0	3.05	2.0	5.31
6.0	0.06	4.0	1.20	6.0	3.08	4.0	5.19
12.0	0.27	6.0	1.87	13.0	3.26	6.0	5.63
24.0	0.02	12.0	1.29	24.0	3.67	12.0	5.40
48.0	0.20	24.0	1.55	48.0	3.90	24.0	6.07
96.0	0.29	46.3	2.15	72.0	4.19	48.0	6.33
144.0	0.54	72.0	2.34	96.0	4.49	72.0	6.44
336.0	0.56	96.0	2.60	144.0	4.58	96.0	6.68
456.0	0.64	142.7	3.12	180.0	4.88	240.0	7.22
600.0	0.58	216.0	3.40	216.0	5.17	360.0	7.52
		288.0	3.59	288.0	5.29	480.0	7.69
		408.0	3.73	408.0	5.27	624.0	7.35
		528.0	3.99	528.0	5.50	768.0	7.54
		408.0	3.70			936.0	7.77
		528.0	3.83			1104.0	8.04

Table F.3. Asphaltene yields from mixtures of MX-B-A1 bitumen and *n*-heptane at 21°C and air atmosphere.

Yield at Specified *n*-Heptane Content			
52 wt%		55 wt%	
Time, h	Yield, wt%	Time, h	Yield, wt%
1.2	0.49	1.1	8.43
2.1	0.75	2.1	8.11
5.2	8.13	5.2	11.46
8.4	8.82	8.4	11.96
23.9	10.19	23.7	13.80
42.1	11.86	42.1	13.92
72.2	12.55	72.1	14.77
145.1	12.79	144.9	15.29
260.4	13.51	260.3	15.50
338.0	14.40	337.9	16.72
452.0	14.43	451.9	15.50
499.3	15.02	499.3	16.17

Table F.4. Asphaltene yields from mixtures of EU-HO-A1 heavy oil and *n*-heptane at 21°C and air atmosphere.

Yield at Specified *n*-Heptane Content							
80 wt%		81.5 wt%		83 wt%		86 wt%	
Time, h	Yield, wt%	Time, h	Yield, wt%	Time, h	Yield, wt%	Time, h	Yield, wt%
1.0	0.01	1.4	0.00	1.3	0.02	1.3	0.20
2.1	0.01	2.2	0.00	2.2	0.00	2.1	0.26
5.0	0.01	5.8	0.01	5.7	0.00	5.7	0.29
7.5	0.02	8.4	0.00	8.3	0.04	8.3	0.40
24.3	0.02	22.5	0.02	22.3	0.09	22.3	0.50
48.7	0.02	44.7	0.01	44.6	0.11	44.5	0.57
95.3	0.02	70.4	0.04	70.4	0.18	70.3	0.74
149.7	0.02	147.2	0.05	147.2	0.24	147.1	0.78
150.3	0.01	240.5	0.09	240.5	0.34	240.4	0.96
263.4	0.03	336.7	0.11	336.6	0.37	336.6	0.96
338.7	0.04	453.4	0.17	453.3	0.45	453.3	1.01
452.7	0.05	499.9	0.19	499.8	0.50	499.7	1.09
502.6	0.06						

Table F.5. Asphaltene yields from mixtures of MSB oil and *n*-heptane at 21°C and air atmosphere.

Yield at Specified *n*-Heptane Content							
45 wt%		47.5 wt%		50 wt%		55 wt%	
Time, h	Yield, wt%	Time, h	Yield, wt%	Time, h	Yield, wt%	Time, h	Yield, wt%
21.2	0.04	26.6	0.08	20.6	0.09	0.6	0.16
22.2	0.05	27.1	0.09	21.0	0.11	1.0	0.17
25.7	0.06	28.1	0.09	22.0	0.11	2.2	0.17
28.3	0.08	31.2	0.10	25.1	0.12	5.2	0.18
42.7	0.08	34.2	0.11	28.1	0.14	8.2	0.19
64.6	0.12	50.1	0.12	44.0	0.14	24.0	0.20
90.4	0.13	50.2	0.12	44.2	0.15	24.3	0.21
167.2	0.16	67.6	0.12	61.5	0.15	41.6	0.21
260.7	0.16	105.1	0.15	99.0	0.17	79.1	0.23
356.9	0.18	176.5	0.17	170.4	0.19	150.5	0.24
473.6	0.20	283.9	0.18	277.9	0.23	258.0	0.28
520.0	0.20	366.1	0.20	360.0	0.24	340.1	0.29
		479.5	0.21	473.5	0.25	453.5	0.30
		528.3	0.21	522.3	0.26	502.4	0.30

APPENDIX G: AERATED BITUMEN DATA

The effect of aeration on asphaltene yields was investigated with the WC-B-A0 bitumen sample diluted with *n*-heptane. These data have been measured in a previously unpublished study. The bitumen samples were first deoxygenated and then aerated at different temperatures (see Section 2.9). Later, asphaltene yields were measured at 24 h using *n*-heptane as precipitant. These data are reported in Table G.1. Table G.2 presents yield data for samples contacted with air and nitrogen at 70ºC. Yields were measured over time at 85 wt% *n*-heptane using aerated bitumen samples and are reported in Table G.3.

Table G.1. Asphaltene yields at 24 h from mixtures of aerated WC-B-A0 bitumen at different temperatures.

	Yields at 24 h (wt%)				
n-Heptane Content, wt%	Base Case	N_2 at 70ºC	Aeriation at 21ºC	Aeriation at 40ºC	Aeriation at 70ºC
50.9	0.53	0.53	0.62	0.7	1.47
58.0	1.06	1.01	1.17	3.6	6.24
67.5	5.11	5.3	5.48	7.6	10.35
73.4	7.25	7.7	7.12	9.7	12.52
87.4	10.73	11.3	10.68	13.5	15.05
96.5	11.35	11.6	11.35	14.1	15.47

Table G.2. Asphaltene yields at 24 h for *n*-heptane diluted WC-B-A0 bitumen. Bitumen samples were contacted with air or nitrogen at 70ºC.

Air contacted at 70ºC		**N_2 contacted at 70ºC**	
n-Heptane	Yield (wt%)	*n*-Heptane	Yield (wt%)
50.9	0.54	50.9	0.58
58.0	1.05	54.7	0.77
67.5	4.8	58.0	0.94
73.4	6.94	60.9	2.1
87.4	10.7	67.5	5.16
96.5	11.4	73.4	7.5
		87.4	10.6
		96.5	11.37

Table G.3. Asphaltene yields from mixtures of WC-B-A0 bitumen at 85 wt% *n*-heptane and 21°C for bitumen samples aerated at different temperatures.

Time, h	**Yield (wt%)**		
	Base Case	Aerated at 40ºC	Aerated at 70ºC
24	8.75	12.18	12.94
96	9.24	12.57	13.78
168	9.68	12.37	13.76
504	9.91	12.92	13.96
1008	9.85	12.61	14.26

APPENDIX H: SIZE DISTRIBUTIONS AND MEAN DIAMETER DATA

H.1. Asphaltene Aggregate Size Distributions

Size distributions of asphaltene aggregates were measured with the FBRM and micrographic methods after 1 h mixing at 195 rpm. Figure H.1 shows the cumulative number frequency distributions of asphaltene aggregates from the diluted bitumen mixtures investigated in Chapter 6. For the *n*-pentane diluted WC-B-A3 bitumen, Figure H.1a, the width of the distributions and the number mean diameter increased with solvent content up to 70 wt% and then decreased at higher dilutions. For both *n*-heptane diluted bitumens (Fig. H.1b and H.1c), the width of the distributions and mean diameters remained almost constant with increased solvent content. All distributions measured in this work were approximately log normal.

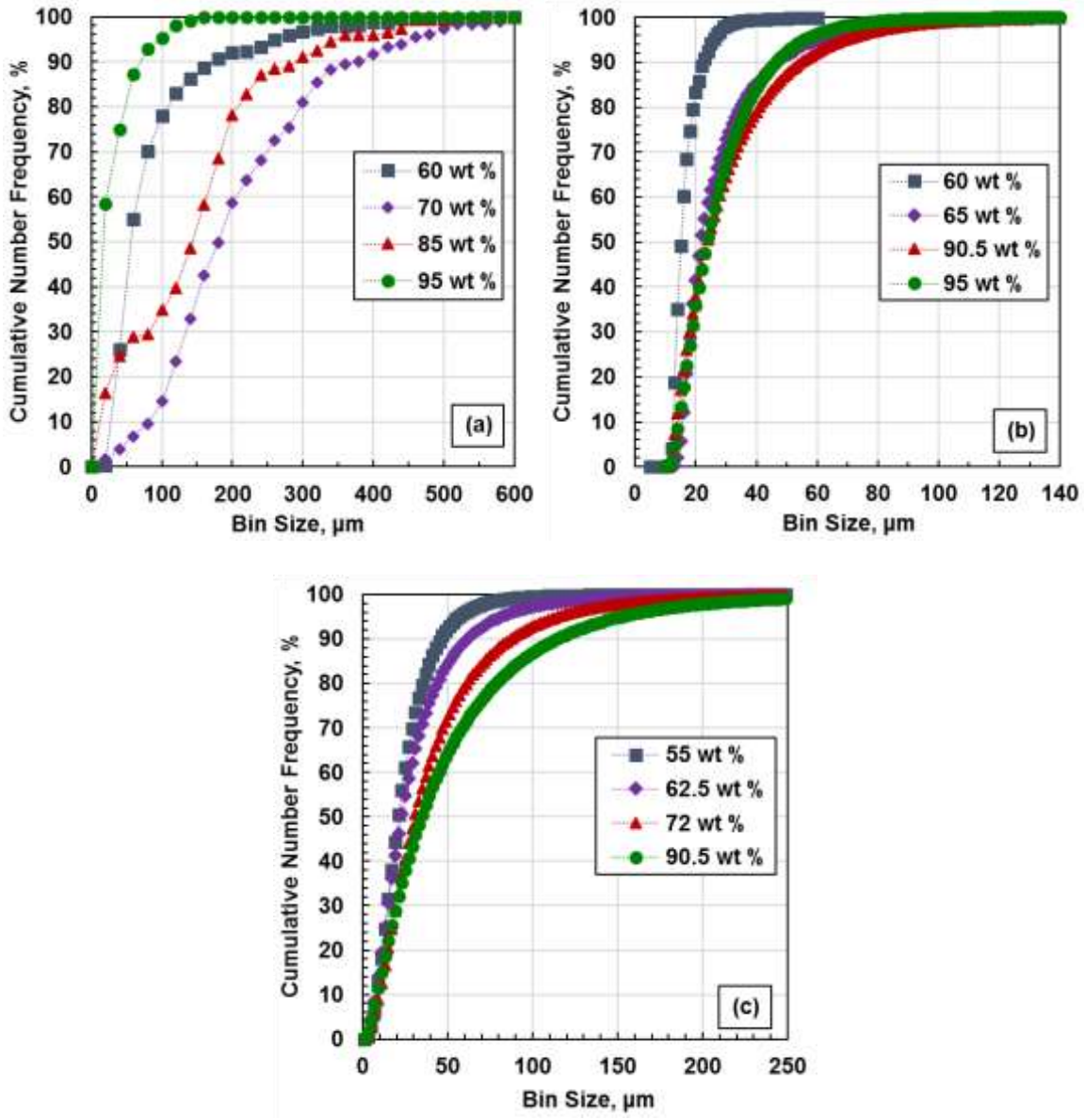

Figure H.1. Cumulative aggregate size distribution of *n*-pentane or *n*-heptane diluted bitumen after 1 h mixing at 21ºC. a) *n*-pentane/WC-B-A3; b) *n*-heptane/WC-B-A3; c) *n*-heptane/WC-B-B2(1). Note horizontal axes have different scales. All distributions in (a) and 60 and 65 wt% in (b) were obtained with the micrographic method. The other distributions were obtained with FBRM method. Data in a) and b) were originally reported by Casas (2017).

H.2. Asphaltene Aggregate Mean Diameters

The five definitions of aggregate mean diameter from Table 2.2 were calculated for all the distributions measured in this work and are provided in Table H.1.

Table H.1. Asphaltene aggregate mean diameters for mixtures of bitumen and precipitant measured after 1 h of mixing at 195 rpm and 21ºC.

***n*-pentane/WC-B-A3**					
Solvent Content, wt%	d_1	d_2	d_3	d_{32}	d_{43}
60.0	89.9	121.0	158.5	241.9	363.1
70.0	211.5	242.5	271.8	311.4	397.2
85.0	148.6	183.6	212.5	254.7	337.2
95.0	54.3	75.0	96.8	131.5	216.5
***n*-heptane/WC-B-A3**					
Solvent Content, wt%	d_1	d_2	d_3	d_{32}	d_{43}
60.0	17.4	19.9	23.7	32.6	44.1
65.0	17.9	20.8	25.1	36.8	45.3
70.0	19.0	22.1	25.2	43.2	51.7
72.0	-	-	-	-	55.4
80.0	22.3	45.6	55.0	58.2	77.5
87.5	28.2	43.9	53.5	63.3	84.8
90.6	-	-	-	-	86.8
95.0	34.5	44.2	53.7	64.4	87.1
***n*-heptane/WC-B-B2(1)**					
Solvent Content, wt%	d_1	d_2	d_3	d_{32}	d_{43}
50.0	13.0	17.7	23.4	40.8	63.9
55.0	27.4	37.0	49.0	85.9	133.3
57.5	33.0	43.2	55.2	90.1	134.2
60.0	45.5	59.2	73.5	113.1	151.3
62.5	39.1	51.9	65.3	103.4	139.8
67.0	40.1	54.3	68.9	110.8	147.7
72.0	44.4	60.6	76.9	123.6	162.5
77.0	52.2	71.0	89.5	141.8	182.9
82.0	62.0	84.2	105.6	165.9	211.5
87.5	60.9	81.0	100.3	153.6	195.5
90.5	60.9	80.7	99.8	152.9	195.8
93.5	57.6	76.3	94.8	146.6	189.9
95.5	56.3	74.8	93.9	148.0	196.7

APPENDIX I: FRACTAL DIMENSION DATA

Fractal dimensions for asphaltene aggregates from the diluted bitumen systems studied in this work were obtained from sediment volume method at 21ºC and atmospheric pressure. Data reported in Figure 6.5 are provided in Table I.1. The repeatability on both compacted and uncompacted fractal dimensions was ± 0.08.

Table I.1. Fractal dimensions of asphaltene aggregates obtained in this work. $D_{f,c}$ = compacted; $D_{f,uc}$ = uncompacted fractal dimension.

***n*-pentane/WC-B-A3**			***n*-heptane/WC-B-A3**			***n*-heptane/WC-B-B2(1)**		
Solvent Content, wt%	$D_{f,c}$	$D_{f,uc}$	Solvent Content, wt%	$D_{f,c}$	$D_{f,uc}$	Solvent Content, wt%	$D_{f,c}$	$D_{f,uc}$
60.0	2.76	2.55	60.0	2.09	1.88	55.0	2.43	2.26
70.0	2.81	2.56	65.0	2.40	2.14	57.5	2.53	2.30
85.0	2.79	2.55	72.0	2.47	2.26	60.0	2.60	2.34
95.0	2.36	2.19	80.0	2.55	2.35	62.5	2.62	2.37
			90.5	2.40	2.17	67.0	2.63	2.41
			95.0	2.21	1.99	77.0	2.66	2.45
						82.0	2.62	2.44
						87.5	2.60	2.35
						95.5	2.33	2.09

APPENDIX J: MEASURED ASPHALTENE YIELDS FOR THE SETTLING STUDY

Yields of asphaltene precipitation were measured for the three mixtures investigated using the gravimetric method. The yield data presented in Fig. 6.1a are reported in Table J.1. Yields were collected at 1.5 h contact time, 21ºC, and 1 atm. The yields were repeatable to ± 0.89 wt% for the *n*-pentane diluted bitumen and ±0.61 wt% for both *n*-heptane diluted bitumen systems.

Table J.1. Yields of asphaltene precipitation at 1.5 h contact for the mixtures investigated in this work.

***n*-pentane/WC-B-A3**		***n*-heptane/WC-B-A3**		***n*-heptane/WC-B-B2(1)**	
Solvent Content, wt%	Yield, wt%	Solvent Content, wt%	Yield, wt%	Solvent Content, wt%	Yield, wt%
49.8	1.1	56.8	0.0	40.3	1.0
53.8	6.1	61.5	3.4	51.3	2.9
58.4	9.6	67.4	6.0	55.4	5.2
63.1	11.8	71.5	7.8	60.1	7.8
67.2	12.5	71.9	8.1	74.6	12.9
69.9	14.8	81.5	10.7	79.4	13.4
70.1	14.7	90.2	12.0	90.8	14.3
80.4	16.7			95.2	14.5
89.9	17.1				

APPENDIX K: SETTLING RATE DATA

K.1. Experimental data

Settling rates were measured for the mixtures *n*-pentane/WC-B-A3, *n*-heptane/WC-B-A3, and *n*-heptane/WC-B-B2(1) at 21ºC and atmospheric pressure. Data collected with the visual and sampling methods are reported in Tables K.1, K.2, and K.3. The repeatability of the measurements is ±0.02 cm/min for the visual method and ±0.10 for the sampling method.

Table K.1. Settling rates of asphaltene aggregates from the *n*-pentane diluted WC-B-A3 bitumen at 21ºC and 1 atm. Data collected with visual method only.

***n*-pentane/WC-B-A3**	
Solvent Content (wt%)	Settling Rate (cm/min)
60.0	2.53
65.0	7.69
70.0	12.64
75.0	22.48
85.0	39.27
90.0	18.92

Table K.2. Settling rates of asphaltene aggregates from the *n*-heptane diluted WC-B-A3 bitumen at 21ºC and 1 atm. Data in bold font were collected with the sampling method. The rest of the data were collected with visual method.

***n*-heptane/WC-B-A3**	
Solvent Content (wt%)	Settling Rate (cm/min)
60.0	**0.23**
65.0	**0.12**
70.0	**0.20**
72.0	**0.26**
80.0	0.31
90.5	0.28
95.0	0.38

Table K.3. Settling rates of asphaltene aggregates from the *n*-heptane diluted WC-B-B2(1) and WC-B-B2(2) bitumen at 21ºC and 1 atm. Data in bold font were collected with the sampling method. The rest of the data were collected with visual method.

***n*-heptane/WC-B-B2(1)**		***n*-heptane/WC-B-B2(2)**	
Solvent Content, wt%	Settling Rate, cm/min	Solvent Content, wt%	Settling Rate, cm/min
50.0	**1.45**	**55.0**	**0.21**
55.0	**0.55**	**57.5**	**0.24**
57.5	**0.43**	**60.0**	**0.39**
60.0	**0.51**	**62.5**	**0.55**
62.5	**0.48**	67.0	1.01
67.0	1.01	72.0	2.00
72.0	2.01	77.0	2.40
77.0	2.40	82.0	2.55
82.0	2.70	87.5	1.39
87.5	1.39	95.5	1.00
90.5	0.99		
95.5	1.00		

K.2. Adjusted Settling Rates with Different Diameter Definitions

Settling rates were adjusted with the modified Stokes' law using the weighting factor (x) for the fractal dimensions and the five definitions of aggregate average diameter. Figures K.1 and K.2 show the adjusted settling rates for the *n*-pentane/WC-B-A3 and *n*-heptane/WC-B-A3 mixtures. The weighting factors for each curve were reported in Table 6.5 of this thesis.

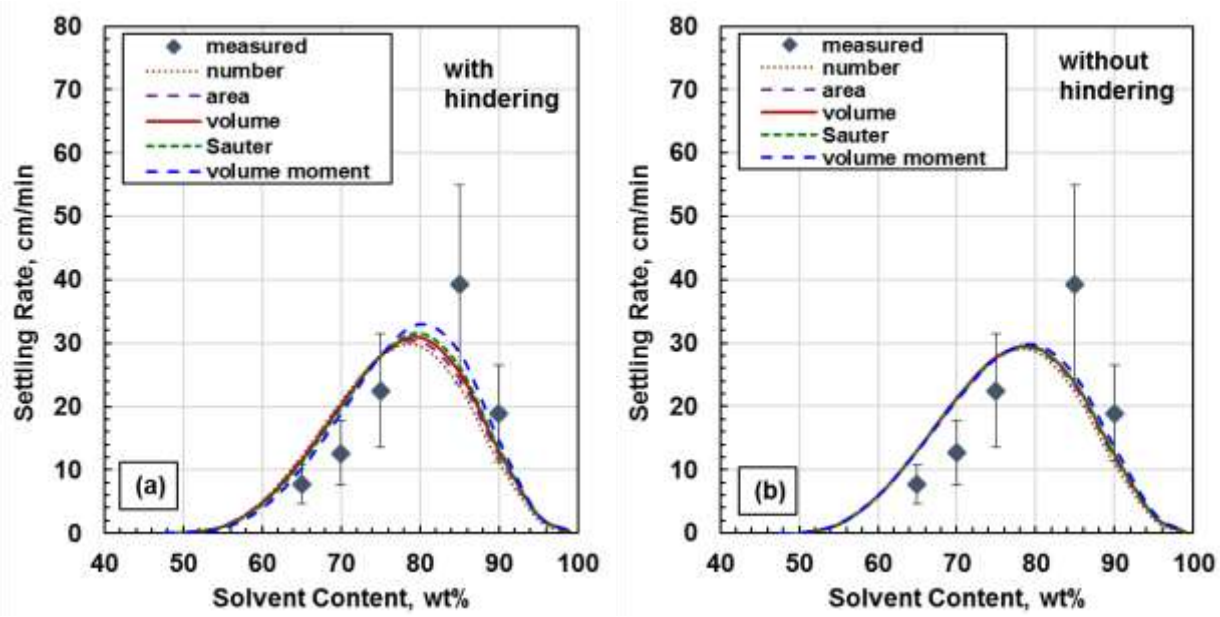

Figure K.1. Adjusted settling rates with the modified Stokes' model for asphaltene aggregates from *n*-pentane diluted WC-B-A3 bitumen mixtures using different definitions of mean diameter. a) model with hindering effect; b) model without hindering. The values obtained for the weighting factor x for each curve are provided in Table 6.5.

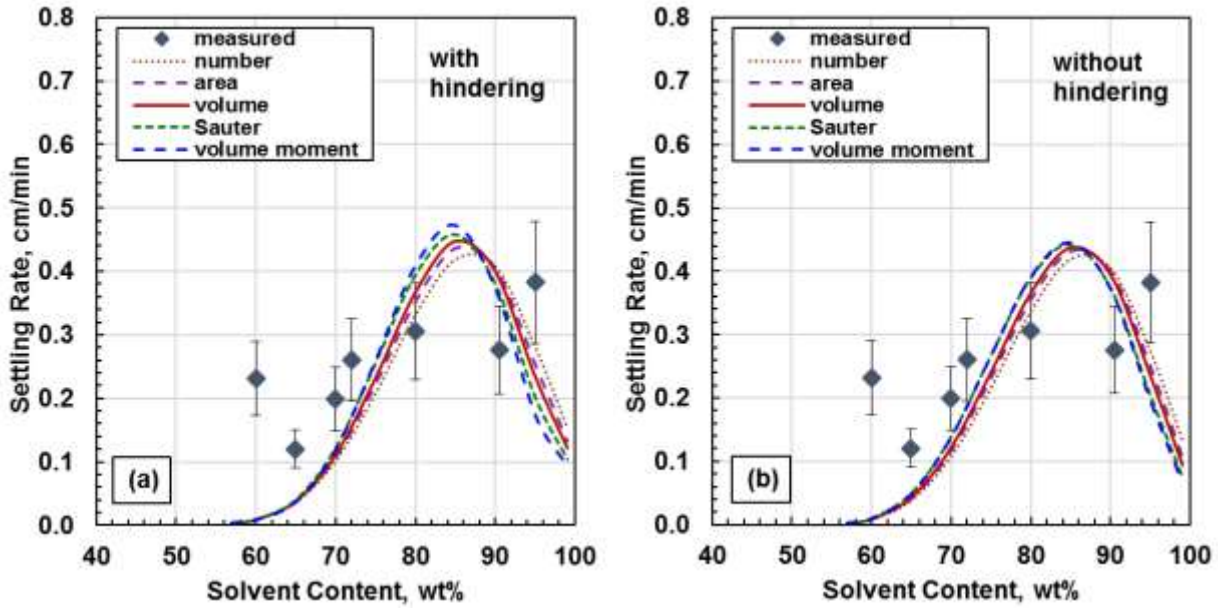

Figure K.2. Adjusted settling rates with the modified Stokes' model for asphaltene aggregates from *n*-heptane diluted WC-B-A3 bitumen mixtures using different definitions of mean diameter. a) model with hindering effect; b) model without hindering. The values obtained for the weighting factor *x* for each curve are provided in Table 6.5.